

AFRL-AFOSR-UK-TR-2013-0024



Study of Mechanisms of Filamentary Pulse Electric Discharge Interaction with Gaseous Flow of Nonuniform Composition

Dr. Sergey B. Leonov

**Institute of High Temperatures
Russian Academy of Science
IVTAN, Izhorskaya str., 13/19
Moscow 125412 Russia**

EOARD ISTC 07-7006/Project 3793p

Report Date: June 2013

Final Report from 1 October 2007 to 31 March 2013

Distribution Statement A: Approved for public release distribution is unlimited.

**Air Force Research Laboratory
Air Force Office of Scientific Research
European Office of Aerospace Research and Development
Unit 4515 Box 14, APO AE 09421**

REPORT DOCUMENTATION PAGE

Form Approved OMB No. 0704-0188

Public reporting burden for this collection of information is estimated to average 1 hour per response, including the time for reviewing instructions, searching existing data sources, gathering and maintaining the data needed, and completing and reviewing the collection of information. Send comments regarding this burden estimate or any other aspect of this collection of information, including suggestions for reducing the burden, to Department of Defense, Washington Headquarters Services, Directorate for Information Operations and Reports (0704-0188), 1215 Jefferson Davis Highway, Suite 1204, Arlington, VA 22202-4302. Respondents should be aware that notwithstanding any other provision of law, no person shall be subject to any penalty for failing to comply with a collection of information if it does not display a currently valid OMB control number.

PLEASE DO NOT RETURN YOUR FORM TO THE ABOVE ADDRESS.

1. REPORT DATE (DD-MM-YYYY) 17 June 2013	2. REPORT TYPE Final Report	3. DATES COVERED (From - To) 01 October 2007 - 31 March 2013
--	---------------------------------------	--

4. TITLE AND SUBTITLE Study of Mechanisms of Filamentary Pulse Electric Discharge Interaction with Gaseous Flow of Nonuniform Composition	5a. CONTRACT NUMBER ISTC Project 3793p
	5b. GRANT NUMBER ISTC 07-7006
	5c. PROGRAM ELEMENT NUMBER 61102F

6. AUTHOR(S) Dr. Sergey B. Leonov	5d. PROJECT NUMBER
	5d. TASK NUMBER
	5e. WORK UNIT NUMBER

7. PERFORMING ORGANIZATION NAME(S) AND ADDRESS(ES) Institute of High Temperatures Russian Academy of Science IVTAN, Izhorskaya str., 13/19 Moscow 125412 Russia	8. PERFORMING ORGANIZATION REPORT NUMBER N/A
--	--

9. SPONSORING/MONITORING AGENCY NAME(S) AND ADDRESS(ES) EOARD Unit 4515 APO AE 09421-4515	10. SPONSOR/MONITOR'S ACRONYM(S) AFRL/AFOSR/IOE (EOARD)
	11. SPONSOR/MONITOR'S REPORT NUMBER(S) AFRL-AFOSR-UK-TR-2013-0024

12. DISTRIBUTION/AVAILABILITY STATEMENT
Distribution A: Approved for public release; distribution is unlimited.

13. SUPPLEMENTARY NOTES

14. ABSTRACT

The work conducted under the project #3793p investigates the problem of multi-component flow mixing intensification by means of unstable low-temperature plasma. This research is related to fundamental plasma technology application in the field of control of airflow parameters. The work performed under this program will also result in obtaining new analytical, computational, and experimental data on filamentary plasma interaction with high-speed flow.

The project formal objective is to study the properties of filamentary transversal pulse-repetitive discharge and mechanisms of plasma-gas interaction under non-premixed conditions in high-speed flow.

The work as a whole was performed during five-year period of time. The tasks of the work include analytical/computational efforts, experimental investigations, and data analysis.

15. SUBJECT TERMS

EOARD, Plasma Physics, Magnetohydrodynamics, Plasma-Induced Mixing, Non-Premixed Composition, Pulse Electrical Discharge, High-speed Flow, Plasma Non-uniformity, Gasdynamic Instability, Measurement's Technique, Simulation of Discharge-Gas Interaction

16. SECURITY CLASSIFICATION OF:			17. LIMITATION OF ABSTRACT SAR	18. NUMBER OF PAGES 224	19a. NAME OF RESPONSIBLE PERSON Gregg Abate
a. REPORT UNCLAS	b. ABSTRACT UNCLAS	c. THIS PAGE UNCLAS			19b. TELEPHONE NUMBER (Include area code) +44 (0)1895 616 021

ISTC Project No. 3793p

**Study of Mechanisms of Filamentary Pulse Electric Discharge
Interaction with Gaseous Flow of Nonuniform Composition**

Final Project Technical Report

on the work performed from Oct 01, 2007 to March 31, 2013

**Joint Institute for High Temperature
Russian Academy of Science**

**Project Manager Sergey B. Leonov
 DrSc**

**Deputy Director Vladimir A. Zeigarnik
 DrSc**



A handwritten signature in blue ink, appearing to be 'S. Leonov', is written over a horizontal line. A second horizontal line is positioned below the first one.

May 2013

This work was supported financially by EOARD and performed under the agreement to the International Science and Technology Center (ISTC), Moscow.

Distribution A: Approved for public release; distribution is unlimited.

Title of the Project: Study of Mechanisms of Filamentary Pulse Electric Discharge Interaction with Gaseous Flow of Nonuniform Composition

Commencement Date: October 01, 2007

Duration: From October 01, 2007 to March 31, 2013 for 66 months

Project Manager: Sergey Borisovich Leonov

phone number: +7-(495) 484-1811

fax number: +7-(495) 483-2285

e-mail address: leonov@ihed.ras.ru

Leading Institute: Joint Institute for High Temperature Russian Academy of Science
Izhorskaya str., 13 bld 2, Moscow, 125412, Russia
+7 (495) 483 22 75
Leonov@ihed.ras.ru
www.oivtran.ru

Participating Institutes:

Foreign Partner: European Office of Aerospace Research and Development (EOARD)
Building 186, 86 Blenheim Crescent, Ruislip, Middlesex, HA4 7HB, UK
Phone: +44 (0) 189 561 6021; Fax: +44 (0) 189 561 6012
E-mail: gregg.abate@crougton.af.mil

Keywords:

Plasma-Induced Mixing, Non-Premixed Composition, Pulse Electrical Discharge, High-speed Flow, Plasma Non-uniformity, Gasdynamic Instability, Measurement's Technique, Simulation of Discharge-Gas Interaction

Contents

- i. List of key personnel
- ii. List of acronyms and definitions

1. Introduction

- 1.1. Project's Objectives.
- 1.2. Tasks' Description

2. Short review of efforts year per year (Review of activity)

- 2.1. Short review of the first year efforts
- 2.2. Short review of the second year efforts
- 2.3. Short review of the third year efforts
- 2.4. Short review of the fourth year efforts
- 2.5. Short review of the fifth year efforts

3. Background

- 3.1. Review based on available literature
- 3.2. Discharges for mixing and ignition assistance
- 3.3. Experimental methods for diagnostic of mixing

4. Task 1. Analytical Efforts

- 4.1. Development of the physical models:
 - 4.1.1. The physical model of spark channel development
 - 4.1.2. Hydrodynamic instability of the after-spark channel boundary
 - 4.1.3. Stabilizing role of the residual current
 - 4.1.4. Physical mechanism of jets formation
 - 4.1.5. Experimental demonstration of the physical model suitability
- 4.2. Computational analysis of plasma channel and low-density zone dynamics in ambient conditions
- 4.3. Discharge specific localization in two-component system
- 4.4. Instability of plasma channel by 1D and 2D computational analysis
- 4.5. Comparison of simulation and experimental data
- 4.6. Adjustment of spectroscopic technique for spatially resolved estimation of mixing

efficiency

4.7. Benefits of double-pulse pattern

4.8. Ignition by filamentary pulse plasma

5. Task 2. Experimental Efforts

5.1. Experimental facility description

5.2. Experimental study of plasma channel and low-density zone dynamics in ambient conditions

5.3. Experimental runs under stable and unstable operational modes

5.4. Experimental study of plasma channel and low-density zone dynamics in high-speed flow

5.5. Experimental study of plasma localization in mixing layer of gas-gas and spray-gas systems at ambient conditions

5.6. Experimental runs with second gas and spray injection in high-speed flow

5.6.1. Experimental runs with co-flowing jet of second gas

5.6.2. Experimental runs with wall jet of second gas

5.6.3. Experimental runs with gaseous hydrocarbons injection, double pulse pattern

5.6.4. Experimental study of efficiency of plasma-based mixing by means of PBF in high-speed flow

5.6.5. Experimental runs with liquid hydrocarbons injection

6. Conclusions

Attachment 1.

List of published papers with abstracts

Attachment 2.

List of presentations at conferences and meetings with abstracts

i. List of Key Personnel.

Dr. Alexander A. Firsov	PhD, Research Staff,
Dr. Yury I. Isaenkov	PhD, Leading Researcher,
Dr. Igor V. Kochetov	PhD, Senior Researcher,
Dr. Sergey B. Leonov	DrSc, Head of Department, Project Manager,
Dr. Yury A. Melnik	PhD, Senior Researcher,
Dr. Alexey B. Miller	PhD, Research Staff
Mr. Konstantin V. Savelkin	Senior Engineer,
Dr. Michail N. Shneider	in collaboration with Princeton University,
Mr. Michail A. Shurupov	PhD Student,
Dr. Victor R. Soloviev	PhD, Senior Researcher,
Mr. Vladimir A. Storozhenko	Technician,
Dr. Valery N. Suchov	PhD, Leading Engineer,
Mr. Dmitry A. Yarantsev	Engineer-Physicist.

Acknowledgements.

Dr. Valentin A. Bityurin,
Mr. Paul G. Makeev,
Prof. Richard Miles,
Prof. Anatoly P. Napartovich,
Dr. Gregg Abate

ii. List of Definitions and Acronyms.

M -	Mach Number of the flow.
Re -	Reynolds Number.
C -	capacitance.
E-	electric field strength.
E/N-	reduced electric field strength.
I, I _d -	electric current.
k-	Boltzman's constant, electrons mobility.
L-	inductivity.
N _e -	concentration of electrons.
N -	concentration of neutral gas particles.
N _n -	concentration of the different chemical species.
P, P _{st} -	static pressure.
P _o -	stagnation pressure in airflow.
R	resistivity.
R _L =ωL	inductive resistivity.
S -	area of midsection.
T _g -	gas temperature.
T _v -	vibrational temperature of molecular gas.
T _e -	temperature of electrons in plasma.
U, U _d -	voltage on discharge gap.
V -	velocity of flow.
W -	power or power density.
ρ ₀ -	gas density in flow.
ε ₀ -	electrostatic constant.
δ-	boundary layer thickness.
λ-	wavelength.
τ -	relaxation time.
ω -	circular frequency of EM wave.
AC -	alternative current.
BL -	boundary layer.
CFD -	computational fluid dynamics
DC -	direct current.
EMF -	electromagnetic field.
HF -	high frequency.
HV -	high voltage.
IR -	infra-red radiation.
MF -	magnetic field.
PD -	pulse discharge.
PG -	plasma generator.
PS -	power supply.
PWT -	pulse wind tunnel.
SW -	shock wave.
TS -	test section.
UV -	ultra-violet radiation.
WT -	wind tunnel.

1. Introduction.

1.1. Project's Objectives.

The work conducted under the project #3793p investigates the problem of multi-component flow mixing intensification by means of unstable low-temperature plasma. This research is related to fundamental plasma technology application in the field of control of airflow parameters. The work performed under this program will also result in obtaining new analytical, computational, and experimental data on filamentary plasma interaction with high-speed flow.

The project formal objective is *to study the properties of filamentary transversal pulse-repetitive discharge and mechanisms of plasma-gas interaction under non-premixed conditions in high-speed flow.*

The work as a whole was performed during five-year period of time. The tasks of the work include analytical/computational efforts, experimental investigations, and data analysis. The results of the project were supposed as follows:

- Data on the pulse discharge dynamics in ambient gas and in flow.
- Result of analysis of physical mechanisms of the discharge channel fast expansion.
- Experimental data on the mixing intensification in two-gases medium by the pulse-repetitive discharge.
- Dependence of the mixing effect on the parameters of flow, discharge, and gas composition.
- Experimental data on the submicrosecond filamentary discharge dynamic in mixing layer of gas1-gas2 and spray-gas systems at static conditions and in high-speed flow.
- Description of kinetic and dynamic physical models of the discharge specific localization in vicinity of two gases and spray-gas boundary.
- Consideration of physical mechanism of strong gasdynamic instability of after-discharge channel.
- Consideration of advantages of the double-pulse scheme for ignition of non-premixed air-fuel composition. Physical demonstration of effectiveness of the two-pulse scheme for ignition of non-premixed air-fuel composition.
- Description of physical models of turbulent motion of the gas affected by the discharge in non-homogeneous media. Experimental and analytical data.
- Quantitative experimental data on the mixing efficiency due to unstable submicrosecond discharge excitation in vicinity of the boundary between two gases, obtained by non-intrusive diagnostics.

It should be considered that the objective of the project was achieved and the results were obtained in full.

The work included several important steps, namely: (1) review of available publications; (2) specification of the experimental configuration and explicit design of plasma generator; (3)

development of the appropriate diagnostics; (4) test runs and getting an experimental data concerning non-homogeneous plasma effect on mixing; (5) analytical and computational analysis at verification by experimental data; (6) analysis of results and recommendations for the further development; (7) demonstration of the plasma mixing effect under conditions of high-speed multi-components flow; (8) experimental data on the discharge dynamic in mixing layer of gas1-gas2 and in spray-gas systems; (9) description of kinetic and dynamic physical models of the discharge specific localization in the vicinity of two gases and spray-gas boundary; (10) diagnostics of the mixing efficiency by Probe Breakdown Fluorescence; (11) recommendations on the improvement of plasma-assisted mixing method and apparatus.

During the first year the work was aimed at available data analysis, the experimental facility modification, and runs under ambient conditions. In a parallel line the diagnostics methods and equipment were prepared. The analytical/computational efforts were done to attend the experimental data and measurements. Mainly two problems were being tried to resolve:

- What are main steering mechanisms of post-discharge instability?
- Which properties of the discharge are distinct in different gases?

During the second year the efforts in frames of the project were arrowed on study of the unstable discharge properties in high-speed flow. Experimental works were supported by analytical and CFD efforts as usually. A main attention was paid for the facility modification in frames of preparation of two-phase flow mixing experiment. This experiment was started to study the features of the discharge interaction with co-flow jet of model gaseous fuel (CO₂ in this particular case).

In the third year of the project a main attention was paid for the experiments in multi-components flow and for analysis of the results based on experimental data and data of analytical/computational efforts. The physical model of the instability development has found a successful experimental verification.

The fourth year efforts were aimed at the study of detail physical mechanism of the specific localization of pulse filamentary discharge in vicinity of boundary between two gases and between liquid spray and gas. The intensification of the effect of jets' instability was also under analysis and experimental optimization. This experimental work was supported by analytical and computational efforts in cooperation with Princeton University. A new spatial-resolved spectroscopic diagnostic was designed and preliminary applied for qualitative estimations of mixing efficiency. The theoretical part on the work included an analysis of kinetic and dynamic physical mechanisms of the pulse filamentary discharge localization in non-homogeneous two-component gas. Detail dynamics of the gas movement after the discharge shoot was modeled based on 3D Navier-Stokes approach. A benefit of two-pulse mode was explored for a fast ignition of combustible gaseous mixture. The experiments were performed to study of the discharge properties in vicinity of two-phase composition (liquid spray in air). Spectroscopic system was constructed to estimate the mixing efficiency. The experimental portion of the work included three topics: (1) tests on the discharge localization affected by thin laminar jet of He and heated air; (2) demonstration of spectroscopic technique ability to detect a presence of secondary gas in the main media (mixing); and (3) tests to study the discharge interaction with spray jet in high-speed flow.

During the fifth year of the project performance two main ideas are considered to be realized for better understanding of physical processes in a system consisting of a submicrosecond pulse discharge – non-homogeneous media in order to move this technique toward practical realization:

- Application of newly developed diagnostic for the mixing efficiency measurements;
- Detailed description of mechanisms of excitation and development of turbulent motion of the gas at interaction with transient plasma.

Due to the previous activity the spectroscopic diagnostic was developed for non-intrusive evaluation of gaseous components presence in small volume after medium disturbance by the unstable discharge. To make a quantitative measurement this system was calibrated and improved. The authors also explored the experimental methods that could be specifically applied to evaluate quantitatively the spectrum and intensity of turbulent motion in gas impacted by the discharge. The experimental study was performed of the mixing enhancement by filamentary discharge in high-speed flow. The probe discharge breakdown spectroscopy technique was applied to explore the optical spectra modification at direct fuel injection in two cases: without filamentary discharge generation and after the mixing intensification by the forestream plasma. Extra simulations were fulfilled to highlight the gasdynamic instability patterns.

1.2. Tasks' Description

The work was divided conditionally on two main tasks in accordance with the methods of research: theoretical and experimental. The first task "Analysis of plasma channel and low-density zone dynamics in high-speed flow" included a development of appropriate diagnostics as well. The second task "Experimental study of plasma channel and low-density zone dynamics in high-speed flow" included eleven subtasks as shown below. Besides of these subtasks several extra efforts were fulfilled to support the analytical and experimental studies: significant modification of the facility, updates in diagnostics, etc.

The tasks of the work include analytical/computational efforts, experimental investigations, and data analysis. The SOW has specified the work's tasks as listed below.

Task 1. Analytical Efforts: Analysis of plasma channel and low-density zone dynamics in high-speed flow

1.1. Review of available publications on filamentary discharge properties and interaction with high-speed flow.

1.2. Development of diagnostic technique applicable for estimation of mixing efficiency.

1.3. Computational analysis of plasma channel and low-density zone dynamics in ambient conditions.

1.4. Computational analysis of plasma channel and low-density zone dynamics in high-speed flow.

1.5. Comparison of simulation and experimental data.

1.6. Analysis of 1-3rd years data.

1.7. Reporting.

1.8. Development of the kinetic and dynamic physical models of the discharge specific localization in two-component system.

1.9. Adjustment of spectroscopic technique for spatially resolved estimation of mixing efficiency.

1.10. Analysis of 4th year data.

1.11. Consideration of physical model of origin and development of turbulent motion of non-homogeneous gas affected by the electrical discharge.

1.12. Analysis of spectra and intensity of turbulence at electrical discharge interaction with gaseous media by non-intrusive diagnostics.

1.13. Analysis of data (analytical, experimental and computational). Reporting.

Task 2. Experimental Efforts: Experimental study of plasma channel and low-density zone dynamics in high-speed flow

2.1. Experimental study of plasma channel and low-density zone dynamics in ambient conditions.

2.2. Experimental runs under stable and unstable operational modes.

2.3. Experimental study of plasma channel and low-density zone dynamics in high-speed flow.

2.4. Experimental runs with two-phase flow.

2.5. Experimental runs with hydrogen and gaseous hydrocarbons injection.

2.6. Analysis of data.

2.7. Experimental study of plasma localization in mixing layer of gas1-gas2 and spray-gas systems at ambient conditions and in high-speed flow.

2.8. Analysis of 4th year data.

2.9. Calibration and improvement of Probe Breakdown Fluorescence system for quantitative measurements.

2.10. Experimental study of efficiency of plasma-based mixing enhancement by means of PBF at ambient conditions and in high-speed flow.

2.11. Analysis of data. Reporting.

The experimental parameters of the JIHT RAS high-speed test are summarized below.

- Mach number of airflow 0.5 and 2.00
- Static pressure 1-0.27 (down to 0.15) Bar
- Inter-electrodes gap D=50-60 mm
- Type of discharge High-voltage pulse repetitive, filamentary
- Energy input to the single plasma shock up to 2J for 50ns
- Typical repetition rate up to 10kHz for 2-3pulses mode
- Operation time of gasdynamic facility up to 1sec

Following measurements are suggested for PAL/ JIHT RAS test.

- Electrical measurements of the discharge characteristics
- OES – optical spectroscopic measurements
- PBS – probe breakdown spectroscopy
- Streak and schlieren-streak observations
- Video records
- Pressure measurements

It can be considered that as a whole the objectives of the Project were reached and the results expected were obtained.

The most of physical results were reported, and published [1-10] due to the project's efforts. Among them: experimental data on the unstable filamentary plasma dynamics in static gas and in high-speed flow; analytical and computational models of the jet-type gasdynamic instability due to pulse discharge generation were described for the first time; development of the spectroscopic diagnostic of mixing based on probe discharge excitation (Probe Breakdown Fluorescence = PBF); dynamics of the discharge in two-components and two-phase flow were studied in single-pulse and multi-pulse modes at variety of conditions; etc. The experimental data were obtained and validated by means of wide set of diagnostic methods.

This Final Technical Report describes the most valuable results obtained in frames of the project ISTC#3057p due to experimental, computational, and analytical efforts.

References to section 1.2:

1. "Control of Flow Structure and Ignition of Hydrocarbon Fuel in Cavity and behind Wallstep of Supersonic Duct by Filamentary DC Discharge", Ed. S. Leonov, Project ISTC-EOARD-IVTAN #3793p, The Annual and Quarterly Technical Reports, 2007-2013.
2. S. B. Leonov, Y. I. Isaenkov, A. A. Firsov, S. L. Nothnagel, S. F. Gimelshein, and M. N. Shneider, "Jet Regime of the Afterspark Channel Decay", PHYSICS OF PLASMAS **17**, 1, 2010
3. M. A. Deminsky, I. V. Kochetov, S. B. Leonov, A. P. Napartovich, "Modeling of plasma assisted combustion in premixed supersonic gas", International Journal of Hypersonics, Vol 1, #4, 2011, pp.209-223
4. Sergey B. Leonov, Dmitry A. Yarantsev, "Instability in Post-Discharge Thermal Cavity", IEEE Transactions, Plasma Science, June 2008, DOI 10.1109/TPS.2008.922479
5. Yuri I. Isaenkov, Sergey B. Leonov, Mikhail N. Shneider "Suppression of the turbulent decay of an afterspark channel with residual current", PHYSICS OF PLASMAS **14**, 123504_2007.
6. Sergey B. Leonov "Visualization of Unsteady electrical discharges in high-speed flow", Journal "International Review of Aerospace Engineering", International Review on Aerospace Science and Engineering by PRAISE, v.3, #4, August 2010, pp214-222.

7. *A. Firsov, Yu. Isaenkov, S. Leonov, M. Shurupov, D. Yarantsev*, “Pulse Filamentary Discharge in Mixing Layer of Reacting Gases”, Proceedings of 18th International Conference on Gas Discharges and Their Applications, Germany, Greifswald, 05 – 11 September 2010
8. *A. A. Firsov, Yu. I. Isaenkov, I.V. Kochetov, S. B. Leonov, A.P. Napartovich, M.N. Shneider, M.A. Shurupov, D. A. Yarantsev*, “Mixing Intensification by Electrical Discharge”, AFOSR Program Review “Fundamental Mechanisms, Predictive Modeling, and Novel Aerospace Applications of Plasma-Assisted Combustion”, November 9-10, 2011, OSU, Columbus, OH
9. *S. Leonov, Yu. Isaenkov, D. Yarantsev, M. Shurupov, J. Michael, A. Dogariu, M. Shneider, R. Miles*, “High-Voltage Breakdown, Guided by Femtosecond Laser and Gas Inhomogeneity”, Proceedings of 19th International Conference on Gas Discharges and Their Applications, Beijing, Sept 2012, paper 159
10. *S. B. Leonov, A. A. Firsov, M. A. Shurupov, J. B. Michael, M. N. Shneider, R. B. Miles, and N. A. Popov* “Femtosecond laser guiding of a high-voltage discharge and the restoration of dielectric strength in air and nitrogen”, PHYSICS OF PLASMAS, vol.19, 123502, 2012

2. Review of activity.

2.1. Short review of the first year efforts.

During the first year the work was aimed at available data analysis, the experimental facility modification, and runs under ambient conditions. In a parallel line the diagnostics methods and equipment were prepared [1]. In the first quarter of the project the analysis of previous efforts has been done, and the future theoretical and experimental work was planned. During the second quarter of the project the efforts were directed on the experimental facility modification, diagnostics analysis, and manufacturing of parts and components for future experiments. In the third quarter the work was aimed at study of discharge properties in ambient medium at variation of gas properties, and power supply parameters. The efforts of the fourth quarter were mainly devoted to the study of plasma instability in unmoved gas. Computational simulations were being done during whole period of time.

Among of others the key point of this work is an adequate measurement of the mixing efficiency. The best way for that is to know the concentrations of main components and their spatial distribution. The Project schedule supposed the efforts for analysis of applicable diagnostic methods. The analysis was made in cooperation with Princeton University. The analysis made shows that for the local measurements the *laser breakdown fluorescence* could be used [2-4]. It possesses important advantages: high temporal and spatial resolutions, and non-intrusive nature. At the same time the result is supposed to be mostly quantitative due to insufficient averaging at short operation of the facility.

The *laser breakdown fluorescence* can give the data on composition in small volume of the gas ($l \times d = 2 \times 0.1 \text{ mm}$, approximately) located in predefined position. Temporal resolution will be less than $1 \mu\text{s}$. *This diagnostic is non-intrusive*. To realize this method several steps are planned: exact design of extra arrangement; purchasing of the pulse laser; assembling of equipment; model test measurements; measurements in supersonic flow. Extra manpower is required as well. The Fig.2.1.1 presents a draft scheme of measurements by means of *laser breakdown fluorescence*. Unfortunately, the project's existing capabilities were very limited to construct the laser system required for this method. In case of possible future extension of the work the diagnostic based on *laser breakdown fluorescence* method can provide critically important extra information on the mixing efficiency.

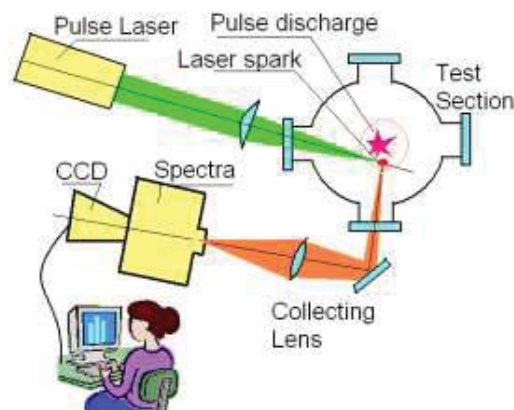


Fig.2.1.1. Draft-scheme, related with local measurement by LBF.

Concluding this analysis the authors have announced that during the further experiments the deeply modified schlieren and schlieren-streak techniques are utilized with appropriate processing of images; measurements of voltage and current to estimate electrical field and power release; optical spectroscopy for qualitative evaluation of the media composition.

In frames of the Task 2, during the 1st year of the project performance the experiments were fulfilled on the pulse discharge dynamics in quiescent air and other gases, namely: argon (Ar), carbon dioxide (CO₂), ethylene (C₂H₄). The experimental facility was designed, assembled, and upgraded by new power supply. Existing diagnostics include: pressure measurements, time-resolved schlieren imaging, electrical measurements, video records, IR frames, light-emission analysis, and other conventional methods. The most diagnostics work in quite specific modes. These methods allow acquiring the data on flow structure, electrical parameters, dynamics of post-plasma channel, and some data on the plasma parameters.

The gas breakdown and afterspark channel cooling and expansion in 5 cm gap in different gases at normal conditions were studied for the basic consideration. The typical voltage-current and power characteristics of the discharge in air at atmospheric pressure are presented in Fig.2.1.2. It is seen that current in air has several vibrations after the main pulse. This rule is not universal (see section 5 for details) but shows that the inductive processes are not negligible. The data were refined for correct evaluation of the power release as it shown in the right picture.

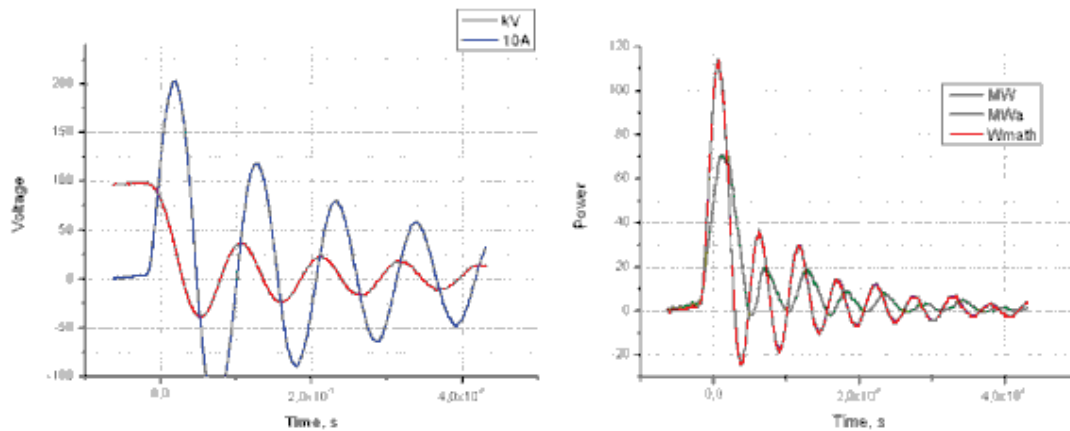


Fig.2.1.2. Voltage-current and power characteristics of electrical pulse in air. Power (in MW): green line taking into account inductive processes. Energy deposition is about 2.5J in this case.

At high level of pressure and fixed 2-electrodes configuration the discharge appears in form of filamentary long spark. The filamentary discharge penetrates cross flow between electrodes with the speed about $V \approx 10^7 \text{ m/s} = 1 \text{ cm/ns}$. This value was estimated based on the schlieren pictures of the shock waves propagation away from initial streamers. The plasma temperature was estimated in $T_{pl} = 15-17 \text{ kK}$ on the base of spectroscopic measurements of continuum luminescence. The analysis of radiation profile concludes the plasma as optically thick at the phase of high current.



Fig.2.1.3. Typical schlieren image of post-discharge thermal distortion, $t=200 \mu\text{s}$.

The behavior of the after-discharge channel can be characterized by generation of intensive lateral jets with sequential fast turbulization of significant volume of the gas (the diameter is inter-gap distance, approximately). The sample of schlieren image of the jets generation is shown in Fig.2.1.3. In such a way the analysis of experimental data gives some not obvious results concerning the size of disturbed zone: its value occurs several times greater than it could be in accordance with laminar or turbulent diffusion law.

The electrical characteristics of the discharge in different gases and the dynamics of disturbed zone were explored in special series of tests. The main pulse duration was $t \approx 100$ ns, rate of the voltage rise before breakdown $dU/dt \approx 3 \times 10^{10}$ V/s, gas pressure $p = 1$ Bar, inter-electrodes gap $d = 50$ mm. The table 1 presents some factual data. Among the molecular gases the gaseous hydrocarbon fuel provides the best conditions for discharge development on the first phase (breakdown itself). With further growth of the electric current the situation can be changed. This statement is confirmed by measuring history of E/N and current in high-current phase of the discharge in different gases.

Table 1: Experimental data, pulse discharge in different gases. Short current $\tau = 100$ ns.

Gas	Air	C2H4	CO2
Typical breakdown voltage, kV	100	98	93
Energy deposition in main pulse, J	2.1	2.4	2.9
Typical plasma channel resistance at $t/2$, Ohm	18	30	65

The visualization of the discharge induced flow dynamics was made using schlieren technique for the short-pulse mode. The observation of those images allows considering some peculiarities of the post-discharge channel behavior in different gases.

- Ar: size of disturbance is minimal, very often the discharge has several channels.
- Air: maximal speed of expansion in time range 20-200 μ s.
- CO2: the turbulence has smaller scale than in the Air, a “bubble” generation of unknown nature.
- C2H4: very similar with CO2.

The next important item is the discharge’s filament localization under nonhomogeneous gaseous medium. There was found experimentally [5] that the voltage on the discharge gap is increased significantly in the most cases of the air-fuel-plasma interaction. The explanation of this fact includes the idea that the discharge localization is managed by the rule of minimal gap voltage along the line. It can be supposed that the discharge “prefers” the place in oxidized, fuel, or between them in dependence on the composition electrical properties. The simulation proves the possibility of such a mechanism.

References to section 2.1.

1. “Study of Mechanisms of Filamentary Pulse Electric Discharge Interaction with Gaseous Flow of Nonuniform Composition”, Project ISTC #3793p, The First Year Report, October 2008.

2. *L. Zimmer, Sh. Tachibana*, “Laser induced plasma spectroscopy for local equivalence ratio measurements in an oscillating combustion environment”, Proceedings of the Combustion Institute, issue 31, 2007, pp.737-745

3. *T.-W. Lee, N. Hegde*, Combustion Flame, 142, 2005, pp.314-316

4. *K. Kohse-Hoinghaus, R.S. Barlow, M. Alden, J. Wolfrum*, Proceedings of the Combustion Institute, issue 30, 2005, pp.89-123

5. *Sergey B. Leonov, Dmitry A. Yarantsev, Campbell Carter* Transversal Electrical Discharge as a New Type of Flameholder, 15th AIAA International Spaceplanes and Hypersonic Systems and Technology Conference, Dayton, OH, Apr-May 2008, AIAA-2008-2675.

2.2. Short review of the second year efforts.

During the second year the efforts in frames of the project were arrowed on study of the unstable discharge properties in high-speed flow. Experimental works were supported by analytical and CFD efforts as usually. In the 5th quarter of the project the computational analysis of plasma channel and low-density zone dynamics was performed based on 2D approach. Mainly two questions were resolved: (1) physical mechanism of jets' instability arising; and (2) a range of gas velocity in jets escaped. The experiments were started on the plasma filament dynamics analysis in high-speed flow. Those experiments were continued in the 6th quarter using modified scheme of the discharge excitation. The pulse-repetitive mode was applied to recognize the features of cross-interaction of individual plasma filaments. The parameters of flow disturbance were estimated based on experimental data. In the 7th quarter of the project performance a 3D model of the after-discharge channel unstable expansion were developed based on CFD++ software. A main attention was paid for the facility modification in frames of preparation of two-phase flow mixing experiment. This experiment was started in 8th quarter to study the features of the discharge interaction with co-flow jet of model gaseous fuel (CO₂ in this particular case).

Physical mechanism of jet formation. Jets are developing in quasi-isobaric stage, when $p(r,t) \approx p_0$. An illustrative sketch of jets formation is shown in the Fig.2.2.1. Depending on whether the surface of the channel boundary is concave or convex, flow from the periphery to the center, arising in a process of cooling, can be contracting or expanding. If the flow is contracting (concave surface), the static gas pressure increases, however, expanding flow from the convex surface decreases the pressure. As a result, we can expect the formation of jets in the direction opposite to pressure gradients. A "cumulative" jets formation is being also studied numerically using a commercial CFD++ flow solver. CFD++ is a flexible computational fluid dynamics software suite for the solution of steady and unsteady, compressible and incompressible Navier-Stokes equations, including multi-species capability for perfect and reacting gases.

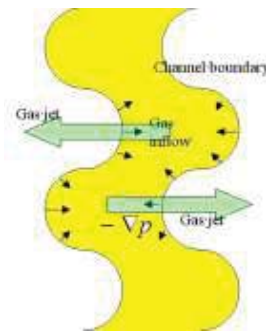


Fig.2.2.1. 2D Schematic of 'cumulative' jet formation during the cooling of a curved channel.

Shape of the plasma channel (3D restoration). The most conventional source of data for analysis in studying the characteristics of the discharge channel form is the picture (photos) of the discharge. However, a more complete visualization of the discharge structure in space can be provided by three-dimensional model reconstructed from photographs obtained. Model recovery was produced in the SolidWorks program. A sample of reconstructed 3D channel is shown in Fig.2.2.2.

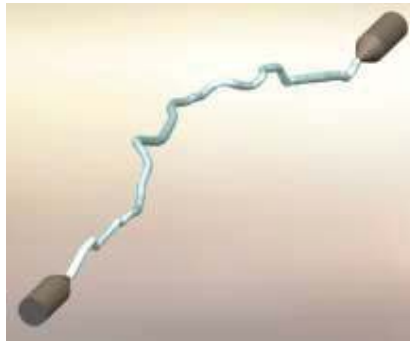


Fig.2.2.2. Sample of restored 3D plasma channel.

Comparison of simulation and experimental data. On the first stage of expansion ($t < 50 \mu\text{s}$) the post-discharge channel looks quite classical: cylindrical thermal cavity. At $t \approx 80\text{-}150 \mu\text{s}$ (depending on conditions) the shape of the after-spark channel occurs unstable. The physical mechanism of this instability is that the cooling of the axial zone leads to the pressure decrease with sequential gas reverse movement. Such a movement occurs unstable due to the Rayleigh-Taylor mechanism. The time of RT instability was compared with the experimentally obtained one. The later stage of expansion can be characterized by generation of intensive lateral jets followed by fast turbulization of significant volume of the gas. The analysis of experimental data gives some not obvious results concerning the size of disturbed zone: its value occurs several times bigger than it could be in accordance with laminar or turbulent diffusion mechanisms. This statement was clearly demonstrated.

Power supply. Several principal changes in electrical scheme have been considered for the spark discharge excitation at high repetition rate within the supersonic airflow.

Experimental study of low-density zone dynamics in high-speed flow. Two experimental series were performed: (1) measurements of the short-pulse discharge parameters in air at variable pressure; (2) and study of pulse discharge dynamic in supersonic flow. The first series appears to be needed because the static pressure in high-speed flow is lower than atmospheric value: $P_{st} = 100\text{-}250 \text{ Torr}$ at $M = 2$. The electrical parameters were measured in coupling with schlieren images acquisition to detect the instability presence. In some range of parameters a shorter pulse may be more efficient in order to energy release to low-density gas. Figures 2.2.3 summarize the electrical parameters of the discharge depending on the gas pressure.

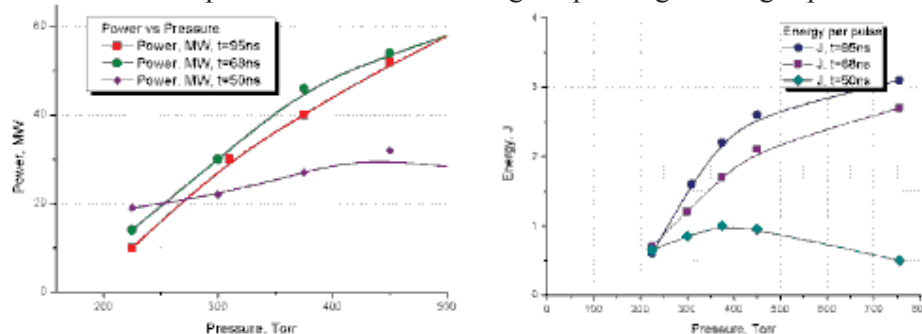


Fig.2.2.3. Comparison of the discharge modes in terms of power and energy deposition.

The second series of tests appears to be needed because the static pressure in the first case was critically lower than atmospheric value: $P_{st} = 100\text{-}250 \text{ Torr}$ at $M = 2$. At the same time there is no any significant modification of the averaged flow parameters. The quantitative analysis of images allows to estimate a main characteristic size of the plasma-induced disturbances. The Fig.2.2.4 presents a comparison of Fourier spectra of the processed images. The statistically averaged value is calculated as of $\Delta y = 1\text{-}3 \text{ mm}$.

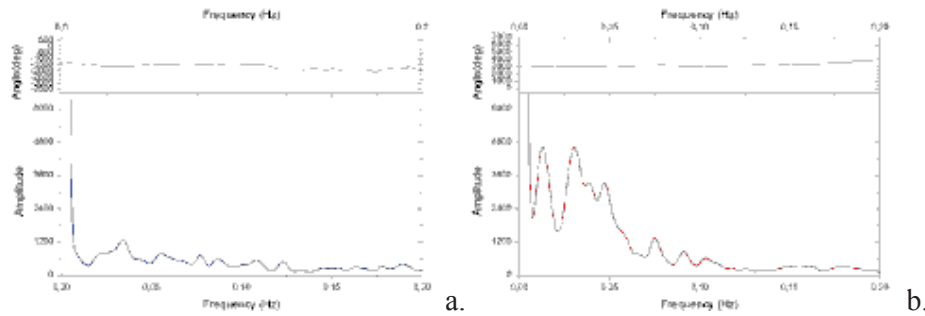


Fig.2.2.4. Fourier spectra of density disturbances in two cases: no discharge (a); and triple pulse (b).

Additional analysis of physical effect of multi-pulse operation mode on gas' characteristics shows that zone of disturbances occupies not less than 70% of gas volume at distance more than 100mm downstream the discharge generation zone (electrodes position). From one side the repetition rate is limited by the effect of strokes conjugation, but, from the other side, must be enough high to disturb as much gas as possible on reasonable distance.

Experimental runs with two-phase flow. Three experimental series were fulfilled to study the discharge interaction with two-component flow:

- Discharge through the jet of second gas, no external flow;
- Discharge in external flow with a central body without the second gas injection;
- Discharge through co-flowing jet of second gas in supersonic airflow.

This work shows that the effect of fast turbulization of the after-discharge channel can be efficient for the improvement of the mixing of the multicomponent flow. Plasma influence on the flow parameters is occurred to be local and it doesn't result in sufficient total pressure loss. It is occurred that for gas parameters studied the shorter spark discharge pulse duration the higher discharge effectiveness in terms of energy release. At the same time instability of the post discharge thermal cavity has lower intensity at the lower gas density in spite of the increasing of the energy release reduced by density. Current channel structure depends on gas type in the main. It was observed experimentally that discharge channel splits in C_2H_4 and CO_2 . It was also demonstrated at the first time that discharge channel is localized along the boundary of two different gases under favorable conditions.

2.3. Short review of the third year efforts.

In the third year of the project a main attention was paid for the experiments in multi-component flow and for analysis of the results based on experimental data and data of analytical/computational efforts. During the 9th quarter of the project performance the work was devoted to study of the filamentary discharge interaction with a secondary gas jet directly injected from the wall into subsonic or supersonic flow. Gaseous fuels were modeled by CO₂ (instead of hydrocarbons) and He (instead of hydrogen). In 10th quarter the theoretical part on the work included an analysis of two distinctive notions: (1) the effectiveness of the pulse filamentary discharge for the fuel ignition under intensive mixing; and (2) the pulse filamentary discharge localization in non-homogeneous gas. Experimental part was directed on study of the filamentary discharge interaction with a fuel jet in high-speed flow. Optical spectroscopy was applied to prove the fact of discharge localization in immediate vicinity of the fuel. In 11th and 12th quarters the analysis of data was being performed based on results of experimental, analytical, and computational efforts. Additionally in 12th quarter the physical model of the discharge instability was successfully verified.

The tool used to conduct the numerical study is CFD++ developed by Metacomp Technologies, Inc. In this work, a turbulent Reynolds Averaged Navier-Stokes capability of CFD++ is applied. The simulations were conducted in three dimensions, with a 2nd order in space, Harten, Lax, van Leer, Contact discontinuity Riemann approximation algorithm. A two equation k- ϵ turbulence model was applied. Time integration scheme was implicit. A P-1 model is used for the radiation heat transfer. Figure 2.3.1 shows main result – strong asymmetry in the gas velocity distribution. The presented results suggest the following mechanism of jet formation. At concave sides of the plasma channel, shock wave propagation results in strong compression followed by strong rarefaction behind the shock. At convex sides, the shock wave is diverging, and thus is characterized by smaller compression followed by weaker rarefaction as compared to the convex sides. As a result, a pressure gradient builds up, with pressure decreasing from convex to the opposite concave sides. This causes jet formation outside of the concave regions, with the general direction of jets from concave to convex.

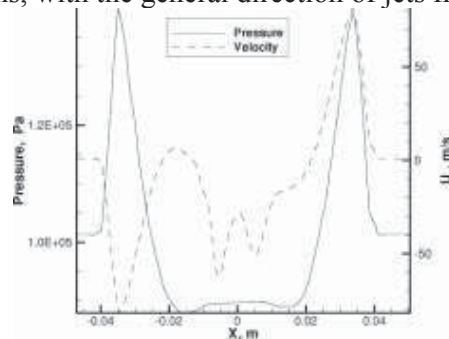


Fig.2.3.1. Gas pressure and temperature for time moment 100 μ s after the pulse.

The next important idea is the discharge's filament localization under nonhomogeneous medium. There was found experimentally that the discharge follows closely a boundary between two gases in the most cases at the air-fuel-plasma interaction. The explanation of this fact includes the idea that the discharge localization is managed by the rule of minimal electrical field, required for the discharge maintenance, along the line of breakdown. It can be supposed that the discharge "prefers" the path in the fuel, oxidizer or between them depending on conditions and the phase of the discharge development. For the short-pulse discharge the physical mechanism appears as the following. The first stage of the spark breakdown is the multiple streamers propagation from the "hot" electrode toward the grounded one. In case of high-power electrical source those streamers occupy a huge volume of the gas, covering all

possible paths for the further development. This statement is illustrated by the well adjusted schlieren photo of the streamers' phase in Fig.2.3.2a, where the spark phase was prevented due to the voltage reducing. The next phase consists of the real selection of the discharge path among the multiple channels with non-zero conductivity. It is the key point – which channel appears to be the best in terms of the current increase, i.e. possessing higher conductivity and lower inductivity. If the media is non-homogeneous the favorite path may not be the shortest one. Sometimes double- and triple-channel structures were observed.

The Fig.2.3.2b shows results of calculations of discharge properties in ethylene-air mixture. Here the coefficient of the ionization rate minus the rate of attachment is presented for variable reduced electrical field. Well seen that the best conditions for discharge development may be realized in reach mixture but not in air or in ethylene. This statement was confirmed by measuring history of E/N and resistance in high-current phase of the discharge at study of the discharge parameters in different gases.

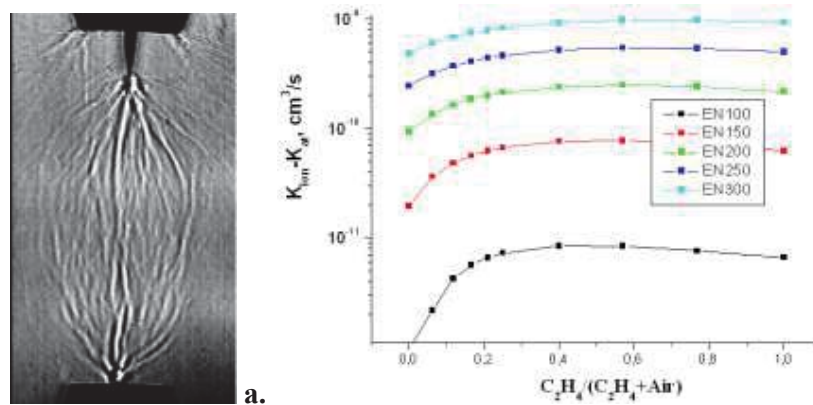


Fig.2.3.2. a – streamer phase of the discharge; b - calculated coefficient of ionization taking into account the electrons attachment in air, ethylene and their mixture.

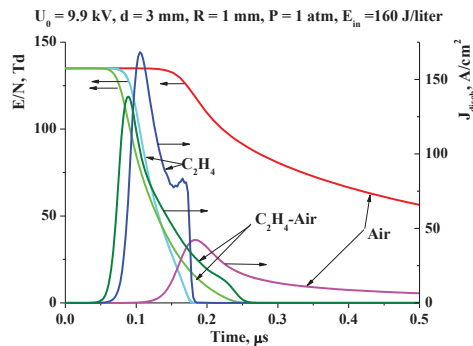


Fig.2.3.3. Dynamics of E/N and current density for the C₂H₄, Air and mixture C₂H₄-Air.

At the same time not all experimentally found phenomena might be explained by that mechanism of the discharge localization. In this part of work a new hypothesis was checked out. The hypothesis supposes that dynamic properties of the gases (fast breakdown) may be not the same as a static behavior. Three variants of the pulse discharge breakdown were calculated: in C₂H₄, in Air, and in C₂H₄-Air (ER = 1) mixture. A simple discharge circuit were used – capacitance (32 pF), inductivity, and the discharge channel self-consistent resistivity. The model of filamentary discharge was utilized: length 3mm, radius 1mm. Initial voltage 9.9 kV, pressure 1 Bar, temperature 300K. Concentration was considered as constant. The model includes kinetics equations, Boltzmann equation, energy equation, and equations of external circuit. Results of calculation of electric field and the current dynamics are presented in

Fig.2.3.3. The fastest current development is considered for the Air-fuel mixture. This fact could be posed as the important to explain the phenomena of selectivity in the discharge channel localization.

The next experimental approach includes the following features: duct-driven airflow $M=0.5$ and $M=2.35$; direct injection of gaseous fuel (C_2H_4); transversal short-pulse electrical discharge along air-fuel boundary. Double pulse discharge excitation scheme was applied in the most runs. Typical fuel mass flow rate $G=1-5g/s$ was provided through sonic nozzle of diameter $d=4mm$. The grounded electrode was combined with the nozzle. The “hot” high-voltage electrode was installed on the opposite wall of the duct in the same cross-section $X=0$ as the grounded one. Typical schlieren image of the discharge interaction with C_2H_4 jet in high-speed flow is shown in Fig.2.3.4.

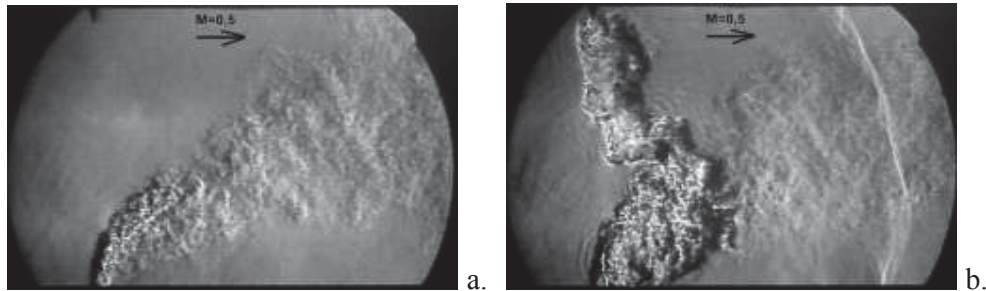


Fig.2.3.4. Schlieren images of the discharge in flow at C_2H_4 jet injection. a, b, – subsonic flow $M=0,5$ without discharge and with discharge, correspondingly.

Spectroscopic observations were performed for better understanding of the dynamics of plasma-jet interaction. Following conclusions/comments may be currently made based on experimental data obtained in this test series:

- Presence of intensive luminosity of CN band at direct fuel injection prove the previously made conclusion that the filamentary discharge strives for the location between two molecular gases, if the experimental arrangement allows it;
- The second pulse breakdown occurs not at the position of the first pulse and not right between electrodes but in some intermediate position – this fact was not emphasized before;
- C_2H_4 ignition by filamentary discharge was detected in this test only in vicinity of the discharge root, probably, due to rather fast cooling of the post-discharge channel. Zone of combustion moves downstream following the main flow.

The physical model of the discharge instability was experimentally verified in the last period of the project fulfillment.

2.4. Short review of the fourth year efforts

In the fourth year of the project performance major efforts were aimed at the study of detail physical mechanism of the specific localization of pulse filamentary discharge in vicinity of boundary between two gases and between liquid spray and gas.

The experiments were performed to study of the discharge properties in vicinity of two-phase composition (liquid spray in air). The experimental portion of the work included three topics: (1) tests on the discharge localization affected by thin laminar jet of He and heated air; (2) demonstration of spectroscopic technique ability to detect a presence of secondary gas in the main media (mixing); and (3) tests to study the discharge interaction with spray jet in high-speed flow. This experimental work was supported by analytical and computational efforts in cooperation with Princeton University.

The actual electrodes configuration to study of the filamentary discharge interaction with a spray medium in vicinity of its boundary is drawn in Fig.2.4.1 below. In this experiments jet was formed by means of long tube connected to externally gated injector. Such configuration allows obtaining uniform cylindrical spray jet.

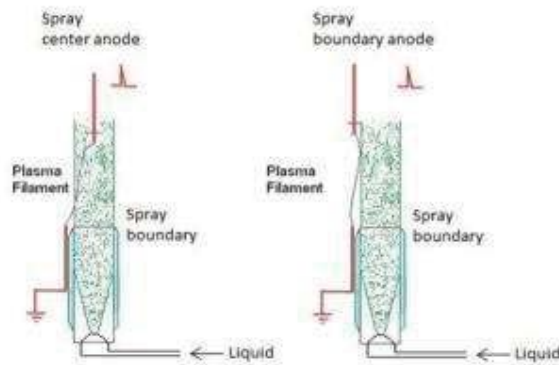


Fig.2.4.1. Variants of electrodes configuration for the first scheme: left – gas-spray, center anode; right – gas-spray, boundary anode.

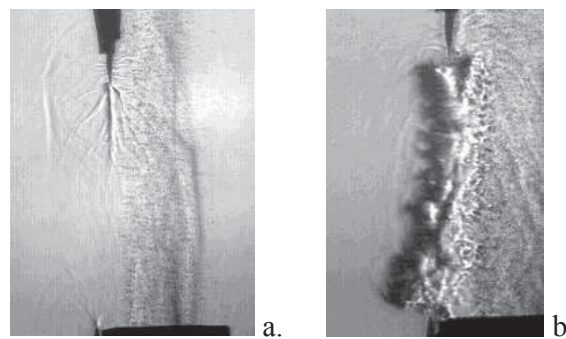


Fig.2.4.2. Schlieren photos of streamers (a) and plasma channel (b) with spray jet.

An influence of spray jet on the process of streamers propagation was observed in runs with intensive spray jet, as it is shown in Fig.2.4.2a. The second stage of development of the discharge is even more responded to the spray jet: as it can be seen in Fig.2.4.2b the discharge tends to propagate along the border of the spray. This effect is rather similar to one in

configuration with gas jet in ambient air. But the plasma filament is not straight as it was in case of gas jet. Contrary it's strongly bended, even more then in air without spray jet.

The next experimental portion of the work included the tests on the discharge localization affected by thin laminar jet of He and heated air. A thin laminar gas jet is blown out from quartz or ceramic pipe in the same plane as the inter-electrode gap with a small angle in respect of axis. Schlieren images and photos were taken in perpendicular directions. In the case of He-jet the effect of specific localization should be appears definitely due to much higher ionization rate in He vs air. In the second case a thermal effect (read: density effects) is revealed. Figure 2.4.3 shows the schlieren image and photo of the high voltage discharge interaction with He laminar jet.

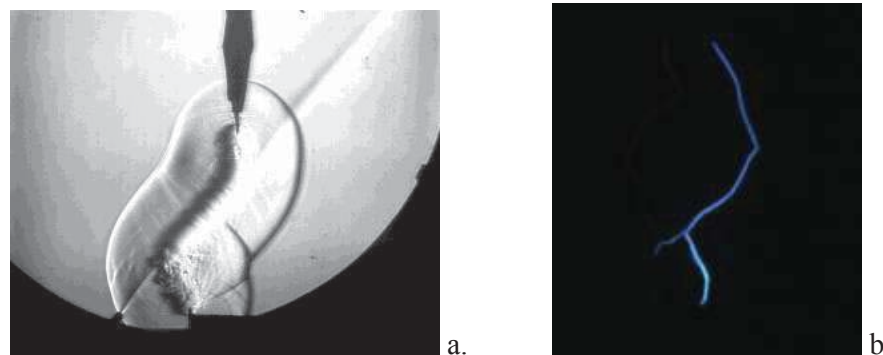


Fig.2.4.3. Schlieren image of HV discharge + He jet (delay 20 μ s) and photo of the discharge.

A new spatial-resolved spectroscopic diagnostic was designed and preliminary applied for qualitative estimations of mixing efficiency.

The theoretical part on the work included an analysis of kinetic and dynamic physical mechanisms of the pulse filamentary discharge localization in non-homogeneous two-component gas. A benefit of two-pulse mode was explored for a fast ignition of combustible gaseous mixture.

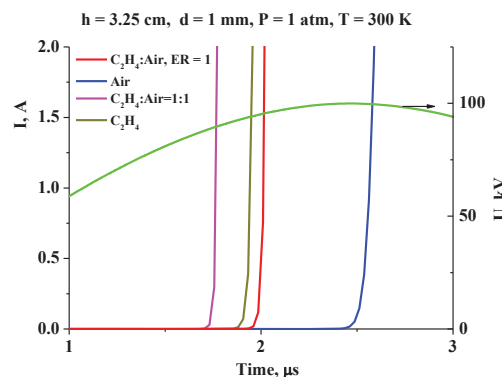


Fig.2.4.4. Electric current evolution in a filament of 1 mm diameter in a discharge with cathode-anode spacing 3.25 cm for various gas compositions.

As it was mentioned above the pulse discharge in co-flowing gas jets has a trend to develop along the boundary between jets composed of two different gases (air, CO_2 , He). This effect may be important in plasma assisted combustion technology as far as correlation between plasma and gas-dynamic movement may enlarge gas mixing rate and make ignition initiation more effective. In order to estimate reality of such effects, the evaluation of plasma properties in fuel/air mixtures of various compositions was performed numerically. The time evolution of plasma in electric field growing in time as $U=U_m \cdot \sin(\pi t/T)$ has been calculated. Calculations

were performed until the discharge current density approaches value about 260 A/cm^2 . In the linear-scale plot (Fig.2.4.4), the discharge breakdown time defined as a moment of current approaching 2 A is ordered for mixtures under consideration as follows: $1.77 \mu\text{s}$ for $\text{C}_2\text{H}_4:\text{air} = 1:1$; $1.95 \mu\text{s}$ for pure C_2H_4 ; $2.02 \mu\text{s}$ for $\text{C}_2\text{H}_4:\text{air} = 6.25:93.75$ (ER=1); $2.59 \mu\text{s}$ for dry air. Thus our model predicts the lowest breakdown voltage (94 kV) for the mixture $\text{C}_2\text{H}_4:\text{air} = 1:1$. Our study for the short (less than $1.3 \mu\text{s}$) times demonstrates that at earlier stage of evolution the discharge current density grows more rapidly in pure ethylene. It means that the plasma filament in a course of development may wander in space searching best local conditions for the breakdown.

Detail dynamics of the gas movement after the discharge shoot was modeled based on 3D Navier-Stokes approach. It was found that shock wave interaction not only determines the direction of disturbances propagation. In some cases it also produces weak fast vortex structure, which is ahead of the main disturbance. This fact was confirmed experimentally. As it shown in Fig.2.4.5, experimental results at an early stage agree well with the simulation data.

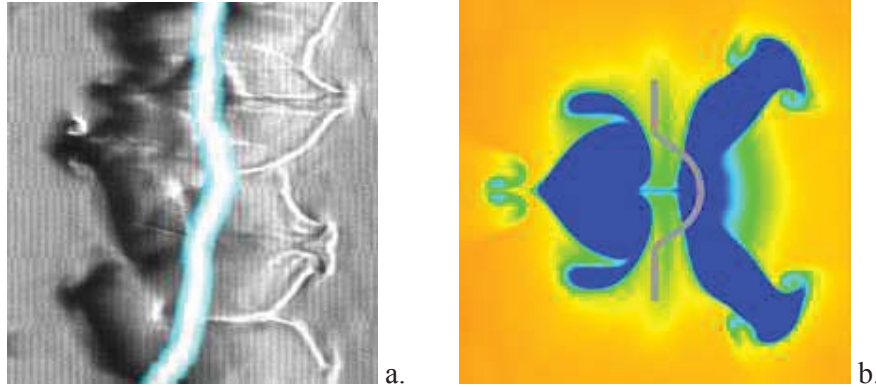


Fig.2.4.5 Fast disturbance structure, $200 \mu\text{s}$. a – schlieren visualization, b – numerical simulation, density.

2.5. Short review of the fifth year efforts

During the fifth year of the project performance two main ideas were considered for better understanding of physical processes in a system consisting of a submicrosecond pulse discharge – non-homogeneous media in order to move this technique toward practical realization:

- Application of newly developed diagnostic for the mixing efficiency measurements. The experimental study was also performed of the mixing enhancement by filamentary discharge in high-speed flow.
- Detailed description of mechanisms of excitation and development of turbulent motion of the gas at interaction with transient plasma.

The calibration and improvement of Probe Breakdown Fluorescence system for quantitative measurements of result of mixing intensification by pulse filamentary discharge were fulfilled at the beginning of the fifth year of the project activity. Due to the previous activity the spectroscopic diagnostic was developed for non-intrusive evaluation of gaseous components presence in small volume after medium disturbance by the unstable discharge. The probe discharge breakdown spectroscopy technique was applied to explore the optical spectra modification at direct fuel injection in two cases: without filamentary discharge generation and after the mixing intensification by the forestream plasma.

The series of the spectroscopic measurements has been fulfilled at variation of the mixing ratio of gases. The result of measurements is a set of spectra that are presented in Fig.2.5.1. Spectrum amplitude and shape for each mixing ratio was stable from run to run that is resulting from the uniformity of the mixture composition and stability of the discharge parameters.

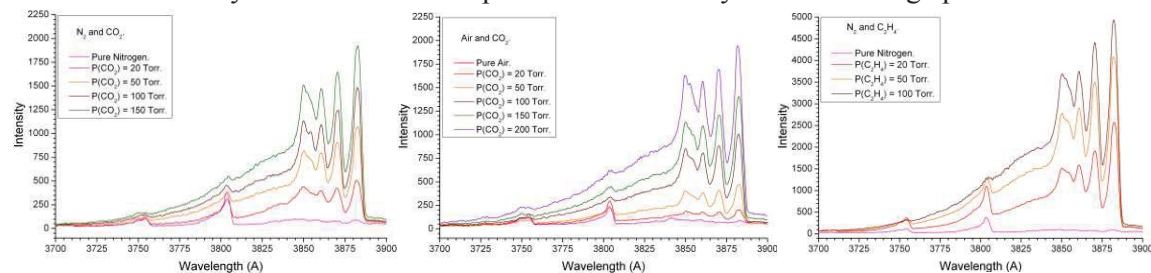


Fig.2.5.1. Spectra at variation of mixing ratio for the N_2/CO_2 , Air/ CO_2 , and N_2/C_2H_4 mixtures.

It was found that there is a notable difference between spectra for different mixtures. It is seen that CN intensity grows much faster with the second gas partial pressure for the ethylene containing mixture than for the CO_2 mixture. As a result the spectrum loses its sensitivity to the ethylene partial pressure for pressures higher than 100 Torr. For CO_2 containing mixtures this limit is 150 Torr. Nitrogen bands intensity is reduced with the growth of the second gas pressure. As a result the method possesses some limitation in terms of second gas partial pressure.

The experiments on mixing evaluation by PBF were performed in high-speed flow. The probe discharge was initiated downstream of the main one. The emission of the discharge was collected from variety of positions along the Y axis. It was observed some unsteadiness of position of boundary between CO_2 jet and main airflow. Fortunately, the width of boundary fluctuation zone was smaller than dimension of the region perturbed by the main discharge. The experimental data for supersonic flow is shown in Fig.2.5.2. It is seen the dramatic

difference between spectrum of probe discharge for CO₂ jet (blue in Fig.2.5.2a) and spectrum of probe discharge for CO₂ jet perturbed by the main discharge. Arising of the strong CN bands and reduction of the N₂ bands mean that there is essential amount of CO₂ within the measurement region in the second case. At the same time CN bands are almost absent with strong N₂ bands are presenting in the spectrum, when CO₂ jet does not perturbed by the main discharge in the first case. According to the calibration curves the mixing ratio may be estimated as 0.45 in this particular case.

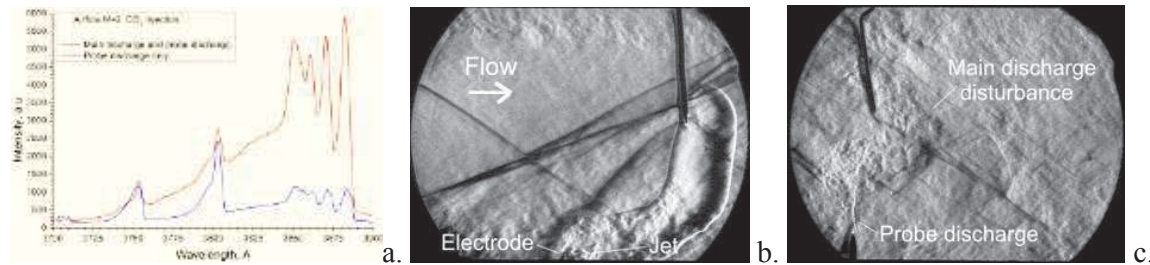
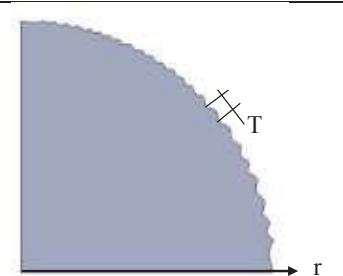
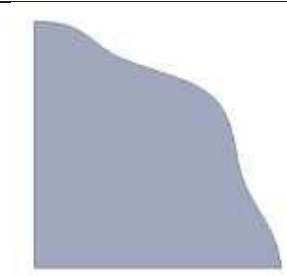
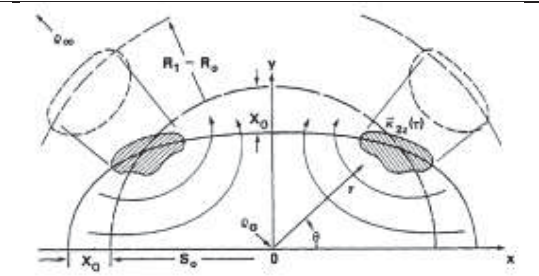


Fig.2.5.2. Spectra (a) and schlieren photos made in supersonic flow. Main discharge is in the 2nd window (b) and probe discharge in the 3rd window of the test section (c).

Extra experiments were carried out for analysis of spectra and intensity of turbulence at electrical discharge interaction with gaseous media. The non-intrusive method of extraction of cross-correlation function from data of schlieren sensors was applied. The dominant frequency of artificial disturbances was measured in a range of 200-400kHz. These data were additionally verified by means of examination of processed schlieren images.

Table 2.5.1. The distortion of the cross section		
		
Small disturbances (HighFreq) ($T \ll r$)	Large disturbances (LowFreq) ($T \sim r$)	Elliptical channel, described in [Boris J.P., Picone J.M. – Vorticity generation by asymmetric energy deposition in a gaseous medium // NRL Memorandum Report 4854, 1982], ($T > r$)

Analysis of the development of after-discharge channel instabilities at distortion of the initial form of the spark discharge cross-section was performed based on analytical prediction, published data and experimental evidence obtained in frames of this project. The most shape's deviations of the discharge channel from the ideal infinitely long cylinder lead to turbulent disturbances generation in gas. Let us consider some variants, see Table 2.5.1.

The vorticity equation describes evolution of the vorticity,

$$\frac{d\xi}{dt} + \xi(\nabla v) = (\xi \nabla) v + \left(\frac{\nabla \rho \times \nabla p}{\rho^2} \right), \text{ where}$$

$$\xi = \nabla \times v \text{ is the vorticity.}$$

It is clearly seen that $\nabla\rho \times \nabla p$ term is a main source of vorticity. In the case of elliptical energy contour the pressure distribution and velocity field become close to cylindrical symmetry while the density distribution remains elliptical. The system obtains a field in which this term is not equal to 0. It was shown by Boris and Picone that elliptical distortion results in 4 large vortices.

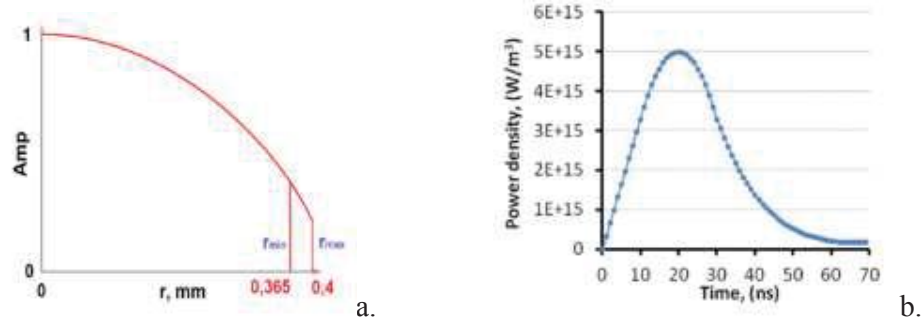


Fig.2.5.3. Power density spatial (a) and temporal (b) profiles.

In the case of low frequency disturbances the same mechanism can be realized. But the size of distortion is smaller than radius of spark channel and it is possible to increase the distortions by Rayleigh-Taylor instability. 2D numerical simulation was provided in FlowVision software for LowFreq case geometry presented in Table 2.5.1. Spark discharge was modulated by volumetric heat source. Maximal radius was 0.4 mm, minimal radius was 0.365 mm, radial profile is presented in Fig.2.5.3a, and time dependence of the power density was the same as in several previous simulations, see Fig.2.5.3b. Some results of this numerical simulation are presented in Fig.2.5.4. As it is seen in Fig.2.5.4a, that vortex-like gas motion formed at $t=100 \mu\text{s}$ and it corresponds to the gasdynamic process described in section above devoted to Rayleigh-Taylor instability. We can conclude that initial vorticity produced by RT instability then develops to significant boundary disturbances, and all evolution depends on initial geometry distortion and power release. Our current problem is that we only can suppose these parameters because there are no experimental information about spark cross section and radial power profile.

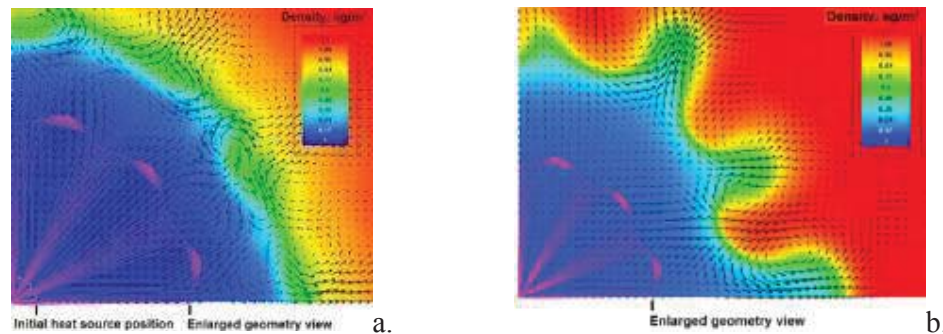


Fig.2.5.4. Simulation results: a – $t=100 \mu\text{s}$, b – $t=2 \text{ ms}$.

Extra simulations were fulfilled to highlight the gasdynamic instability patterns and analysis of spectra and intensity of turbulence at electrical discharge interaction with gaseous media. Discharge breakdown is simulated by volumetric heat source which is placed on xz boundary of calculation domain. The most important information can be attracted from 2D distributions for different time moments. As it shown in Fig.2.5.5 both bends of spark channel

produce vortex-like structures, and boundary of each disturbance moves away from place of initial heat source position. Disturbances propagate in a wide sector, about 80° . The data obtained allow one to conclude that disturbances are spiral vortex structures, which moves and expand in main directions, specified by both bends of heat source curved cylinder.

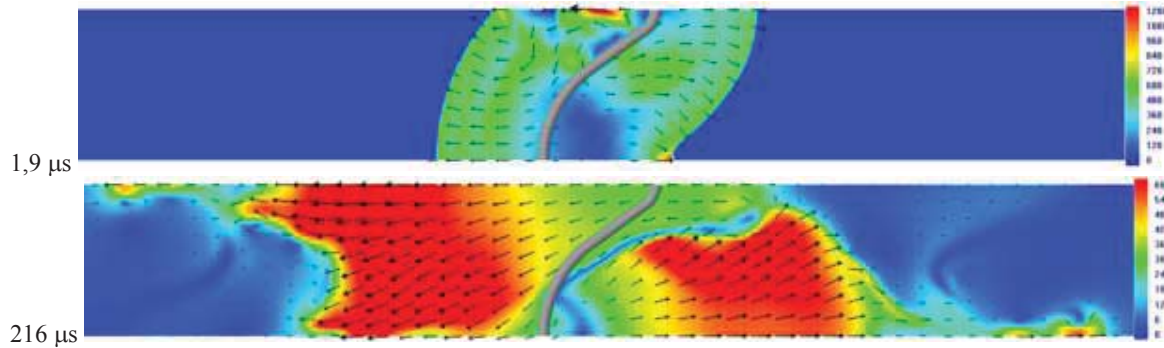


Fig.2.5.5. Velocity field, (m/s).

A physical (experimental) demonstration of effectiveness of the two-pulse scheme for ignition of non-premixed air-fuel composition were performed in high-speed flow with direct fuel injection from the combustion channel's wall. The results obtained in this part of work show that the effect of strong instability can be efficient for improvement of the mixing in multicomponent flows. It was demonstrated also that the discharge channel localizes along the boundary of two media at favorable conditions. At operating within the high speed flow, if the discharge gap is longer than distance to the previously disturbed zone than the next breakdown occurs along the channel of the previous discharge, igniting the previously activated portion of flammable gas. At such mode the generation of sequential pulses at some optimal repetition rate causes the most effective pattern of plasma-assisted mixing and ignition. At the same time, in mode without ignition, plasma influence on the flow parameters is occurred to be local and it doesn't result in sufficient total pressure loss.

3. Background.

3.1. Review based on available literature (prior 2008).

A spark discharge attracts attention of scientific community due to development of prospective plasma technologies. Among these technologies the following ones may be listed: plasma-chemical reactions excitation in the systems of exhaust gases cleaning; ozone generation by the DBD; the powerful fast spark switches; modification of the flow structure by discharge over bodies with different shape in order to reduce gasdynamic drag; powerful discharges application for increasing of the oil extraction from the wells, and so on. Our field of interest includes processes of the spark channels development and their interaction with high speed gas flows. Spark discharges is characterized by the manifold of the existence modes. There is no comprehensive theory that is able to describe all the discharge modes by now.

The realization of the ignition and combustion control in high-speed non-premixed flows is one of the most important issues of air-breathing propulsion. Due to the rather limited time available to complete the combustion process, from the one hand, and the finite rate of chemical reactions and mixing from the other hand an external way to assist to intensify these processes is urgently needed. Plasma production by the electrical gas discharge is considered now as a very promising candidate to play such a role. Well known idea of the “plasma-assisted combustion” comprises several important approaches: plasma-induced ignition due to chemical activation of oxidant and fuel, mixing intensification, flame-holding, combustion of lean mixtures, burnup completeness, etc. However up to now only limited number of works is devoted to the problem of fast mixing inflow and/or ignition of non-premixed compositions by electrical discharge treatment [1-7].

An electrical discharge’s properties strongly depend on the conditions of excitation, flow parameters and characteristics of supplying electromagnetic power. The mechanisms of the plasma of electrical discharges influence on mechanical, physical, and chemical processes in high-speed flow may be considered and listed as follows: (1) fast local heating of the medium; (2) volumetric forces generation due to electrostatic and MHD interaction; (3) turbulence and instabilities promotion; (4) shock waves generation; (5) active radicals, excited molecules, and particles deposition; (6) photo-dissociation and ionization by electron impact.

The modification of flow structure may be done by means of controlled energy deposition. At enough large level of the power release the artificial separation of the flow may be realized. It is a method to increase a local residence time, and the real mechanism of the mixing intensification. Active radicals’ deposition occurs due to molecules’ dissociation and excitation by electron’s impact in electric field and by more complex processes. If the chain chemical reactions are realized, the deposition of active particles may lead to large (synergetic) benefit in reactions’ rate as well as in required amplitude of power deposition. Local shock waves generation promotes the mixing processes in heterogeneous medium and initiates chemical reactions due to heating in shock’s front zone.

Recently several experimental and analytical works were published in frames of plasma-assisted combustion concept. Among of them we can review only a few ones shortly. The paper [8] presents nonequilibrium RF plasma assisted combustion experiments in CO-air, ethylene-air, and methane-air flows using FTIR absorption spectroscopy and visible emission spectroscopy. Results of combustion completeness and emission spectroscopy measurements suggest that O and H atoms, as well as OH radicals are among key species participating in plasma chemical fuel oxidation reactions. Consistent with their previous measurements, the results show the highest fuel oxidation efficiency in lean air-fuel mixtures, as well as significant fuel conversion at the conditions when there is no flame in the test section. In the latter case, fuel species oxidation occurs in plasma chemical reactions, which are not related to

combustion. However, since the net fuel oxidation process is exothermic, heat release during these reactions may result in achieving thermal ignition and flameholding in the plasma. Since CH emission peaks only after thermal ignition is achieved in hydrocarbon-air flows, CH radical is unlikely to be among key species in plasma chemical reactions. This indicates that to obtain further insight into the mechanism of plasma assisted ignition, future research effort should be focused on O and H atom, as well as OH radical concentration measurements, especially in lean air-fuel flows before thermal ignition occurs.

In the paper [9] the numerical simulations of hydrogen-air ignition by nonequilibrium gas discharge in supersonic flow was considered. The model of the discharge parameters simulation in chemically-active mixture was developed for the first time. The results demonstrate that the electrical discharge of glow type is quite prospective candidate for ignition technique. The combustion acceleration effectiveness strongly depends on initial temperature and energy release. At the 700K of static temperature, atmospheric pressure, and power release about 200J/l the induction time occurs 3.4 times shorter than at the thermal initiation. That calculation was done for the conditions of real experiment, described in [10].

Numerous publications were offered by NEQ-Lab MIPT group [11, 12, for example], where a deep analysis of plasma-chemical kinetics under the plasma-assisted combustion was announced. As it was considered, nonequilibrium plasma of nanosecond pulse discharge can affect a flame blow-off velocity significantly due to active radicals' deposition. It occurs with energy input negligible in comparison with burner's chemical power.

The group of "Applied Plasma Technology" announced some devices for fuel ignition and flame stabilization [13]. Positive results of performed investigations indicated significant advantages of selected non-equilibrium plasma generator in comparison with the thermal plasma sources.

The successful efforts are being performed for plasma-assisted combustion in WPRL with colleagues. One of the last publications [14] is devoted to development of plasma igniter for use in high-speed and high-altitude air vehicle. Such an igniter produces a rich pool of radicals that would drive pre-ignition chemistry leading to ignition. The ignition concept demands non-equilibrium plasma characterized by a high degree of feed-gas dissociation and little direct heating of the gas.

A serious experimental work is being carried out by joint Russian team of MSU, CIAM and IGP [15]. The efforts are arrowed on a comparative test of different plasma sources by the criteria of ignition efficiency in high-speed flow.

Several groups of investigators demonstrate a successful ignition of premixed air-fuel composition and flame acceleration by non-equilibrium corona or barrier discharges; see for example [16-17]. As a rule in those works the conditions are rather far from practical schemes of high-speed combustion. Unfortunately, specific information available now is not quite sufficient for consideration of critically specific mechanisms and, consequently, for proper choice of the discharge type.

Character of the discharge development stages that are previous to the spark initiation depends on many factors: gas pressure, electrodes shape, length of the discharge gap and so on. For example, at conditions of small discharge gap and smooth electrodes (uniform electric field) the discharge is caused by sequence of electron avalanches [18], which transform to the spark mode when self-maintaining condition is met. Avalanche mechanism of the breakdown development has been studied well enough in classical experiments with Wilson chamber. Well known Townsend condition of the self-maintaining discharge:

$$\gamma[\exp(\alpha d) - 1] = 1,$$

where α – first Townsend coefficient of ionization, γ – second Townsend coefficient, allows to obtain explicit expression for breakdown voltage and electric field strength:

$$U = \frac{B(pd)}{C + \ln(pd)}; \quad \frac{E}{p} = \frac{B}{C + \ln(pd)}; \quad C = \frac{A}{\ln\left(\frac{1}{\gamma} + 1\right)}.$$

Constants A and B are determined by semiempirical Townsend relationship:

$$\alpha = Ap \exp\left(-\frac{Bp}{E}\right).$$

These relationships describe the shape of the dependence $U(pd)$ – Paschen curves, if the constants A and B are correct.

The streamer mechanism of the breakdown is observed in case of highly nonuniform field, which is generated by electrodes, radius of which is much smaller than the discharge gap. Streamer mechanism is realized also at the conditions of uniform field and overvoltage within the discharge gap. Spark arising is caused due to ionization of atoms and molecules by the electron impact. Ionization rate depends strongly on the electric field magnitude and on the processes of the free electrons loss. The magnitude of the critical field for the air at the atmospheric pressure is 30 kV/cm ($E/p = 40$ V/cm·Torr). When discharge is generated in the highly nonuniform field, the ionization processes take place at the points of the field where electric field amplitude is lower (sometimes much lower) than critical one. This fact indicates that discharge, which is propagating to the area of the electric field with low intensity, generates field for itself with intensity that is enough for ionization. Naturally, the start of the process is determined by the development of the electron avalanche that is transformed to the streamer form. Approximate estimate of the avalanche-streamer transition condition has been done on the base of the experimental results in the Wilson chamber firstly [18]:

$$\alpha x_{kp} \cong 20,$$

where x_{kp} – distance from the cathode to the point of the streamer initiation.

Modern diagnostics techniques allow to resolve the process of the streamer generation. For example, the instantaneous images of the streamer have been obtained by means of the shutter camera in the discharge gap 13 cm long. The dynamics of the spark development has been studied by means of the streak-camera [21]. The time resolution of the camera was 10 ns. The instantaneous images at the exposure time 10 ns and time step 40 ns look like groups of the glowing points that start from the sharp part of the one of the plain electrodes and move to the opposite electrode at conditions of gap voltage 100 kV and atmospheric pressure. After the streamers' are having gained the opposite electrode a plasma channel starts to propagate from the electrode sharp part, with the structure being time- and space-continuous.

Instantaneous images were changed rapidly depending on mixture composition (percentage of oxygen). Localization of the gliding objects occurred concurrently with reducing of their quantity when the oxygen concentration increases from 1% up to 15%. Streamer propagation velocities obtained in experiments depended on applied voltage as well as on gas composition. These velocities varied from $5 \cdot 10^7$ cm/s to $3,5 \cdot 10^8$ cm/s. Authors give the estimation of the charge of the streamer head on the base of the photos, synchronized oscillograms of the current and relationship for the current – $I = qv$. If the propagation velocity of the streamer is 10^8 cm/s and the current of a single streamer is 1A, which is evident from the photos and oscillograms, than space charge per one streamer head is 10^{-8} Cl or $6 \cdot 10^{10}$ of electron charges.

The leaner dimension of the positive charge concentration is estimated as $\Delta x = 14$ um that is followed from the photos, which give geometrical parameters of the streamers, and from the assumption that the positive ions density within the head is $6 \cdot 10^{13}$ cm⁻³. These data allow to determine the order of magnitude of the electric field intensity in front of the streamer head.

$$E = \frac{U_0}{4\pi\epsilon_0 r^2} \approx \frac{10^{-8}}{4\pi \cdot 8.85 \cdot 10^{-12} (0.46 \cdot 10^{-2})^2} = 42.5 \text{ kV/cm}$$

or $E/P = 55,9 \text{ V/cm}\cdot\text{Torr}$, that agrees the conditions of the ionization processes.

The avalanche-streamer mechanism of the ionization wave propagation precedes the initiation of the spark breakdown. Nevertheless, crossing of the discharge gap by the streamer that causes to the generation of the plume of the weakly ionized plasma, which crosses the discharge gap, does not cause to the initiation of the spark breakdown itself. Such a breakdown is characterized by the low resistance of the channel, high current density and temperature [20]. Direct transition of the streamer to the spark is possible only for very short discharge gap (shorter than 1 cm). Multifold reduction of the streamer channel resistance is needed for such a transition at conditions of the longer discharge gaps. Therefore, fast and intensive heating of the channel up to temperature of 5000-6000K have to occur in order to ionization has achieved the same character as one for the arc channel, when dropping voltage-current characteristic is realized ($dU/d\tau < 0$).

Streamer mechanism of the breakdown may be observed for the noble gases because there is no electron attachment and no energy loss on the molecular vibrations. Streamer mechanism of the breakdown is complicated for the molecular electropositive gases (for example for nitrogen) due to the high energy loss on the excitation of the molecular vibrations. VT relaxation time is longer by the orders of magnitude than life time of the streamer plasma at the low temperature. The worst conditions for the streamer breakdown are realized in the molecular electronegative gases, for example in the air. Besides the energy loss on the molecular vibrations excitation, electrons die due to the attachment with characteristic time of the process being equal to the $10^{-8} - 10^{-7}$ s. So, in order to realize the streamer mechanism of breakdown it is need to obtain maximal streamer propagation velocity $\sim 10^9$ cm/s, which is possible at applying pulses with very steep edge and at high overvoltage of the discharge gap.

In real case the heating of the channel and its transition to the spark is realized due to the joining of the many streamer channels into the union current within the relatively thin “tree-like” channel with “branches” – separate streamers. Electron charge has gone to the anode quickly due to the high conductivity of the heated channel and tree begins to grow. Such a process is repeated many times and effect of the plasma channel is realized due to the feeding by the cathode streamers’ currents in front of the hot channel head. Short streamers that are directed to the opposite electrode during the process of the “tree” development save its conductivity and continue to feed the growing channel with the current. Long streamers and streamers that are directed across the tree movement lose its conductivity quickly but save its charge, so, the tree is surrounded with charge layer during the development. It causes to the increasing of the plasma formation capacity. Such a two-stage process, in which “tree” growth has its own velocity that is on the order of magnitude smaller than streamer velocity, was named as leader. If the power of the power source is high enough leader process is finished by the spark channel, which is the narrow bright discharge with the low impedance and high current density.

Formation of the spark channel is accompanied with the shock waves generation and intensive light emission. Electron emission from the cathode accompanied with the cathode spot have to be realized in order to generate the spark discharge with low impedance [22]. The experiments on the study of the spark channel expansion were fulfilled in the forties of the last century [23]. Dynamic images of the emission of the visible spark diameter depending on time have been obtained by means of the high speed photo cameras with the rotating mirrors and slit projection. It results from the research of the authors [24] that there is fast expansion of the channel at the start of the current through the spark channel, with the velocity being equal to the thermal velocity of the gas atoms. The channel expands much slower during the late stage.

If the initial velocity of the spark channel expansion is equal to the velocity of the shock wave propagation, than expansion velocity has to meet the Tailor law [25] that describes expansion of the semispherical shell at the explosion of the nuclear bomb. Dependence of radius on time from the Tailor equation is the following $r^2 \sim t$ for the case of cylindrical wave. Dependence of the $(\lg t)$ on $(2 \lg r)$ has been obtained by authors [26]. This dependence is the linear one.

Current density in the spark channel changes during the expansion process. Current density was 30 kA/cm^2 and intensity gradient of the electric field in the spark was $\sim 30 \text{ V/cm}$ at the start of the process ($t=0,5 \text{ us}$, discharge of the capacitor facility at the vibrational mode, nitrogen, 1 atm). At the 8 us discharge current reduced down to $\sim 2-3 \text{ kA/cm}^2$ and gradient to $\sim 30 \text{ V/cm}$. Length of the spark was $10-35 \text{ cm}$. It should be noted that discharge parameters depends mainly on capacitors batteries and velocities of the currents' changes can be determined by the value of the power source inductance. Characteristics time of the current change was 20 ns in [27].

If it is possible to neglect the effects caused by the electrodes in comparison with the processes of the charge transfer to the region of the spark volume than the following relationship can be written:

$$I = \pi R^2 n_e k_e E e,$$

where R – spark radius, n_e – electrons concentration, k_e – electron mobility. Energy balance equation for the spark channel can be presented as following [22]:

$$IE = S + W + \frac{dU}{dt},$$

where W – energy loss per time due to the thermal conductivity; S – energy loss on the emission, U – internal energy of the spark channel. There can be a relation between the electrical conductivity

$$\sigma = \frac{I}{E} = \pi R^2 n_e k_e e$$

and internal energy [27] if the following assumption is true: electron gas have no time to change kinetic energy of the ions, atoms and molecules, no time to change excitation degree of the vibrational and rotational levels during the time period under consideration. Listed assumptions are true for the short discharges at the high electric field. At the same time an internal energy can be presented as:

$$U = \pi R^2 n_e \left(\frac{3}{2} kT + eV_i \right),$$

where the first term is a kinetic energy of the electrons, the second one is the energy loss on the ionization. If dependence of internal energy and electrical conductivity on the temperature is negligible than electrical conductivity may be estimated as following:

$$\sigma = aU, \quad a = \frac{k_e e}{\frac{3}{2} kT + eV_i}.$$

If there is a thermal equilibrium within the spark channel than values σ and a can be expressed in terms of temperature. The following equation that connects electrical conductivity with parameters of the external circuit can be obtained for the very short discharge at neglecting of the emission and thermal conductivity losses:

$$IE = \frac{I^2}{\sigma} = \frac{dU}{dt}, \quad I^2 = \frac{\sigma}{a} \frac{d\sigma}{dt} = \frac{1}{2a} \frac{d\sigma^2}{dt}, \quad \text{or } \sigma^2 = 2a \int I^2 dt.$$

Temperature of the spark channel can be estimated by means of the Saha equation. Electron concentration can be estimated by means of Stark broadening of the line. Typical ionization degree for the discharge in the air is $\sim 1\%$ or $N_e = 2,7 \cdot 10^{17} \text{ sm}^{-3}$.

Recovery time of the breakdown strength of the gap is important for the pulse-repetitive discharges. Limit frequencies of the spark discharge at the pulse-repetitive mode are determined by the velocity of the breakdown strength recovery. An empirical relationship for the recovery voltage has been obtained in early experiments [22] for the spark current of 5 kA in the air at atmospheric pressure and discharge duration of 10-15 us:

$$V = V(1 - e^{-at}),$$

where $a = 1515$ for the single discharge gap, t – is measured in seconds, V – constant breakdown voltage. Recovery time of the gap breakdown strength for the air at atmospheric pressure is 1-1.5 ms.

It is possible to achieve much higher velocities of the breakdown strength recovery by means of the blowing the discharge gap. Frequency of the discharge generation achieves 1 kHz and higher if the flow velocity is ~ 100 m/s [28].

The modern state of the researches in the field of spark discharge is reflected in the number of publications. Calculation results of the streamer propagation velocity are presented in [29]. Calculations have been done in frames of simple model of the background electrons reproduction and in frames of the detailed diffusing-drift model. Experimental results of the short gap ($d \sim 5$ mm) breakdown are presented in [30]. It has been found out that spark channel is a combination of the number of micro-channels (up to 1000) with diameter of 5-10 micrometers and current density about 10^7 A/sm². This phenomenon is explained by the instability generation at the front of the ionization wave. Spatial structure and propagation process of the positive streamer has been studied experimentally by means of CCD camera in the edge-plane gap of 40-80 mm at the peak voltage of 60 kV. It is noted that the streamer diameter is within the limits of 0,02–2,5 mm. Propagation velocity is 0,07–15 mm/ns. There were two types of power source, namely: capacitor with the external resistance of 1 kOhm, or transmitting line with wave resistance of 200 Ohm.

Properties of the high-current discharge (60 kA) 1,6 ms long are studied in [32] at atmospheric pressure in the gap 10 cm long. High velocity of the residual spark channel cooling has been found out. Such a phenomenon is due to hydrodynamic turbulent process that is caused by the Rayleigh-Taylor-like instability.

New theoretical model has been proposed and applied in [33]. This model allows to calculate for the given non periodic pulse the process of the spark discharge generation, sequential cooling of the postdischarge channel and recovery of the breakdown strength taking into account generation and dissipation of the gas turbulent movement.

It is known that a turbulent gas flow forms in a cooling down after-spark channel. This causes a more efficient heat transfer than what is possible due to the molecular mechanism. Therefore, the speed with which the channel cools down and expands increases drastically. (As a result the channel's cooling and expansion rates speed up significantly) This kind of a cooling regime may be realized, for instance, after the interruption of powerful spark discharges [34-37], pulse arcs and laser sparks [37,38]. It is possible (It may be supposed) that the dynamics of the channel decay of natural lightning as well as that in a long artificial spark, which models it, is also defined by the formation of a turbulent flow in the after-discharge channel [39]. The dependence of the gas cooling process characteristics on a relatively small residual current in the channel has been demonstrated for the first time in (paper) reference [40]. As it has been shown theoretically each current pulse has its corresponding critical value of the residual current stabilizing the cooling channel under the quasi-stationary arc condition (featuring relatively high temperature and conductivity of the channel). Later a one-dimensional model was used to study the dynamics (behavior) of the hydrodynamic parameters of the lightning channel in the return stroke and after the pulse current is damped [41]. The effect of the continuous residual electric current during pauses between the successive strokes on the plasma

cooling in the channel was analyzed as well. It was shown that a continuous electric current, that is several orders of magnitude lower than the maximal current in the return stroke, is capable of maintaining the channel conductivity. This effect cannot be explained merely by Joule heating but it is largely governed by the fact that the turbulent heat transport is suppressed substantially. In this case, even a continuous current as low as $I_{res}=50-100A$ is capable of maintaining the conductivity of a lightning channel at a such level that only M-components can develop in the channel rather than the dart leader of the subsequent stroke [41].

Preliminary promising analytical and experimental works done recently show that a spark discharges can provide a significant enhancement for mixing, ignition, and flameholding in high-speed combustor, because of fast turbulent expansion of the igniting afterspark media [42,43].

It is of great interest to investigate the relationship between the inner and external parameters of the channel prior to the formation of a fully developed turbulent flow as well as the origin of turbulence and its dynamics. As was shown in references [40,41,44], the theory predicted the effect of turbulent decay stabilization at small residual current presence for post-pulse heating of the central part of the after-spark channel.

References to section 3.1.

1. *L. Jacobsen, C. Carter, R. Baurie, T. Jackson* "Plasma-Assisted Ignition in Scramjet", AIAA-2003-0871, 41st AIAA Aerospace Meeting and Exhibit, 6-9 January, Reno, NV, 2003.
2. *Morris R.A., Arnold S.T., Viggano A.A., Maurice L.Q., Carter C., Sutton E.A.* "Investigation of the Effects of Ionization on Hydrocarbon-Air Combustion Chemistry". 2nd Weakly Ionized Gases Workshop, Norfolk, 1998.
3. *S.O. Macheret, M.N. Shneider, and R.B. Miles*, "Energy Efficiency of Plasma-Assisted Combustion in Ram/Scramjet Engines", AIAA 2005-5371
4. *Sergey B. Leonov, and Dmitry A. Yarantsev* "Plasma-induced ignition and plasma-assisted combustion in high-speed flow" // *IOP*, Plasma Sources Science and Technology, **16** (2007), p.132-138, stacks.iop.org/PSST/16/132.
5. *S. Leonov, V. Bityurin* "Hypersonic/Supersonic Flow Control by Electro-Discharge Plasma Application.", AIAA-2002-5209.
6. *Bocharov A., Bityurin V., Klement'eva I., Leonov S.* Experimental and Theoretical Study of MHD Assisted Mixing and Ignition in Co- Flow Streams // Paper AIAA 2002- 2228,
7. *Buriko Yu., Vinogradov, V., Goltsev, V.*, "Influence of active radical concentration on self-ignition delay of hydrocarbon fuel/air mixture". "Applied physics", 2000, P.10.
8. *Ainan Bao, Guofeng Lou, Munetake Nishihara, Igor V. Adamovich* "On the Mechanism of Ignition of Premixed CO-Air and Hydrocarbon-Air Flows by Nonequilibrium RF Plasma", AIAA-2005-1197.
9. *A. Napartovich, I. Kochetov, S. Leonov* "Calculations of dynamics of hydrogen-air ignition by nonequilibrium discharge in high-speed flow", J. Thermophysics of High Temperature (rus), 2005, #2.
10. *O. Voloschenko, S. Leonov, A. Nikolaev, N. Rogalsky, V. Sermanov, S. Zosimov*, "Experimental study of hydrogen combustion in model supersonic duct", International Scientific Conference "High-Speed Flow: Fundamental Problems", Zhukovskiy, 21-24 September 2004.
11. *A. Starikovskii* "Plasma Supported Combustion", invited lecture for 30th International Symposium on Combustion, Proceedings of the Combustion Institute, Chicago, 2004. Invited Lecture. P 326 .
12. *S. Starikovskaia, I. Kosarev, A. Krasnochub, E. Mintousov, A. Starikovskii* "Control of Combustion and Ignition of Hydrocarbon-Containing Mixtures by Nanosecond Pulsed Discharges", AIAA-2005-1195.
13. *I. Matveev, S. Matveeva, A. Gutsol, A. Fridman* "Non-Equilibrium Plasma Igniters and Pilots for Aerospace Application", AIAA-2005-1191.

14. *M. Brown, R. Forlines, B. Ganguly, C. Campbell, F. Egolfopoulos*, "Pulsed DC Discharge Dynamics and Radical Driven Chemistry of Ignition", AIAA-2005-0602.
15. *V. Vinogradov, I Timofeev* "Initial Study of Different Plasma Discharges in a M=2 Air Flow", AIAA-2005-0988, 43rd AIAA Aerospace Meeting and Exhibit, 10-13 January, Reno, NV, 2005.
16. *J. Liu, F. Wang, L. Lee, N. Theiss, P. Ronney, M. Gundersen*, "Effect of Discharge Energy and Cavity Geometry on Flame Ignition by Transient Plasma", AIAA-2004-1011.
17. *P. Magre, V. Sabel'nikov, D. Teixeira, A. Vincent-Randonnier* (ONERA) "Effect of a Dielectric Barrier Discharge on the Stabilization of a Methane-Air Diffusion Flame", ISABE-2005-1147.
18. *Reter G.* Electron avalanches and breakdown in gases. Moscow: Mir, 1968, 390pp.
19. *Rayzer Yu. P.* Physics of gas discharge. Moscow: Science. 1992.
20. *Baselian E.M., Rayzer Yu. P.* Spark discharge. Moscow: MIPT, 1997.
21. *Won J.Yi., Williams P.F.* Experimental study of streamers in pure N₂ and N₂/O₂ mixtures and a \approx 13 cm gap. J. of Phys. D: Appl. Phys. V. 35 (2002) P. 205-218.
22. *Mick J., Kregs J.* Electrical discharge in gases. Moscow: Foreign literature, 1960.
23. *Flowers J.W.* Phys. Rev. V. 64 (1943) P. 225.
24. *Norider H., Rarsten O.* Ark.Mat.Astr.Fys., A36, Pt.4 (1949).
25. *Naylor G.I.* Proc.Poy, Soc. A201, 159, 175 (1950).
26. *Higham J.B., Meek J.M.* Proc. Phys Soc. B63, 649, 1950.
27. *Davies D.R.* Proc. Phys.Soc. 61, 105, 1948.
28. *Isaenkov Yu.I., Bublik N.P., Makeev P.G.* Triggered spark gap switches and their erosion characteristics. Int. Power Modulators Conf., Hollywood, USA, 2002, P. 487.
29. *Yakovenko S.I.* The mechanism of streamer propagation. JTP (rus), 2004, V. 74, # 9, p.47-53.
30. *Perminov A.V., Trenkin A.A.* Microstructure of current channels of nanosecond discharge. Journal of Technical Physics (rus), 2005, v.75, #9, p.52-55.
31. *Briels T.M.P., Kos J., vanVeldhuizen E.M., Ebert U.* Circuit dependence of the diameter of pulsed positive streamers in air. J. Phys. D: Appl. Phys. (2006) V. 39, P. 5201-5210.
32. *Azizov E.A., Kravchenko S.A., Solodovnikov S.G.* The properties of high current high pressure discharges. Plasma Physics Reports, (2005), V. 31, No. 7, P. 616
33. *Shneider M. N.* Turbulent cooling of the gas after spark discharge. Journal of Technical Physics (rus), 1998, v. 68, #2, p.30-35.
34. *E.P.Bel'kov*, Sov. Phys.Techn. Phys. 16, 1321 (1972)
35. *E.P.Bel'kov*, Sov. Phys.Techn. Phys. 19, 1210 (1974)
36. *J.M Kulman, G.M. Molen*, AIAA J. 24, 1112 (1986)
37. *J.P. Greig, R.E. Pechacek, M. Releigh*, Phys.Fluids 28, .2357 (1985)
38. *S.N.Kabanov, L.I.Maslova, T.I.Tarkhova, V.A.Trukhin, V.T.Yurov*, Sov. Phys.Techn. Phys. 35, 655 (1990)
39. *J.M. Picone, J.P.Boris, J.R. Greig., M.Releigh, R.F. Fernsler*, J.AtM.Sci. 38, 2056 (1981)
40. *M. N. Shneider*, The effect of residual current on turbulent cooling of after-spark channels, AIAA 2000-0721, Reno, Nevada, 2000; Available from the AIAA: www.aiaa.org, Washington, DC
41. *N. L. Aleksandrov, E. M. Bazelyan, M. N. Shneider*, Plasma Physics Reports 26, 893 (2000)
42. *S. B. Leonov, Y. I. Isaenkov, M.N. Shneider*, Effect of the Post - Pulse Discharge Channel's Fast Turbulent Expansion on the Gas Flow, AIAA-2007-1352, Reno 2007
43. *Yu. I. Isaenkov, S. B. Leonov, M. N. Shneider*, Mixing Intensification by Electrical Discharge in High-Speed Flow, Proceeding of the Fifth International Conference on Fluid Mechanics, Aug.15-19, 2007, Shanghai, China
44. *M.N.Shneider*, Physics of Plasmas, **13**, 073501-11, (2006)

3.2. Discharges for mixing and ignition assistance

Typical conditions for discharge maintenance in aerospace science: pressure $P=0.1-1\text{Bar}$, velocity of the flow $V=100-1000\text{ m/s}$. Characteristic temperature of gas varies from $T=200\text{K}$ (ambient conditions) to $T\leq 2\text{ kK}$ for combustion chamber. As a rule, at such conditions the plasma of electric discharges appears in filamentary form due to instabilities mostly associated with the mechanism of electrical field enhancement in a vicinity of heated plasma channel. At present, there are no reliable universal rules for appearance of any electric discharges at high temperature. Under high pressure and high-speed flow the most types of discharges are nonuniform and nonequilibrium. The high-pressure glow discharge is rather homogeneous one; and high-current longitudinal arc produces the equilibrium plasma. A strong non-uniformity of the plasma inflow renders a chance for significant decrease of required electrical power for predefined effect. This idea is in local multi-points influence with sequential expansion of flame fronts.

Some data for different types of discharges and their merits/drawbacks in plasma assistance for combustion are shown in table below. Here a large domain of non-selfsustained and combined type of electric discharges is not included. These data are averaged and should be considered as quite evaluative.

Discharge type	Typ. power	“+”	“-”
Longitudinal arc	1-100 kW continuous	High temperature	Location in boundary layer, electrodes erosion, low efficiency.
Transverse DC	1-100 kW	Mixing, high temperature	Electrodes erosion, low efficiency, low volume of treatment.
Arc in separation zone	1-100 kW	Mixing, high temperature, auto-adjustment	Location in separation zone.
HF filamentary	1-10 kW	High speed of penetration, mixing, single-electrode.	Low input power, unpredictable position.
HF and MW torch	1-10 kW	Single-electrode or electrodeless	Very sensitive to flow
MW filamentary	0.1-10J/pulse	Electrodeless, high efficiency in radicals generation.	Complex equipment, large breakdown threshold at high pressure.
Laser spark	Wide range	High density of energy deposition.	Small volume of interaction, low efficiency of lasers.
High-pressure glow	1-100 kW, continuous	Large volume, effective in radicals generation.	High level of required power, multi-electrode system is required.
Nanosecond pulse discharge	0.01-1 J/pulse	Effective in radicals generation, high-speed of penetration.	Low-pressure application for homogeneous appearance.
Short-pulse transverse spark	1-100 J/pulse	High density of energy deposition, effective mixing.	Multi-electrode system is required.
Barrier/Corona	1 W/cm ²	Effective in radicals generation.	Location in near-surface layer, low density of energy deposition.

The complete management of the combustion process under any conditions requires a large level of additional energy deposition (in a range of the flow enthalpy) that is out of practical interest. The idea is not related to strong effect of energy release but to gentle control of mixing processes, flow structure, and chemical reactions rate. The second direction is to give the gear to force combustor to work under off-design conditions. It may be a temporal mode, when the level of required electric energy is not vitally important. Unfortunately, specific information available now is not quite sufficient for proper choice of the discharge type. Our understanding is that there is no versatile solution to a design and method of application of plasma for combustion. Each specific situation has to be considered separately. But it seems clear that the nonequilibrium, unsteady, and nonuniform operation modes are preferable. Current understanding also is that plasma has to be generated “in situ” just in the location of fuel-oxidizer interaction but not by external device. The **pulse filamentary discharge** satisfies with the most of those requirements.

We might consider several mechanisms of the short-pulse high-voltage discharge effect on the parameters of gas and flow structure, if it was excited in dense, high-speed flow of air with a fuel. Among of them are the following ones:

- ◇ Local Superheating of gas;
- ◇ Discharge-Induced Shock Wave increases temperature and pressure locally and intensify a mixing;
- ◇ Photo-dissociation and photo-ionization of air and fuel yields in chemically active radicals production;

This section analyzes the magnitude of the effects.

Shock wave effect. The gasdynamic effect of instantaneous heat deposition by filamentary plasma has been simulated numerically. In this stage of the problem’s study the calculations have been limited by cylindrical symmetry, rectangular profile of the energy deposition and neglect of the plasma radiation (it was took into account by means of energy loses). Cylindrical channel with radius $r=r_0$ (range $r_0=0.25\text{-}2\text{mm}$) was supplied by instantaneous energy release with amplitude $W=0.2\text{-}0.5\text{J/cm}$ in suggestion of constant gas density. The scheme is shown in Fig.3.2.1.

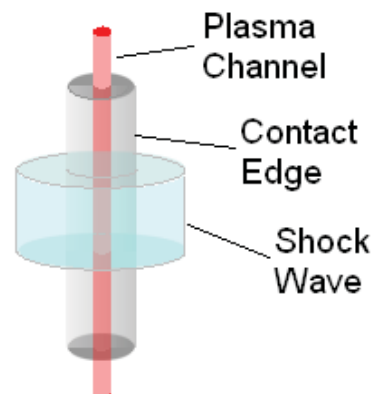


Fig.3.2.1. Scheme of plasma channel arrangement for CFD.

The model of inviscid perfect gas was put on the basis of the numerical simulation (Euler's equations). Godunov's explicit non-stationary scheme of the second order of accuracy was used for the solution of gas dynamic equations. The results of simulation have been verified by Sedov's formulae at small radial distances (large amplitude of the shock wave). The simulations were executed for ambient conditions ($T_0=300\text{K}$ and $P_0=1\text{Bar}$) and "hot" air ($T_0=800\text{K}$ and $P_0=1\text{Bar}$). The graphs below show main results.

The pressure and temperature redistribution due to shock wave propagation are presented in Fig.3.2.2 and 3.2.3 for ambient conditions and temperature redistribution in Fig.3.2.4 for initial temperature $T_0=800\text{K}$. The energy deposition was $W=1.3\text{J}$ to the cylinder with radius $r_0=0.25\text{mm}$ in both cases.

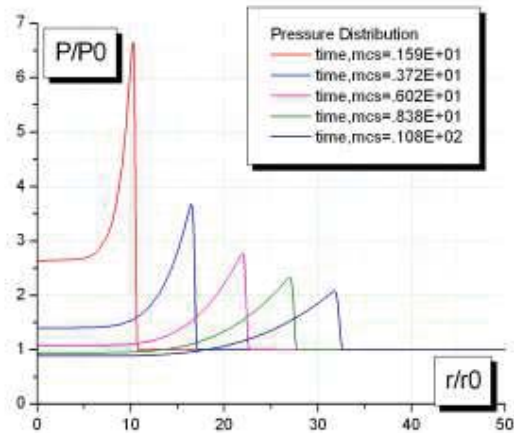


Fig.3.2.2. Pressure profiles at SW propagation. $T_0=300\text{K}$.

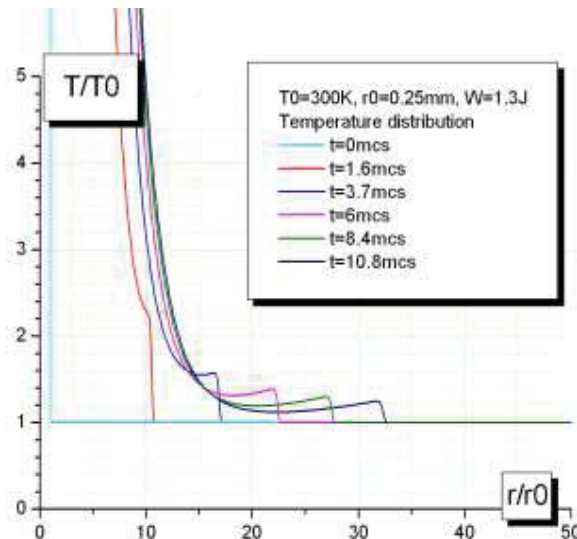


Fig.3.2.3. Temperature profiles at SW propagation. $T_0=300\text{K}$.

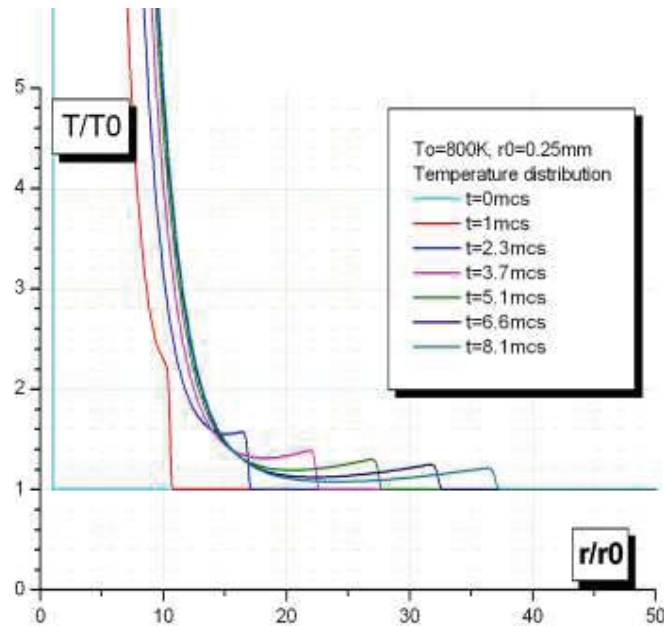


Fig.3.2.4. Temperature profiles at SW propagation. $T_0=800\text{K}$.

It is well seen that the significant pressure and temperature jump are occurred in the vicinity of plasma channel. The gas density is also increased that is important for chemistry enhancement. In the first $10\mu\text{s}$ the temperature rises on 20% in the area about $d=16\text{-}20\text{mm}$ in diameter. The raised temperature (5-20% of extra value) is conserved in that zone during about $\Delta t=10\mu\text{s}$. It might be quite enough for some chemical reactions intensification.

Photo-dissociation of the gas. The estimations of the photo-dissociative and photo-ionization processes in air due to radiation of the short-pulse high-voltage electrical discharge were done under the following conditions:

- ◇ Air at ambient conditions $P=1\text{Bar}$, $T_0=300\text{K}$;
- ◇ The temperature in discharge channel is $T=16\text{kK}$ that is correlated with energy deposition in about 1.7J ;
- ◇ The discharge channel is optically thick;
- ◇ Initial diameter of the discharge channel is 0.5mm , length – 50mm .

The direct mechanisms of photo-ionization were only taken into account. A significant absorption of the radiation by air occurs at the wavelength of external source less than $\lambda=186\text{nm}$ due to strong excitation of Shuman-Runge band of molecular oxygen O_2 . At $\lambda=176\text{nm}$ ($\epsilon=7.05\text{eV}$) the absorption spectrum transforms to continuum that leads to dissociation of the oxygen. An effective dissociation of molecular nitrogen N_2 begins at $\lambda<140\text{nm}$. At $\epsilon>12.1\text{eV}$ the photo-ionization of oxygen and nitrogen takes place with a large cross-section of process.

It is clear that plasma never illuminate as absolutely black body. The real intensity of radiation is always less than it could be predicted on base of Plank's law. In our case the intensity of the plasma channel radiation in visible part of the spectrum lies not far from Plank's law. The estimations of energy being transformed to radiation give the value about 25%, which is in agreement with conventional radiation share for such discharges [1-4]. The

handbook on physical properties [5] gives the value of integral thermal radiation factor for the air:

$$J_{air}/J_{black\ body} = 0.82;$$

for $T=16\text{kK}$ and $P=50\text{Bar}$. In the case of the pulse discharge the initial pressure in discharge channel is much more: $P \approx 2N_0 k T (1+\alpha)$, where α is ionization degree ($\alpha \approx 0.9$) and factor 2 is due to full dissociation. Therefore, we can expect that the intensity of radiation is close to Plank's value.

It allows one to evaluate the whole irradiative energy in our conditions in a range $W=0.3-0.5\text{J}/\text{cm}^2$ meaning the lateral surface of the plasma channel. This value was utilized for calibration of integral radiation of the discharge. In accordance with the Plank's law the maximum of spectral distribution at $T=16\text{kK}$ lies at $\lambda \approx 200\text{nm}$ (for $I(\lambda)$) or $\lambda \approx 300\text{nm}$ (for $I(\varepsilon)$). The comparison of radiation spectral density and absorption factor [2] is shown in Fig.3.2.5.

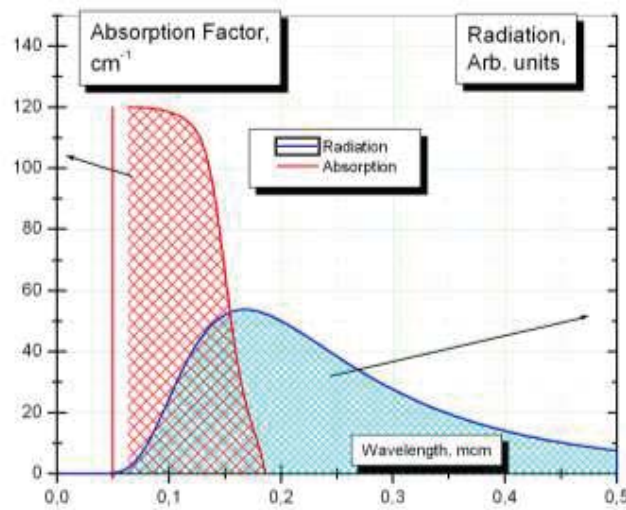


Fig.3.2.5. Plasma radiation and absorption factor.

In the case of cylindrical symmetry the radiation field outside the plasma filament (in a distance r) can be expressed as following one:

$$J(r, \varepsilon) = J_0(\varepsilon) \times \frac{r}{r_0} \times \exp(-\mu(\varepsilon) \times (r - r_0));$$

where ε - is a photon energy, μ - is absorption factor. The relative fraction of dissociated molecules of oxygen (it is the main fraction) can be calculated by the following expression:

$$\frac{\delta N_{O_2}}{N_{O_2}} = \frac{1}{N_{O_2}} \times \int_0^{\infty} \frac{1}{\varepsilon} \times \frac{\partial J(r, \varepsilon)}{\partial r} \times d\varepsilon;$$

when the plasma channel in not expanded yet.

An absorbed irradiative energy flux has been estimated numerically for different distances from the axes. The result is shown in Fig.3.2.6.

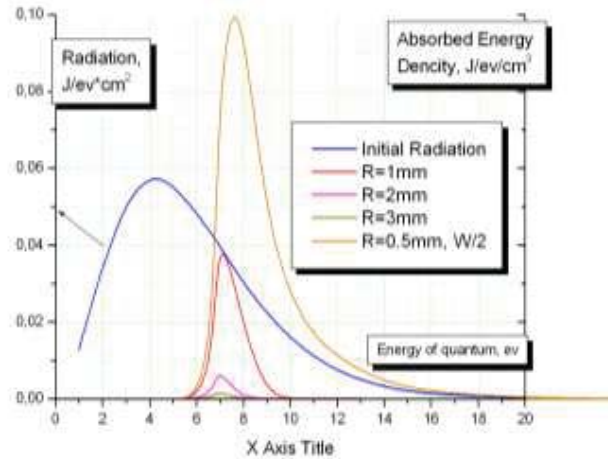
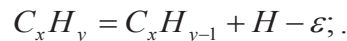


Fig.3.2.6. Irradiated energy dissipation for ionization and dissociation in ambient air.

It may be expected the intensity of dissipated energy decreases with the distance fast. The photo-ionization zone locates not far than 1mm from the axes. The photo-dissociation processes are significant for the distances up to $r=3\text{mm}$ from the plasma. The estimations gave the value of dissociated oxygen in range 1% for $d=2\text{mm}$ and about 0.1% for $d=4\text{mm}$. Together with the channel expansion the zone of significant level of excitation and dissociation will expand rapidly up to diameter $d\approx 10\text{mm}$.

It is important that the cross-section of the molecular oxygen and nitrogen excitation and photo-dissociation are decreased with the temperature rise. At the same time the energetic threshold of the effect is slightly falls due to primary thermal excitation of the molecules. Therefore, under the high-temperature conditions we could expect some increase of the zone of dissociation. Besides of that the excitation of metastable states of molecular oxygen (singlet ΔO_2) can be realized effectively.

A large fraction in efficiency of dissociation mechanism can give molecules of any hydrocarbon fuel. The most hydrocarbon substances have the specific dissociation energy in a range $\varepsilon_{\text{dis}}=3.95\text{-}4.3\text{ev}$ for the reactions of hydrogen detachment:



Such a reaction (free hydrogen appearance) plays a key role in combustion of heavy fuels. From the other side the photo-dissociation of heavy molecules can be executed by the photons with less energy (higher wavelength) than in air.

References to section 3.2.

1. A. Aleksandrov, A. Ruchadze, "Physics of high-current sources of radiation", Moscow, Atomizdat, 1976, pp184.
2. M. Sultanov, "Shock-compressed plasma in powerful pulse discharges", -Dushanbe: "Donish", 1981, pp280.
3. Ya. Zeldovich, Yu. Raizer, "Physics of shock waves and high-temperature hydro-dynamic phenomena", Moscow, Science, 1966, pp687.
4. N. Gegechkory, "Experimental study of the channel of spark discharge", JETPh, 21, 493, 1951.
 5. "Physical values", Handbook under I. Grigoriev and E. Meylichov edition: Moscow, Energoatomizdat, 1991, 1233pp (p791).

3.3. Analysis of non-intrusive diagnostics of spectra and intensity of turbulence at electrical discharge interaction with gaseous media.

This part is based on the literature, mostly cited in [1-6].

It is clear that almost all natural and most of artificial flows of liquids and flows are turbulent. Technical progress needs to describe such flows. Main equation describing fluid viscous dynamics is Navier-Stokes equation. However, in most cases it is very difficult (sometimes impossible) to solve or compute this equation therefore, the accurate measurement and calculation of turbulent flows has wide ranging application and significance.

One of the first developed methods for flow speed measurements was Hot Wire Anemometry (HWA). Method is based on measuring of intensity of thermal heat removal from thin hot probe (wire of foil), which depends on flow velocity. The great majority of the HWA systems in use employ the Constant Temperature Anemometry (CTA) implementation. Main disadvantage of described method is necessary probe installation within the flow. It makes CTA method intrusive in general, because of influence of probe at process in flow and flow itself. However, CTA systems offer a very high frequency response, reaching into hundreds kHz range. It makes CTA almost the only method of measuring turbulence. Need to precise calibration and essential nonlinearity of response of system to flow direction and probe position may be refer to additional shortcoming of the system. Moreover, with presence of high voltage discharge the existence of conductive wires in discharge area is almost inconvenient. The conductive electrodes transfer some potential, which rearrange the electric field in discharge area. Therefore, the streamers from first stage of discharge may be connected on the probe of CTA. In this case, all the electronics in CTA setup will be damaged. All this makes CTA almost inconvenient for flow measurements in conditions of high voltage discharge.

Developing and fast progress in LASERs in 60-s make it possible to evolve non-intrusive methods of measuring flows in fluids and gases. One of the first such methods was Laser-Doppler Anemometry (LDA) developed at the first by Yeh and Cummins. Method is based on light scattering on seeding particles, which occur with the frequency shift due to Doppler Effect. This makes the output is exactly linear, no calibrations are required, the output has low noise, high frequency response and velocity is measured independently of other flow variables. Progress in signal processing and fiber optics make this method useful for practice. Frequency response of such a technique may be attributing to average – in practice it is tens of kilohertz. One of the limitations of this method is directional ambiguity of measured velocities. This ambiguity can be removed using a Bragg cell (to add a constant frequency shift to main signal), but only for small velocities – to 50-60 m/s.

Relatively small power of lasers using in LDA allows us to concern interaction of laser with flow to be negligible. At the same time with non-intrusive action of laser, LDA assumed to seed small particles into flow to scatter the light. Existence of seeding particles does not disturb the flow itself, but, considering the high voltage discharge, it can affect both streamer and main stage of discharge propagation. In case of LDA seeding particles may be from different material, which allow choosing particles the most inert according to electrical point of view. In comparison with other techniques, LDA have the smallest particle size.

Both described methods are local – they measure the flow velocity in one point or small area. This area is 5 μm to 1 mm in case of thermo anemometry and from 100 μm to 1 mm in

case of LDA. Rapid development of digital camera and lasers make possible to visualizing and quantifying of whole flow field. The development of Particle Image Velocimetry (PIV) has become one of the most popular instruments for flow measurements. This method is based on processing of image particle seeded into discharge and illuminated by laser knife. The modern approach to PIV assumed to obtain two images of particles in flow with small delay in time. Subsequent processing of images with cross-correlation function analysis allows obtaining particle displacement and, consequently, flow speed. Cross-correlation function is made for small interrogation region containing 10-20 particles.

Consider the interaction with flow PIV have the same highs and lows as a LDA system. Spatial resolution strongly depends on exact system, but measuring is carrying out in whole velocity field. As in LDA the PIV system assumed to seed foreign particles in to flow. In this case, the particles must be bigger and concentration of it must be higher. However, the spatial resolution defined not by concentration of particles, but by interrogation region. Unfortunately, the PIV systems have the slowest temporal resolution – about 15 Hz, due to requirement of two images obtaining for one shot. On spatial resolution, most of limitations contributed by spatial resolution of camera used and dimensions of interrogation region. Temporal resolution also limited by camera and laser frequency. There is an opportunity to build PIV system using high-speed camera and high frequency laser. But in such case one needed to build an auto-correlation function instead of cross-correlation, which reduces the spatial resolution. Moreover, in burst mode of operation, laser energy is small and camera sensitivity is low which makes such configuration useful for limited range of applications.

Along with PIV systems similar techniques were developed: 1) Particle Tracking Velocimetry (PTV) 2) Laser Speckle Velocimetry (LSV). In LSV scattered light interfere to make a registered speckle. LSV distinguished from PIV mostly with concentration seeding particle on which light scattering occur. It is bad from electrical point of view. Higher concentration of seeding particles results increasing of its effective influence of electro technical parameters of medium and the process of streamer propagation.

PTV most important feature is very low concentration of seeding particles. This method is based on registration of individual particle tracks within the flow. In order to be able to track individual particles the concentration of particles must be very low. In PTV, the acquired data is a time sequence of individual tracer particles in the flow. PTV results in velocity information in random locations. On the other hand, it makes it the least intrusive methods of flow field measurement, from the electrical and flow interaction point of view.

In comparison with a gasdynamic test a quantity of parameters to be measured in plasma-assisted experiment is larger significantly. The conditions for diagnostic are more complex and some widely used methods are not applicable. For example, so powerful methods as hot-wire velocimetry can't be used in plasma due to an extra heating by heterogeneous molecular recombination and relaxation. The PIV method also has limited possibility for application in plasma and strong electrical field. Two physical mechanisms impede the particles movement in flow: charging in plasma and polarization in electrical field. By the first mechanism the particle acquires the charge up to potential in order $\varphi \approx kT_e$, where T_e = electron temperature. It leads to arising the Coulomb force in external electrical field $F = qE$, where $q = 4\pi\epsilon \times r \times q$, r = particle's radius. By the second mechanism, which works in plasma and without plasma both, the particle has got a dipole momentum in external electrical field $p \approx 16\pi\epsilon E r^3$. In nonuniform electrical

field an effective force $E=p \times grad E$ can be quite strong. The calculations show that the extra velocity of the particles due to plasma and electrical field can be in a range $V=(15 \div 5)m/s$ for $r=(10^{-4} \div 10^{-3})cm$ under typical conditions. It means that the smoke visualization and the PIV can be applied only in high-speed areas and has very limited capabilities in zones of low-speed flow.

Correlation method is one of the novel and not fully developed techniques of flow measurements. It based on processing of consequent schlieren images and does not need to seed particles into flow at all. So this method does not influence on flow or any stage of discharge propagation. It can be considering like non-intrusive method of flow field measurement with presence of high voltage discharge. Still, one has to serious improving of processing of image technique to obtain good results from this method. In addition, schlieren images are integrated along the cross-section.

On turbulent pulsation spectrum measurement.

Next, we will analyze of suiting of techniques described for measuring turbulence. In order to measure spectrum of turbulent pulsations with good precision one needed to satisfy strict condition of temporal and spatial resolution. For turbulent flows, accurate measurement of turbulence requires that scales as small as 2-3 times the Kolmogorov scale be resolved - $\left(\frac{v^3}{\epsilon}\right)^{\frac{1}{4}}$. The frequencies of pulsation reach hundreds of kilohertz. Briefly, the main properties of different techniques are collected in Table 3.

Table 3 [1].

	Constant temperature anemometry	Laser-Doppler anemometry	Flow field measurement			
			Particle image velocimetry	Particle Tracking velocimetry	Laser speckle velocimetry	Image Correlation Velocimetry
Proportionality of output signal S(t)	Non-linear	linear	linear	linear	linear	linear
Spatial Resolution	Single point typically ~ 5 μm x 1 mm	Single point typically 100 μm x 1mm	Depending on measurement volume	Low, random location of tracks	Depending on measurement volume	Depends on Schlieren system and processing algorithm
Frequency Distortion	Sensor is in contact with flow – very High frequency response, follows flow behavior	Good frequency response – tracer particles assumed to follow flow (particle lag)	Particle motion frozen at 2 instants in time assumes line displacement Sample frequency ~30 Hz	Acquired data is a time sequence of individual tracer particles in the flow	Similar to PIV. Laser speckle detection instead of image	Depends on Schlieren system
Dynamic Range; Resolution	Depends on analog-to-digital conversion 12- and 16-bit typical; can be higher	16-bit digitization of Doppler frequency within selected bandwidth	Depends on subpixel resolution of particle displacement 6- to 8-bit typical	Depends on subpixel resolution of particle displacement 6- to 8-bit typical	Depends on subpixel resolution of particle displacement 6- to 8-bit typical	Depends on Schlieren system
Concentration of seeding particles	none	Average to high	average	Very low	high	none
Particle size	-	<100 μm	>1 mm	>1 mm	>1 mm	-
Interaction with high voltage discharge.	Very high	low	Depending on type of seeding particles	Depending on type of seeding particles	Depending on type of seeding particles	none

The most suitable method for turbulence measure in conditions of high voltage discharge is Laser-Doppler Anemometry as it can be seen from Table N. Firstly, due to its high frequency

response – modern electronics allows to build system in hundreds of kilohertz range. Secondly, due to nonintrusive operation of system: the seeding particles are small, and its concentration can be not too high. Correct choice of seeding particles material can reduce their influence on different discharge stages.

The most common tool for turbulence measure is constant temperature anemometry. In condition of high voltage discharge it cannot be applied due to necessarily of probe installation into discharge zone. Other techniques failed due to spatial and temporal resolution. So one can conclude, that the most interesting technique for turbulence measuring under conditions observing is LDA.

Reference to the section 3.3.

1. K. D. Jensen “Flow Measurements” Review. – J. of the Braz. Soc. of Mech. Sci. & Eng. 2004, Vol. XXVI, No. 4 / 417
2. Adrian, R.J.(1991) “Particle Imaging Techniques for Experimental Fluid Mechanics”, Annual Review of Fluid Mechanics, vol 23, p 261-304
3. Tropea, C. (1995) “Laser Doppler anemometry: recent developments and future challenges”. Meas. Sci. Technol. 6: 605-619.
4. N. Cézar, C. Besson, A. Dolfi-Bouteyre, L. Lombard, “Airflow Characterization by Rayleigh-Mie Lidars”, Aerospace lab, the ONERA Journal, Issue 1 - December 2009
5. ULF HÖGSTRÖM, J. C. R. HUNT and ANN-SOFI SMEDMAN, “THEORY AND MEASUREMENTS FOR TURBULENCE SPECTRA”, Boundary-Layer Metrology 103: 101–124, 2002, Kluwer Academic Publishers.
6. Springer Handbook of Experimental Fluid Mechanics, Springer, 2007

4. Task 1. Analytical Efforts.

"When I meet God, I am going to ask him two questions: Why relativity? And why turbulence? I really believe he will have an answer for the first."

Werner Heisenberg

One of the problems of high-speed combustion is the effective mixing of fuel and oxidized in the combustor at compressible conditions [1-2]. The problem is difficult to be solved due to very short residence time of supersonic flow in the combustor of restricted length. Besides of this a compressible flow possesses poor mixing because of a reduced expansion rate of the shear layers. In order to solve those problems the extra method is required to keep mixing efficiency high enough with a minimum total pressure loss [3].

It is a well-known fact that the turbulent gas motion develops in a cooling post discharge channel, replacing molecular heat conduction as the dominant mechanism of the heat transfer. As a result, the rates of cooling and expansion of the channel increase considerably. The turbulent motion may therefore significantly increase the rate of the fuel-gas mixing, which may in turn be used to control the mixing rate in high-speed directly fuelling combustors.

1. *J. M. Seiner, S. M. Dash, and D. C. Kenzakowski*, "Historical survey on enhanced mixing in scramjet engines," *J. Propul. Power* 17, 1273 (2001)
2. *E. J. Gutmark, K. C. Schadow, and K. H. Yu*, "Mixing enhancement in supersonic free shear flows," *Annu. Rev. Fluid Mech.* 27, 375 (1995).
3. *Shigeya Watanabe, M. G. Mungal* "Velocity fields in mixing-enhanced compressible shear layers" *J. Fluid Mech.* (2005), vol. 522, pp. 141–177.

4.1. Development of the physical models

4.1.1. The physical model of long spark channel

It is considered a spark channel development in the cold unperturbed surrounding air at pressure $P_0=1 \text{ atm}$ for current pulses

$$I = I_a \cos(2\pi ft) \exp(-t/\tau_a) + I_{res}, \quad (1)$$

typical for spark discharge. Here I_a is the amplitude of an aperiodic current pulse of frequency f , τ_a is the characteristic decay time; I_{res} is the residual after-discharge current ($I_{res} \ll I_a$). It is convenient to look for the solution in Lagrange's mass coordinates $dm = \rho r dr$ within the framework of the standard equations of one-dimensional gasdynamics:

$$\begin{aligned} \frac{\partial r}{\partial t} &= v, \\ \frac{1}{\rho} &= \frac{1}{2} \frac{\partial r^2}{\partial m}, \\ \frac{\partial v}{\partial t} &= -r \frac{\partial}{\partial m} (p + Y), \\ \frac{\partial \varepsilon}{\partial t} + (p + Y) \frac{\partial}{\partial t} (1/\rho) &= Q, \end{aligned} \quad (2)$$

Here Y is the artificial viscosity, Q gives the influx and the losses of heat: where Q_J , Q_{rad} , Q_λ correspond to Joule heating, losses by radiation and heat conductivity. Equations (2) are solved together with the equation of state of the gas in the channel.

At time $t = 0$ we set the initial channel radius $r_0 \approx 0.1 \text{ cm}$ and the gas temperature

$$T(r, 0) = T_0 + T(0, 0)/(1 + r^2/r_0^2),$$

where $T_0 = 300 \text{ K}$, $T(0, 0) = 10^4 \text{ K}$. Our calculation shows that in the process of discharge evolution the solution quickly 'forgets' the initial conditions. Note, that choosing a preheated thin channel of radius r_0 for the initial condition corresponds to a "precursor" breakdown heating, which itself can be a source of initial channel explosive expansion. Initial thermal energy stores in the channel of unit length $q_0 \approx 2\pi\rho_0 \int_0^{r_0} (\varepsilon - \varepsilon_0) r dr$ should be $\ll q(t)$ - thermal energy deposited into the channel during the current pulse.

A similar problem to the one formulated in this work is discussed in [1], where radiation is treated in multiple band diffusive approximation. In this approximation [1] the equation for radiation diffusion is solved for each k -th spectral band:

$$\frac{1}{r} \frac{\partial}{\partial r} \left(\frac{r}{3k_\nu} \frac{\partial U_\nu}{\partial r} \right) + k_\nu (U_{p\nu} - U_\nu) = 0,$$

The term Q_{rad} corresponding to losses by radiation in Q has the form

$$Q_{rad} = -\frac{1}{\rho} \sum_k \nabla \vec{W}_k = \frac{c}{\rho} \sum_k k_{\nu} (U_{k\nu} - U_{kp\nu}) \quad (5)$$

The molecular heat conductivity gives the contribution to Q, which is given by

$$Q_{\lambda} = \frac{1}{\rho} \frac{\partial}{\partial r} \left(r \lambda \frac{\partial T}{\partial r} \right) = \frac{1}{\rho} \frac{\partial}{\partial m} \left(\rho r^2 \lambda \frac{\partial T}{\partial m} \right), \quad (6)$$

where $\lambda(T)$ is the heat-conductivity coefficient. Local Joule heating intensity is determined from the formula

$$Q_J = \frac{E^2 \sigma}{\rho}, \quad (7)$$

where $\sigma(T)$ is the conductivity of plasma; $E(t) = IR$ is the electric field, $R(t)$ is channel resistance per unit length.

At $P > P_0$, the gas temperature T was determined by calculating internal energy ε , and density ρ by interpolating the function $T(\varepsilon, \rho)$ from the corresponding tabulated data presented in [2]. For the relatively high temperatures ($T > 10^4$ K), the following interpolation formula for specific internal energy of air [3]:

$$\varepsilon = 8.3 (T_{[K]}/10^4)^{1.5} (\rho/\rho_0)^{0.12} \text{ eV/molecule} \approx 27.7 T \frac{1.5}{[K]} (\rho/\rho_0)^{0.12} \text{ J/kg}$$

was used. The values of the channel plasma conductivity, partial air composition (including the molecular dissociation and ionization), and gas temperature T dependent heat conductivity coefficient have been taken from [4, 5], where the local thermodynamic equilibrium (LTE) in each time moment was assumed. In this assumption, the degree of ionization and the channel conductivity completely determined by the air 4 plasma thermodynamic parameters: pressure, density, and internal energy (or temperature). Note, that rate of the afterspark channel cooling relates to the channel conductivity. Therefore the turbulent regime of the afterspark cooling strongly influences the channel conductivity: the faster temperature decreasing results into the faster drop of conductivity from $\approx 10^4 \text{ Ohm}^{-1}\text{m}^{-1}$ at $T > 10^4$ K, to negligible small values at $T < 3000$ K.

Most of presented calculations were done for the current pulse (1) with $I_a = 1 \text{ kA}$, $\tau_a = 0.1 \mu\text{s}$, and different values of the residual current, I_{res} . At the levels of Joule's heating intensities for the discharges under study, the channel expansion is accompanied by the formation of a shock wave (SW). The radial distribution of gas parameters in the channel and the shock wave for the pulse current of a spark discharge at various times are identical to those obtained in previous works [4, 5]. The dynamics of the gas parameter's evolution at the center of discharge,

the channel radius, r_{ch} , and the front of the shock wave, r_{sw} , for a given current pulse is shown in Fig.4.1.1. Radiation plays a very important role in the total balance and transport of energy during the evolution of the spark channel. Most of the irradiated energy gets absorbed at the channel border, while heating the adjacent layers of cold gas. During the evolution of the spark discharge, when temperature in the channel $T > 10^4$ K, the contribution of the molecular heat transfer to the total energy balance is relatively small (Fig.4.1.2a and b). The radiation heat losses are falling with time, and, as the channel temperature decreases down to $T(0) < 10^4$ K, the molecular heat transfer becomes the dominant heat loss mechanism (Fig.4.2.2c and d).

The after-spark channel cools down due to molecular heat transfer, and this is a very slow process. However, the intensity of the channel cooling down and expansion processes will increase sharply in the case of gas turbulization in the cooling channel. The mechanisms that may lead to instabilities of the channel boundary and the development of turbulent flow will be discussed below. The so-called "negative pressure drop", known from the explosion theory (see, for example [6]), clearly shows up in the results of the calculations (Fig.4.1.1,a).

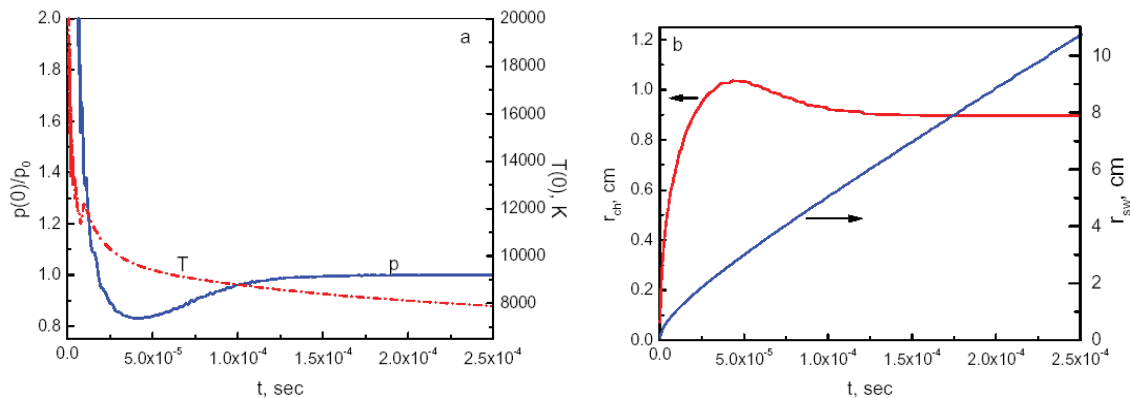


Fig.4.1.1: Gas dynamical parameters of spark discharge formation: a — pressure and temperature on the channel axis; b - radii of the shock wave, r_{sw} , and of the channel, r_{ch}

There comes a moment during the process of channel expansion, when the pressure drops down to $P \approx P_0$ (P_0 is the pressure of the unperturbed surrounding cold gas), but the channel expansion goes on due to inertia. Then the pressure drop becomes negative (the negative drop phase), and the channel boundary expansion slows down to a halt. At this point cold gas begins flowing backward accompanied by compression of the channel gas and, consequently, by pressure and temperature build-ups. Below it will argue that the channel boundary's slow motion toward the center may be among possible causes of the Raleigh-Taylor instability in the region with a large density gradient at the channel boundary, which finally brings about the gas

flow turbulization in the channel. As a result, the speed, with which the channel cools down and expands, greatly increase.

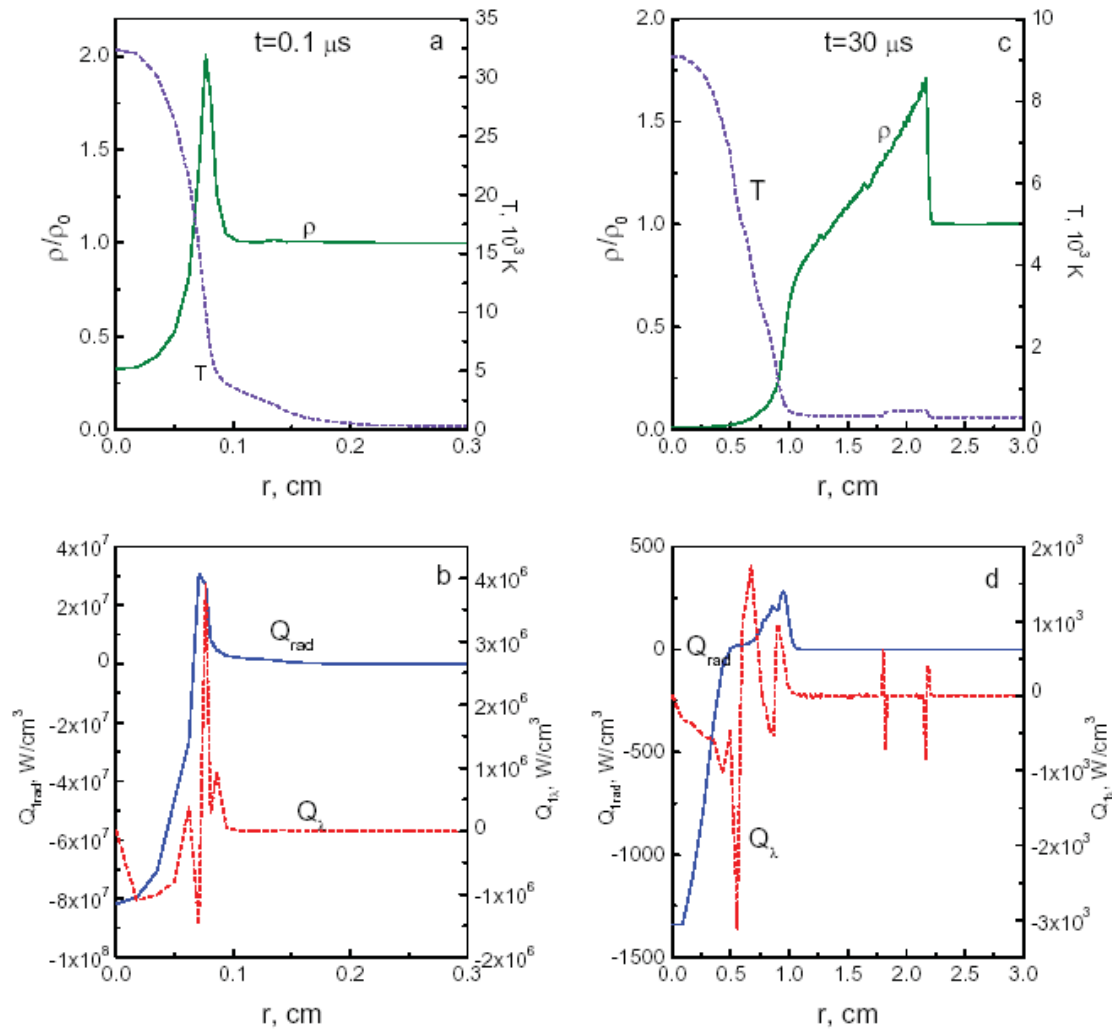


Fig.4.1.2: Radial distributions of the gas density ρ/ρ_0 , temperature, T/T_0 — a, c and the volume losses of energy by the radiation, Q_{rad} , and by the molecular heat conductivity, Q_λ - b, d at two times after the initiation of the current pulse: $t = 0.1 \mu s$ - a,b and $30 \mu s$ - c,d

The residual current hardly influences the cooling process or the channel plasma characteristics up to the end of the phase of the negative pressure drop. Therefore, as we will see below, the residual current does not affect the evolution of the hydrodynamic instability of the channel boundary, which takes place during the channel boundary's motion back toward the center. However, the turbulent flow development in the cooling channel is suppressed, because the cooling is stabilized with the Joule heating caused by the residual current. As a matter of fact after the pressure inside the channel is restored (from its minimum up to P_0), the cooling process becomes almost isobaric ($P \approx P_0 = \text{const}$). Therefore, the temperature drop is

accompanied by the gas density rise, which requires a gas mass influx from the peripheral regions to the center. This radial flow of cold gas is the source of kinetic energy of turbulence pulsations, which are generated in the cooling channel. If there is a mechanism that is able to stop the temperature drop (and, thus, stabilize the gas density rise), generation of turbulent pulsations in the channel is suppressed. Such a stabilizing mechanism in this case is the Joule's heating by a relatively small residual current.

4.1.2. Hydrodynamic instability of the after-spark channel boundary

The pressure in the cooling channel becomes practically equal to the external one, when the gas temperature is still as high as $T \approx 10^4$ K. A further temperature decrease occurs at an almost constant pressure that is accompanied by a gas density rise and requires a gas influx from the channel periphery. This radial flow is unstable and results in the development of a turbulent flow of the gas inside the channel. As was shown earlier [7], one of the possible causes of this generation of the turbulent pulsation in the cooling after-spark channel may be a deviation of the channel geometry from the ideal cylinder at the heating stage (e.g., the channel cross-section ellipticity or/and winding, energy-release discreteness etc). Intense vortical flows of the gas form at the isobaric stage with a characteristic scale defined by the original non-uniformity whose size is of the same order as or exceeds the channel radius. However, on schlieren-photographs by the time $t \approx 10^{-4}$ s elapsed after the start of the cooling down process one can see the incipient instability at the channel boundary with the typical size being noticeably smaller than the radius. Only following the appearances of these small instabilities, is when larger scale vortex motions develop [7]. This scenario of turbulence creation is presented in experiments irrespectively of a degree of the channel geometry imperfections.

A possible mechanism to observe the hydrodynamic instability in experiments can be the Raleigh-Taylor instability in the region of large density gradient at the channel boundary. In the non-inertial frame of reference, set at the accelerating boundary, inertial force is exerted on the gas with the corresponding effective acceleration \mathbf{a}_{eff} in the boundary region. The evolution of the Raleigh-Taylor instability is then possible in the transition layer at the channel boundary when $\mathbf{a}_{eff} \times \nabla \rho < 0$ is fulfilled [8].

Such motion is possible when the condition $\nabla p \times \nabla \rho < 0$ is satisfied at the channel boundary. In Fig.4.1.3 on the magnified scale we show a typical distributions of density and pressure calculated for $t=30\mu\text{s}$ (when channel expands as a consequence of inertia) and for $t =$

100 μs (during channel compression). The condition $\nabla p \times \nabla \rho < 0$ is satisfied at the boundary of the expanding channel (Fig.4.1.3,a) and, therefore, the expansion process is stable.

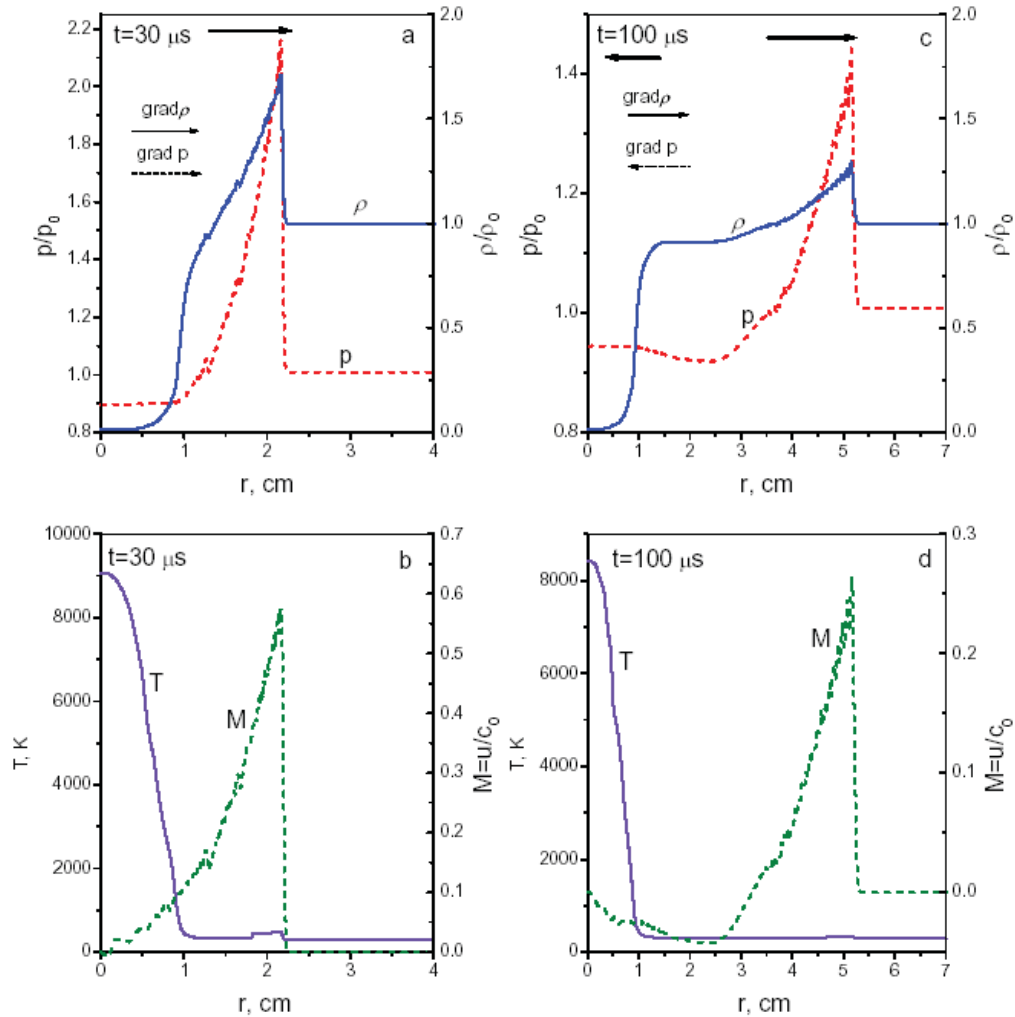


Fig.4.1.3: Radial distributions of density, pressure, temperature and mass velocity $M = v_r/c_0$ (c_0 - sound velocity of unperturbed cold air) during the channel boundary expansion ($t = 30 \mu\text{s}$) — a, b and at the time when the boundary moves back to the center ($t = 100 \mu\text{s}$) — c, d. The thick arrows show the gas flow directions. The thin arrow shows the pressure and density gradients directions.

The high gas pressure in the external region leads to deceleration of the channel boundary expansion bringing it to a halt. Then the expansion is followed by the compression. With the channel volume decreasing the increased gas pressure in the channel impedes the further compression. Thus, after some time the pressure and density gradients will have opposite directions and, therefore, $\nabla p \times \nabla \rho < 0$ (Fig.4.1.3, b). As a result, the conditions for the Raleigh-

Taylor instability are satisfied at the channel boundary. Taking into account that the gas density $\rho \ll \rho_0$ in the channel, we estimate the time of the instability development using the formula:

$$\tau_{inst} \sim (2\pi r / \lambda)^{-1/2}, \delta r < \lambda \lesssim r_{ch}$$

where λ is the perturbation wave length, and δr is the size of the region at the channel boundary, where the essential density drop takes place. For example, from our results obtained for the considered current pulse, we estimate $\tau_{inst} \approx 10^{-4}$ s; this time scale is commensurable with the duration of the negative pressure drop. Note that this estimation is correct only in the linear stage of the instability development.

The non-linear stage of the hydrodynamic instability and the transition process to the developed turbulence in the after-spark channel is another complicated problem, which, as far as we know, has not been considered before. However, the experimental results yielded by the studies of processes in the after-spark channel support the argument that the duration of the non-linear stage is of the same order of magnitude as the aforementioned estimate of τ_{inst} .

4.1.3. Stabilizing role of the residual current

The calculations have shown that the residual current I_{res} (which is small compared to the current's amplitude value) can stop the channel cooling while preserving the channel's relatively high temperature and conductivity, which are peculiar to the quasi-stationary free arc (Fig.4.1.4). Moreover, each pulse of the discharge current has a corresponding minimal value of the residual current which stabilizes the channel decay. For the magnitude of the current pulse considered in the present work, the cooling stabilization occurs at $I_{res} = 25A$ (Fig.4.1.4). It follows from computed results that a continuous electric current, which is several orders of magnitude lower than the peak discharge current, is capable of maintaining the channel conductivity. This effect cannot be explained merely by Joule heating but is largely governed by the fact that the turbulent heat transport (effective turbulent heat conductivity (Fig.4.1.4,c)) is substantially suppressed. The cascade development of low scale turbulent pulsations gets also suppressed in the case with the residual current (Figs.4.1.5 and 4.1.6).

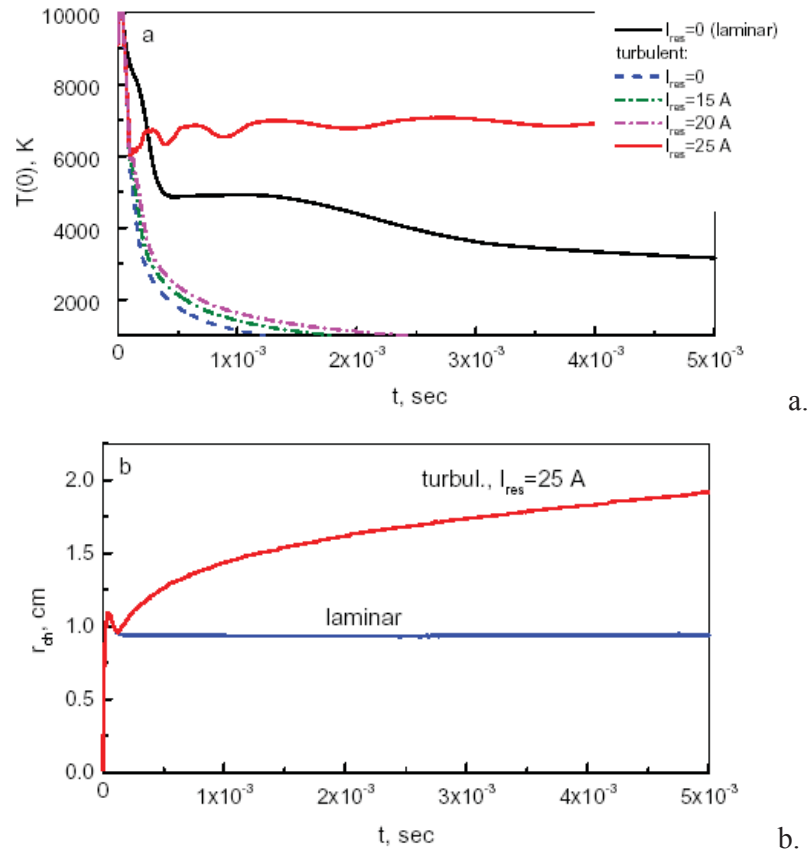


Fig.4.1.4: Temperature on the axis of the cooling down after-spark channel — a: 1 —with not accounting for the turbulence motion in the channel ('laminar' cooling); 2 — 5 with accounting for the turbulent motion developed in the channel; b - the channel radius.

The process of the after-spark channel cooling takes place with a much higher intensity at the developed turbulent flow in comparison with the regular quasistationary arc. Therefore, at equal temperatures and radii, the field in the stabilized turbulized channel, E_T , exceeds that in the regular quasi-stationary arc, E_λ , which got stabilized via the molecular heat conductivity, see Fig.4.1.7. This approximated relationship follows from the condition of the quasi-stationary balance between Joule's heating in the channel and the heat losses through its lateral surface. It must be noted that the rise of the electric field E in the channel at a given I_{res} is limited by the voltage drop, ΔU , across the entire channel. As the degeneration process of the intensive turbulent flow in the channel continues, E_T approaches the value of E_λ . (appr. 10 V/cm, typical value for the quasistationary free arc at atmospheric pressure, see, for e.g., [9]).

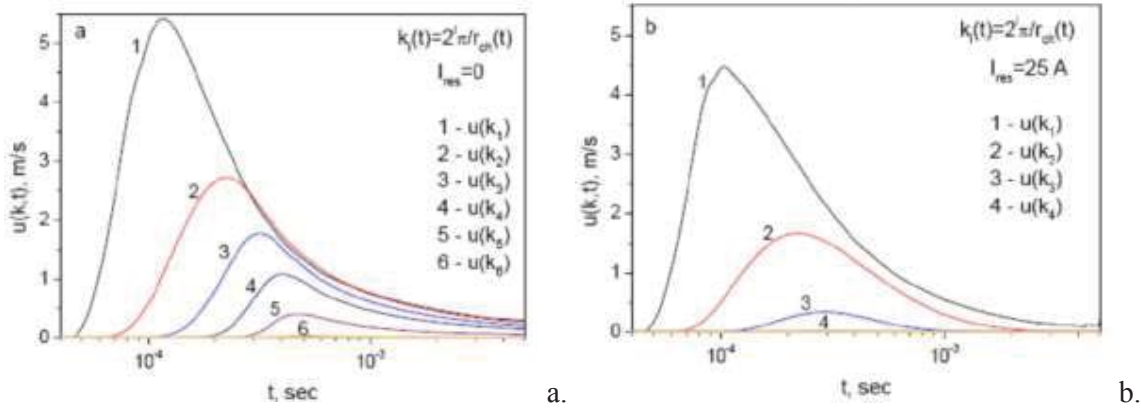


Fig.4.1.5: Spectrum of the turbulent pulsations development: a $I_{res} = 0$, b - $I_{res} = 25A$

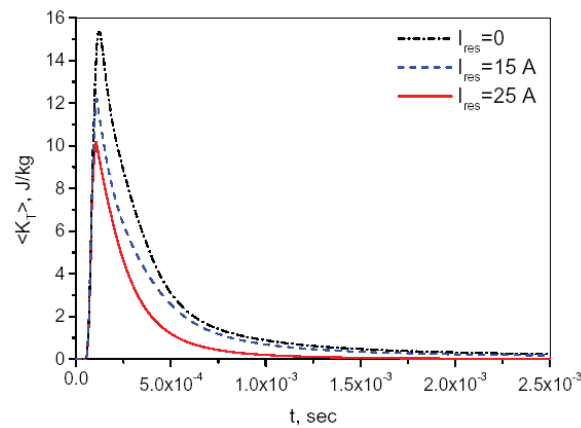


Fig.4.1.6: Kinetic energy of the turbulent pulsations per unit mass: effect of the I_{res} .

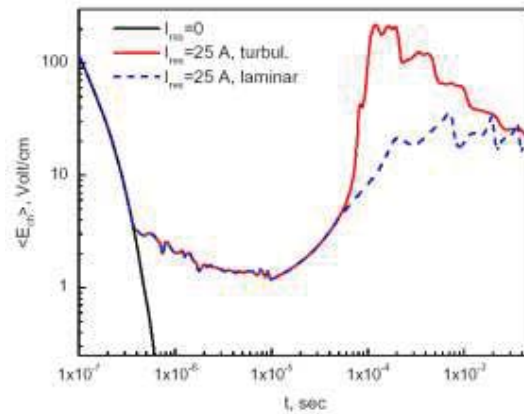


Fig.4.1.7: The electric field in the channel without the residual current and with taking into account the gas turbulent motion in the channel and without it.

The processes that govern the behavior of filamentary pulse discharge and after-spark channel decay have been reviewed. The role and influence of a small residual current in a decaying channel on the cooling characteristics have been studied. It has been shown that each current pulse has its corresponding critical value of the residual current stabilizing the cooling

channel under the quasi-stationary arc condition (featuring relatively high temperature and conductivity of the channel).

The suggested model [10] can be applied to describe the development and the decay of the after-spark channel in a wide range of dimensions: the main stage of lightning and a long laboratory spark or the relatively narrow inter-electrode gap of a high-current spark discharger. However, the typical time for the development of the turbulent pulsations as well as their characteristics remain adjustable parameters. To develop a more rigorous theory, we need to carry out comprehensive experimental investigations of the post-discharge stage to obtain enough information about the values of electrical, gas dynamical and thermodynamical parameters of a decaying channel and their relationship with the characteristics of a passed discharge current pulse. This task is one of the most important due to this work.

4.1.4. Physical mechanism of jets formation.

Jets are developing in quasi-isobaric stage, when $p(r,t) \approx p_0$. An illustrative sketch of jets formation is shown in the Fig.4.1.8. Depending on whether the surface of the channel boundary is concave or convex, flow from the periphery to the center, arising in a process of cooling, can be contracting or expanding. If the flow is contracting (concave surface), the static gas pressure increases, however, expanding flow from the convex surface decreases the pressure. As a result, we can expect the formation of jets in the direction opposite to pressure gradients.

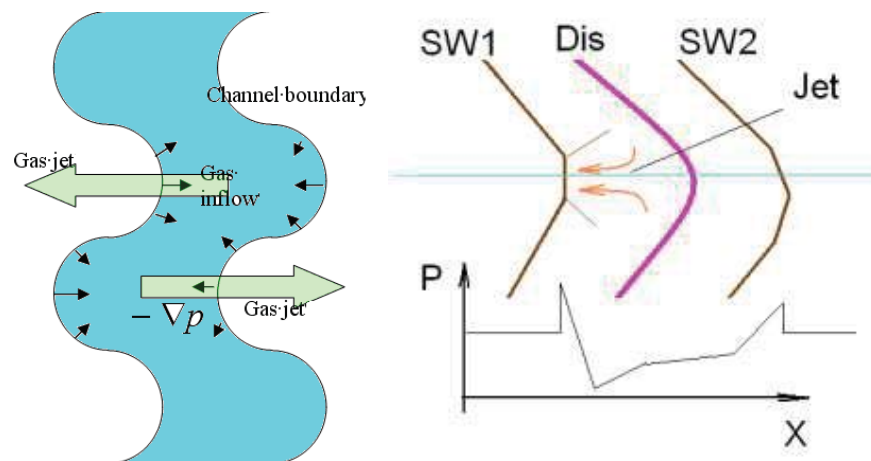


Fig.4.1.8. 2D Schematic of ‘cumulative’ jet formation during the cooling of a curved channel. SW1 – shock wave from concave side. Sketch of pressure distribution.

Shape of the plasma channel (3D restoration). The most conventional source of data for analysis in studying the characteristics of the discharge channel form is the picture (photos) of the discharge. But it misses much of the information, because in the general case, the discharge

develops in the volume, but not on the plane. More information can be obtained by producing shots by two cameras in mutually perpendicular planes. However, a more complete visualization of the discharge structure in space can be provided by three-dimensional model reconstructed from photographs obtained.

In the case where the discharge is a filament or a set of several filaments, its model can be constructed as follows: if there is only one filament on the photos (let's assume its vertical position), then a graph from the first photo represents a set of coordinates (X,Y) and from the second photo – (Z,X) , that allows us to construct a three-dimensional structure (X,Y,Z) , see Fig.4.1.9.

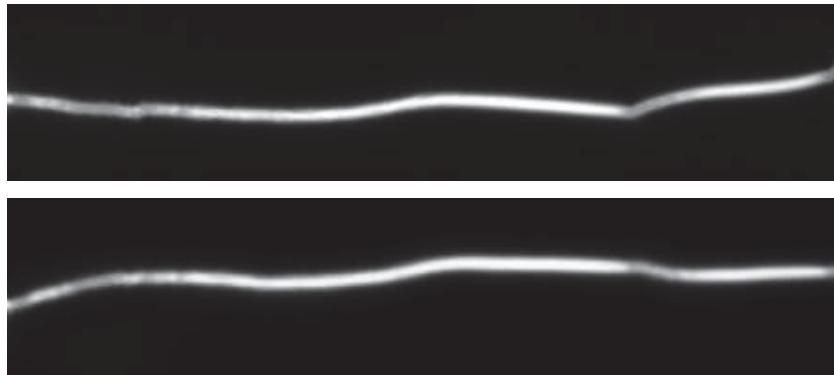


Fig.4.1.9. Sample of two images of the discharge in orthogonal projection.

The first phase of the model creation is photograph preprocessing that includes translation from the current color space to gray scale and fields cropping. The pictures are vertically cropped in such way that each horizontal line contains a discharge fragment. Then a smaller picture is enlarged with maintaining the same proportions so that the vertical dimensions of both frames coincide. Then the photographs are uploaded into LabView-based program that can create a dependence of intensity from horizontal coordinate for each horizontal set of points for preliminary processed pictures.

The serial number of line is the coordinate Y_i , and the coordinate of maximum intensity is X_i or Z_i for the first and second images, respectively. The function of the Gaussian approximation of the data is used to determine X_i , that allow to obtain more accurate coordinate of the absolute maximum, since it takes into account the neighboring points. In addition to this program determines coordinates that let to construct discharge channel volume. The manual selection of threshold intensity fixes coordinates x_i and x'_i ($x_i < X_i < x'_i$). Approximation of the discrete data also let to obtain more accurate coordinates. If the distance between the electrodes is known, all received coordinates can be transferred from the

dimensionless quantities into millimeters. The result of the program is a generation of 5 files, the first of which describes the axial line in three-dimensional space, and 4 others are three-dimensional envelope curves, that define the discharge volume.

Model recovery was produced in the SolidWorks program. This program can import files obtained by LabView and construct curves in three dimensional spaces. In addition to the curves creation it's necessary to make an elliptic (close to circular) profile. By pulling the profile along the axial line with account of envelope curves (of all four or only some of them, since the creation of an element using 5 curves is not always successful) to construct a solid-state element - the model of the discharge. A sample of reconstructed 3D channel is shown in Fig.4.1.10.

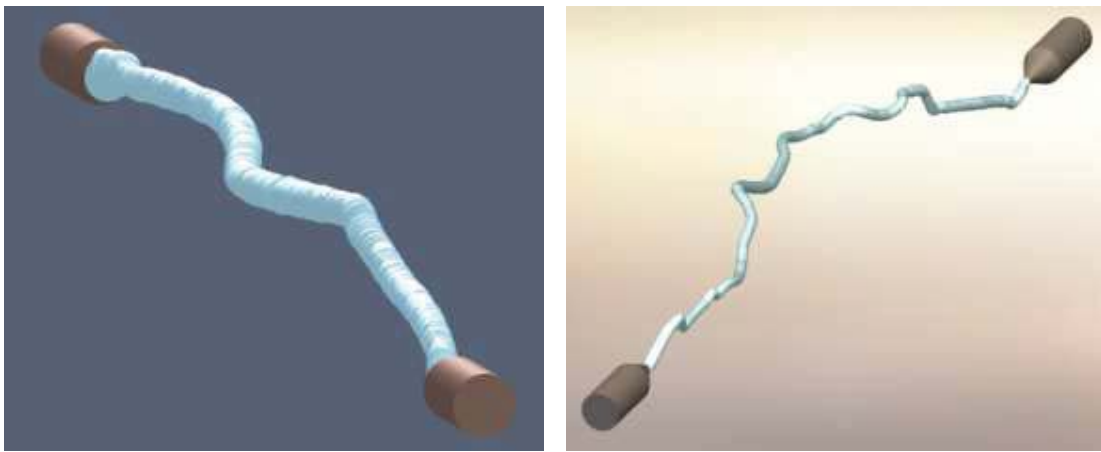


Fig.4.1.10. Sample of restored 3D plasma channel. 7 steps and 14 steps.

The described method allows us to quickly construct the three-dimensional structure of the discharge in simple cases where the discharge is not branching or little branched. *Disadvantages:* if the discharge have a fragment of the channel, located in a horizontal or close to horizontal, the program described above, will give an incorrect result. The proposed method does not allow for the construction of highly branched discharge.

Well seen that the discharge channel shape is curved and consists of several individual fragments-steps. The number of steps depends on the discharge gap as it is shown in Fig.4.1.11. The dependence is not linear, of course: a longer filament usually has much more bends. Typically, the discharge breakdown occurs by one step if the discharge gap is $p \times D \leq 20 \text{ Bar} \times \text{mm}$.

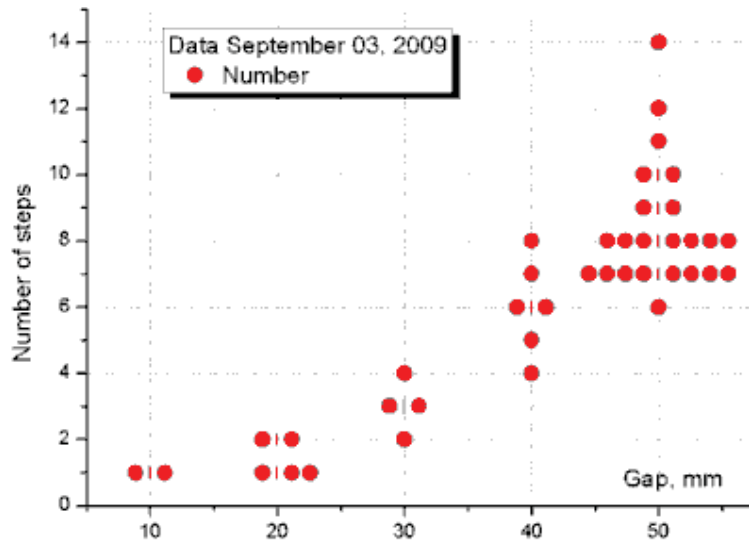


Fig.4.1.11. Trend of discharge breakdown steps depending on the gap.

An absence of bends strongly affects the instability appearance and intensity. The Fig.4.1.12 demonstrates comparison of typical schlieren images of the after-discharge caverns at variation of the discharge gap and pressure. Well seen that there is no similarity in respect of the $P \times D$ parameter.

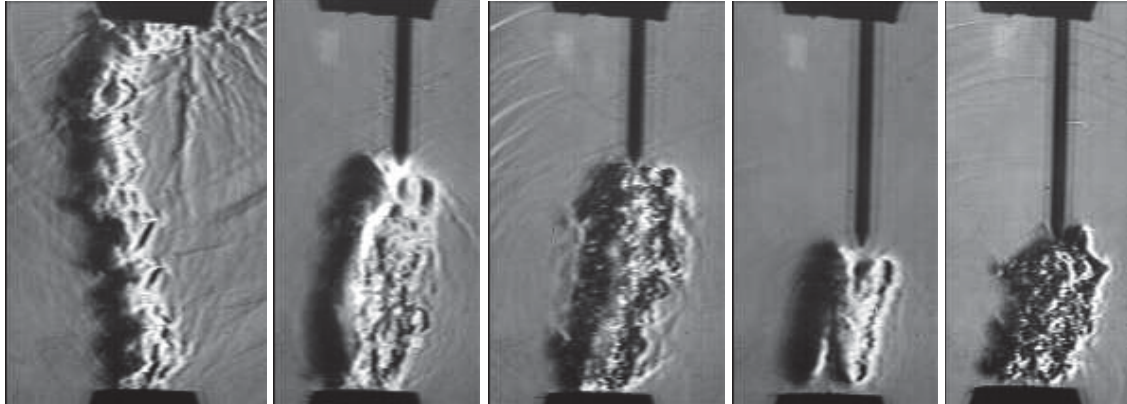


Fig.4.1.12. Schlieren images of the thermal cavern at delay time 100us: 1Bar, 50mm; 1Bar, 30mm; 1.7Bar, 30mm; 1Bar, 20mm; 2.5Bar, 20mm, sequentially.

4.1.5. Experimental demonstration of the physical model suitability.

A special test was performed to prove the physical model of the lateral jets generation. The key point of the model is that the jets are generated from concave side of curved plasma filament. Usually the plasma filament has uncontrollable 3D complicated shape. A third electrode (it is visible on right side of images) was installed in the test chamber to distort the electrical field distribution. This electrode was grounded through the resistor of high value. At

zero current it possesses the potential of earth. After the streamer breakdown the potential of third electrode appears as floating. Such a method allows making a controllable bending of the discharge filament. Figure 4.1.13 below shows the dynamic of the hot cumulative jet at artificial curvature of the discharge channel, right as it is predicted by the theory.

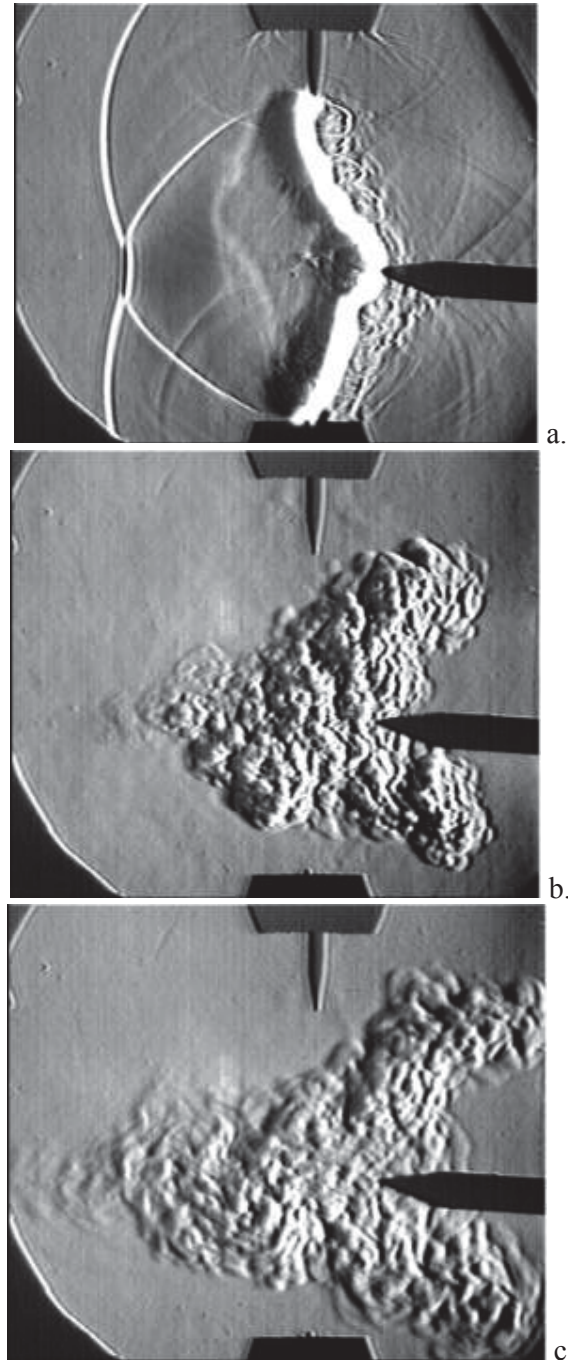


Fig.4.1.13. Fast jet development after the filamentary discharge breakdown. Third electrode is for controlled bending of the discharge channel. (a) – $t=40\mu\text{s}$, strong plane-front shock generation; (b) - $t=540\mu\text{s}$; (c) - $t=1040\mu\text{s}$.

References to the section 4.1.

1. A.H.Paxton, R.L.Gardner, L..Baker, Phys.Fluids 29, 2736 (1986)
2. N.M.Kuznetsov, Thermodynamic Functions and Air Shock Adiabates at High Temperatures. Mashinostroenie, 1965. (in Russian)
3. Ya.B.Zel'dovich, Yu.P.Raizer, Physics of Shock Waves and High Temperature Hydrodynamic Phenomena, Academic Press, 1968
4. M.N.Plooster, Phys.Fluids 14, 2111 (1971)
5. M.Akram, J.Phys.D: Appl.Phys. 29, 2137 (1996)
6. F.A.Baum, K.P.Stanyukovich, B.I.Shikhter, Physics of Explosion (ch.13), Moscow: GIFML, 1959. (in Russian)
7. J.M. Picone, J.P.Boris, J.R. Greig., M.Releigh, R.F. Fernsler, J.Atm.Sci., 38, 2056 (1981)
8. G.Taylor Proc.Roy.Soc. (London) A201,192 (1950)
9. Yu.P.Raizer, Gas Discharge Physics, Springer-Verlag, Berlin, New York, 1991
10. M.N.Shneider, Physics of Plasmas, 13, 073501-11, (2006)

4.2. 3D Computational analysis of plasma channel and low-density zone dynamics at ambient conditions.

Three-dimensional simulation of after spark channel breakup was executed by using FlowVision™ 3.08 software. Numerical modeling was based on solution of 3D time-dependent Reynolds averaged Navier-Stokes equations with the utilization of the wide used two-equation $k-\varepsilon$ model of turbulence. Calculation was provided in one quarter ellipsoid domain, which dimensions are following: $R_x = R_y = 32$ mm и $R_z = 36$ mm. Calculation domain is shown in Fig.4.2.1. Initial conditions in calculation area are following: pressure $P = 101325$ Pa and temperature $T = 273$ K. Reference pressure for results is 101325 Pa. Symmetry condition was used on xz and xy plans to decrease a number of computational grid cells, and Riemann condition was used on spherical boundary of calculation domain. Riemann condition fixes gas parameters on infinite distance. This condition takes into account the direction of disturbance propagation and disturbances do not reflect from such boundary. Parameters of the Riemann boundary are equal to initial conditions.

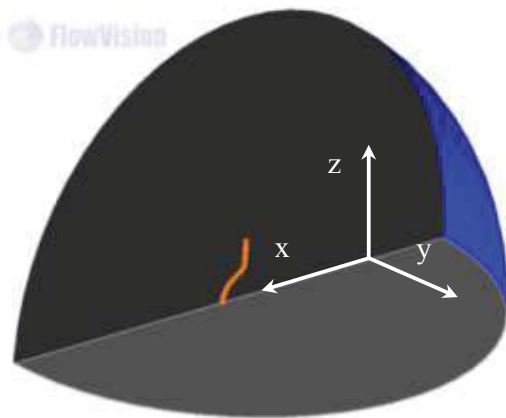


Fig.4.2.1. Calculation domain.

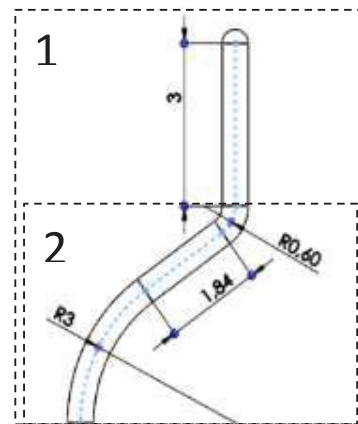


Fig.4.2.2. Scheme of volumetric heat source.

Discharge breakdown is simulated by volumetric heat source which is placed on xz boundary of calculation domain. Volumetric heat source was used in a half of curved cylinder 8,257 mm long and 7 mm height. Scheme of cylinder is presented in Fig.4.2.2(1). Radius of the curved cylinder is gradually increased from 0.25 mm to 0.34 mm during volumetric heat source operation.

The calculation was performed on a reconfigurable rectangular grid based on reference grid with $32 \times 16 \times 18$ 2 mm cubic cells. During of 1st level adaptation each base cell was divided into eight smaller cells. Cells size of $31,25 \mu\text{m}$ (6th level adaptation) were used in a small volume around and inside the curved cylinder at the start of calculation. Fragments of the computational grid are shown in Fig.4.2.3. During the calculation the maximal level of adaptation is gradually declining, different levels of adaptation based on the characteristic dimensions of the gasdynamic perturbations for different regions was used. Number of grid cells was varying in a range from 0.45×10^6 to 2.27×10^6 meshes.

Volume of half of the curved cylinder is $8.27\text{E-}10\text{ m}^3$, but a total volume of all cells affected by volumetric heat source is $9.67\text{E-}10\text{ m}^3$. So maximal power released by volumetric heat source (at recalculation to full volume including area cut off by a XZ plane of symmetry) is $\sim 10\text{ MW}$ for 8.5 mm length, or $\sim 20\text{ MW}$ for 17 mm length, because it more correct considering XY plane of symmetry (30 mJ/mm). Time dependence of power density of volumetric heat source is presented in Fig.4.2.4(a). Time-dependent calculation was provided to 2 ms time point. Time dependences of different gas parameters in calculation domain are presented in Fig.4.2.5. But main information can be obtained from 2D distributions for different time moments. As it shown in Fig.4.2.6 both bends of spark channel produce vortex like structures, and boundary of each disturbance moves away from place of initial heat source position. Final disturbances position caused by R3 mm bend presented in Fig.4.2.6 (XY, 2 ms). Disturbances propagate in a wide sector $\sim 80^\circ$. Time dependency of propagation velocity is presented in Fig.4.2.4(b).

Velocity and temperature fields for different time moments are presented in Fig.4.2.7 and Fig.4.2.8 respectively. The data obtained allow one to conclude that disturbances are spiral vortex structures, which moves and expand in main directions, specified by both bends of heat source curved cylinder. 3D views of vortex formation and expansion are presented in Fig.4.2.9, and final density isosurface for 1.25 kg/m^3 at 2 ms are presented in Fig.4.2.10. The grey color in last figure is volume, affected by afterspark vortexes and disturbances, and violet is initial spark channel.

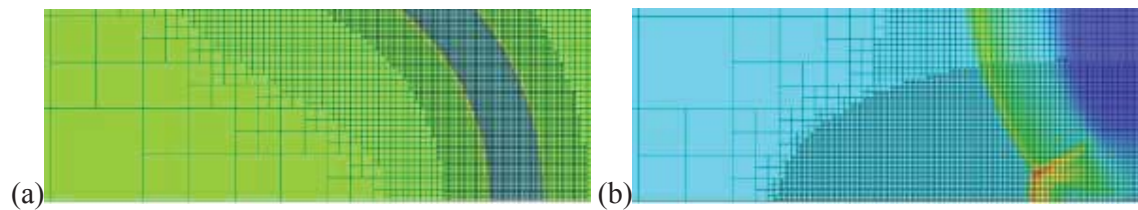


Fig. 4.2.3. Grid examples for 10 ns (a) and $5\mu\text{s}$ (b). Adaptation up to 6^{th} level.

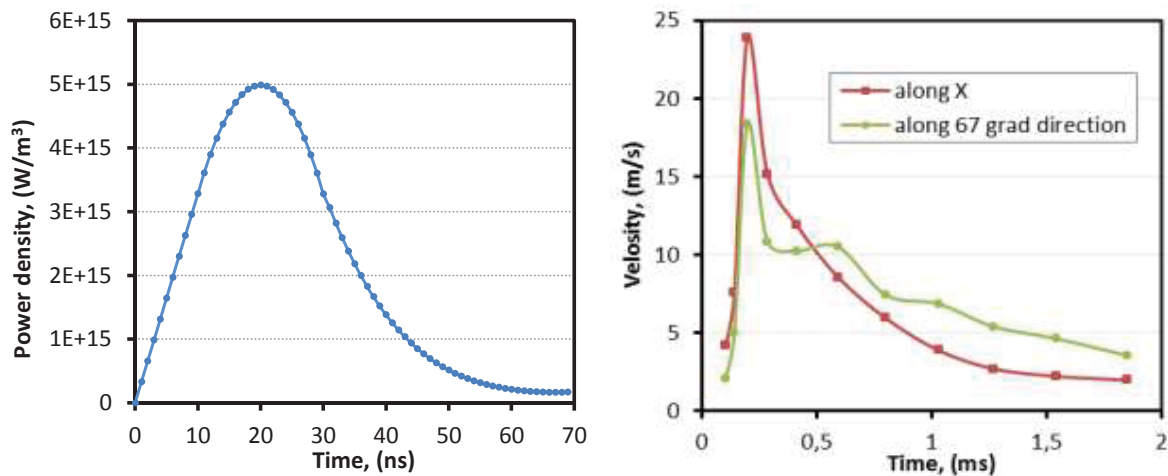


Fig.4.2.4 (a) Power density of volumetric heat source. (b) Velocity of isoline 1.25 kg/m^3 on XY plane.

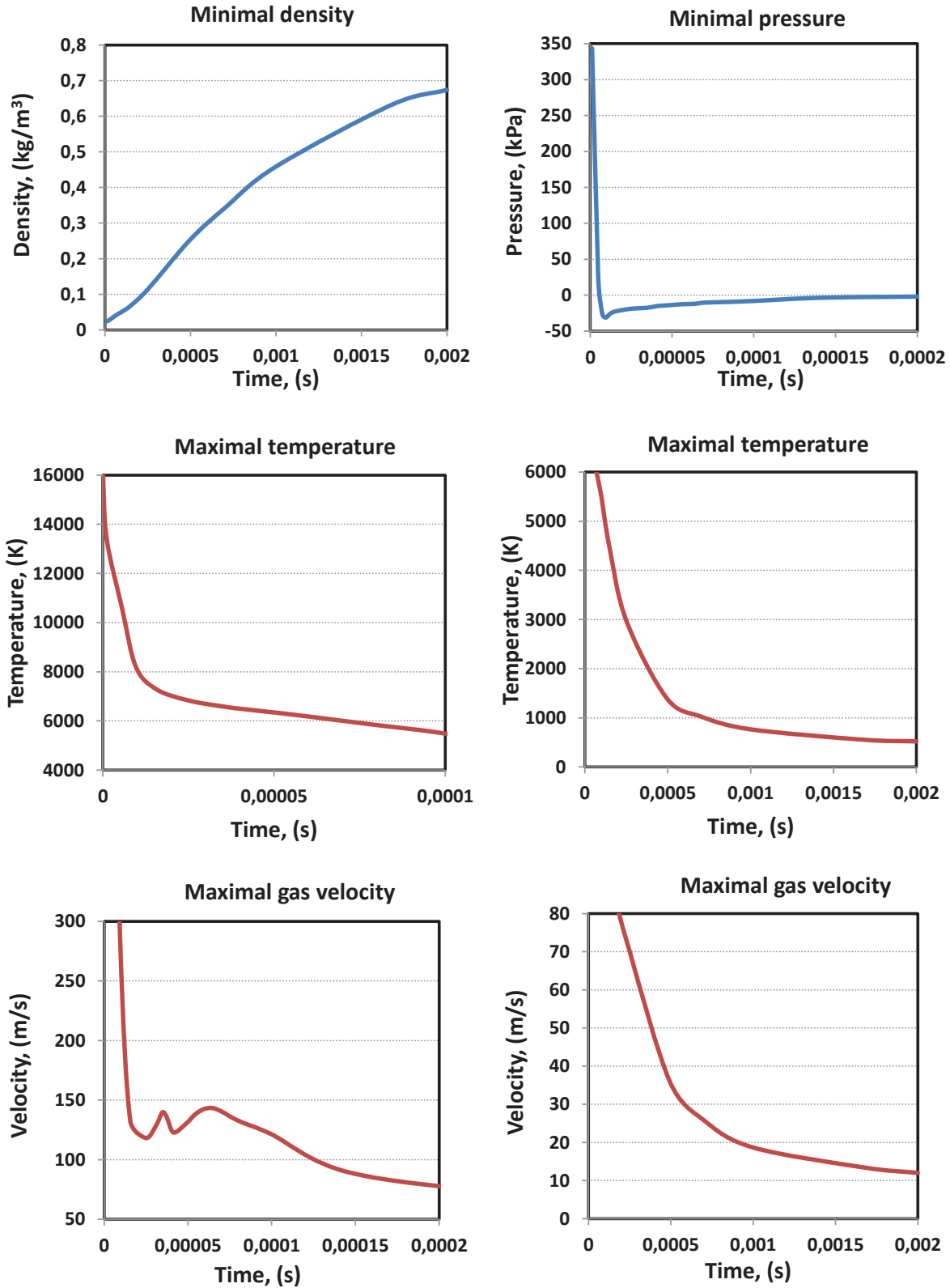


Fig.4.2.5. Gas parameters inside after spark channel (not including shock wave) vs Time.

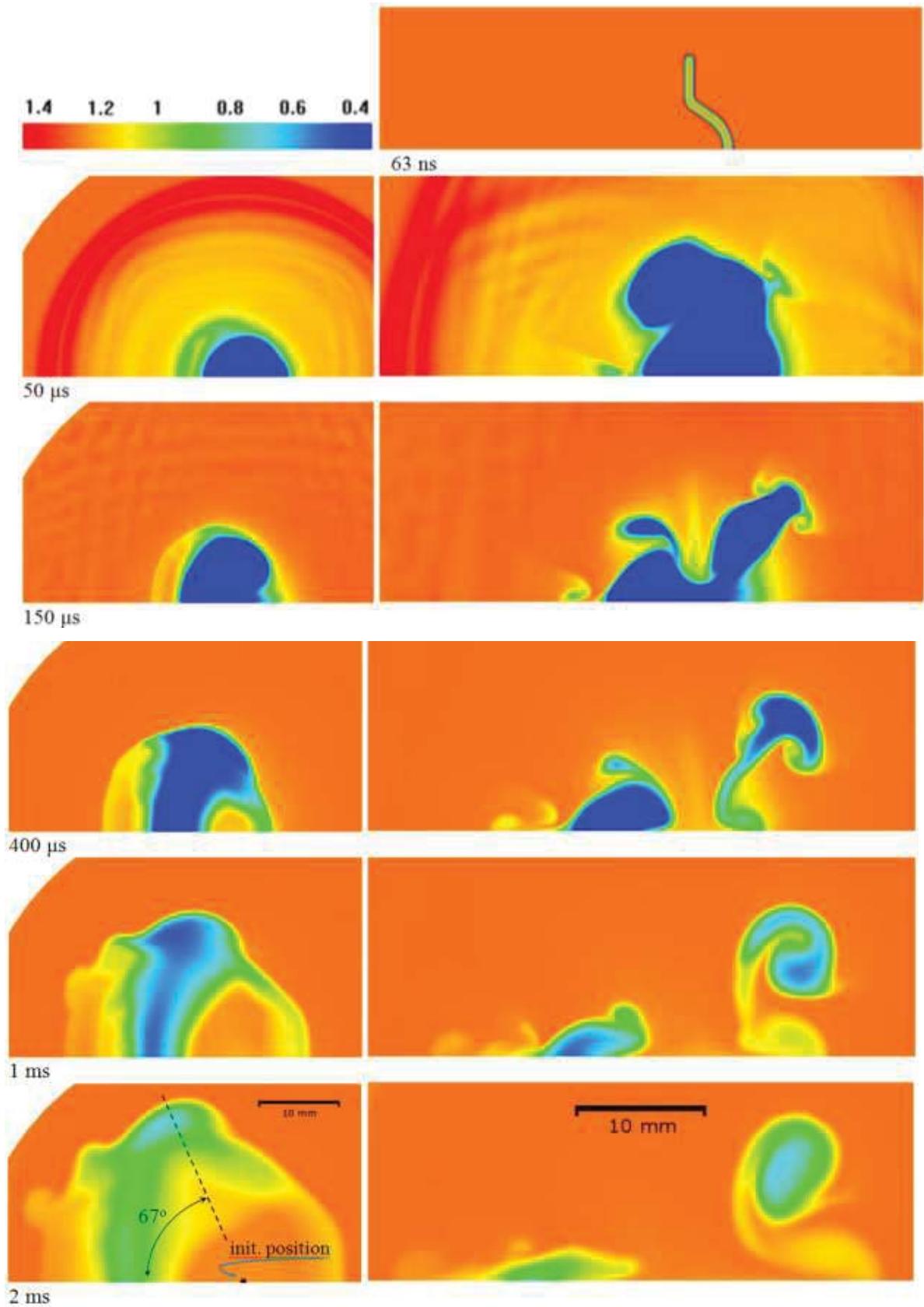


Fig.4.2.6. Density distribution at XY plan (left) and XZ plan (right), (kg/m^3).

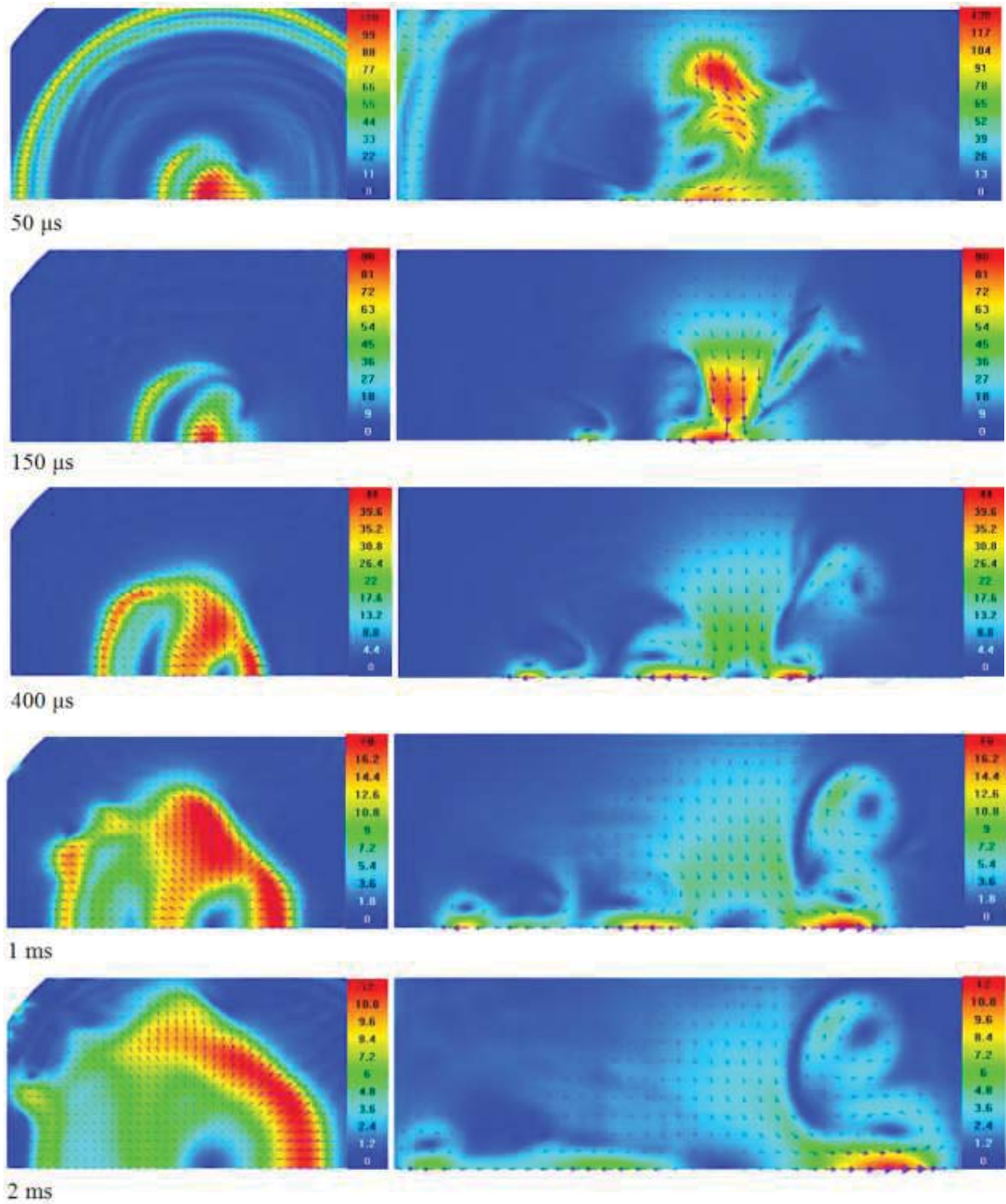


Fig.4.2.7. Velocity field at XY plan (left) and XZ plan (right), (m/s).

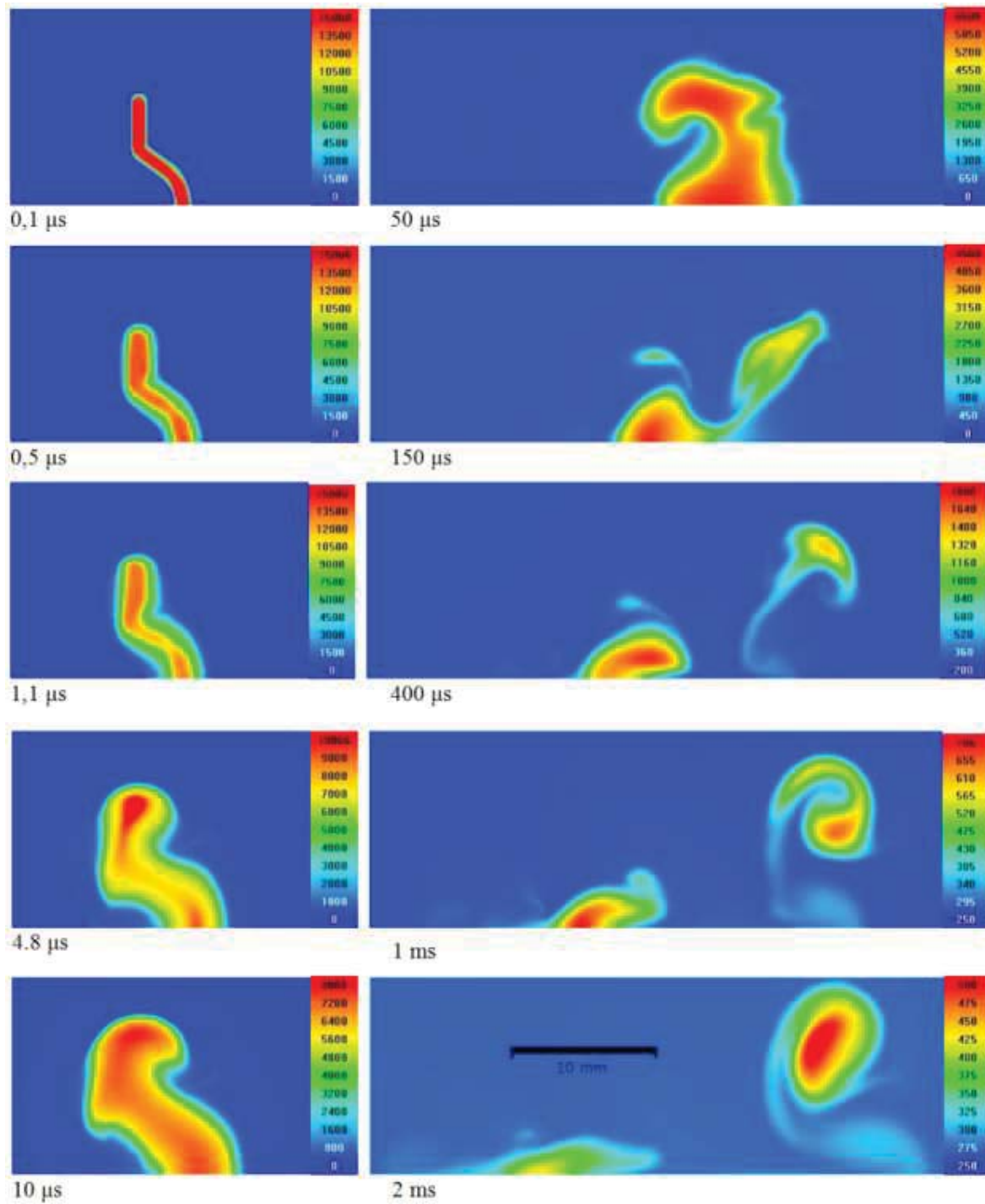


Fig.4.2.8. Temperature distribution at XZ plan, (K).



Fig.4.2.9. Density isosurface (1 kg/m³).

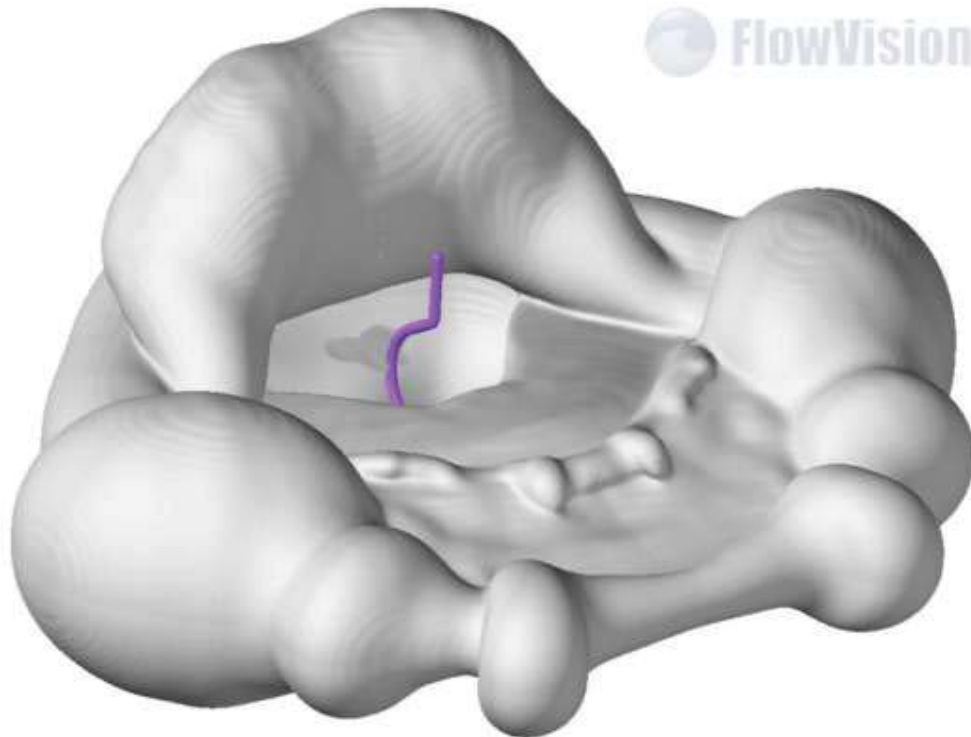


Fig.4.2.10. Density isosurface 1.25 kg/m³ at 2 ms (grey) – volume, affected by afterspark vortexes and disturbances. Violet – initial spark channel.

The analysis of turbulence produced by pulse electric discharge is based on calculation model used in simulation. It is important to understand the difference between most popular approaches at numerical simulation for further report.

- 1) Steady Reynolds-averaged Navier-Stokes (SRANS or usually RANS) simulation uses Reynolds's decomposition: time-averaged term plus turbulent fluctuations.
- 2) Unsteady Reynolds-averaged Navier-Stokes (URANS) simulation uses the same Reynolds decomposition, but transient (unsteady) term in Navier-Stokes equation makes possible to present the results as a sum of time-averaged part, resolved fluctuations and modeled turbulent fluctuations (averaged by turbulence spectrum).
- 3) In Large-Eddy Simulation (LES) solution is represented as a sum of resolved and sub-grid parts. As compared with URANS there is no averaging in this approach: resolved «large-eddy» part is only filtered usually by grid, and sub-grid turbulent fluctuations are taken into account by turbulent model.

In the current simulation 3D URANS approach with $k-\epsilon$ model of turbulence was used. Main large eddies was resolved, and small fluctuations are characterized by turbulent energy k (m^2s^{-2}). Also turbulence intensity can be used for description: turbulence intensity is a ratio

between the root-mean-square of the turbulent velocity fluctuations and the mean velocity. The short exhibition of typical results is presented below in Fig.4.2.11 and Fig.4.2.12 for two time delays after the discharge pulse.

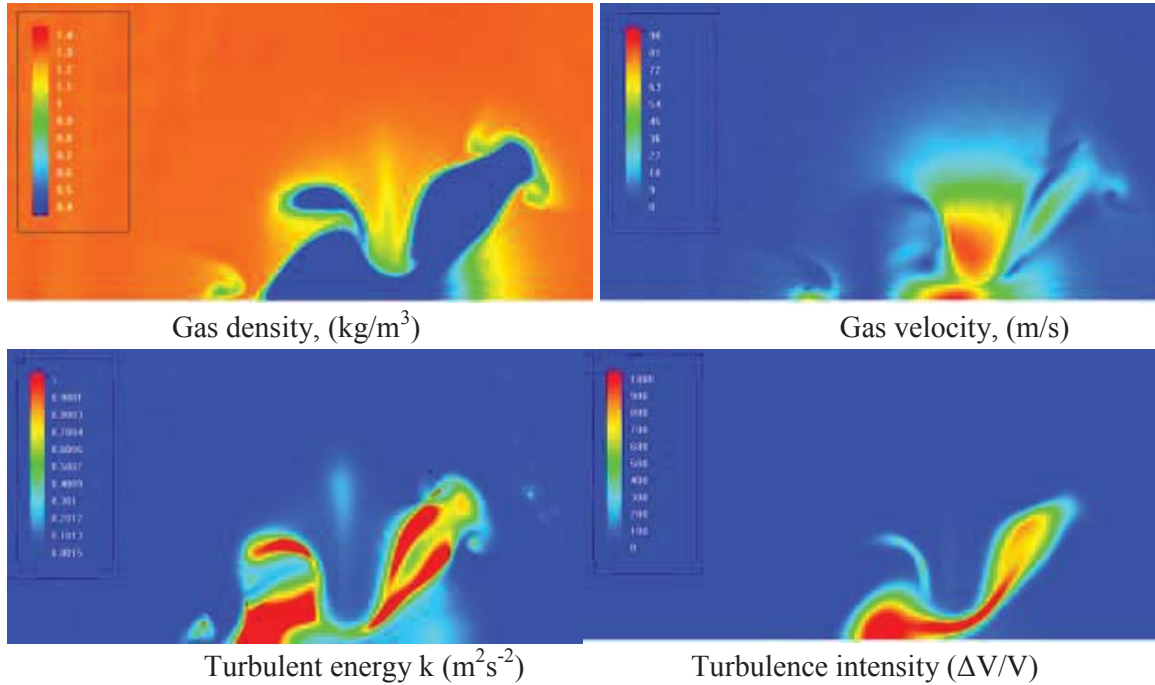


Fig.4.2.11. Simulation results for 150 μs

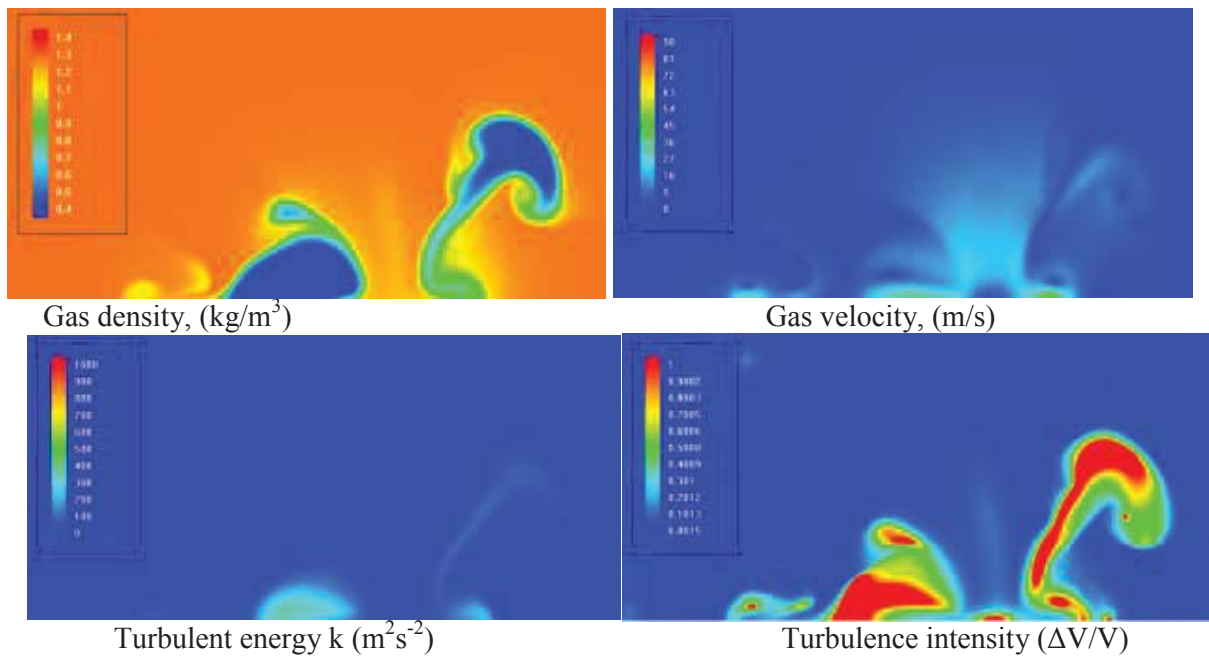


Fig.4.2.12. Simulation results for 400 μs

The extra series of the numerical simulation was performed to indicate a range of discharge parameters, where the maximal jet velocity may be expected. The following mechanism of jet formation is suggested, see Fig.4.1.8. At concave sides of the plasma channel, the shock wave propagation results in strong compression followed by strong rarefaction behind the shock. At convex sides, the shock wave is diverging, and thus is characterized by smaller compression followed by weaker rarefaction when compared with the concave sides. As a result, a pressure gradient builds up, with pressure decreasing from convex to the opposite concave sides. This causes jet formation outside of the concave regions, with the general direction of jets from concave to convex.

As previously the numerical simulation of breakdown and afterspark channel development was performed by using FlowVision™ software. Calculation of air flow in configuration close to experimental one was based on solution of 3D time-dependent Navier-Stokes equations with the utilization of the wide-used two-equation $k-\varepsilon$ model of turbulence. Model of perfect gas with realistic expansion to high-temperature zone (molecular dissociation and ionization are taken into account) was used at modeling of air flow. Geometry of calculation was changed to decrease number of cells in calculation domain. Calculation domain (half of cylinder R32×4 mm) and structure of afterspark channel are presented in Fig.4.2.13. Breakdown was simulated by pulse activation of volumetric heat source inside afterspark channel. Scheme of cylinder is presented in Fig.4.2.2(2). The afterspark channel consists of 7 curved coaxial cylinders. Radiuses and power densities of these cylinders are varied (see Fig.4.2.13(b)), and only one cylinder radiate in each individual cell (power density is not summed up). Dependency of total power on time is multiplied by a factor of 1.5 in comparison with Fig.4.2.4(a).

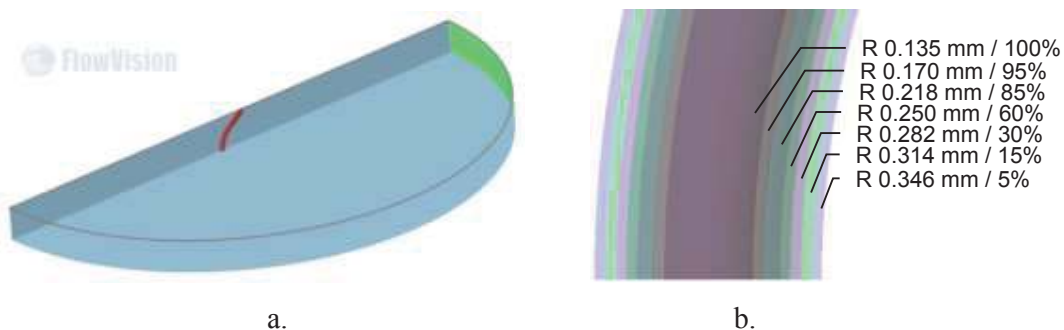


Fig.4.2.13. Calculation domain (a) and heat source structure (b).

Percentage of power density is specified.

Riemann based condition was used on the radial boundary of calculation domain. Initial and boundary air parameters are follows: $V=0$ m/s, $P_0=1$ Atm, $T_0=290$ K. Reference pressure for results is 1Atm. Symmetry conditions were used on all other boundaries. The calculation was

performed on a reconfigurable rectangular grid based on reference grid with $64 \times 32 \times 4$ 1 mm cubic cells. During of 1st level adaptation each base cell was divided into eight smaller cells. Cells size of $31,25 \mu\text{m}$ (5th level adaptation) were used in a small volume around and inside the curved cylinder at the start of calculation. During the calculation the maximal level of adaptation is gradually declining, different levels of adaptation based on the characteristic dimensions of the gasdynamic perturbations for different regions were used. Fragment of the computational grid is shown in Fig.4.2.14. Number of grid cells was varying in a range from 0.6×10^6 to 3.5×10^6 meshes.

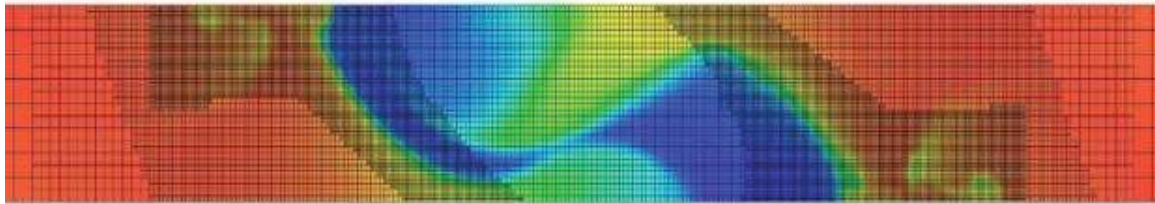


Fig.4.2.14. Grid example for $100 \mu\text{s}$. Adaptation up to 3th level.

Relative pressure distribution is shown in Fig.4.2.15. Clearly seen that pressure in the shock wave is approximately the same for both cases, but in 1050 kW/mm case internal relative pressure is three times higher. In both cases shock wave interaction caused by R3 arc produces a notable rarefaction. Significant pressure gradients lead to the formation of fast swirls in front of main disturbances. Density distribution (side view) for different time moments is presented in Fig.4.2.16. It is seen that these fast swirls are presented for both R3 and R0.06 cases, but it is greater on R3 side. As it is presented in Fig.4.2.17, these perturbations propagate into the sector, and for R3 case main disturbance are also greater and wider than for small radius bending.

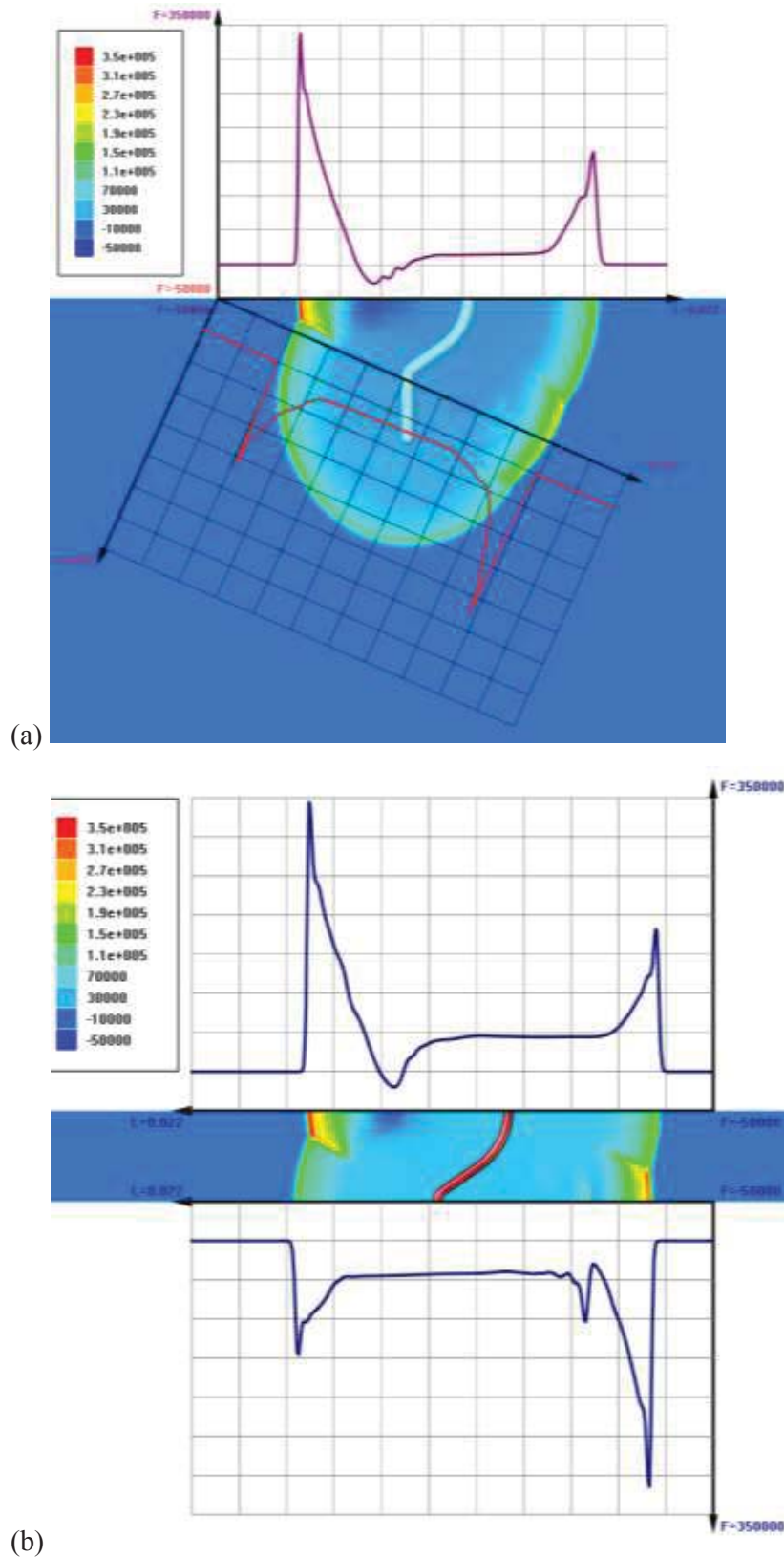


Fig.4.2.15. Relative pressure for 7.7 μs .

(a) – 1st simulation, 30 mJ/mm; (b) – 2nd simulation, 45 mJ/mm.

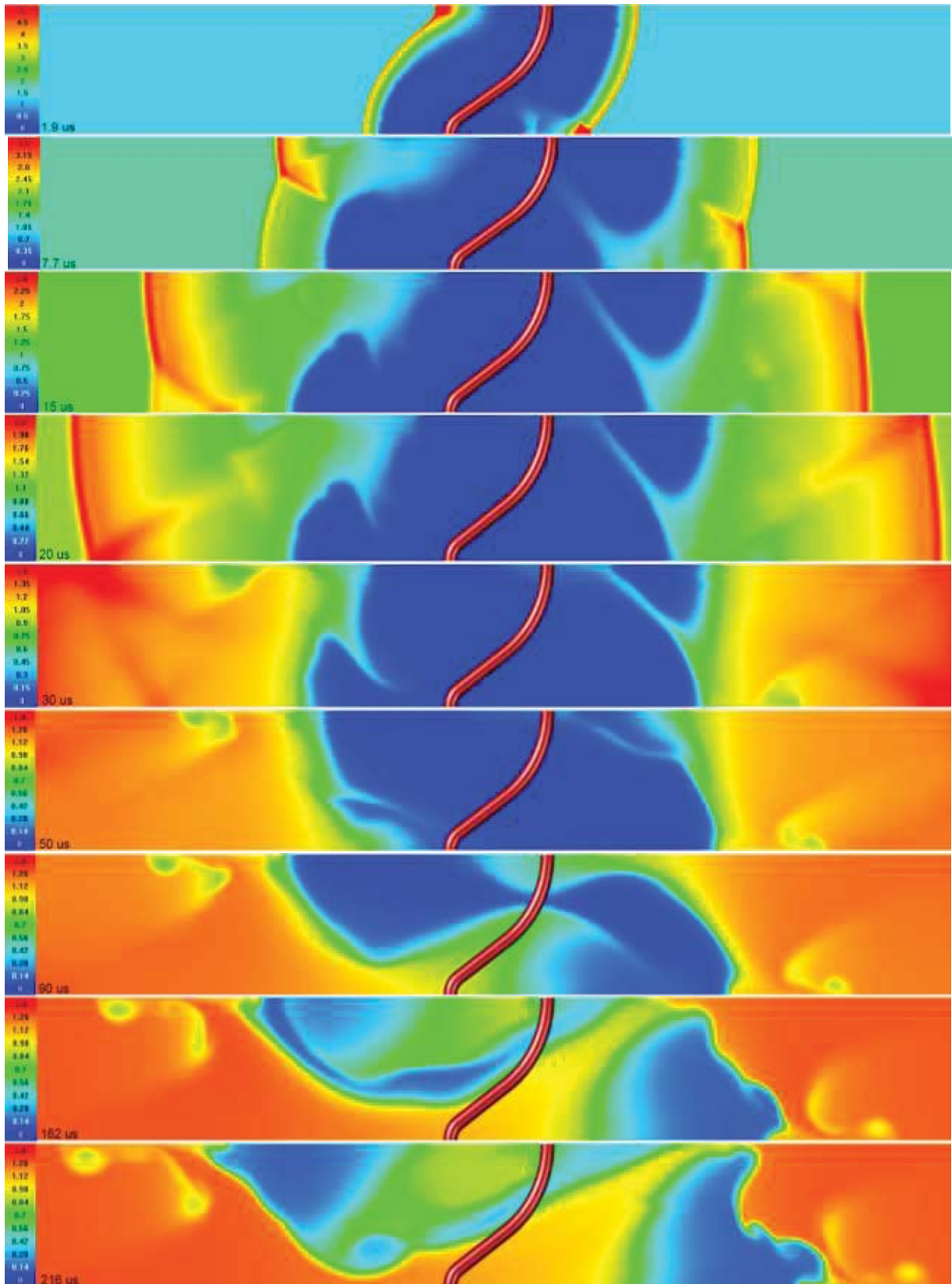
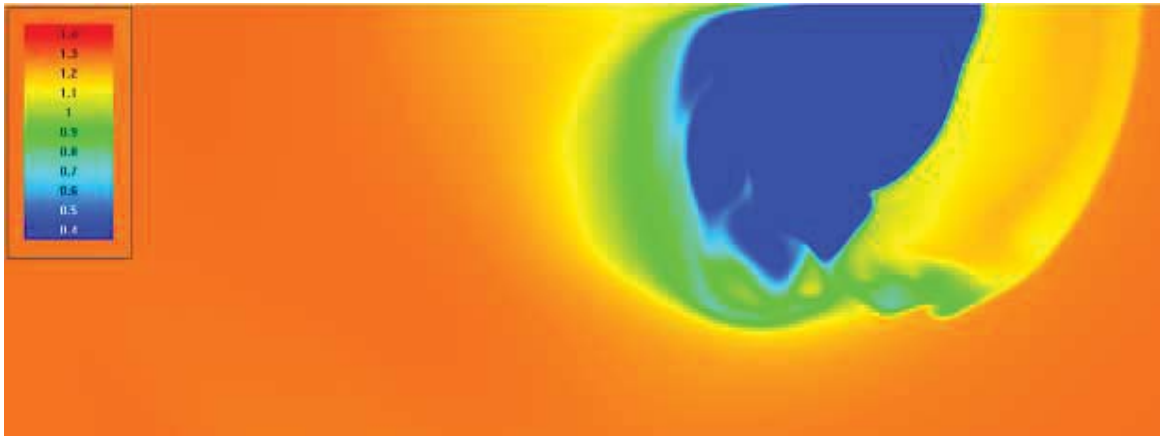
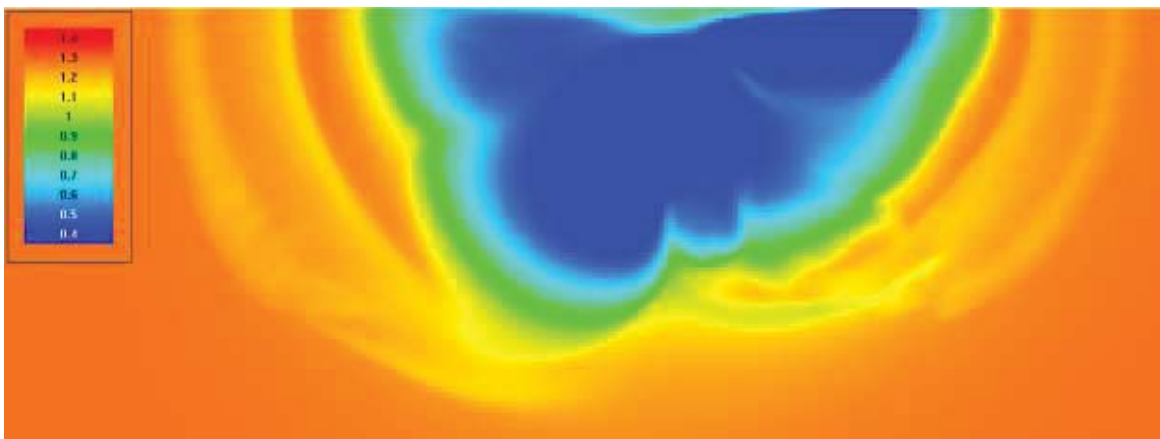


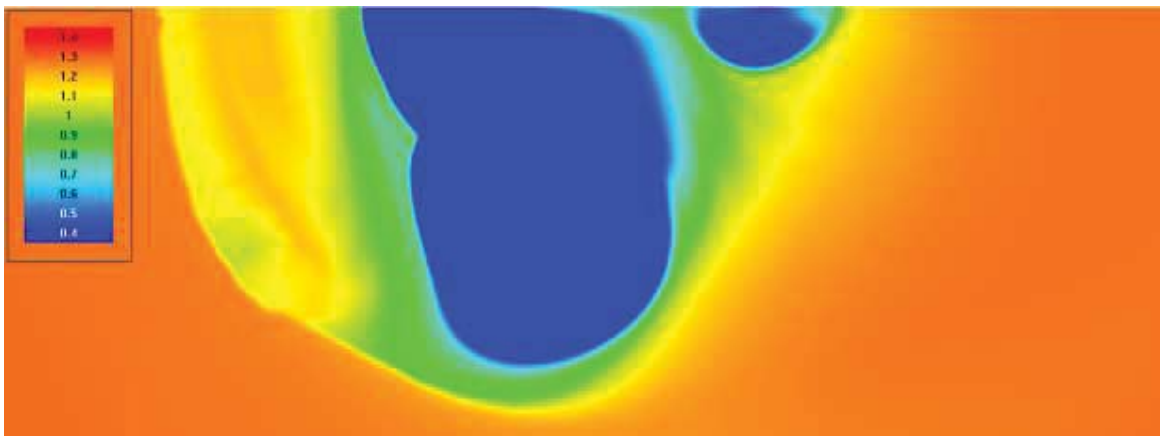
Fig.4.2.16. Density distribution (side view)



(a) R0.06 plan



(b) Density averaged over the height of computational domain (4 mm)



(c) R3 plan

Fig.4.2.17. Density distribution, 216 μ s (top view)

On the basis of previous works and results of numerical simulation the following mechanism of jet formation may be proposed. Strong shock waves from two parts of discharge channel move in intersecting directions. As a result of their interaction the direct shock occurs between them. Pressure, density and velocity of propagation of this shock is greater than these parameters of other basic shock. Also the speed of gas behind this wave is higher than usual. This results in some portion of hot low density gas leads away from main volume of afterspark channel and rarefaction zone is formed between main volume and detached gas portion. Rarefaction zone supports internal gas movement and routes it followed by fast detached gas portion. Detailed information about flow parameters at moment of rarefaction generation are presented in Fig.4.2.18. Result density field based on jet movement is presented in Fig.4.2.19. There are two fast detached low density gas portions to the left and right sides of image and main jets follow them.

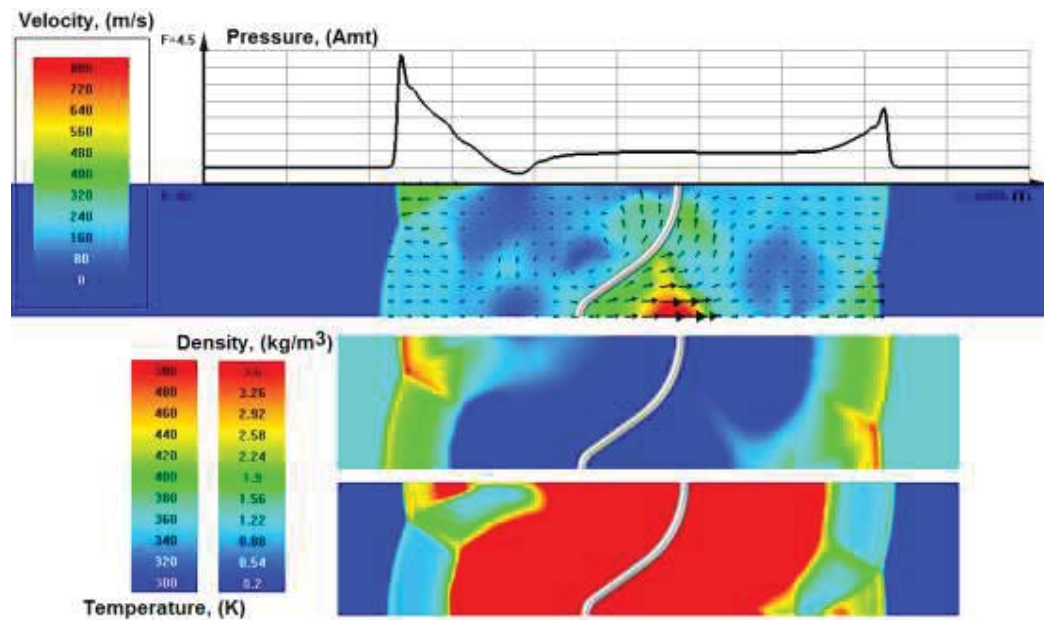


Fig.4.2.18. Results of 2nd simulation at 7.7 μ s.

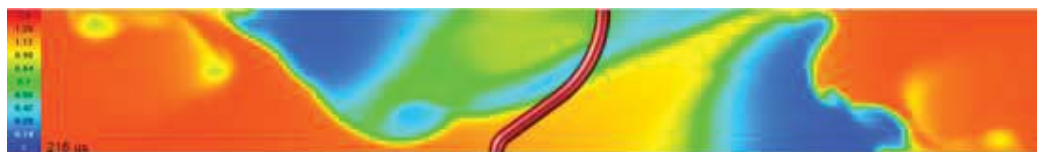


Fig.4.2.19 Density distribution of 2nd simulation at 216 μ s.

4.3. Discharge specific localization in two-component system.

The idea to be analyzed is the discharge's filament localization under non-homogeneous medium. As there was found experimentally, the discharge follows closely a boundary between two gases in the most cases at the air-fuel-plasma interaction. The explanation of this fact includes an impression that the discharge localization is managed by the rule of minimal electrical field, required for the discharge maintenance, along the line of breakdown. It can be supposed that the discharge "prefers" the path in the fuel, oxidizer or between them depending on conditions and the phase of the discharge development. For the short-pulse discharge the physical mechanism appears as the following. The first stage of the spark breakdown is the multiple streamers propagation from the "hot" electrode toward the grounded one. In case of high-power electrical source those streamers occupy a huge volume of the gas, covering all possible paths for the further development. The next phase consists of the real selection of the discharge path among the multiple channels with non-zero conductivity. It is the key point – which channel appears to be the best in terms of the current increase, i.e. possessing higher conductivity and lower inductivity. If the media is non-homogeneous the favorite path may not be the shortest one.

The idea to be analyzed is the discharge's filament localization under non-homogeneous medium. There was observed in number of experiments that the discharge follows closely a boundary between two gases in the most cases at the air-fuel-plasma interaction. There was found also [1] that the voltage on the discharge gap is increased significantly in the most cases of the air-fuel-plasma interaction. A sample of oscillograms is shown in Fig.4.3.1.

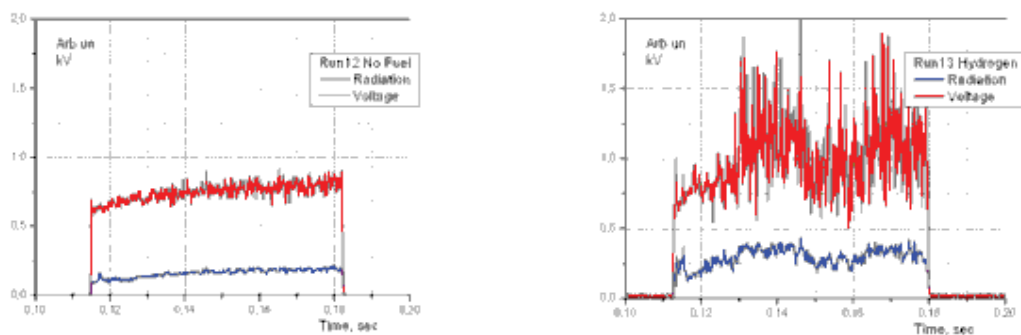


Fig.4.3.1. Voltage-radiation records of the discharge in airflow and under the hydrogen injection.

The explanation of this fact includes the idea that the discharge localization is managed by the rule of minimal electrical field, required for the discharge maintenance, along the line of

breakdown, as it shown in Fig.4.3.2 on simplified manner. It can be supposed that the discharge “prefers” the path in the fuel, oxidizer or between them depending on conditions and the phase of the discharge development. The preliminary simulation proves the possibility of such a mechanism (see result in Fig.4.3.2 - right). The complexity of the problem is due to the gas movement.

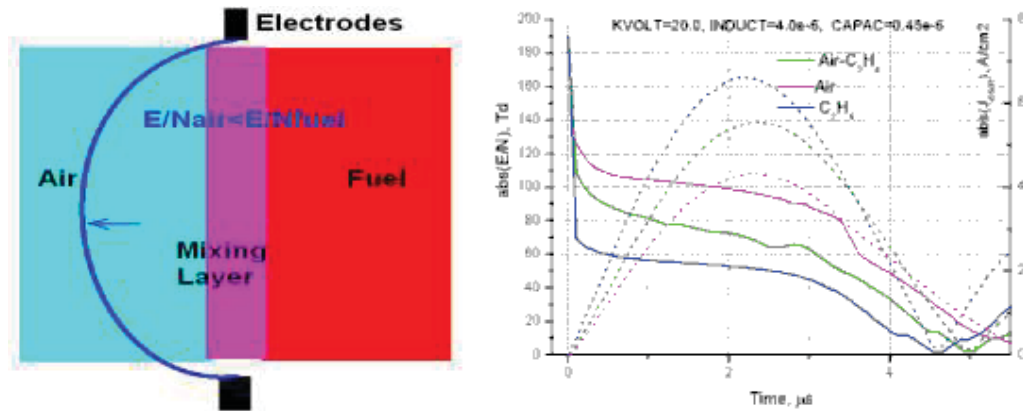


Fig.4.3.2. Scheme: why the plasma filament can move from one media to another (left). Result of the reduced field simulation at pulse discharge generation in different gases (right).

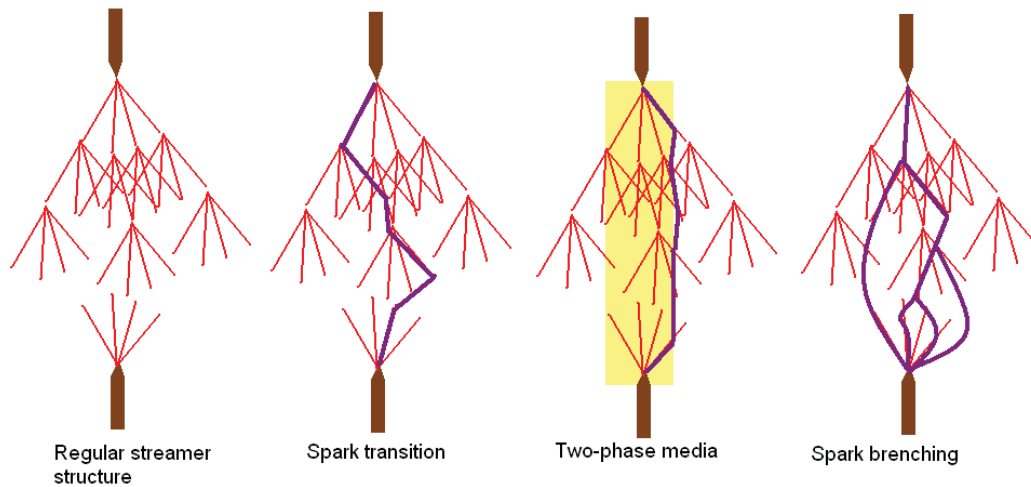


Fig.4.3.3. Scheme: how the pulse plasma filament find the boundary between two gases.

For the short-pulse discharge the physical mechanism appears as the following, see Fig.4.3.3. The first stage of the spark breakdown is the multiple streamers propagation from the “hot” electrode toward the grounded one. In case of high-power electrical source those streamers occupy a huge volume of the gas, covering all possible paths for the further development. This statement is illustrated by the well-adjusted schlieren photo of the streamers’ phase in Fig.4.3.4, where the spark phase was prevented due to the voltage reducing. The next phase consists of the real selection of the discharge path among the multiple channels with non-zero conductivity. It is the key point – which channel appears to be the best in terms

of the current increase, i.e. possessing higher conductivity and lower inductivity. If the media is non-homogeneous the favorite path may not be the shortest one. Sometimes double- and triple-channel structures were observed, as it is shown in Fig.4.3.3d.

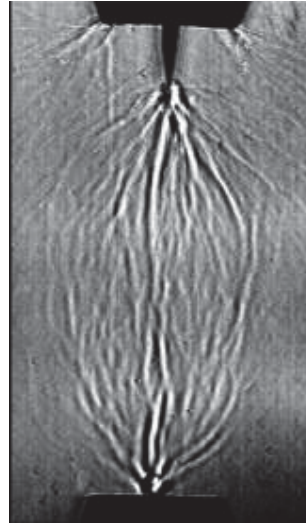


Fig.4.3.4. Schlieren photo of streamer phase of the discharge.

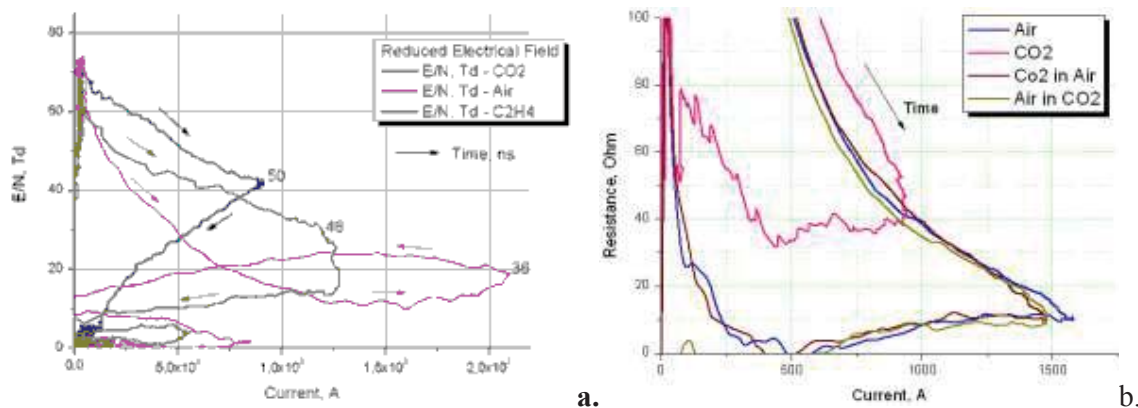


Fig.4.3.5. a - dynamics of reduced electrical field data for 100ns discharge in Air, C₂H₄, and CO₂; b – dynamics of discharge resistance in Air, CO₂, air jet in CO₂ and CO₂ jet in air.

The Fig.4.3.11 in the next subsection shows result of calculations of discharge properties in ethylene-air mixture. Here the coefficient of the ionization rate minus the rate of attachment is presented for variable reduced electrical field. Well seen that the best conditions for discharge development may be realized in reach mixture but not in air or in ethylene. This statement is confirmed by measuring history of E/N and resistance in high-current phase of the discharge at study of the discharge parameters in different gases. Besides discharges in air and ethylene the experiments were fulfilled for discharge in CO₂ (one of combustion products) and in vicinity of boundary between air and CO₂. The pulse duration was $t \approx 100$ ns, rate of the voltage rise before breakdown $dU/dt \approx 3 \times 10^{10}$ V/s, gas pressure $p = 1$ Bar, inter-electrodes gap $d = 50$ mm.

Figure 4.3.5a presents the result of reduced electrical field recalculation based on experimental data. It is seen that in first stage of the discharge the highest field is observed in CO₂, but in the second stage the higher value is realized in air. One more experimental series was carried out to compare the discharge behavior in non-homogeneous medium. The weak laminar jet of secondary gas was arranged between two electrodes: CO₂ jet in air and air jet in CO₂. The result is shown in Fig. 4.3.5b. In this particular case, when the discharge can select the path, it locates in air mostly but in immediate vicinity of secondary gas. This type of behavior was predicted by calculations of ionization rate in Air-CO₂ mixture, as it is shown in Fig.4.3.6. Of interest and for the further analysis is the fact that the localization may depend on the local electrical field: for lower field the preferable position is in CO₂, for higher field magnitude is in air.

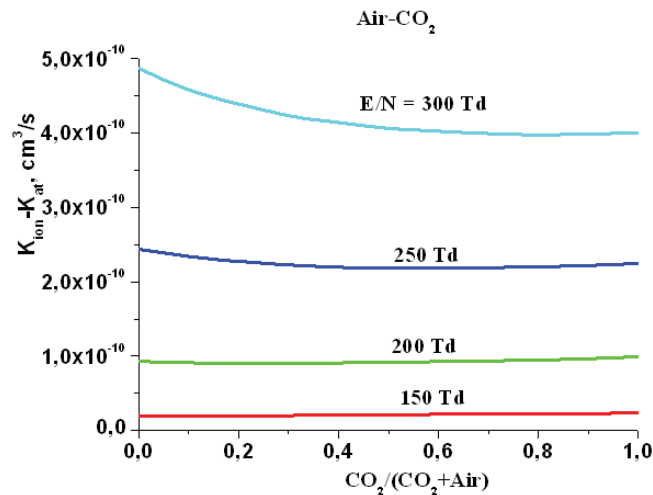


Fig.4.3.6. Calculated coefficient of ionization taking into account the electrons attachment in air-CO₂ mixture.

At the same time not all experimentally found phenomena might be explained by that mechanism of the discharge localization. In this part of work a new hypothesis was checked out. The hypothesis supposes that dynamic properties of the gases (fast breakdown) may be not the same as a static behavior. By the other words a fast change of the electric parameters could affect the discharge channel localization.

Three variants of the pulse discharge breakdown were calculated: in C₂H₄, in Air, and in C₂H₄-Air (ER = 1) mixture. A simple discharge circuit were used – capacitance (32 pF), inductivity, and the discharge channel self-consistent resistivity. The model of filamentary discharge was utilized: length 3mm, radius 1mm. Initial voltage 9.9 kV, pressure 1 Bar, temperature 300K. Concentration was considered as constant. The model includes kinetics equations, Boltzmann equation, energy equation, and equations of external circuit.

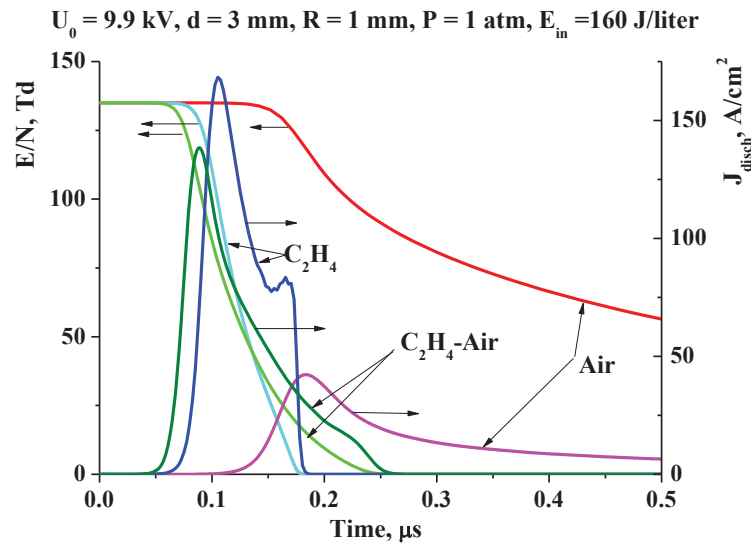


Fig.4.3.7. Dynamics of E/N and current density for the C₂H₄, Air and mixture C₂H₄-Air (ER= 1).

Results of calculation of electric field and the current dynamics are presented in Fig.4.3.7. The fastest current development is considered for the Air-fuel mixture. This fact could be posed as the important to explain the phenomena of selectivity in the discharge channel localization. The C₂H₄ molecules have a bigger ionization cross-section than molecules O₂ and N₂.

The second pike in a current curve shape for pure ethylene is the result of specific behavior of its differential conductivity. The electron drift velocity dependence on the electric field has a local minimum for the C₂H₄ as it is shown in Fig.4.3.8 (comparison of our theory and the experiment).

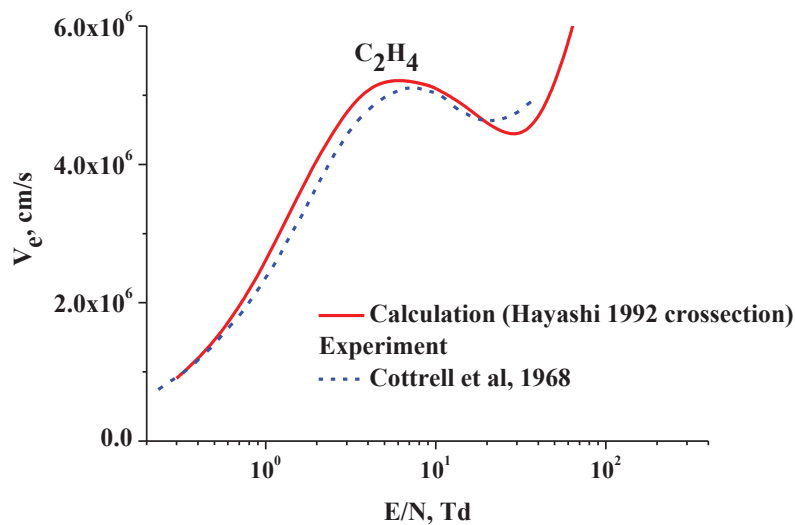


Fig.4.3.8. Drift velocity of electrons vs reduced electric field in C₂H₄. Solid line – calculation based on cross-sections (Hayashi 1992), dashed line - experiment (Cottrell et al, 1968).

Figures 4.3.9 and 4.3.10 show dynamics of the electron concentration and the discharge channel resistance for C₂H₄, Air, and C₂H₄-Air (ER = 1 mixture). Well seen in Fig.4.3.9 that the electron concentration grows much faster in plasma of C₂H₄-Air mixture.

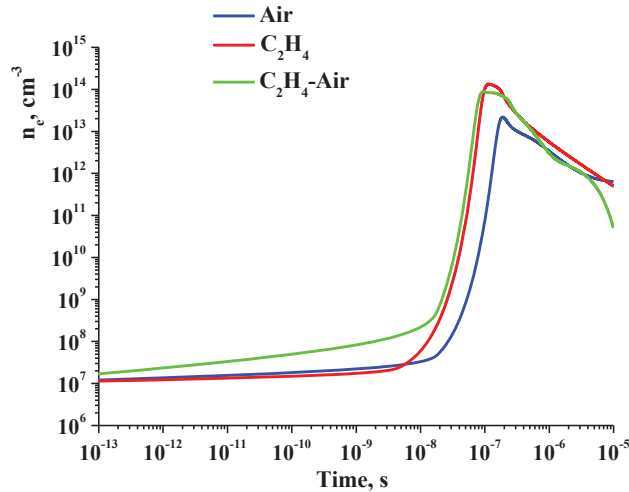


Fig.4.3.9. Electron concentration vs time for C₂H₄, Air и C₂H₄-Air (ER = 1).

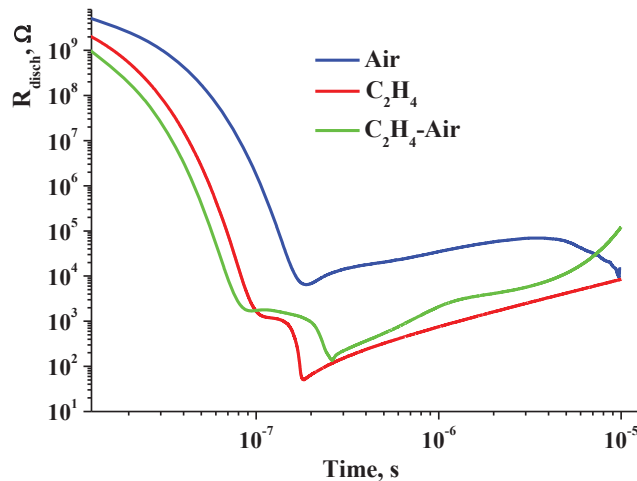


Fig.4.3.10. Dynamics of the discharge channel resistivity on initial stage of breakdown for C₂H₄, Air, and C₂H₄-Air (ER = 1).

At the same time not all experimentally found phenomena might be explained by that mechanism of the discharge localization. In this part of work a new hypothesis was checked out. The hypothesis supposes that dynamic properties of the gases (fast breakdown) may be not the same as a static behavior. By the other words a fast change of the electric parameters could affect the discharge channel localization.

Discharge evolution in C₂H₄/air mixtures in growing voltage applied

The pulse discharge in co-flowing gas jets has a trend to develop along the boundary between jets composed of two different gases (air, CO₂, He). This effect may be important in plasma assisted combustion technology as far as correlation between plasma and gas-dynamic movement may enlarge gas mixing rate and make ignition initiation more effective. In order to estimate reality of such effects, the evaluation of plasma properties in fuel/air mixtures of various compositions was performed numerically. Here C₂H₄/air mixtures are considered with variable composition. The most important quantity governing discharge breakdown is the rate of electron multiplication equal to difference between electron impact ionization and attachment rates.

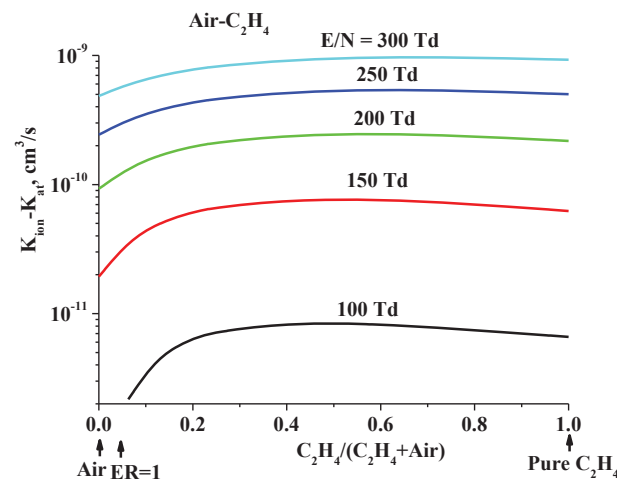


Fig.4.3.11. Electron multiplication rate as a function of gas composition for various values of the reduced electric field strength E/N , $ER=1$ is stoichiometric mixture (6.25% of C₂H₄)

Figure 4.3.11 shows the difference between the total ionization and attachment rates as a function of relative ethylene concentration at various E/N parameter values. Ionization and attachment rates were calculated from numerical solving of electron Boltzmann equation for steady state conditions in two-term approximation for the electron velocity distribution function [2]. The necessary electron scattering cross sections for N₂, O₂ and C₂H₄ molecules were taken from refs. [3-5]. It is seen that at $E/N = 100$ and 150 Td (1 Td = 10^{-17} V·cm²) the multiplication rate as a function of ethylene concentration has a maximum around its value 0.5. It means that in a course of mixing of two jets most probably the discharge would be located within a region with nearly equal concentrations of ethylene and air.

Under conditions of experiment the discharge evolves to a high current form. Then, numerous secondary processes leading to electron multiplication and destruction of negative

ions start to play an important role. Much more extended model is required to describe correctly plasma dynamics at the later stage. We took as a basis the model formulated in ref. [3], which is applicable for modeling uniform non-thermal plasma in air, and added the processes associated with appearance of the new components.

We have calculated time evolution of plasma in electric field growing in time as

$$U=U_m \cdot \sin(\pi t/5);$$

here U_m , the amplitude of the voltage applied, t is the time measured in microseconds. In calculations $U_m=100$ kV, the inter-electrode distance $d=3.25$ cm, and duration of voltage pulse wave quarter is $t=T/4=2.5\mu s$, the initial gas temperature was set equal to 300 K, and pressure 1 Bar. The initial electron concentration was taken equal to 100 cm^{-3} . Calculations were performed until the discharge current density approaches value about 260 A/cm^2 . At higher current densities our model is inapplicable.

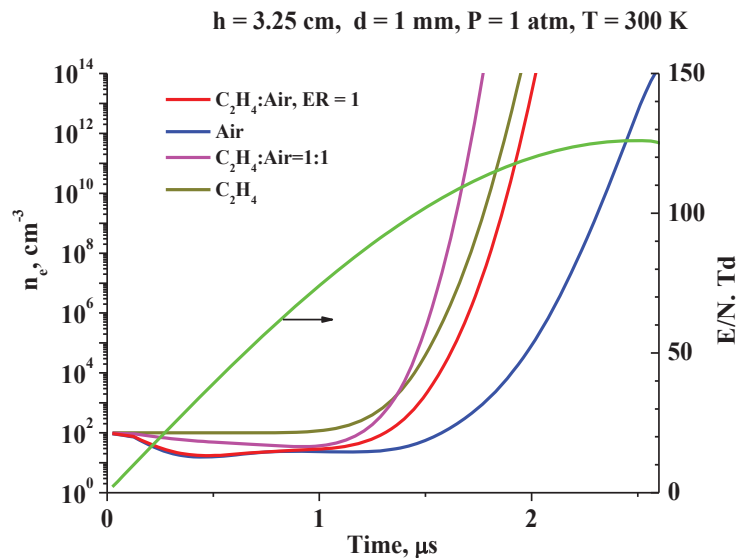


Fig.4.3.12. Electron number density (left axis) evolution for various gas compositions, and the reduced electric field strength (green line, right axis) as a function of time.

Figure 4.3.12 shows time evolution of the electron number density for various gas compositions. In the pure ethylene, the electron number density grows monotonously, while dilution by air leads to appearance of its decreasing at short times. This effect is explained by the role played by three-body and dissociative attachment of electrons to O_2 molecules. The most interesting effect observed in Fig.4.3.12 is appearance of crossing of curves for pure ethylene and C_2H_4 :air =1:1 mixture. The ionization rate (in absence of the attachment) for pure ethylene is the highest. Electron attachment processes with addition of air lead to decrease of

the electron number density at times shorter than 1 μs . Then detachment processes are coming into force due to concentration growth of negative ions and excited molecules, which result in compensation of the attachment processes. As a result, the electron multiplication rate for $\text{C}_2\text{H}_4:\text{air}=1:1$ is becoming larger than for pure ethylene at E/N value about 40 Td.

The appearance of two minima in curve for electron concentration is explained by competition of three-body and dissociative attachment processes, rates of which have opposite dependence on E/N . At low E/N the three-body attachment dominates and leads to falling down the electron number density. With E/N growth it diminishes resulting in some growth of electron number density. With further increase of E/N the dissociative attachment comes into play and diminishes the electron number density again. Transition to final growth of n_e is due mainly to effect of the detachment processes.

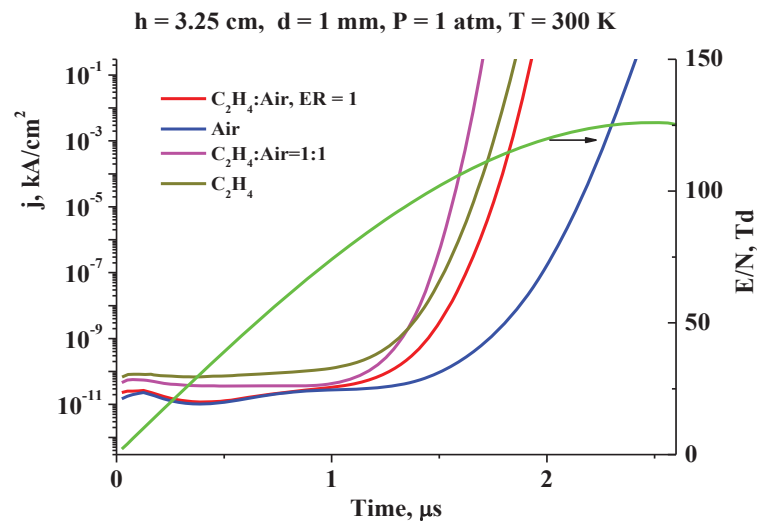


Fig.4.3.13. Discharge current density (left axis) evolution for various gas compositions, and the reduced electric field strength (green line, right axis) as a function of time.

Evolution of electric current density shown in Fig.4.3.13 for various $\text{C}_2\text{H}_4/\text{air}$ mixtures is qualitatively similar to the electron concentration evolution in Fig.4.3.12. Slight differences in shapes of curves in Fig.4.3.12 and Fig.4.3.13 originate from the E/N dependence of electron drift velocity shown in Fig.4.3.14. Time variation of the voltage applied results in change in time of the electron drift velocity, which is shown for convenience in Fig.4.3.15 as a function of time. It is seen, in particular, that a slight decrease of the electric current at time shorter than 0.5 μs is explained by the decrease of the drift velocity. Fig.4.3.13 demonstrates that the current density for mixture grows at the start slower than in pure ethylene, then accelerates and approach the same value as for the pure ethylene at about 1.4 μs and since that moment grows

faster. This fact allows us to expect that the discharge development in the C_2H_4 partially mixed with air will prefer the path in space with nearly equal concentrations of ethylene and air. Moreover, the current channel should move with time from a region with high ethylene concentration to a region with gas composition C_2H_4 :air=1:1.

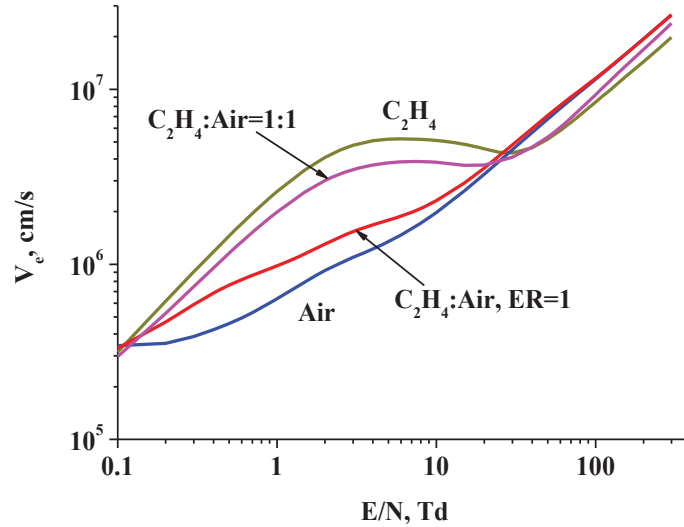


Fig.4.3.14. Electron drift velocity as a function of E/N for various C_2H_4 /air mixtures.

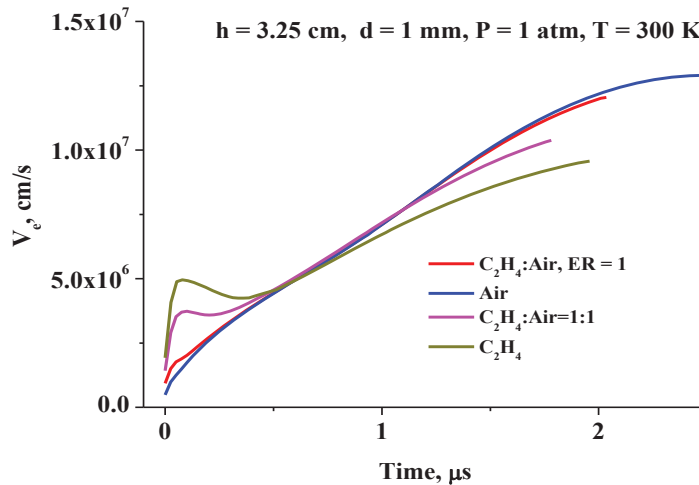


Fig.4.3.15. Electron drift velocity as a function of time for various C_2H_4 /air mixtures.

Finally, the electric current evolution in a filament of 1 mm diameter in a discharge with cathode-anode spacing 3.25 cm is shown in Fig.4.3.16 at discharge voltage growing up to 100kV for various gas compositions using linear scales for the current and time.

In the linear-scale plot, the discharge breakdown time defined as a moment of current approaching 2 A is ordered for mixtures under consideration as follows: 1.77 μs for C_2H_4 :air =1:1; 1.95 μs for pure C_2H_4 ; 2.02 μs for C_2H_4 :air= 6.25:93.75 (ER=1); 2.59 μs for dry air. Thus

our model predicts the lowest breakdown voltage (94 kV) for the mixture $C_2H_4:air = 1:1$. Our study for the short (less than $1.3\mu s$) times demonstrates that at earlier stage of evolution the discharge current density grows more rapidly in pure ethylene. It means that the plasma filament in a course of development may wander in space searching best local conditions for the breakdown.

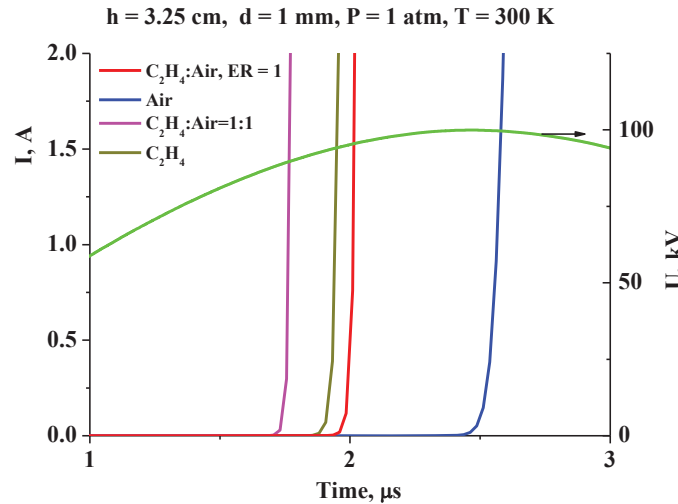


Fig.4.3.16. Electric current evolution in a filament of 1 mm diameter in a discharge with cathode-anode spacing 3.25 cm for various gas compositions. The discharge voltage (green curve, right axis) grows as $100 \text{ kV} \cdot \sin(\pi t/5)$.

References to the section 4.3.

1. Sergey B. Leonov, Dmitry A. Yarantsev, Campbell Carter, “Transversal Electrical Discharge as a New Type of Flameholder”, AIAA-2008-2675.
2. Shkarofsky I. P., Johnston T. W., Bachynski M. P., The particle kinetics of plasma, Addison-Wesley Publishing Company, London, 1966.
3. Akishev Y.S., Deryugin A.A., Karalnik V.B., et. al., Numerical simulation and experimental study of an atmospheric-pressure direct-current glow discharge, *Plasma Phys. Rep.*, 1994, 20, 511-524.
4. Ionin A.A., Kochetov I.V., Napartovich A.P., Yuryshev N.N., Physics and engineering of singlet delta oxygen production in low-temperature plasma, *J. Phys. D: Appl. Phys.*, 2007, 40, R25-R61.
5. Hayashi M., Electron collision cross sections determined from beam and swarm data by Boltzmann analysis in “Nonequilibrium Processes in Partially Ionized Gases” Eds. M. Capitelli and J. N. Bardsley, *NATO ASI Series B: Physics* v. 1990, 220, 333-340, Plenum Press, N-Y.

4.4. Rayleigh-Taylor and other instabilities of plasma channel due to 1D and 2D computational analysis

Decay of the discharge channel is a complex process which depends on several factors. Different research groups in their paper [1–4] consider two main reasons of turbulent gas cooling of low density channel after discharge breakdown. These reasons are Rayleigh-Taylor instability and different geometrical deviations of discharge filament from ideal cylinder. Previously thought that the thermodynamic conditions in the discharge prevent appreciable growth of Rayleigh-Taylor instability [1], but contemporary experimental and numerical results suggest the importance of this effect at the early stage of the low density channel decay [4].

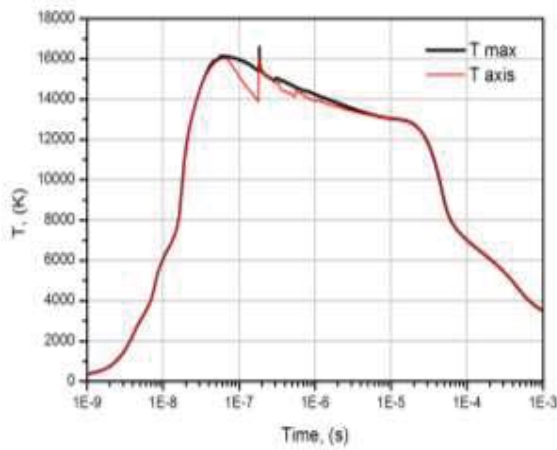


Fig.4.4.1. Temperature vs time

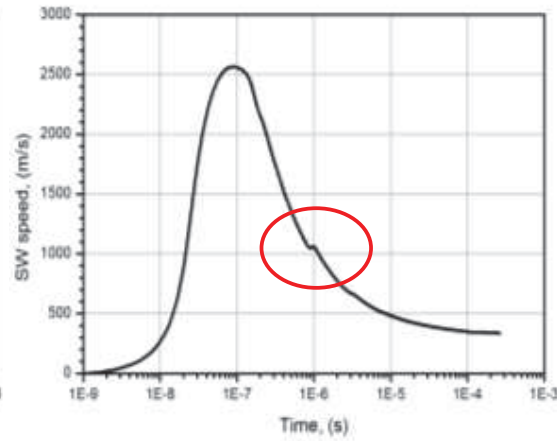


Fig.4.4.2. Shock wave speed vs time

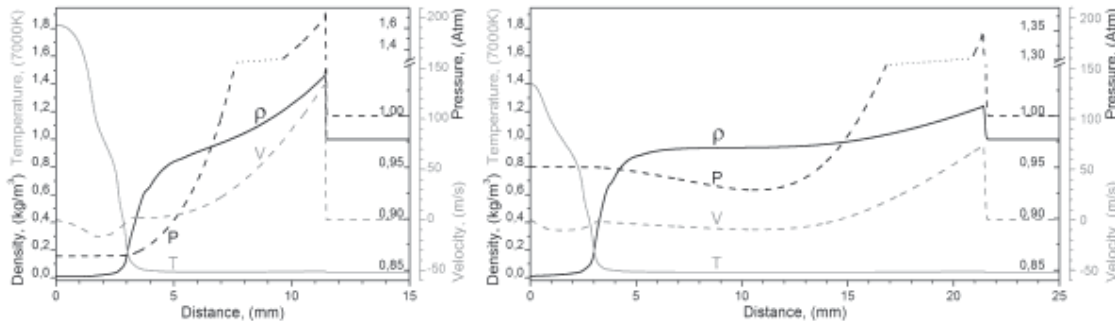


Fig.4.4.3. Profiles of gas parameters at 20 μs and 45 μs.

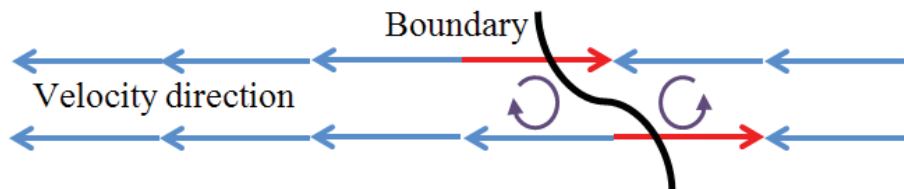


Fig.4.4.4. Rayleigh-Taylor instability on a curved boundary

Rayleigh-Taylor (RT) instability is usually considered as a process on a boundary between two fluids (gases or liquids) with different density. Accelerated motion of a real boundary with fluctuation roughness or bends accompanied by vortex motion and increasing of the border length. This is two main factors to improve mixing of different gases: increase of the border length by vortex motion results in the increase of diffusion mixing area.

In the case of discharge breakdown we have only one gas, but at the initial time there are two highly different areas. Breakdown filament has very low density (about 0.03 kg/m^3) and high temperature (more than 5000K). Surrounding gas is close to the initial, and there is strong density gradient between him and the filament. So this situation can be considered like two different gases. The evolution of the Rayleigh-Taylor instability is possible then the condition $\nabla p \nabla \rho < 0$ is satisfied at the channel boundary. It was shown that this condition is satisfied at $100 \text{ } \mu\text{s}$ after discharge for conditions that are close to the considered conditions [4].

1D numerical simulation similar to described in article [4] was performed for typical energy deposition 300 mJ per 10 mm , described in Fig.4.2.4(a). Simulation was performed by using FlowVision 3.08 software. Thin sector $0,57^\circ$ ($100 \text{ mm} \times 1 \text{ mm}$) with thickness 0.01 mm was used as computational domain. Pressure 1 atm and temperature 283 K was fixed on smallest boundary. Symmetry condition was used on all other faces of domain. The computational grid is a set of 10000 cells with concentration to an axis aligned along the radius. So the spatial resolution is 5 cells per 0.01 mm near axis. Model of turbulence was not used because of high spatial and time resolution. Radius of volumetric heat source was 0.255 mm .

Two interesting facts were found by 1D simulation. 1st one is the maximum temperature is achieved not at heat source enabled but some time later because the fast reverse motion of the gas to the axis and axis pressure increase. Time dependencies of the maximal and axis temperature are presented in Fig.4.4.1. 2nd fact is the internal pressure wave moves from axis to shock wave and catches up and speeds up the shock wave at the time $1 \text{ } \mu\text{s}$. Time dependency of the shock wave speed is presented in Fig.4.4.2.

Gas flow follows a shock wave in radial direction and it is accompanied by a decrease of pressure on the axis of breakdown filament. This leads to a reverse movement of some part of the gas inside and around the filament starting from $20 \text{ } \mu\text{s}$. Gas motion to the axis of channel causes pressure increase in the center of afterspark filament and the negative pressure gradient crosses positive density gradient starting from $45 \text{ } \mu\text{s}$: $\nabla \rho \nabla P < 0$. Profiles of gas parameters at $20 \text{ } \mu\text{s}$ and $45 \text{ } \mu\text{s}$ are presented in Fig.4.4.3. Due to pressure equalization two turning points of velocity vectors are formed at $90 \text{ } \mu\text{s}$ near the filament boundary: 1st inside and 2nd outside

filament. This leads to increasing of initial perturbations. This process is schematically shown in Fig.4.4.4 for 2D case. Consequently possible initial distortions are highly important for the development of instability.

Any shape deviations of the discharge channel from the ideal infinitely long cylinder can lead to turbulent disturbances. Let us consider some variants.

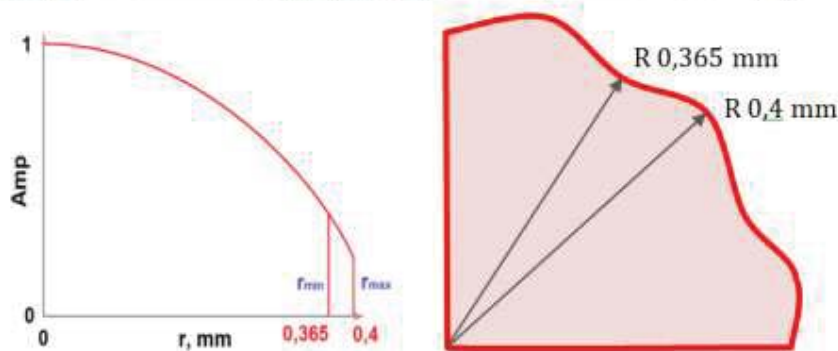
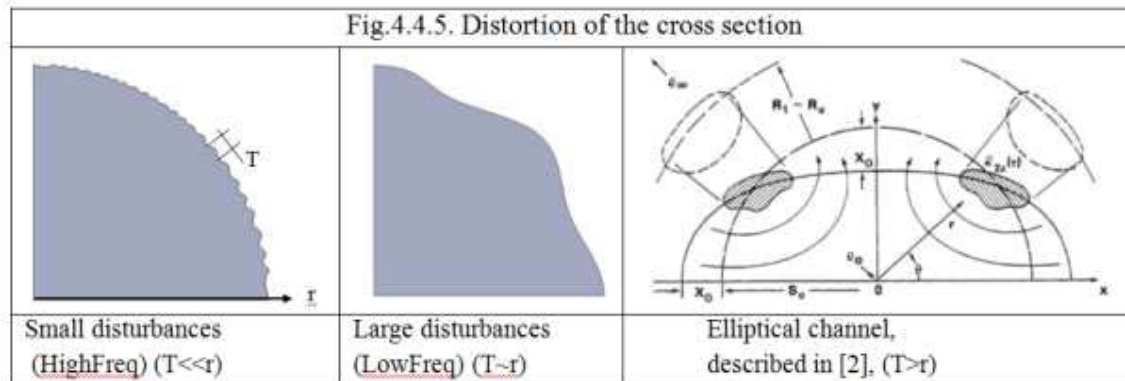


Fig.4.4.6. power density radial profile and geometry of heat source for 2D simulation

The vorticity equation of fluid dynamics describes evolution of the vorticity,

$$\frac{d\xi}{dt} + \xi(\nabla v) = (\xi \nabla) v + \left(\frac{\nabla \rho \times \nabla p}{\rho^2} \right)$$

$$\xi = \nabla \times v \quad - \text{vorticity}$$

and it is clearly seen that $\nabla \rho \times \nabla p$ term is a main source of vorticity. In the case of elliptical energy contour pressure distribution and velocity field become to cylindrical symmetry while the density distribution remains elliptical. So we obtain a field in which this term is not equal to 0. It was shown by Boris and Picone in paper [2] that elliptical distortion results in 4 large vortices.

In the case of low frequency disturbances the same mechanism can be realized. But the size of distortion is smaller than radius of spark channel and it is possibility to increase the distortions by Rayleigh-Taylor instability. 2D numerical simulation was provided in FlowVision software for LowFreq case geometry presented in Fig.4.4.5. Spark discharge was modulated by volumetric heat source. Maximal radius was 0.4 mm, minimal radius was

0.365 mm, radial profile is presented in Fig.4.4.6, and time dependence of the power density was used the same as in several previous simulations (see Fig.4.2.4(a)). Model of turbulence was not used because of high spatial and time resolution. Some results of this numerical simulation are presented in Fig.4.4.7. It is clearly seen in Fig.4.4.7(a), that vortex like gas motion formed at 100 μ s time and it corresponds to the gasdynamic process described in section devoted to 1D calculation of Rayleigh-Taylor instability. So we can conclude that initial vorticity produced by RT instability then develops to significant boundary disturbances, and all evolution depends on initial geometry distortion and power release, but we only can suppose these parameters because there are no experimental information about spark cross section and radial power profile.

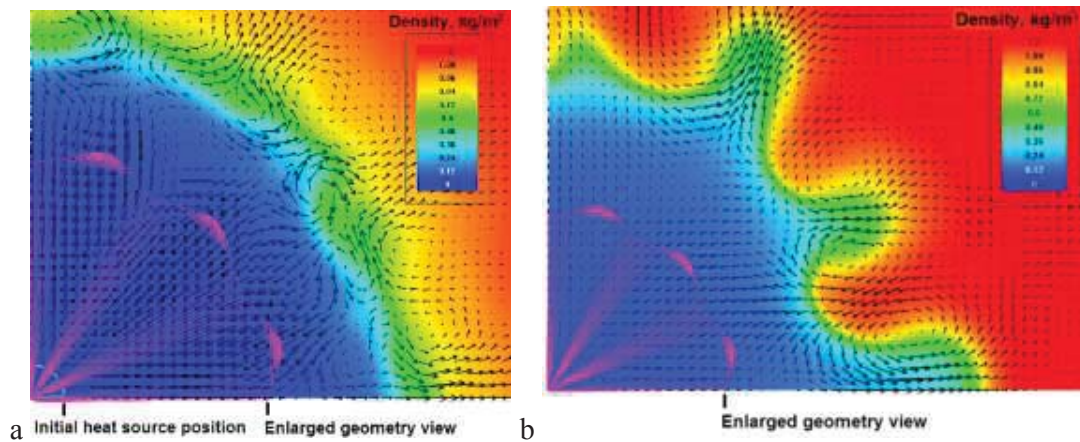


Fig.4.4.7. Simulation results: a – 100 μ s, b – 2 ms

However there is a lot of experimental information about lengthwise spark distortions (see Fig.4.4.8). Initial distortion and separate stages of disturbance development was investigated by photo and Schlieren visualization consequently in a large number of different research groups. Major shift was described in part 4.2: shock wave interaction produces a zone of low pressure behind a shock wave. This leads to a significant gas motion following the zone of SW interaction, and then it causes vortex generation. Typical pressure distribution for major bend at 7.7 μ s is presented in Fig.4.2.15. Results of provided numerical simulation are in a good agreement with experimental Schlieren visualization (see Fig.4.3.4.).

Local shift was earlier described in paper [1-2]. In this case the flow field approaches cylindrical symmetry about the center of mass (z -axis) while the density distribution is offset from the z -axis by X_0 , which varies with position along the z -axis. Supposedly this disturbance formation is also accelerates by RT instability.

Filament constriction is a very interesting type of lengthwise spark distortion. Presumably, it is observed in several experiments with increased spatial resolution of photo and Schlieren technique (see Fig.4.4.9). Probably it is a main type of initial density fluctuations for Rayleigh-Taylor instability evolution. 2D numerical simulation of this case was provided for refinement of this assumption. Simulation was performed by using FlowVision 3.08 software. Geometry of calculation domain was 1° sector of the cylinder with $h=3.4$ mm height (h along z). Geometry of axisymmetric heat source is presented in Fig.4.4.10. Value of power density $P(z)$ is satisfies to the condition: $P(z)S(z)\Delta h = \text{const}$, where $S(z)$ is the cross sectional area of heat source geometry. Model of turbulence was not used because of high spatial and time resolution.

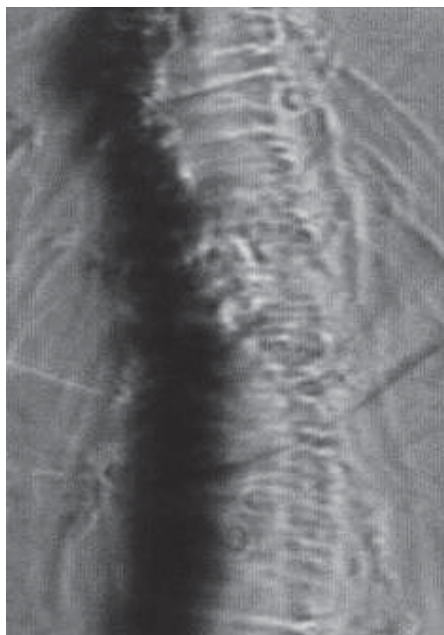
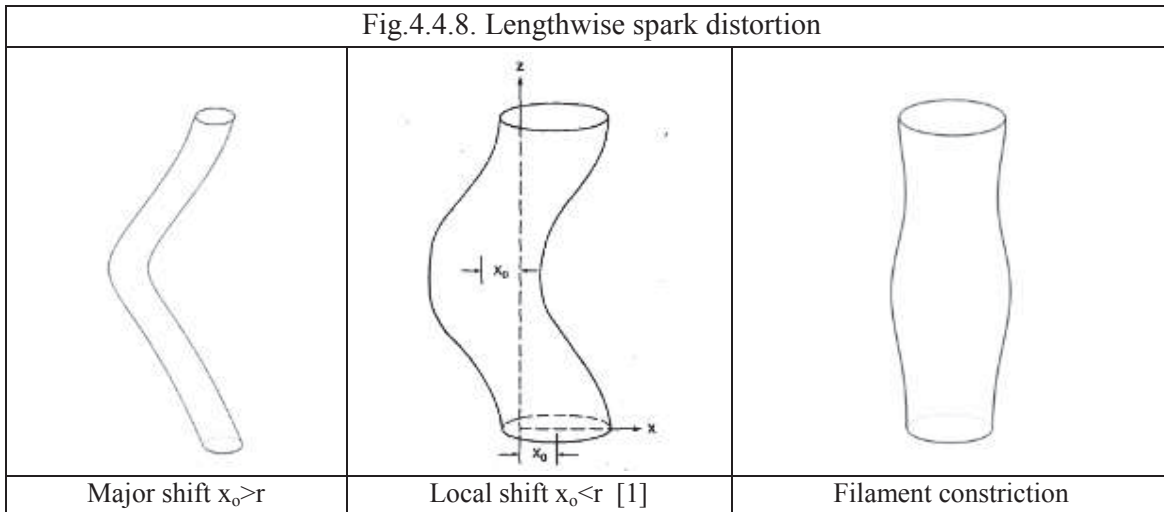


Fig.4.4.9. Enlarged Shlieren image

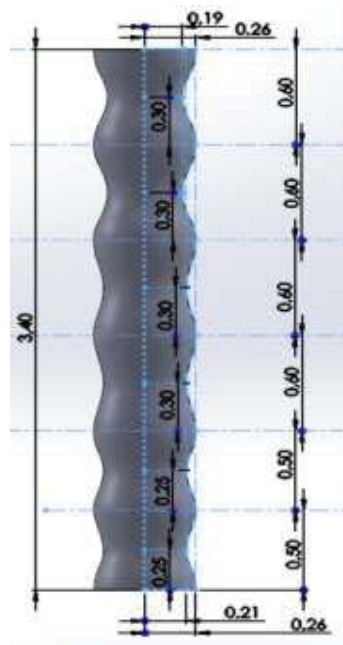


Fig.4.4.10. Geometry of heat source

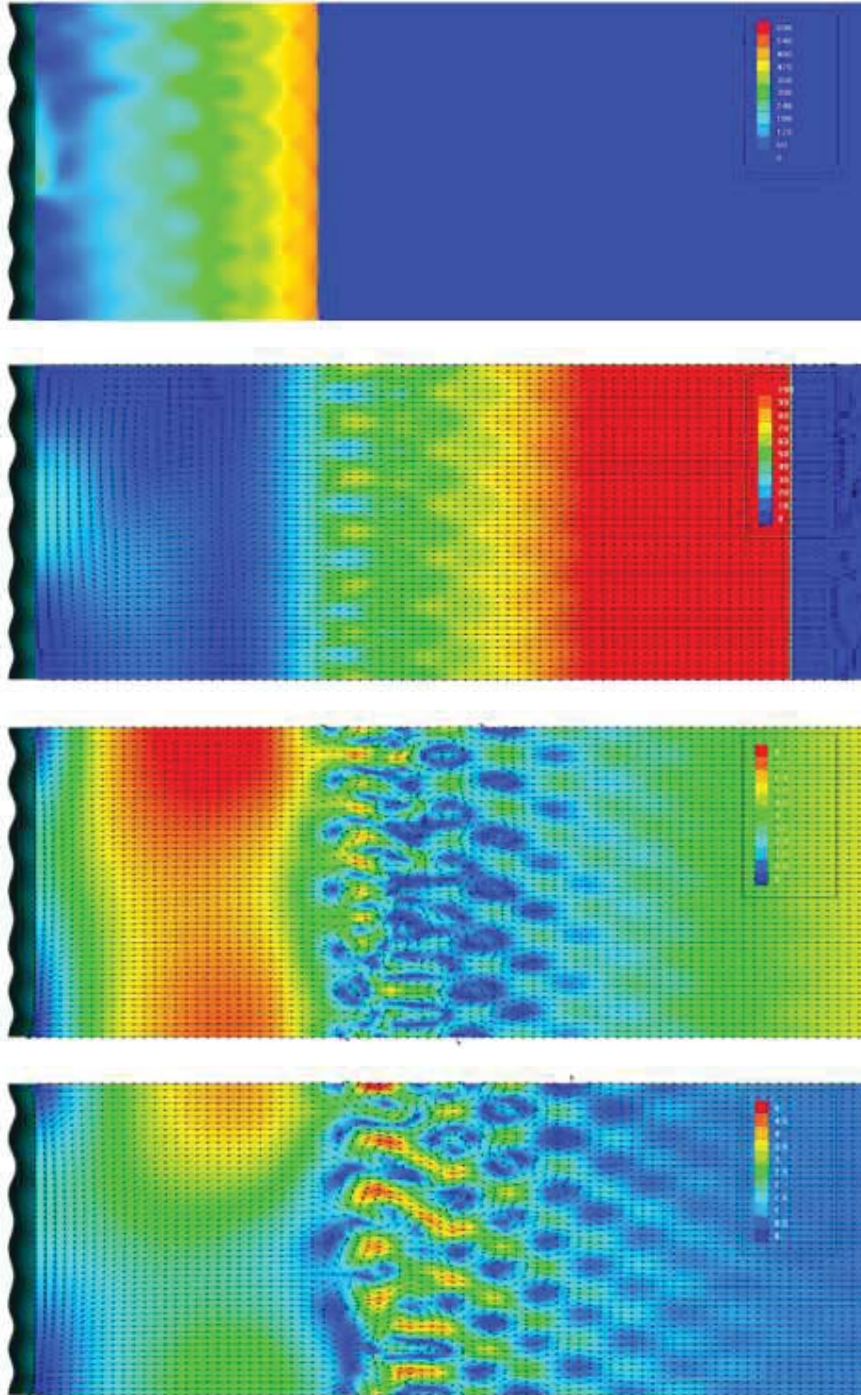


Fig.4.4.11. Velocity field (m/s): 2, 10, 50 and 100 μ s

As it shown in Fig.4.4.11, vortex structures was formed at the time of RT-instability development: 50-100 μ s. Results obtained are significantly closer to the proposed scheme presented in Fig.4.4.4. The density field is presented in Fig.4.4.12 and demonstrated the increase of interface between the main low density core and dense medium.

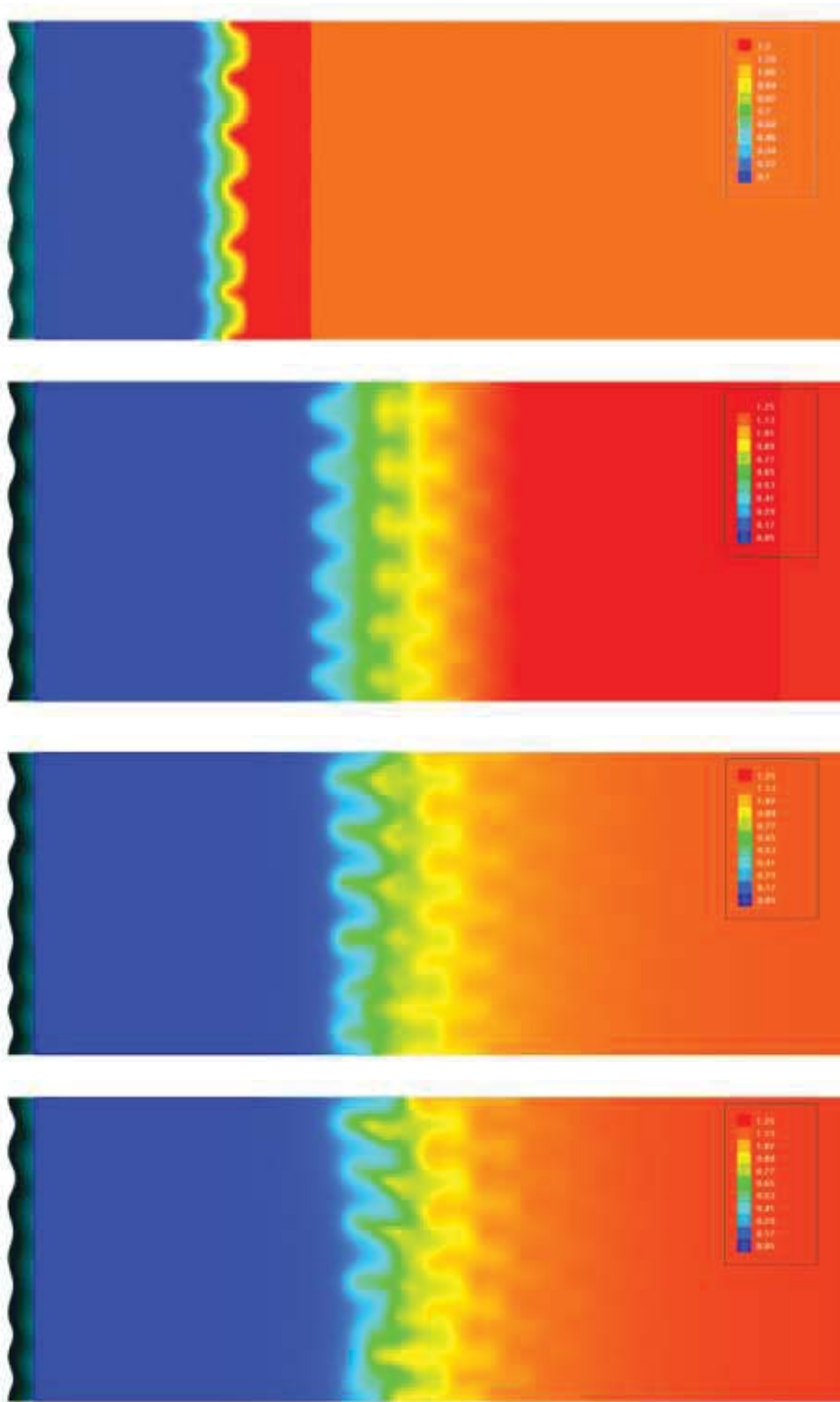


Fig.4.4.12. Density (kg/m³): 2, 10, 50 and 100 μ s

Ramification of spark discharge channel and double (multiple) pulses also can cause additional vorticity. One of possible reason of additional vorticity can be Richtmyer–Meshkov instability (RMI). RMI is an extreme case of Rayleigh-Taylor instability: RMI occurs when an interface between fluids of differing density is impulsively accelerated, e.g. by the passage of a

shock wave. So then shock wave from one branch (or pulse) passes through the density gradient of second branch (or pulse), the Richtmyer–Meshkov instability may occur, if the shock wave is strong enough. And all previous disturbances of initial spark filament form are possible sources of RMI development.

Additional gas motion is also caused by finite length of spark filament. Directed movement toward the center of the discharge gap is occurred after spark discharge breakdown. Experimental and numerical confirmations of this effect are presented in Fig.4.4.13. Regions S1 and S2 are free from disturbances near the electrodes that are clearly seen in Schlieren visualization, and velocity field obtained by CFD for finite spark confirms this result.

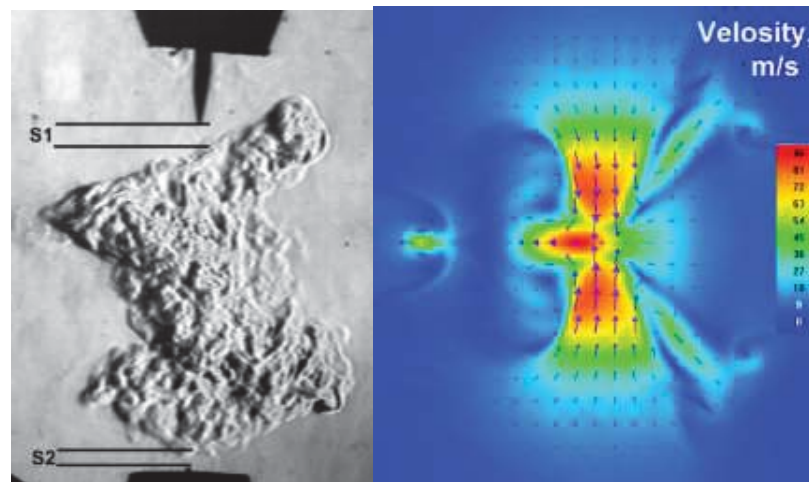


Fig.4.4.13. Gas movement toward the center of the discharge gap

Reference to the section 4.4:

1. *Picone J.M., Boris J.P., Greig J.R., Raleigh M., Fernsler R.F.* – Convective cooling of lightning channels // NRL Memorandum Report 4472, 1981
2. *Boris J.P., Picone J.M.* – Vorticity generation by asymmetric energy deposition in a gaseous medium // NRL Memorandum Report 4854, 1982
3. *Greig J.R., Pechacek R.E., Raleigh M.* – Channel cooling by turbulent convective mixing // NRL Memorandum Report 5280, 1984
4. *Shneider M.N.* - Turbulent decay of after-spark channels // Phys. Plasmas 13, 073501 (2006)

4.5. Comparison of simulation and experimental data.

On the first stage of expansion ($t < 50 \mu\text{s}$) the post-discharge channel looks quite classical: cylindrical thermal cavity. At $t \approx 80\text{-}150 \mu\text{s}$ (depending on conditions) the shape of the after-spark channel occurs unstable as shown in Fig.4.5.1. The physical mechanism of this instability was determined in [1-2]: cooling of the axial zone leads to the pressure decrease with sequential gas reverse movement. Such a movement occurs unstable due to the Rayleigh-Taylor mechanism. The graph in Fig.4.5.1 shows comparison between the experimental and computational data that proves the fact of the reverse flow.

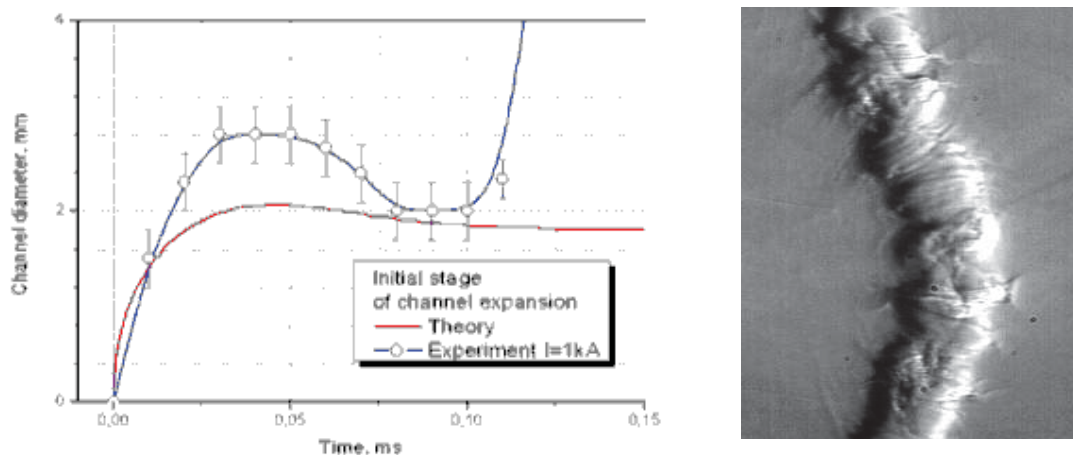


Fig.4.5.1. Dynamics of the after-spark channel expansion and schlieren photo of the disturbed zone in early stage of instability development.

The later stage of expansion can be characterized by generation of intensive lateral jets followed by fast turbulization of significant volume of the gas (the diameter is inter-gap distance, approximately). The analysis of experimental data gives some not obvious results concerning the size of disturbed zone: its value occurs several times bigger than it could be in accordance with laminar or turbulent diffusion mechanisms. The result of measurements and of respective simulation is presented in Fig.4.5.2. It is well seen that the second phase of expansion is not predicted by the model. An observation of the experimental graph allows us to conclude two important points: the diameter of the plasma zone after the fast expansion is about $d = 8 \text{ mm}$, and the mean “velocity” of the plasma disturbances expansion on the phase of jets generation is more than $V = 100 \text{ m/s}$ under the conditions of this experiment. The data on the base of fast-response pressure transducers have verified the data of schlieren observations as a whole.

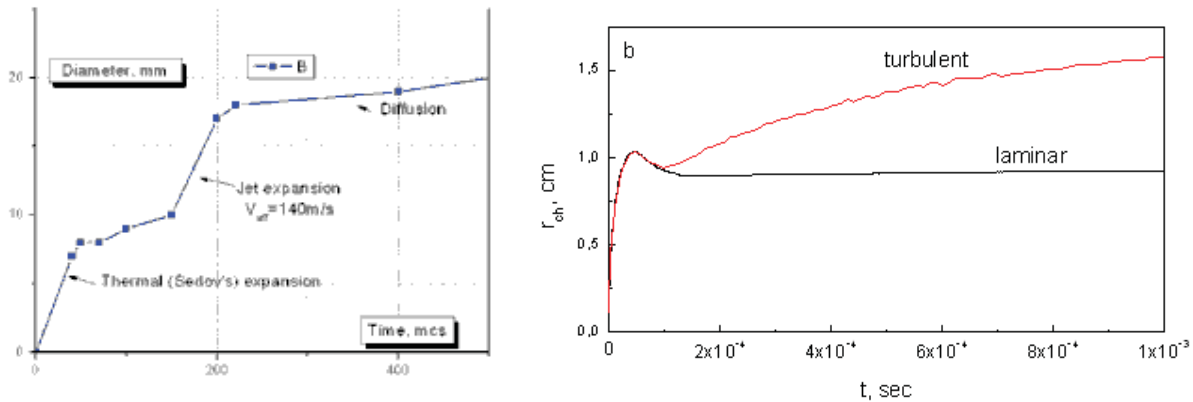


Fig.4.5.2. Plasma disturbance expansion as a function of time. Experiment (left) and simulation (right). Air, $P_0=1$ Bar; initial flow velocity $V=0$.

All theoretical results presented below are obtained on a basis of theoretical model proposed in [10]. This model describes the spark (pulsed arc) development for the given current pulse as well as cooling down of a post-discharge channel with accounting of the generation and dissipation of the turbulent flow. Theoretically predicted threshold for the afterspark channel stabilization at experimentally specified conditions was about $I_{res}=3$ A as shown in Fig.4.5.3, where the calculated gas temperatures at the channel axis are shown for different values of I_{res} .

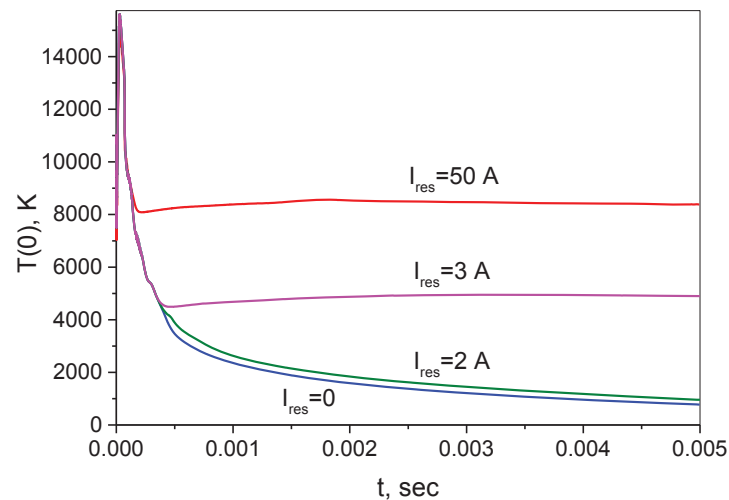


Fig.4.5.3. Calculated temperature on the channel axis. Cases $I_{res}=0$ and 50 A correspond to a current pulses shown in section 5.

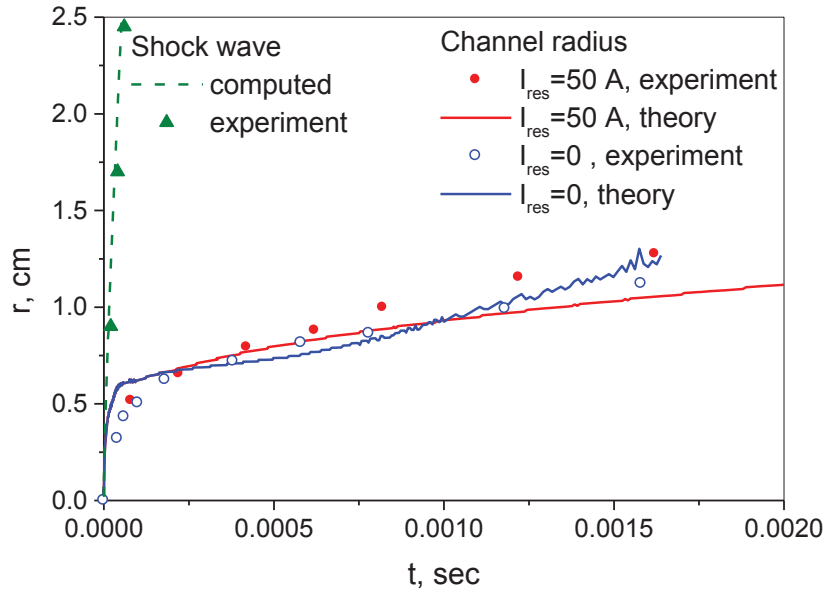


Fig.4.5.4. Comparison of the computed channel effective radii ($\rho(r,t) / \rho_0 \leq 0.85$) with the corresponding data obtained with the schlieren-streak images. The measured and computed shock wave positions are shown.

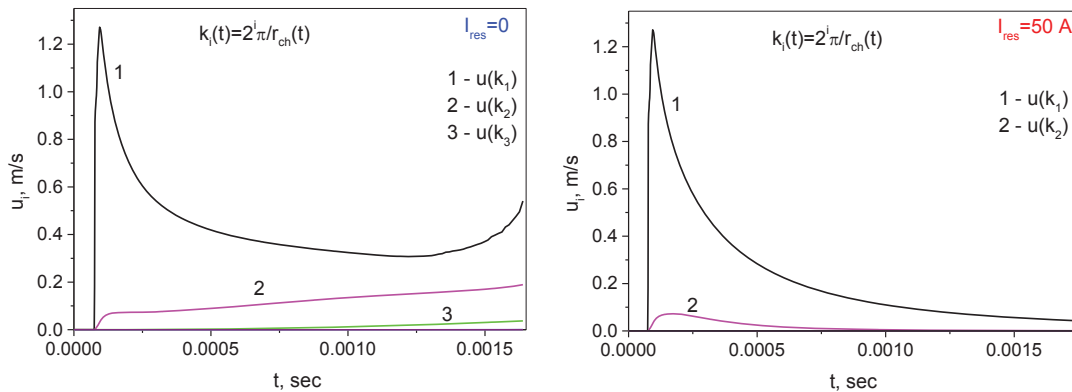


Fig.4.5.5. Computed turbulent velocity spectrum at $I_{res}=0$ and 50 A.

It is interesting to compare the velocity spectrum of the turbulent pulsations which develops in an afterspark channel. We can see that a small-scale spectrum develops in time (Fig.4.5.5, left) at $I_{res}=0$, whereas all small scale turbulent pulsations are suppressed at $I_{res}=50A$ (Fig.4.5.5, right). It is clearly seen the suppression of the development of the turbulent spectrum in agreement with experimental data. All these results with corresponding experimental data are shown in [4].

The Fig.4.5.6 shows the result of comparative analysis of the shock wave position due to the experimental measurements, analytical prediction for a strong wave, and computational

data for weak cylindrical wave propagation. The Sedov's formalism in frames of cylindrical symmetry is valid for the strong wave:

$$R_{sw} = \alpha(\gamma)(E_1 / \rho_0)^{1/4} t^{1/2}; \quad \alpha(\gamma) \approx 1$$

It can be considered a good consistency of the results.

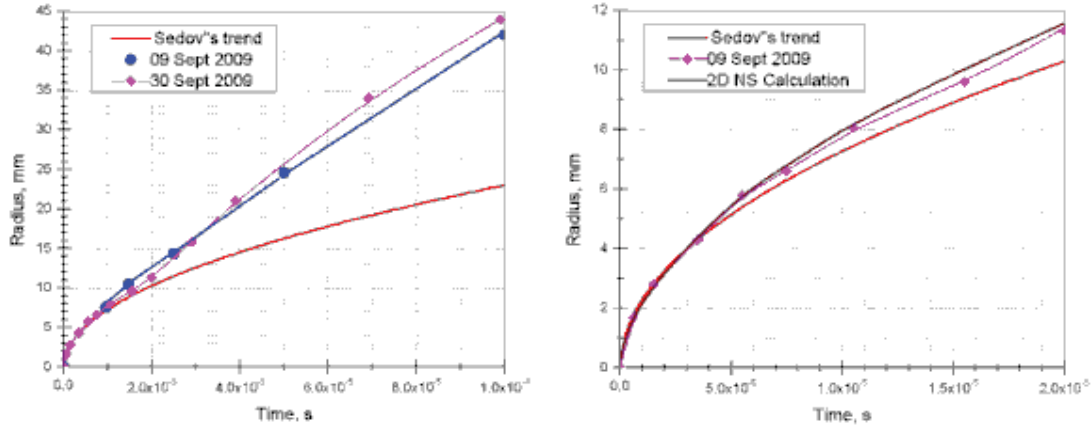


Fig.4.5.6. Experimental data on the discharge-excited SW runaway in two time scales. Symbols - experiment; red line - Sedov's law for $E/D=0.4\text{J/cm}$; brown line – 2D NS simulation ($r_0=0.25\text{mm}$, $E/D=0.4\text{J/cm}$).

One of the most important parameters of the pulse discharge is a time of breakdown τ_{br} , which affects the discharge performance in high-speed flow particularly. The physical mechanism of spark discharge breakdown is called as “streamer to spark transition” because a primary ionized channel is formed by the streamer propagating between electrodes. For a successful operation of the discharge in transversal flow the time of breakdown (time period between the voltage feeding and spark realization) must be less than characteristic gasdynamic time:

$$\tau_{br} < d/V, \quad V = \text{speed of gas}, \quad D = \text{characteristic length.}$$

In geometrical configuration of described test [4] the characteristic length is close to electrode diameter (the mechanism of flow effect on breakdown was announced in [5]). It means that the breakdown time has to be not longer than a few microseconds; otherwise the flow blows down an initial ionized channel, which was created by the streamer. The Fig.4.5.7 below compares the experimentally measured value of breakdown time and the values predicted in [6]. Well seen that to avoid an increase of the breakdown time, the duration of voltage pulse can't be elongated (with simultaneous reduction of amplitude).

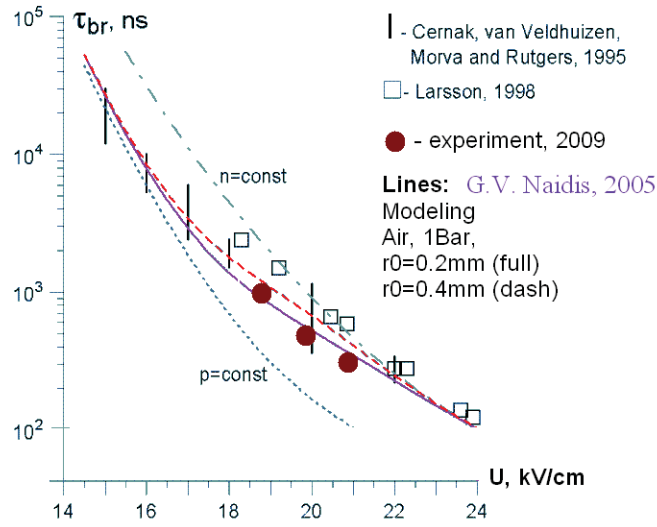


Fig.4.5.7. Comparison of experimental values of breakdown time with theoretical prediction [6].

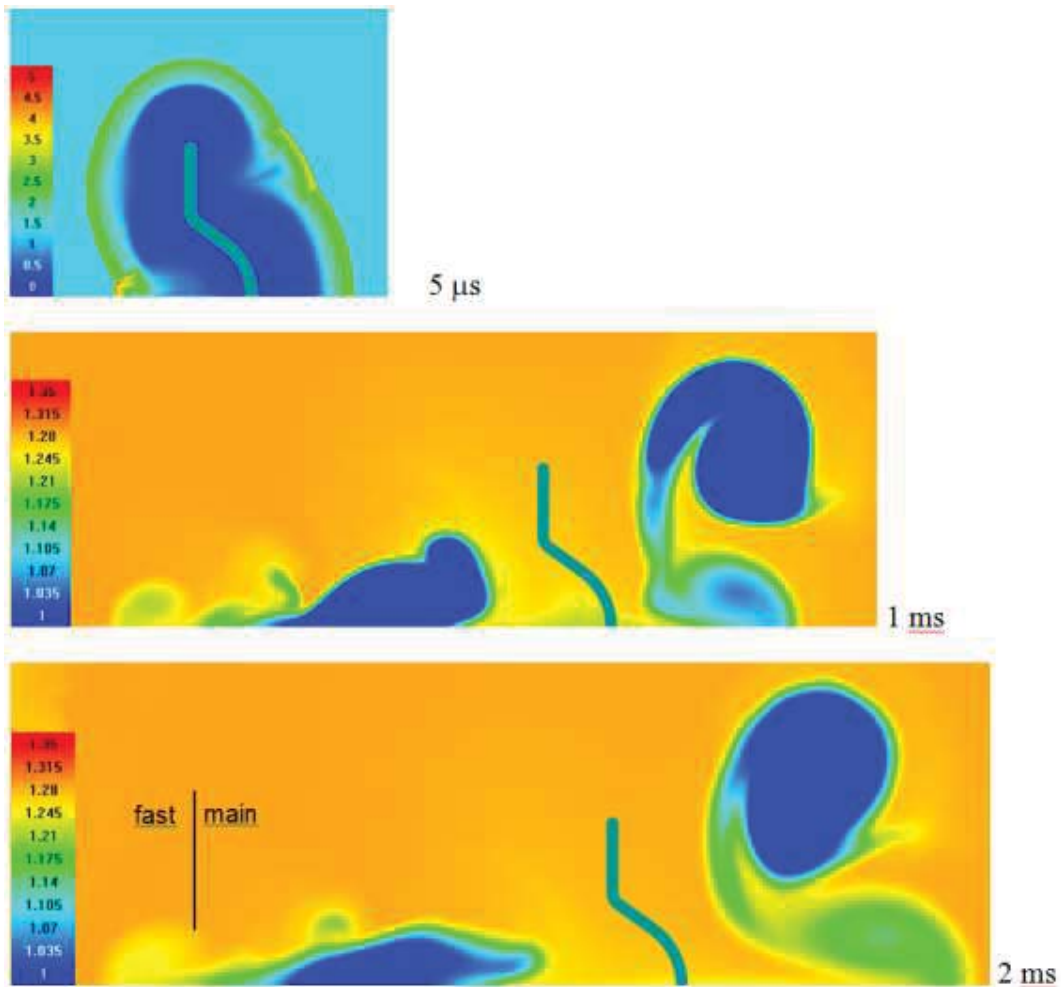


Fig.4.5.8. Fast disturbance caused by shock wave interaction. CFD. Density, (kg/m^3)

It was found in CFD investigations that shock wave interaction not only determines the direction of disturbances propagation. In some cases it also produces weak fast vortex structure (Fig.4.5.8), which moves ahead of the main disturbance. This fact was confirmed experimentally. Schlieren images of fast structure propagation are presented in Fig.4.5.9. As it shown in Fig.4.5.10, experimental results at an early stage agree well with the simulation data. Additional comparison of numerical simulation with experiment is presented in Fig.4.5.11. As it shown in all experimental images the weak fast vortex structure is not symmetrical. Symmetry of this structure in numerical simulation is caused by using symmetry boundary condition.

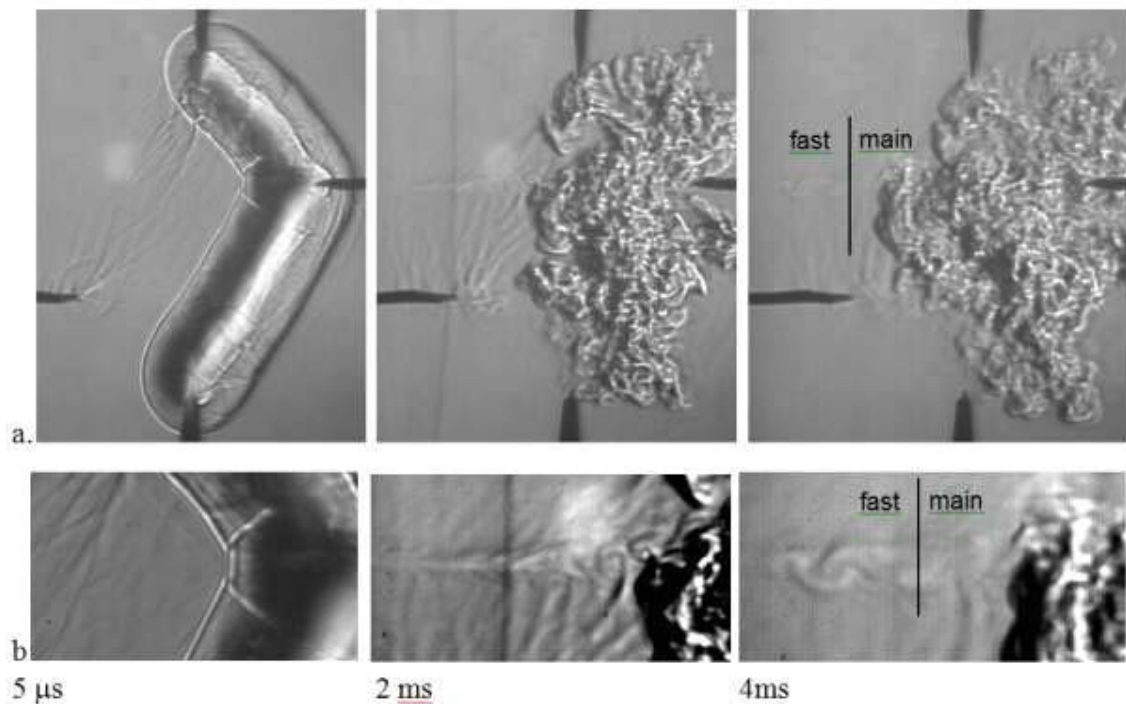


Fig.4.5.9. Fast disturbance caused by shock wave interaction. Experiment.

a – full image, b – fast disturbance

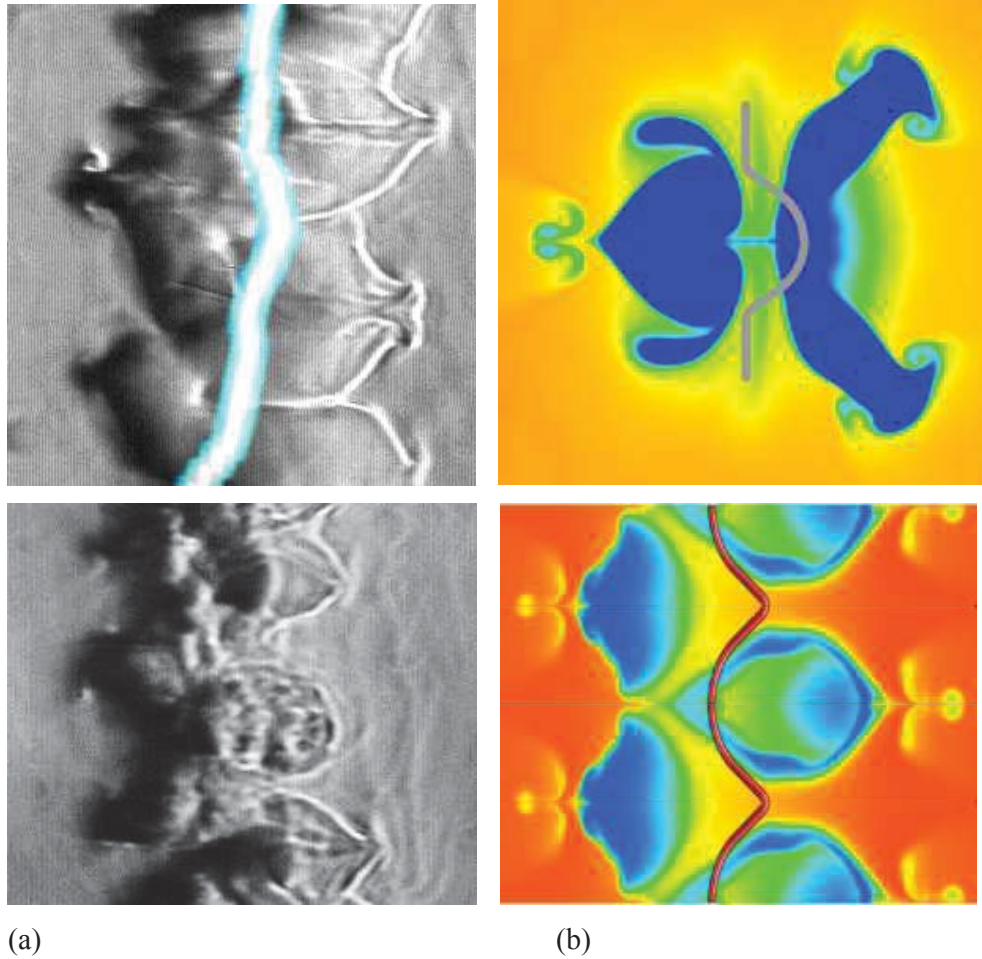


Fig.4.5.10 Jet formation, 180 μ s.

a – schlieren visualization, b – numerical simulation, density.

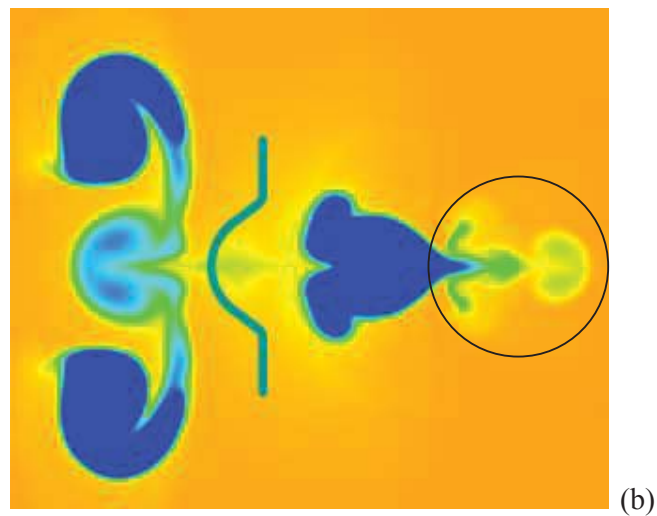
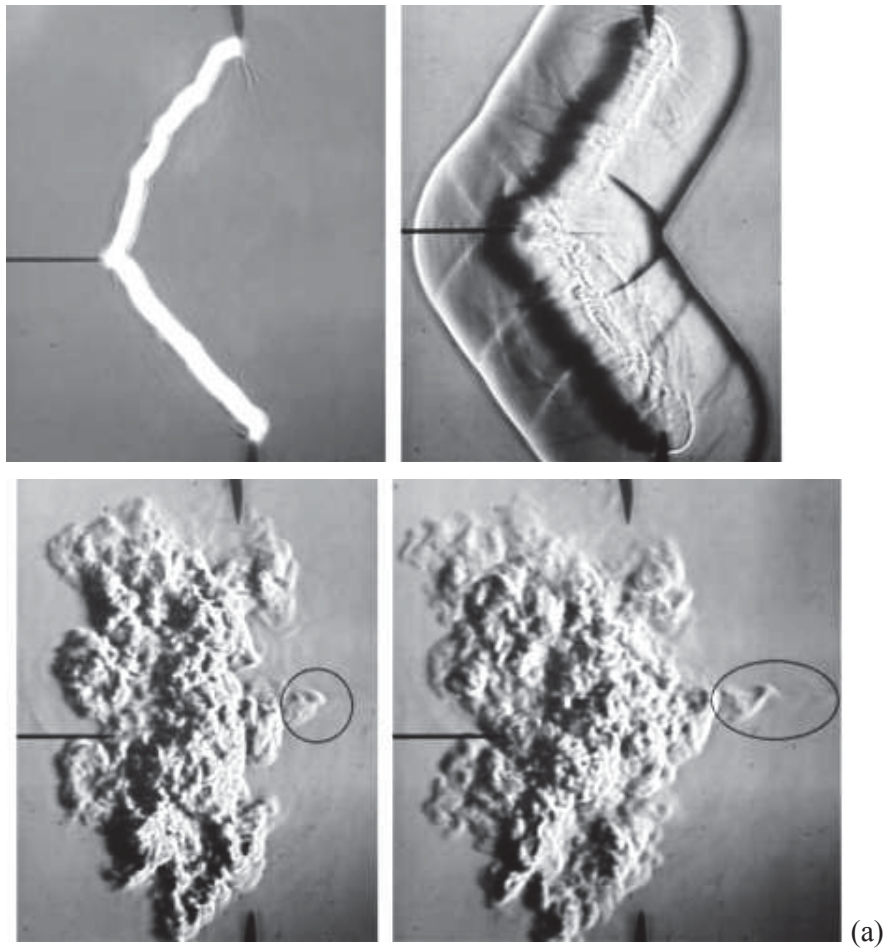


Fig.4.5.11. Comparison of fast jet formation.

(a) Schlieren visualization – $0 \mu\text{s}$, $40 \mu\text{s}$, 2 ms , 4 ms

(b) Density, CFD – 1 ms

References to the section 4.5.

1. N.M.Kuznetsov, Thermodynamic Functions and Air Shock Adiabates at High Temperatures. Mashinostroenie, 1965. (in Russian)
2. Ya.B.Zel'dovich, Yu.P.Raizer, Physics of Shock Waves and High Temperature Hydrodynamic Phenomena, Academic Press, 1968
3. 10. M.N.Shneider, Physics of Plasmas, 13, 073501-11, (2006)
4. "Study of Mechanisms of Filamentary Pulse Electric Discharge Interaction with Gaseous Flow of Nonuniform Composition", Project ISTC #3793p, The First Year Report, October 2008.
5. Sergey B. Leonov, Dmitry A. Yarantsev, Yury I. Isaenkov "Properties of Filamentary Electrical Discharge in High-Enthalpy Flow", 43rd AIAA Aerospace Sciences Meeting & Exhibit, 10-13 January 2005/ Reno, NV, AIAA-2005-0159.
6. G.V. Naidis, "Dynamics of streamer breakdown of short non-uniform air gaps", 2005, J. Phys. D, **38** 3889

4.6. Adjustment of spectroscopic technique for spatially resolved estimation of mixing efficiency.

Among of others the key point of this work is an adequate measurement of the mixing efficiency. The best way for that is to know the concentrations of main components and their spatial distribution. The Project supposed some efforts for analysis of applicable diagnostic methods. At the beginning the analysis was made in cooperation with Princeton University.

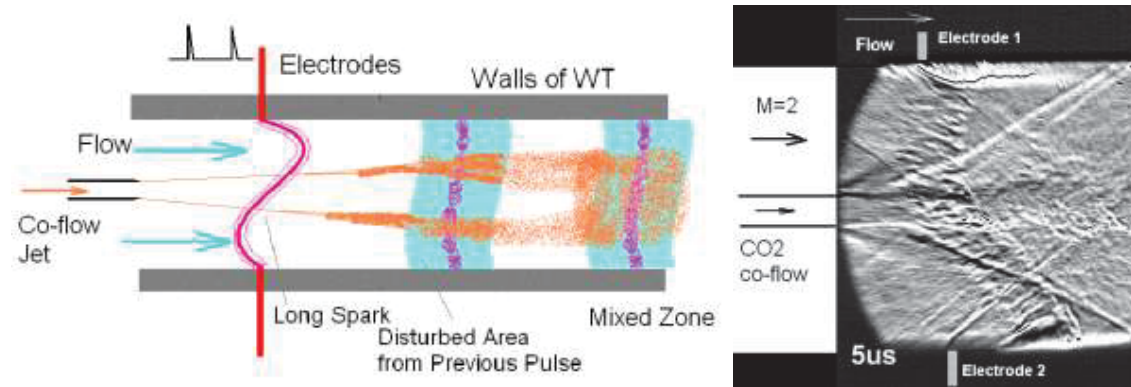


Fig.4.6.1. a - scheme, related with an experimental approach; b – schlieren photo obtained experimentally in M=2 airflow.

The experimental approach consists of the following key points: supersonic duct-driven airflow $M=2$; direct injection of gaseous fuel (co-flow jet of model gas, He or CO₂, preliminary); transversal short-pulse repetitive electrical discharge, crossing air-fuel-air zone or along air-fuel boundary; plasma-induced artificial turbulence; zone of improved mixing. Figures 4.6.1a and 1b show a scheme of test and experimental schlieren photo. A preferred result of measurements is a spatial distribution of concentration of second gas in air depending on the discharge operation mode.

In many previous studies of multi-component flows the mixing is measured by examining the local concentration of a conserved scalar (usually seeded into one of the two streams) or by the formation of a chemical product, which occurs due to mixing and reaction between the two streams. However, these methods, known as passive scalar and chemical product methods respectively, can be severely affected by either measurement resolution or finite chemical rate effects [4-7]. Rayleigh/Mie scattering (from flow-field ice crystals, for example) can be also used to study mixing and penetration of a supersonic jet in a supersonic cross stream [8]. The paper [3] compares in details PIV, Mie, and schlieren techniques to measure the mixing efficiency in planar shear layer. We recognize the PIV method as possessed very limited

capability for application in strong electrical field [9]. The Mie scattering method requires the development of complex laser system.

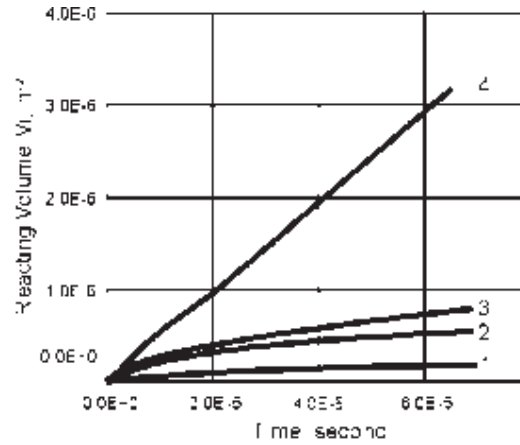


Fig.4.6.2. Reacting volume vs. time. Curve 1: diffusion only, constant temperature 300K; Curve 2: diffusion only, hydrogen temperature 3000K; Curve 3: diffusion and combustion, hydrogen temperature 300K; Curve 4: MHD-assisted combustion. The figure is from [10].

One of the most important parameters of diagnostics applied for the mixing estimation is the spatial resolution. Mixing process include two stages: kinematic mixing and diffusion. In the case of low resolution the measurement method may show both fractions (fuel and oxidizer) while the diffusion is not completed. The concept of “reacting volume” was established in [10]. The reacting volume value can be define as

$$V_r = \int_{V_o} \sum_i X_{i,O} \cdot \sum_j X_{j,F} dV ;$$

where $X_{i,O}$ and $X_{j,F}$ are the mole fraction of i-th oxygen-containing species and the mole fraction of j-th fuel-containing species. The summing should be made on all species in the mixture.

In principle, such a definition of the reacting volume value could be normalized with a limiting value corresponding to uniform mixture. However, the constant factor omitted in the expression written above is non-important in the further analysis. One can see also that at the initial state when two uniform volumes of fuel and oxidizer are put into contact the reacting volume V_r defined here is equal to zero, Fig.4.6.2. It is also clear that the reacting volume is a measure of “combustion” reactions rate between fuel- and oxygen-containing molecules [10].

A strong difficulty in simultaneous measurement of spatial picture of interaction and relative concentration of components in each small volume can be considered currently. This statement leads to conclusion that a combination of methods is reasonable to be applied. As it was announced in project’s quarterly reports, to see the flowfield in experiments the deeply modified schlieren and schlieren-streak techniques are planned to be utilized with appropriate

processing of images. The Fig.4.6.3 shows a sample of schlieren image for analysis and processing. Here the pulse discharge locates inside of CO₂ jet in ambient air.

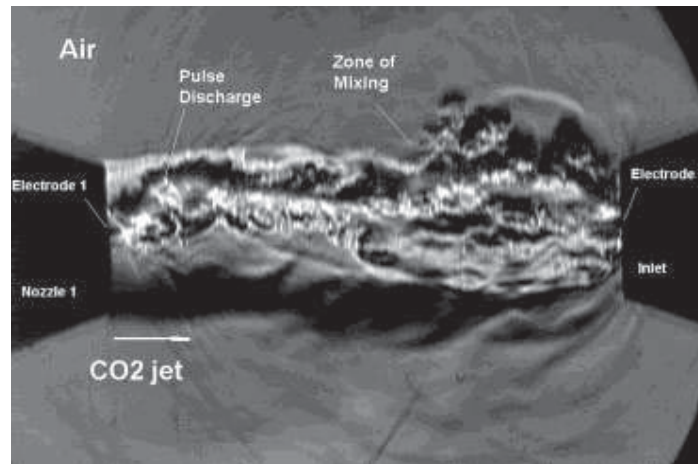


Fig.4.6.3. Sample of the pulse discharge interaction with CO₂ jet in air. Time delay 100 μ s.

The analysis made shows that for the local measurements the *laser breakdown fluorescence* could be used [11-13]. It possesses important advantages: high temporal and spatial resolutions, and non-intrusive nature. At the same time the result is supposed to be mostly quantitative due to insufficient averaging at short operation of the facility.

The *laser breakdown fluorescence* can give the data on composition in small volume of the gas ($l \times d = 2 \times 0.1 \text{ mm}$, approximately) located in predefined position. Temporal resolution can be less than 1 μ s. *This diagnostic is non-intrusive.* To realize this method several steps were planned: exact design of extra arrangement; purchasing of the pulse laser; assembling of equipment; model test measurements; measurements in supersonic flow. The Fig.4.6.4 presents a draft scheme of measurements by means of *laser breakdown fluorescence*.

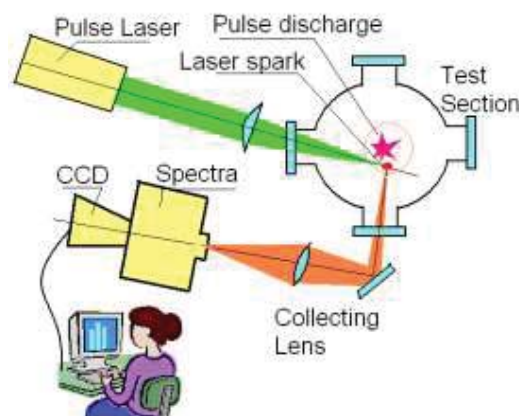


Fig.4.6.4. Draft-scheme, related with local measurement by LBF.

In spite of all advantages of LBF (high temporal and spatial resolution, non-intrusive) this method cannot be applied in frames of this project due to the high cost of the laser system required. It has been proposed to modify this method and to use a weak electrical discharge instead of laser breakdown. The idea is to realize breakdown of the so-called “probe” discharge that possess much less power than the main one at some delay after the main breakdown. The temporal resolution of this method is equal to the probe discharge fluorescence duration – $< 1 \mu\text{s}$ - it is reasonably small. The spatial resolution is determined by the collecting optical system and can be not more than $l \times d = 3 \times 1 \text{ mm}$, approximately. It is a little bit worse than spatial resolution of the LBF but it still seems satisfactory for mixing efficiency estimation. Figure 4.6.5 presents a draft scheme of measurements by means of *Probe Breakdown Fluorescence* = *PBF*.

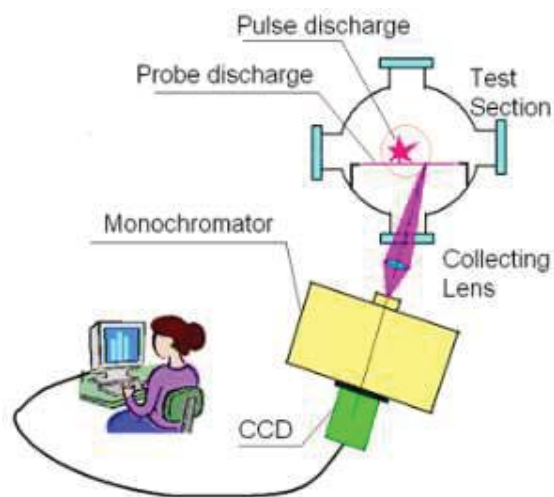


Fig.4.6.5. Draft scheme of the PBF measurements.

It must be ensured that main discharge is not influenced by the probe discharge electrodes significantly. In order to provide this the probe electrodes have floating potential. Otherwise the parasitic capacity of second winding of probe discharge transformer will lead to intensive streamer growth from the probe electrodes. In this case main discharge breakdown will tend to arise through the probe electrode. It was found experimentally that configuration with probe electrodes under floating potential is preferable.

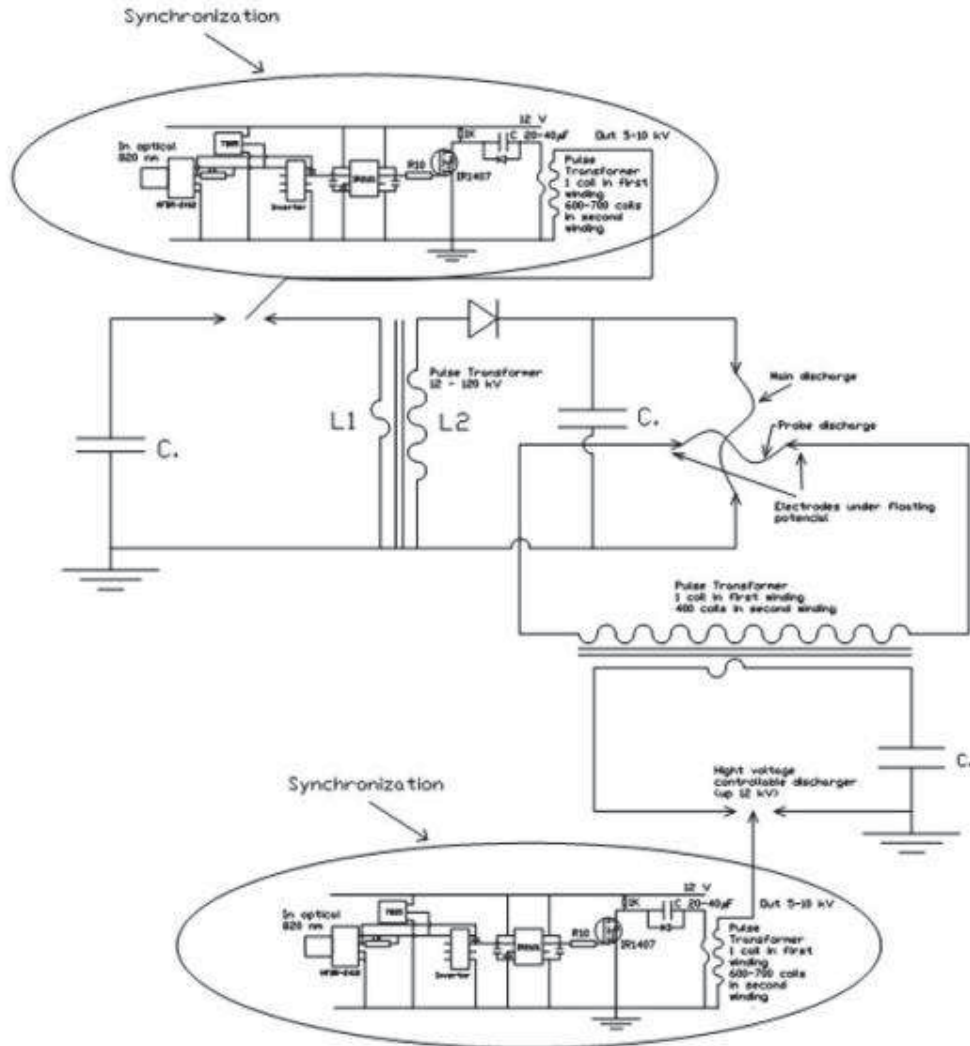


Fig.4.6.6. Electrical scheme of the main and probe discharge.

The principal scheme is presented in the Fig.4.6.6. This scheme allows synchronization of main and probe discharges by means of optical pulse generator.

It has been demonstrated during the series of tests that main discharge breakdown occurs in the same manner as in case without probe discharge electrodes, see schlieren photo on the Fig.4.6.7a. To check the influence of the probe discharge electrodes in more details the streamer tree arising at the first stage of the main discharge has been visualized, Fig.4.6.7b. It is seen that there are some streamers on the probe electrodes but these streamers are weak and rare and do not disturb the streamer tree of the main discharge significantly.

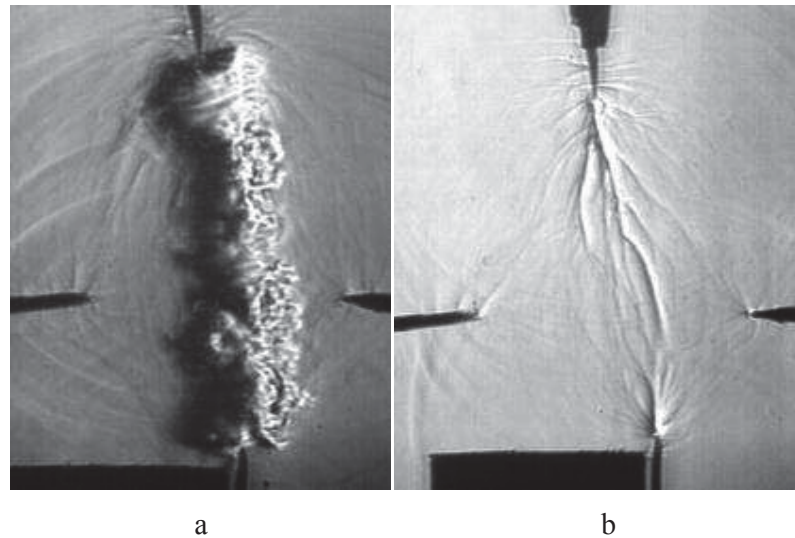


Fig.4.6.7. Main discharge breakdown (a) and streamer phase (b) at presence of the probe electrodes.

The next important task of spectroscopic technique adjustment is to obtain spectra of probe discharge in gaseous hydrocarbons and in the air. Comparison of these spectra will give ideas for mixing efficiency estimation based on such diagnostic method. Spectroscopic observations were carried out by means of high luminosity MDR-2 monochromator combined with ANDOR DU420 spectroscopic camera. Dispersion of this system is $0.5 \text{ \AA}/\text{pixel}$ and spectral resolution is about 2.5 \AA .

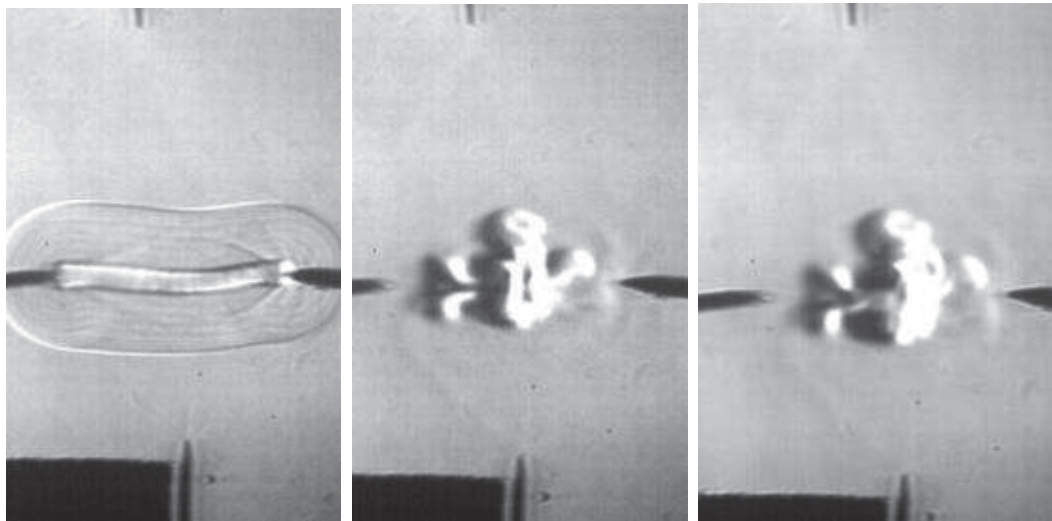


Fig.4.6.8. Schlieren visualization of probe discharge filament decaying.

Spectrum of the main discharge contains high intensity continuous emission that arises due to high temperature within the main discharge channel. The power of the probe discharge must be low in order to avoid this effect. It is seen on the schlieren visualization of probe discharge

filament decaying on the Fig.4.6.9 that gas dynamics disturbances are weak. Power release in probe discharge is measured as low as 0.03-0.1J per pulse.

A survey spectrum of the probe discharge has been obtained in air and in spray of C_2H_5OH , Fig.4.6.9 (a). Low power spark discharge in air excites mostly the second positive system of molecular nitrogen (N_2 , $C^3P_u \rightarrow B^3P_g$). A high intensive emission of CN violet system is observed if breakdown occurs in carbon containing media, as it is seen in Fig.3.4.5 (b). Even small amount of carbons is enough for CN emission to be much more intensive than nitrogen emission.

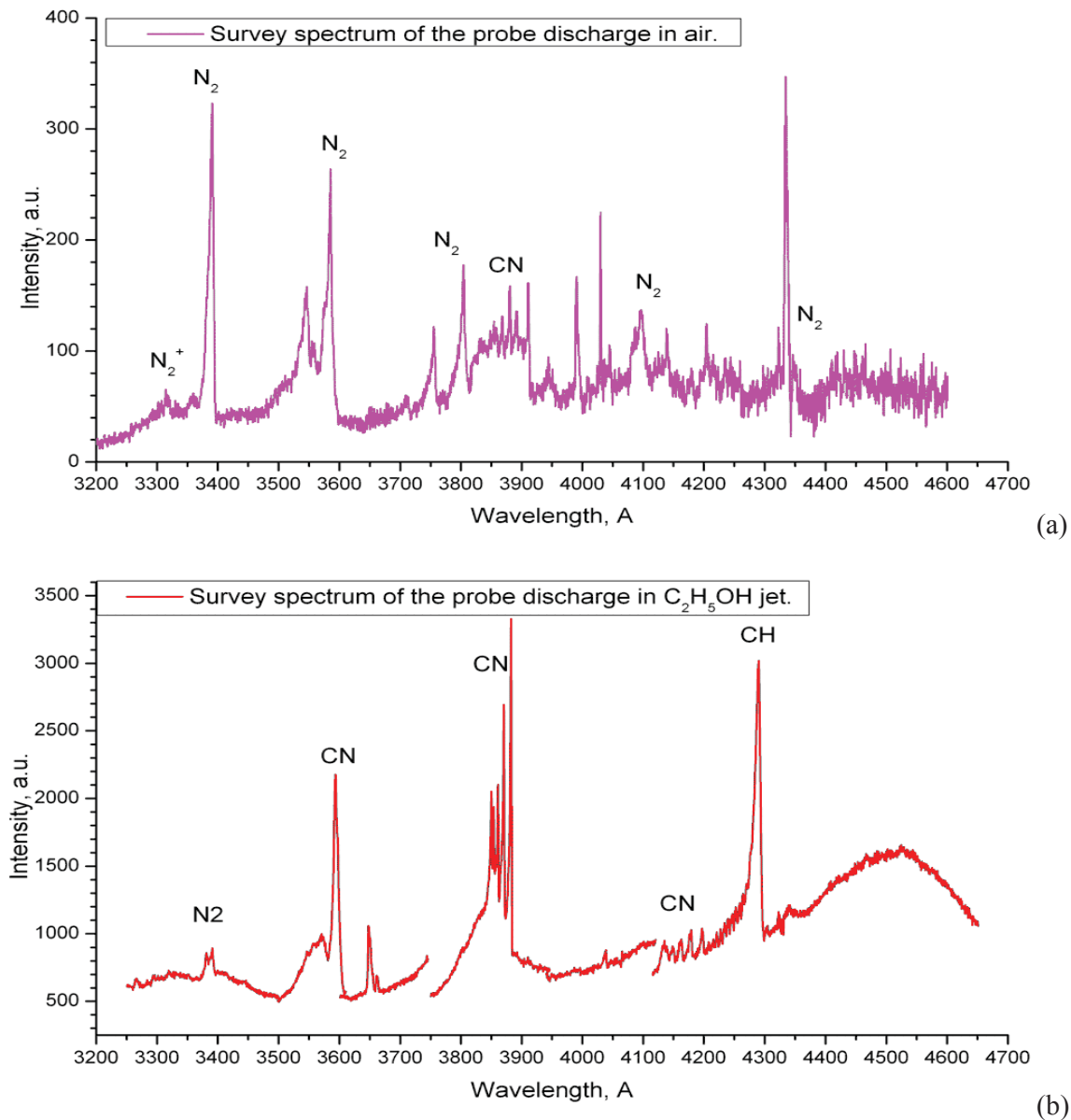


Fig.4.6.9. Survey spectrum of the probe discharge: (a) – in air, (b) – in C_2H_5OH spray jet.

As far as discharge channel has not fully predictable shape, the information needed for mixing efficiency estimation should be obtain during single run. It means that only one relatively narrow (nearly 20nm) spectral range can be captured and be available for analysis. The most proper spectral range is seemed to be a range, containing both nitrogen and CN bands, for example $\lambda=375\div 390\text{nm}$. Probe discharge spectra in this range for two gases are presented in the Fig.4.6.10.

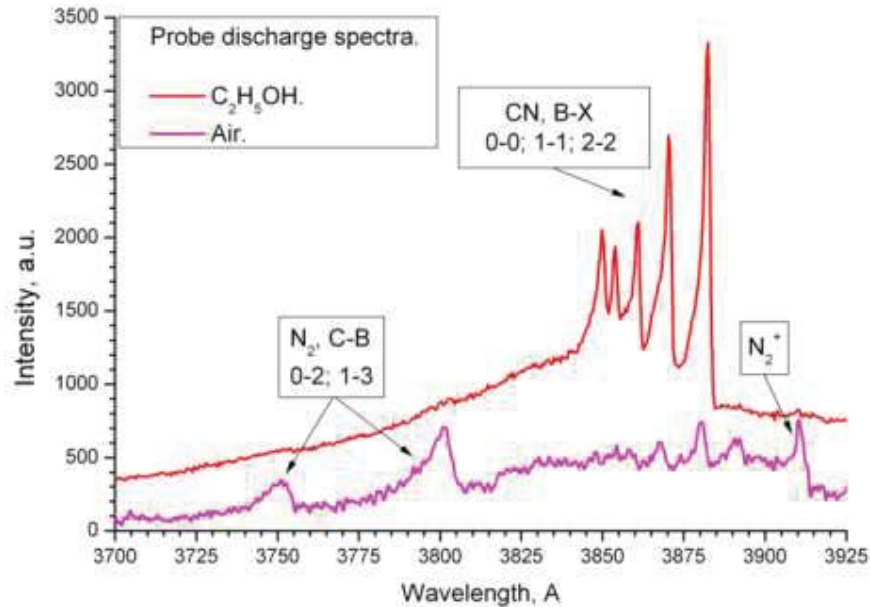


Fig.4.6.10. Probe discharge spectra within the range $\lambda=375\div 390$ nm for $\text{C}_2\text{H}_5\text{OH}$ (red) and air (magenta).

The fact of mixing can be considered due to the presence of CN emission. The procedure of experimental adjustment looks like following: at the first step it is need to find a measuring point containing no $\text{C}_2\text{H}_5\text{OH}$ in vicinity of jet by means of probe discharge spectrum analysis in terms of CN band arising; then this point should be analyzed after the main discharge breakdown. Moving the measuring point in normal direction to the jet axis can give information about the mixing region size.

The estimations of the mixing efficiency as the result of interaction with the pulse filamentary discharge must be studied in non-homogeneous medium. In our case it was a thin laminar jet of CO_2 in ambient air. Jet was formed by means of long cylindrical tube with cone nozzle. The inlet gage, connected to the tube, allows controlling the CO_2 flow rate. Long tube causes to the Poiseuille profile of gas flow near the nozzle. Such configuration allows obtaining long laminar jet of the secondary gas in air. Schlieren photo of jet is shown in Fig.4.6.11.

During the experiments described above the CO₂ jet was oriented at small angle to the main discharge vertical.

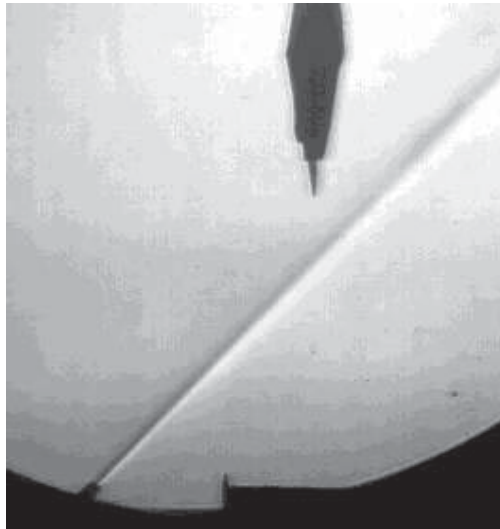


Fig.4.6.11. Laminar CO₂ jet in ambient air

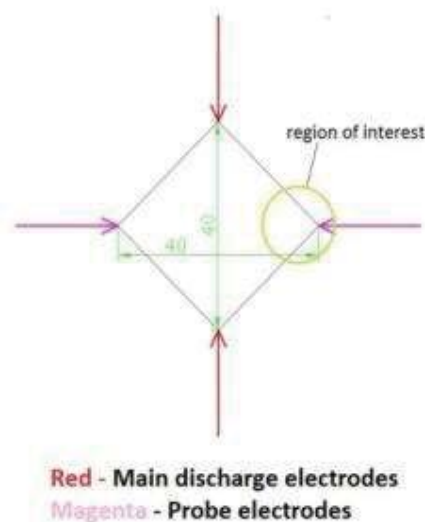


Fig.4.6.12. Experimental configuration of electrodes.

The experiments have shown that designing of particular electrodes configuration of the main and probe discharges face some difficulties. First of all, probe electrodes must not impact the main discharge. To satisfy this demand one must increase the gap between the probe electrodes. On the other hand, increasing gap between probe electrodes makes probe discharge harder to breakdown and makes it more dislocated. Particular configuration of electrodes of both discharges is compromised between two problems described above. It was found experimentally that the best configuration is the following: probe discharge gap is

approximately equal to the main discharge gap; electrodes are placed in the corners of virtual square (see Fig.4.6.12). It has been demonstrated during the series of tests that breakdown of the main discharge occurs in the same manner as in case without probe discharge electrodes. Region of interest for spectroscopic measurements shown in Fig.4.6.12. The electrical current and the power deposition in the probe discharge were >10 times less than in the main discharge.

Such a configuration could be applied to obtain two non-interacting discharges – main discharge aimed to mix non-homogeneous medium, probe discharge is excited to estimate gas composition by light emission from the discharge zone. Visualization of this situation is shown in Fig.4.6.13 (in this picture dischargers flat is not perpendicular to the laser beam of the schlieren scheme).

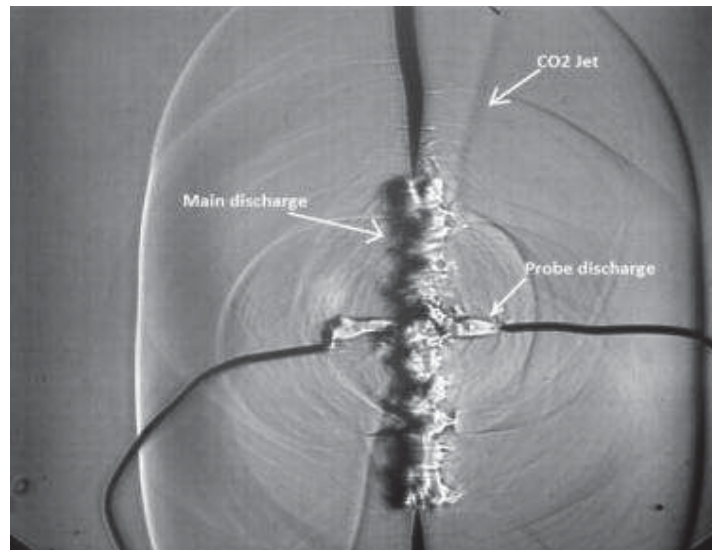


Fig.4.6.13. Visualization of main discharge and probe discharges. Time delay 100 μ s.

Another important point of the technique developed is the delay between the main and probe discharges. It has been found experimentally that such delay must be at least 100 μ s in ambient air. With smaller delay probe discharge feels the residual conductivity of streamer phase of the main discharge. In those cases the shape of the probe discharge becomes unpredictable.

According to the main idea a probe discharge breakdown occurs in zone strongly disturbed by previous main discharge. It means that the delay between discharges must be in a range of 150-500 μ s. The thing is that the jet type instabilities of decaying of main discharge filament needs some time to come to the region of interest. Visualization of such situation may be seen in Fig.4.6.14.

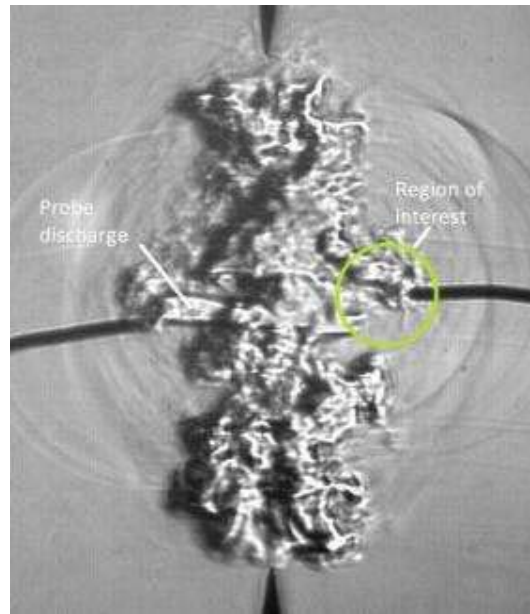


Fig.4.6.14. Schlieren photo of probe discharge in strongly turbulized zone. Time delay 400 μ s.

As it is mentioned above the spectral range that is the most suited for the measurements has been chosen as 3700A – 3925A. It contains both nitrogen and CN spectra. Spatial resolution of the measurements was estimated as 4mm; temporal resolution is equal to the duration of the probe discharge and it was nearly 500ns. The scheme of measurements described above has been tested for two modes: 1) measurement of the probe discharge spectrum at presence of the CO₂ jet; and 2) measurement of the main discharge spectrum at presence of CO₂ jet. Spectrum of the N₂ 2nd positive system was detected in both cases. Spectrum of the main discharge from the off-axis area was rather weak and it was observed not every run. The reason is the variation of the main discharge shape from run to run – sometimes it crosses the region of measurements. Such test has shown that there is no CO₂ jet within the region of interest and the only reason for CN band to appear during measurements is the turbulent gas motion appeared due to influence of the main discharge.

Probe discharge spectrum was measured at variation of the delay time between main and probe discharge. Typical spectra are shown in Fig.4.6.15.

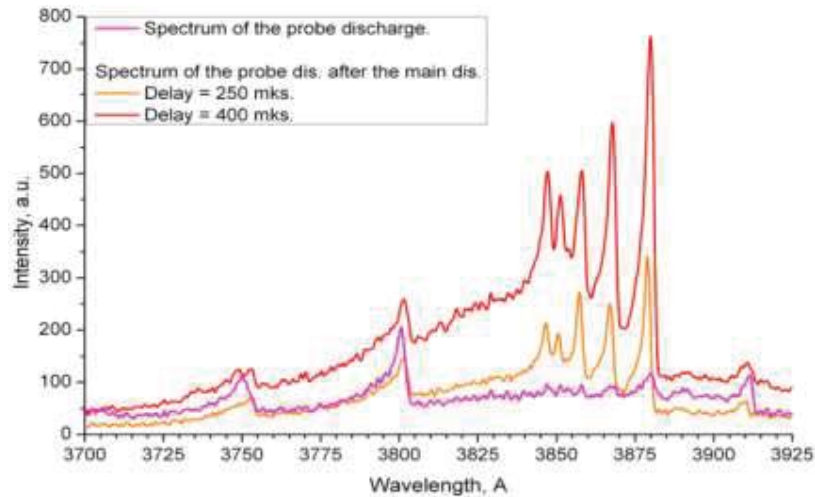


Fig.4.6.15. Spectrum of the probe discharge at variation of the delay time in respect of the main discharge.

It is clearly seen that spectrum of the probe discharge doesn't contain CN at all without preceding breakdown of the main discharge. If main discharge is applied for mixing, the CN emission arises in spectrum of the probe discharge. Its intensity grows with growth of the probe discharge delay that means increasing of the CO₂ concentration. It is also seen that intensity of the N₂ bands tends to reduce, when disturbances reach the measurements region. The data is illustrated by Table 4.6.1 and Fig.4.6.16 below:

Table 4.6.1. Intensity of the CN and N₂ emission for different delays of the probe discharge.

Delay, μs	Intensity of CN at 3883Å, a.u.	Intensity of N ₂ at 3804Å, a.u.	Ratio CN/N ₂
0	53	205	0.3
200	93	123	0.8
250	304	78	3.9
400	661	88	7.5
1500	890	96	9.3

The graph in Fig.4.6.16 illustrates the dynamics of the jet disturbances penetration. We paid attention at the graph on the front position, when jet of mixture reaches the measurements region, and plateau at bigger delays from breakdown. These features reflect the max achievable in this test mixing efficiency. It is clear that the spectrum of the probe discharge depends on position of the measurements region very much – increasing the distance from the main discharge causes the shifting and smearing of the front in Fig.4.6.16. The jets developed after

the discharge breakdown has unpredictable configuration, so it was needed to perform a lot of runs in order to obtain each point on graph in Fig.4.6.16.

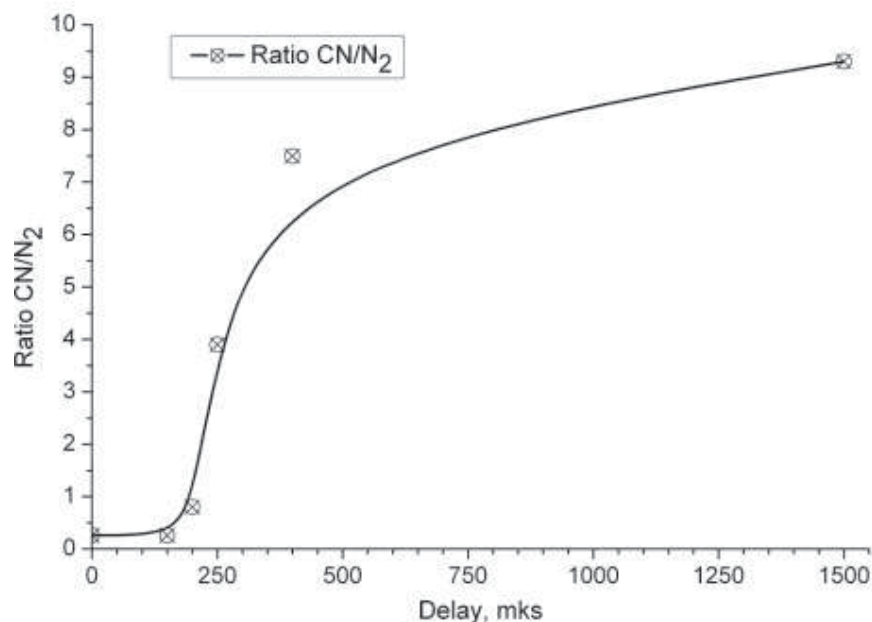


Fig.4.6.16. Emission intensity ratio of CN (3883A) and N₂ (3804A) depending on probe discharge delay time.

It seems that calibration of the method may even allow measuring of the mixing ratio, not only qualitative estimation of the fact of mixing.

In order to calibrate the measuring system the facility for the calibration measurements has been assembled and the scheme is presented in Fig.4.6.17. Pumped out test cell is filled with controllable amounts of gas1 and gas2. The mixing ratio was controlled by means of the pressure measurements. The measuring cell was filled with the main gas (air or N₂) up to atmospheric pressure, and then pumped out to the required pressure. After that, the cell was filled with the second gas up to the atmospheric pressure. Then uniform mixture is prepared by means of the micro-fan installed within the cell. Due to the flammability of the C₂H₄/Air mixture, in some cases the C₂H₄ was modeled by the CO₂ and air was modeled by the N₂. In result, three different mixtures were tested – CO₂/Air, CO₂/N₂ and C₂H₄/N₂.

Probe discharge breakdown is initiated and spectrum of the discharge is registered in waveband at range 370 nm ÷ 390 nm. Spectroscopic observations were performed by means of high luminosity MDR-2 spectroscope combined with ANDOR DU420 spectroscopic camera. Dispersion of this system is 0.5 Å/pixel and spectral resolution is about 2.5 Å. Pressure measurements and electrical measurements are carried out within the measurement cell in order to estimate energy release of probe discharge.

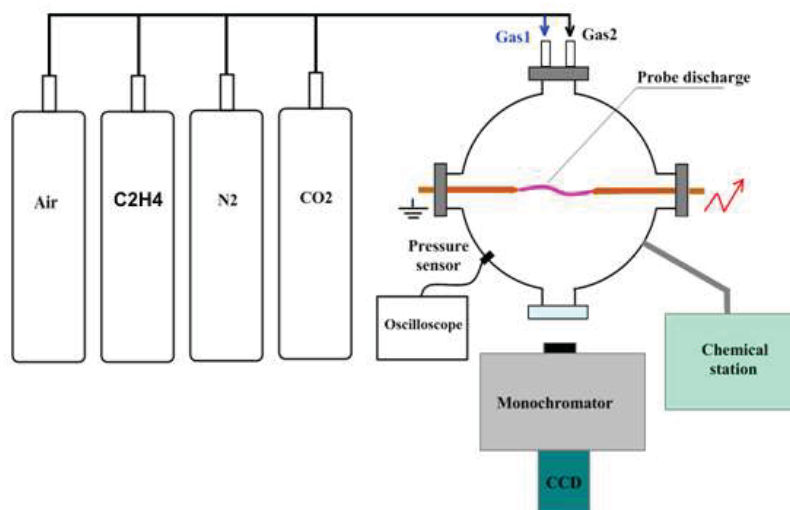


Fig.4.6.17. Scheme of calibration measurements.

The scheme of the probe discharge power supply is presented on the Fig.4.6.18. Power supply is based on Tesla transformer with impulse excitation. Energy deposition in probe discharge should be low enough, so the load to transformer is the capacity of secondary coil circuit. However, even in this case, energy deposition in discharge filament heated the gas, so the gas mixture radiated much of continuum spectra. To decrease the baseline magnitude an additional resistance was added in secondary circuit reducing the energy deposition.

Discharge voltage and current were measured by means of high-voltage probe of Tektronix P6015A and Rogovskiy coil; signals were registered by means of oscilloscope Tektronix DPO 7054. Discharge power occurs to be rather stable from run to run and it was within the range from 0.3 J to 0.45 J. This value is low enough to avoid spectrum to be perturbed much by continuum.

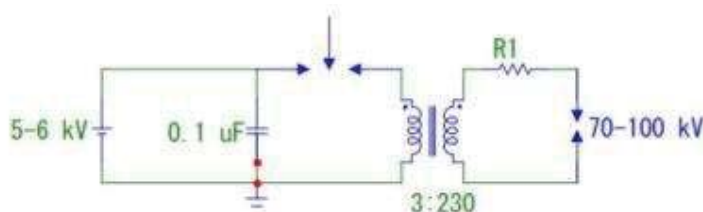


Fig.4.6.18. Scheme of the probe discharge power supply.

The series of the spectroscopic measurements has been fulfilled at variation of the mixing ratio of gases. The result of measurements is a set of spectra that are presented on the Fig.4.6.19-21. Spectrum amplitude and shape for each mixing ratio was stable from run to run that is resulting from the uniformity of the mixture composition and stability of discharge parameters.

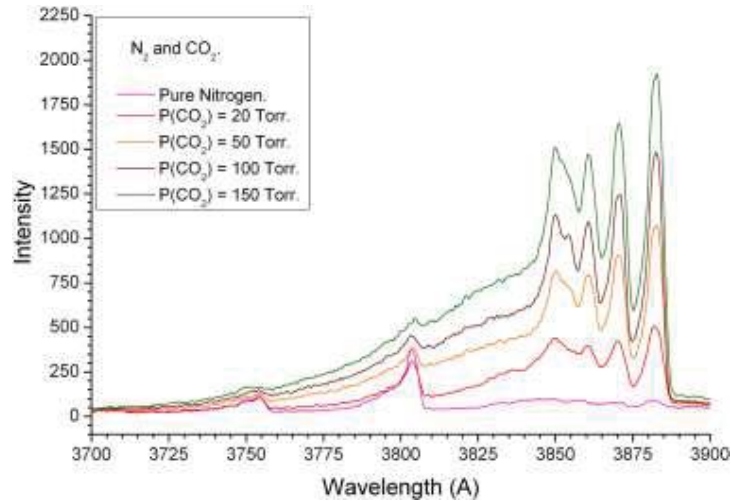


Fig.4.6.19. Spectra at variation of mixing ratio for the N₂/CO₂ mixture.

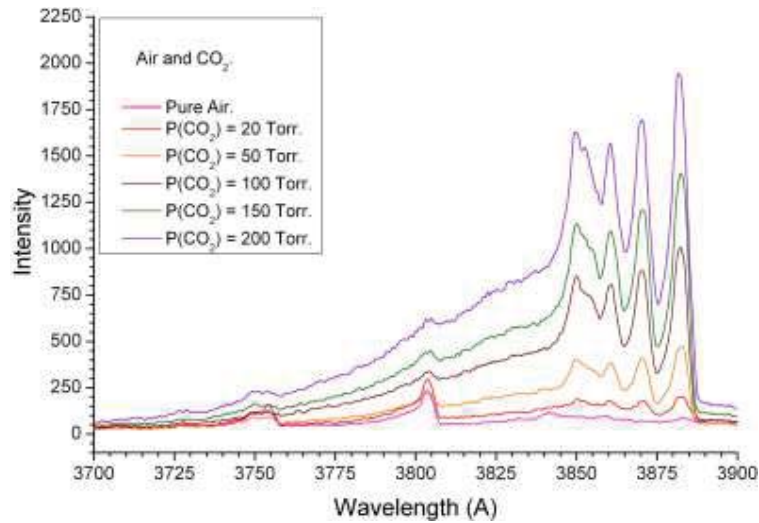


Fig.4.6.20. Spectra at variation of mixing ratio for the Air/CO₂ mixture.

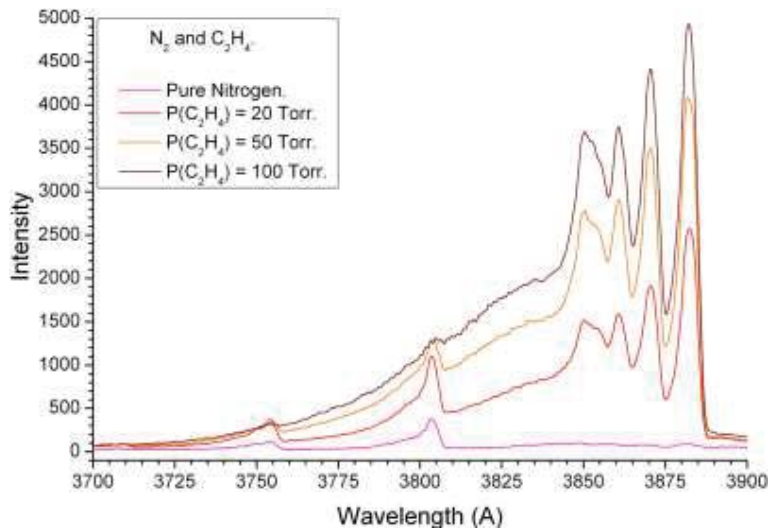


Fig. 4.6.18. Spectra at variation of mixing ratio for the N₂/C₂H₄ mixture.

It was found that there is a notable difference between spectra for different mixtures. It is seen that CN intensity grows much faster with the second gas partial pressure for the ethylene containing mixture than for the CO₂ mixture. As a result the spectrum loses its sensitivity to the ethylene partial pressure for pressures higher than 100 Torr (Fig.4.6.21.). For CO₂ containing mixtures this limit is 150 Torr. Nitrogen bands intensity is reduced with the growth of the second gas pressure, as it is seen in Fig.4.6.22. As a result the method possesses the undesirable limitation in terms of second gas partial pressure. This limitation can be overcome by choosing another spectral range to register N₂ emission, for example 0-0 band of nitrogen second positive system at 337.1 nm. Nitrogen spectrum here is not overlapped by the CN emission. The spectrometer should be modified in order to register spectral range from 320 nm to the 400 nm at one shoot.

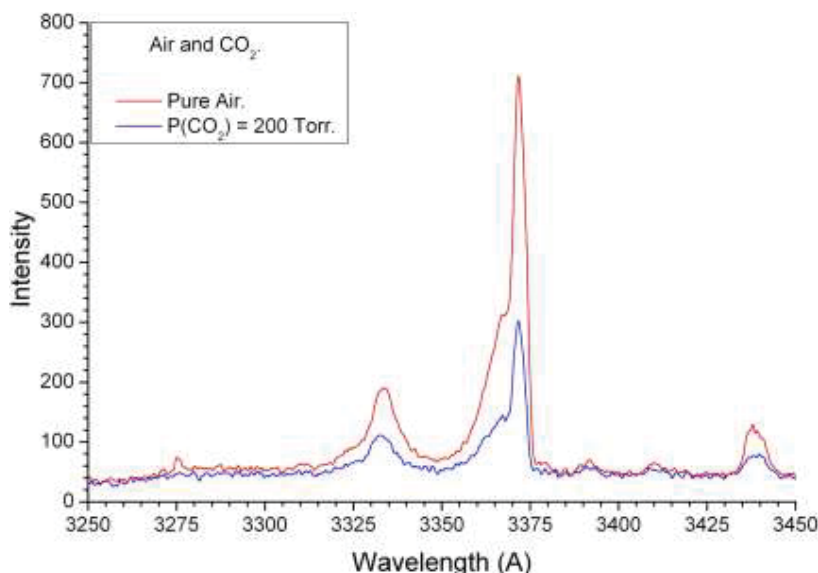


Fig. 4.6.19. Spectra for different mixing ratios for the Air/CO₂ mixture. N₂ (C³P_u→B³P_g, 0-0) band.

Spectra are processed to obtain a parameter that is depending on relative intensities of the CN and N₂ spectral bands. The parameter is calculated as a ratio of the intensities for two peaks: N₂ (C³P_u→B³P_g 0-2) at 380.3 nm and CN (B²Σ⁺→X²Σ⁺, 0-0) at 388.3 nm by the following equation $-S = I_{N_2}/(I_{N_2}+I_{CN})$. The calibration dependency is evaluated in the form of $S=f(P)$, where P is a partial pressure of the second gas (CO₂ or C₂H₄), Fig.4.6.23.

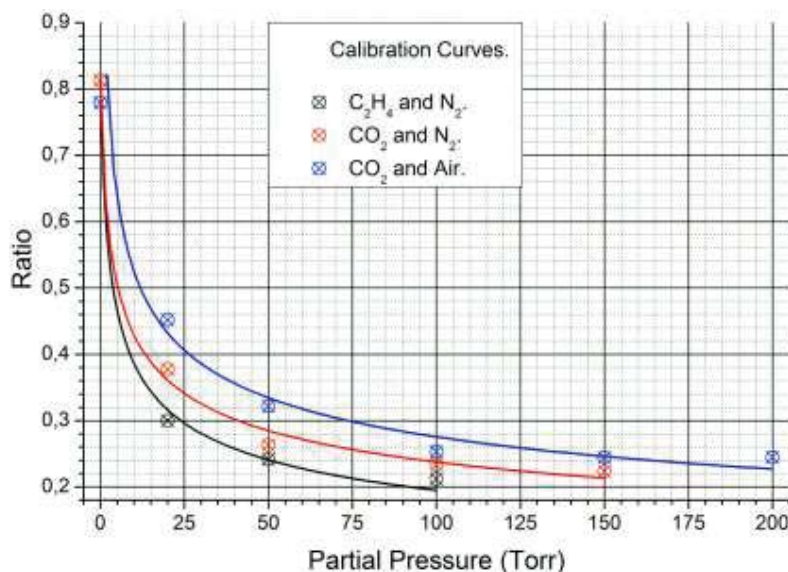


Fig.4.6.23. Calibration curves for different mixtures. Fitting by the $a/(1+x)^b$.

It is seen that the method is rather sensitive only for small amounts of the second gas (below the 75 Torr). Fortunately, the level of equivalence ratio $ER=1$ corresponds to partial pressure of C_2H_4 in Air as low as $P=47$ Torr. Nearby this value the system demonstrates the maximal sensitivity. Another important fact is that there is relatively big difference between different mixtures, for example ratio=0.3 means 25 Torr for C_2H_4/N_2 , 40 Torr for CO_2/N_2 and 75 Torr for CO_2/Air . It means that accuracy of the method, if using for the C_2H_4/Air , should be estimated separately.

Schlieren system was improved for the purposes of this work to raise the repetition rate up to the camera capability and to enhance the temporal resolution. The main improvement is the changing of the light source. The new light source is the pulse laser that possesses high repetition rate of the pulses. Parameters of the diode laser are listed in the table below.

Table 4.1. Diode laser's parameters.

Type	Diode laser
Wavelength, nm	805
Pulse duration, ns	100
Repetition rate, kHz	up to 3.5
Pulse power, W	150
Beam angle of expansion	20°

Such light source has several advantages in comparison with the continuous lamp and with a flash-lamp. The narrow wavelength range of the laser light allows reducing chromatic

aberrations in the camera lens, i.e. the sharpness of the image increases. The extremely short duration of the pulse causes the obtaining of the schlieren photos that are instantaneous in comparison with gasdynamic times (the shift of the flow structures during the pulse is about 0,05 mm, which is much smaller than spatial resolution of the system). The main advantage of the light source is the high repetition rate of 3.5 kHz. This rate allows using the high speed camera at the highest possible speed rates. It was impossible when applying the flash-lamp and/or halogen lamp.

The next improvement of the schlieren device is the modification of the synchronization system. According to a new synchronization scheme the framegrabber generates pulse at the start of the each camera frame. This pulse comes to the laser driver through the optical coupler that allows avoiding of the triggering caused by the EM noise. The accuracy of the synchronization is about 0.1 μ s. It enables to set the shortest exposure time of the camera – 10 μ s. As a result, only laser light is detected by the camera, all other light sources (emission of the combustion and discharge in the test section) are quite weak for such exposure time. The synchronization of the framegrabber, i.e. the triggering of the whole schlieren system, is controlled by the pulse generator through the optical coupler.

Spectroscopic system is typically used to get spectra during the discharge luminosity. Temporal resolution is of 30 μ s, spatial resolution is about $\Delta X * \Delta Y = 2$ mm, the best spectral resolution is $\Delta \lambda = 1.2$ Å, moderate sensitivity. Sensor for record of integral plasma radiation on the base of photomultiplier gage is used as well. Temporal resolution is of 0.1 μ s.

Important information can be also obtained by detail analysis of electrical parameters of the discharge because a dynamics of the channel resistance depends on sort of gas (see Section 5).

Concluding this section we have to announce that during the experiments the deeply modified schlieren and schlieren-streak techniques were utilized with appropriate processing of images; measurements of voltage and current to estimate electrical field and power release; optical spectroscopy for the temperature measurements; and high-speed photography to study the discharge dynamics in flow.

References to Section 4.6.

1. *J. M. Seiner, S. M. Dash, and D. C. Kenzakowski*, "Historical survey on enhanced mixing in scramjet engines," *J. Propul. Power* 17, 1273 (2001)
2. *E. J. Gutmark, K. C. Schadow, and K. H. Yu*, "Mixing enhancement in supersonic free shear flows," *Annu. Rev. Fluid Mech.* 27, 375 (1995).

3. *Shigeya Watanabe, M. G. Mungal* “Velocity fields in mixing-enhanced compressible shear layers” *J. Fluid Mech.* (2005), vol. 522, pp. 141–177.
4. *T. Rossmann, M. G. Mungal & R. K. Hanson* “Mixing Efficiency Measurements Using a Modified Cold Chemistry Technique,” *Expts. Fluids*, 37, 566-576, (2004).
5. *N. T. Clemens & M. G. Mungal* “Large Structure and Entrainment in the Supersonic Mixing Layer,” *J. Fluid Mech.*, Vol. 284, 171-216, (1995).
6. *J. E. Broadwell & M. G. Mungal* “Large-Scale Structures and Molecular Mixing,” *Phys Fluids A*, 3 (5), 1193-1206, (1991).
7. *M. G. Mungal & P. E. Dimotakis* “Mixing and Combustion with Low Heat Release in a Turbulent Shear Layer,” *J. Fluid Mech.*, (1984), 148, 349-382.
8. *S. Murugappan, E. Gutmark, C. Carter*, “Control of penetration and mixing of an excited supersonic jet into a supersonic cross stream”, *Phys. Fluids* 17, 106101(2005)
9. *S. Leonov* “Plasma-Assisted Aerodynamics: Approach and Problem of Measurements”, Keynote Lecture, Proceedings of FLUCOME2007, September 17-19,2007, Tallahassee, FL, USA
10. *A. Bocharov, V. Bityurin, I. Klement'eva, and S. Leonov*, A Study of MHD Assisted Mixing and Combustion, In: 41st Aerospace Sciences Meeting and Exhibit, Reno, NV, 2003, AIAA Paper 2003-5878.
11. *L. Zimmer, Sh. Tachibana*, “Laser induced plasma spectroscopy for local equivalence ratio measurements in an oscillating combustion environment”, Proceedings of the Combustion Institute, issue 31, 2007, pp.737-745
12. *T.-W. Lee, N. Hegde*, *Combustion Flame*, 142, 2005, pp.314-316
13. *K. Kohse-Hoinghaus, R.S. Barlow, M. Alden, J. Wolfrum*, Proceedings of the Combustion Institute, issue 30, 2005, pp.89-123

4.7. Benefits of double-pulse pattern.

During the previous experiments on HV discharge generation in high-speed flow (“Control of Flow Structure and Ignition of Hydrocarbon Fuel in Cavity and behind Wallstep of Supersonic Duct by Filamentary DC Discharge”, Ed. S. Leonov, Project ISTC-EOARD-IVTAN #3793p, The Annual Technical Reports, Oct 2010) some benefits of double-pulse mode were considered in terms of fuel mixing and ignition. The idea is understandable from the figure below on two-pulse pattern of mixing/ignition at direct fuel injection in high-speed flow. The first pulse is responsible for mixing and the medium preliminary activation. The second pulse provides fast controllable ignition at the best synchronization of the moment with the position of fuel portion.

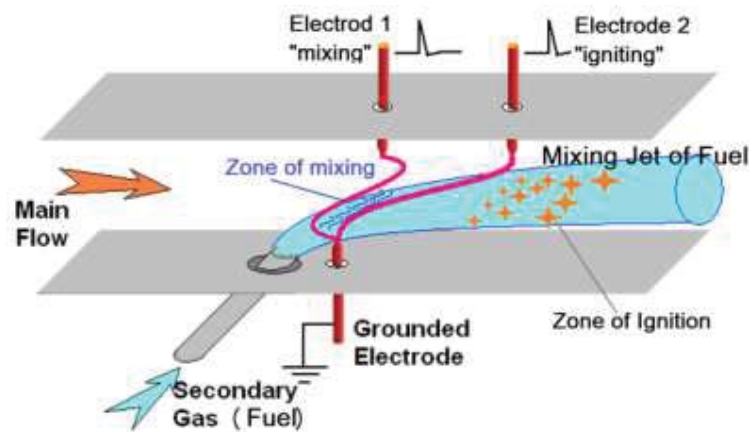


Fig.4.7.1. Principal schemes for double-pulse ignition physical demonstration.

Plasma-chemical kinetic simulation was performed to verify the idea, whether any actual energetic benefit and synchronization accuracy may be achieved due to this scheme of combustion initiation. Some results are presented below.

Simulations were performed by CWB software with kinetic mechanisms “Kintech”. Initial conditions $P = \text{const} = 1 \text{ Bar}$, the discharge was simulated at fixed E/N , in all cases $E/N = 120 \text{ Td}$. The mixture was stoichiometric $\text{C}_2\text{H}_4 - \text{Air}$, initial gas temperature 300 K. Concentration of CN was indicated for diagnostic purposes. Figures 4.7.2 and 3 compare the result for single and double pulse with the same total power. At energy release in the first pulse 0.2 eV/mol the time of ignition $t = 735 \mu\text{s}$. At extra 0.07 eV to the second pulse in time moment $245 \mu\text{s}$ after the first pulse, the ignition occurs at $t = 256 \mu\text{s}$. If the time between the first and the second pulses is bigger than the ignition time after the single pulse with the same total energy, than the ignition is observed right after the second pulse with a minimal delay.

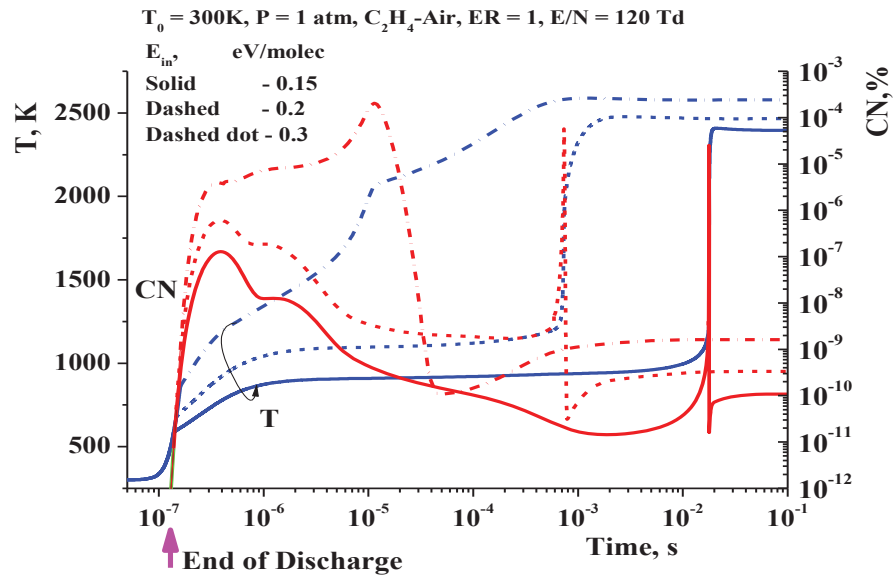


Fig.4.7.2. Dynamics of gas temperature and CN concentration at variation of the discharge energy (0.15, 0.2 and 0.3 eV/mol). Single pulse mode. Logarithmic scale.

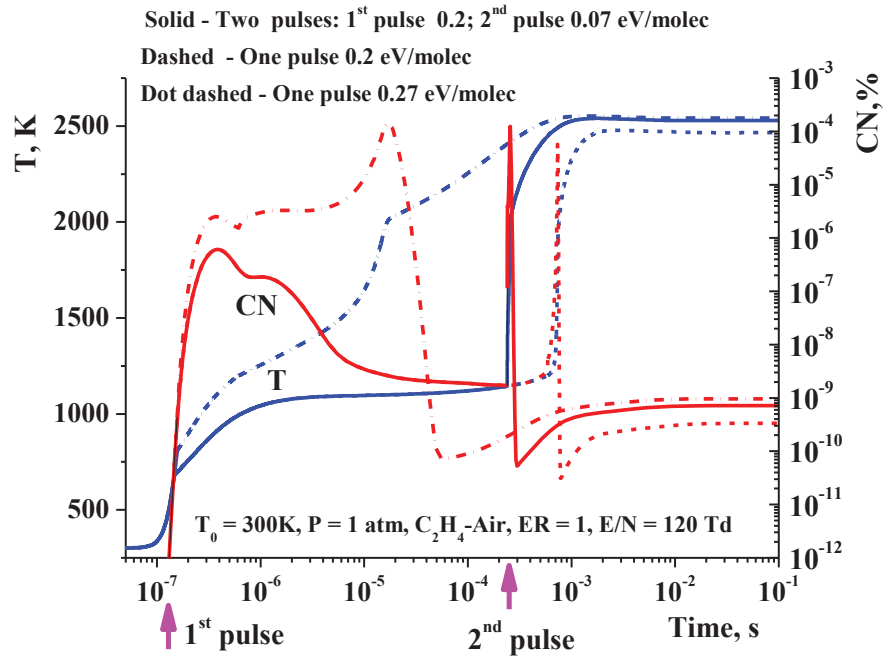


Fig.4.7.3. Dynamics of gas temperature and CN concentration at variation of the discharge energy (0.15, 0.2 and 0.3 eV/mol). Double pulse mode. Logarithmic scale.

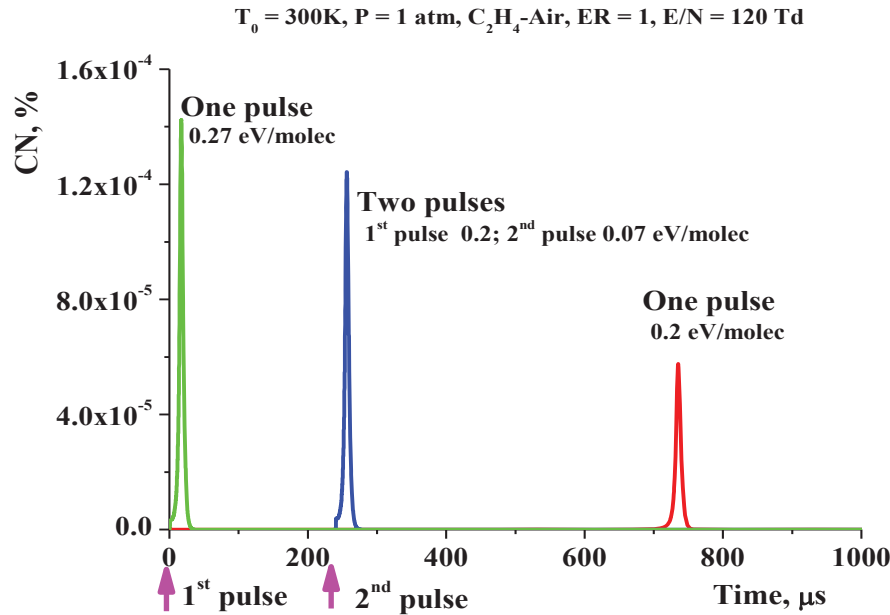


Fig.4.7.4. Dynamics of CN concentration at single pulse and double pulse mode. Linear scale.

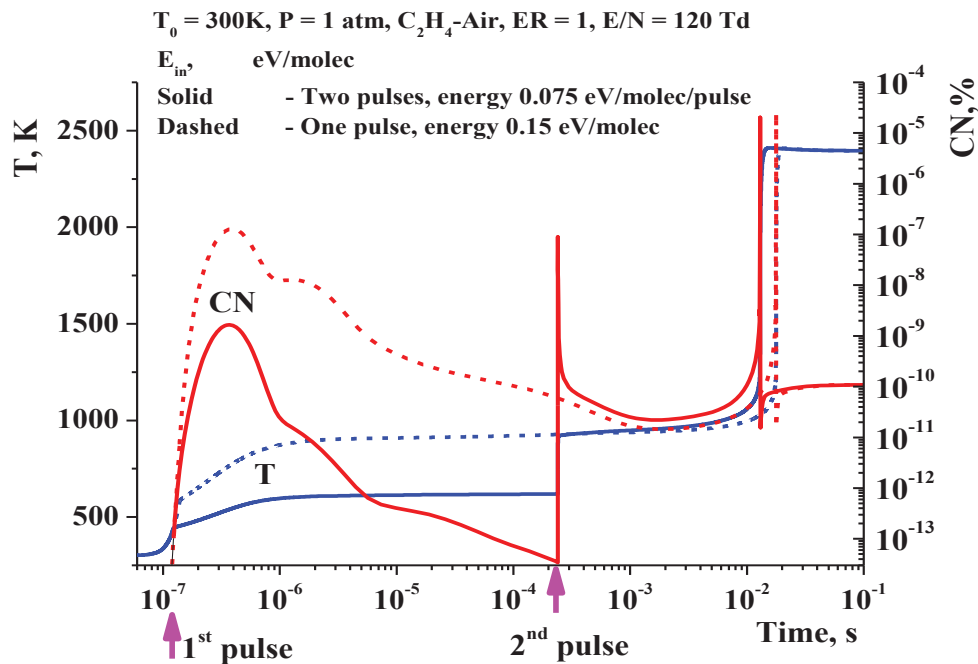


Fig.4.7.5. Dynamics of gas temperature and CN concentration. Single and double pulse mode.

Logarithmic scale.

If the time between the first and the second pulses is less than the ignition time after the single pulse with the same total energy, than the ignition delay reduces on 30% approximately, as it is demonstrated in Fig.4.7.5.

The effect of double pulse mode is especially significant for a lean mixture, as it is shown in Figs.4.7.6-7. It should be considered the effect of accurate synchronization of the ignition in wide range of the second pulse delay as it is shown in Fig.4.7.8.

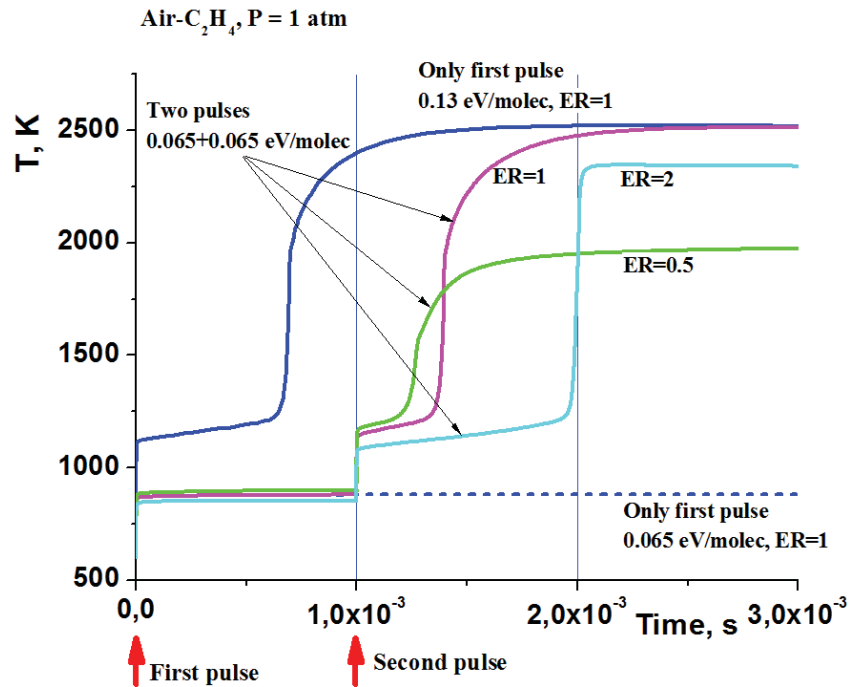


Fig.4.7.6. Dynamics of gas temperature at variation of mixture ER. Double pulse mode.

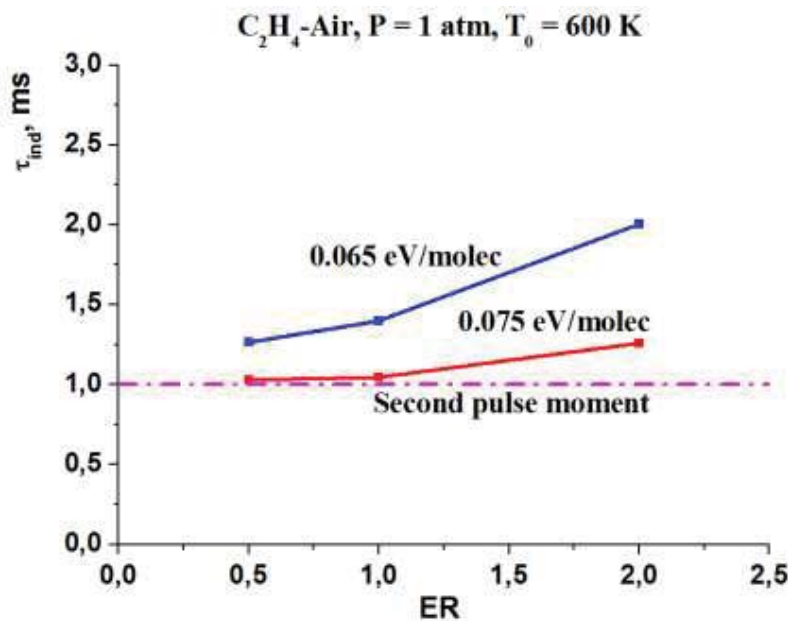


Fig.4.7.7. Induction time in double pulse mode vs equivalence ratio of gas mixture.

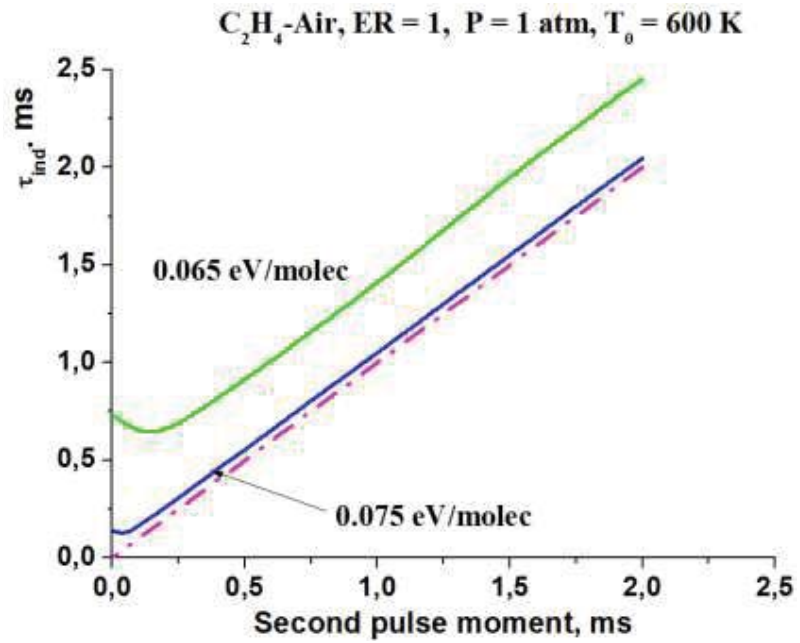


Fig.4.7.8. Induction time in double pulse mode vs time moment of the second pulse.

4.8. Ignition by filamentary pulse plasma.

Despite of instability and the discharge localization modeling in non-homogeneous gas (see sections 4.1-4.4) the effectiveness of the pulse filamentary discharge for the fuel ignition under intensive mixing was analyzed in details.

The problem encountered in modeling plasma of inflammable gases is the necessity to combine approaches of high non-thermal plasma kinetics and of classic thermal combustion. Such unification was made by the authors [1] who showed numerically that for plasma ignition of ethylene-air mixture within a reasonable length of a supersonic flow rather high energy input per mass of gas flow is required (about 210 J/g).

Such parameters of a discharge as E/N (E is the electric field strength, N is the gas number density) and electric current density or electron number density are strictly correlated by discharge nature. In order to find rates of processes involving electrons it is necessary to address the electron Boltzmann equation where from the electron energy distribution function (EEDF) could be calculated. To account properly excitation and dissociation of molecules in the discharge one has to guarantee acceptable accuracy of electron scattering cross sections used in the model. The key criterion for evaluation of their accuracy is a good agreement between calculated and available measured transport and kinetic coefficients for each component of the gas mixture. Traditionally, a set of cross sections for a given species, which satisfies this criterion, is called the 'self-consistent' set.

Actually, development of a non-thermal discharge with required characteristics in high-speed, high-pressure supersonic gas flow is questionable. As was noted by authors [2], there are experimental data indicating that plasma chemical conversion of methane is more effective when discharges have filamentary form. We anticipate that usage of non-uniform (filamentary) plasma may accelerate essentially ignition of premixed fuel – air flows.

One of the most attractive schemes of the ignition of combustible mixture is figured as a system of filamentary discharge located periodically in front direction, as it is shown in Fig.4.8.1. Such type of discharge can be formed by special multi-electrodes system. In this section the result of numerical experiment in a model gasdynamic situation is presented.

Typical duration of the discharge's electrical pulse is much shorter than the characteristic gasdynamic time. That is why the power release can be described as in a fixed volume V_0 . The excited gas zone is expanded and mixed with non-excited gas. Two physical processes are appeared at this moment: a cooling due to the mixing and the thermal power deposition as the

result of combustion. A comprehensive model of mixing and combustion is rather complex, especially in a real kinetic approach.

To examine this approach the model was developed for burning initiation by a series of periodically positioned transverse filamentary-like discharges in approximation of distributed mixing of excited and non-excited gas streams. The model includes self-consistent simulations of the discharge of a small radius in supersonic flow of ethylene-dry air mixture [1] with followed gradual mixing of excited gas with main flow, see Fig.4.8.1. Mixing process was characterized by time interval between beginning of mixing and its termination by exhaust of main stream, Δt_{mix} , and the ratio of the final volume to the initial plasma volume, V/V_0 . The calculations were performed for the ethylene-air premixed composition at initial pressure 1Bar and initial temperature 700K.

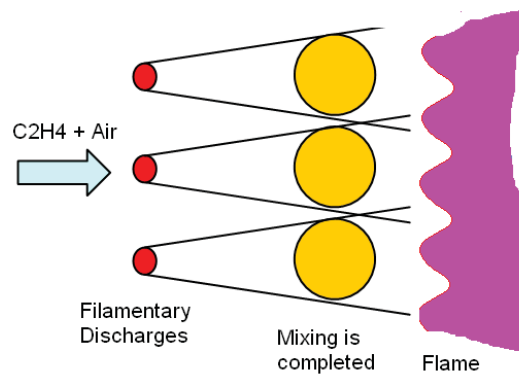


Fig.4.8.1. Scheme of analysis of ignition by filamentary discharge.

In the model the expansion from the volume V_0 to the volume V and mixing are supposed to be started right after the electrical pulse ($1\mu s$) and completed in predefined time t_{mix} . The temperature is being found based on energy balance equation. Components' concentration is reduced due to redistribution in a current volume as follows:

$$\frac{dN_i}{dt} = \left(\frac{dN_i}{dt} \right)_{UNIFORM} - \frac{N_i}{t_{mix}} \left(1 - \frac{V}{V_0} \right).$$

An initial diameter of the discharge's filament is small comparing with a location's space period. At the same time the mixed zone covers whole exposed area during a short time. Concentration of radicals and molecules formed by the discharge is reduced in accordance with the volumetric law (mixing + expansion). Extra molecules N_2 , O_2 , and C_2H_4 are come from the fresh mixture:

$$\frac{dN_i}{dt} = \left(\frac{dN_i}{dt} \right)_{UNIFORM} - \frac{N_i - N_i^0 \frac{T_0}{T}}{t_{mix}} \left(1 - \frac{V}{V_0} \right),$$

where N_i^0 , T_0 – concentration and temperature of initial gases; T – current temperature in mixed volume. Under these conditions the most correct approach is the approximation of the constant gas pressure.

The physical-chemical model is a consistent combination of two approaches [2]: classical thermal combustion theory (close to GRI Mech3 combustion mechanism) and glow discharge plasma kinetics. The equations of thermal and plasma chemistry are solved in isochoric approximation in parallel with the Boltzmann equation for the electron energy distribution function. It was shown previously that isochoric model is in a satisfactory agreement with results computed in frame of a system of 1D gas-dynamic equations in a plug flow model. GRI Mech3 combustion mechanism is widely used, its applicability is proven at temperatures higher than about 1100 K. Plasma kinetic model was validated for low temperature 300 K atmospheric pressure glow discharge in air. This model includes evolution equations for charged particles' densities, excited atom and molecules' densities, and electric circuit equation.

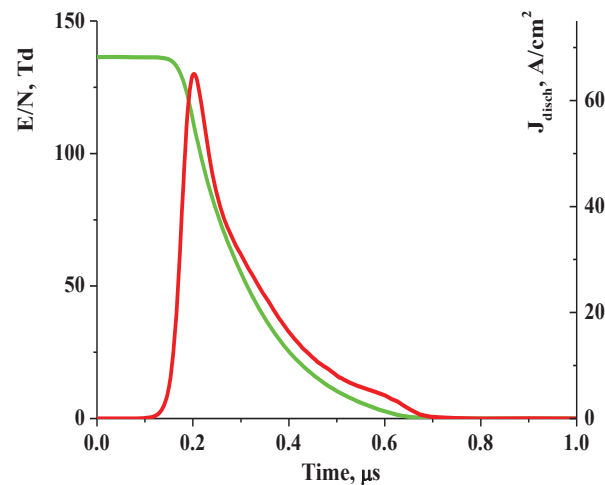


Fig.4.8.2. Dynamics of reduced electric field and current density. Specific power deposition 480 J/g. $T=700\text{K}$, $P=1\text{Bar}$, $\text{N}_2:\text{O}_2:\text{C}_2\text{H}_4=12:3:1$, $R=0.5\text{mm}$.

The discharge and external electrical circuit were modeled by a capacitance and the discharge channel resistivity (self-consistent model). The discharge filament radius was predefined as 0.5mm, energy deposition in this case was 480 J/g. Typical waveforms of the reduced electrical field and the current density are shown in Fig.4.8.2. The electrical field at the current maximum was $E/N=150\text{Td}$. A main mechanism of the plasma effect on chemical reactions rate is the atomic oxygen generation. The part of discharge energy, which is spent for the oxygen generation, is shown in Fig.4.8.3 depending on the electric field. The calculations are fulfilled for the initial gas parameters and composition. The direct molecular dissociation by

electron impact takes about 14% at $E/N = 160\text{Td}$. A total effective dissociation includes collisions with electronically excited nitrogen. The maximal part of energy taken for the O_2 dissociation is about 58% at $E/N = 205\text{Td}$, when the direct heating is taken into account as well.

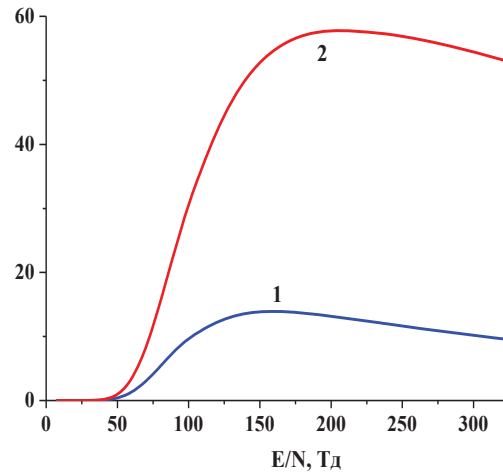


Fig.4.8.3. Part of discharge energy (%) spent for O_2 dissociation in mixture $\text{N}_2:\text{O}_2:\text{C}_2\text{H}_4=12:3:1$. 1 – direct dissociation by electron impact; 2 – total effect including electronically excited N_2 .

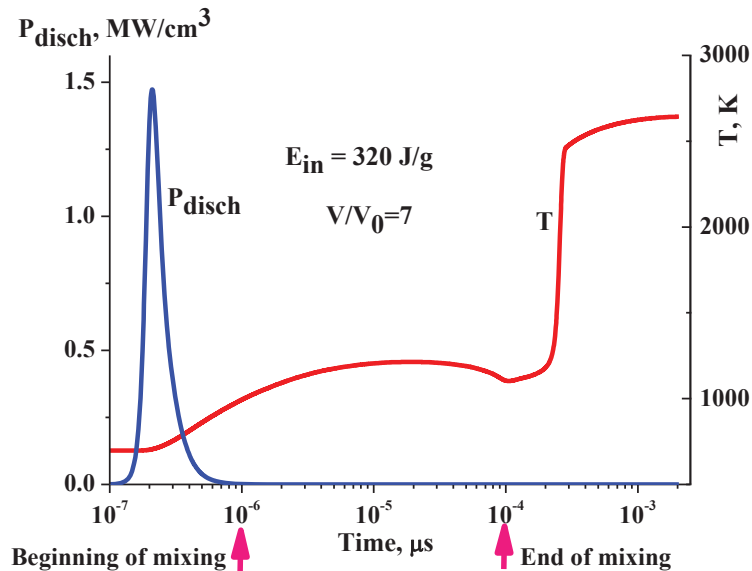


Fig.4.8.4. Dynamics of plasma power and the gas temperature at distributive mixing. $V/V_0=7$, $t_{\text{mix}}=100\mu\text{s}$.

Figure 4.8.4 presents dynamics of the discharge power and the gas temperature. One of important features is non-monotonous behavior of the gas temperature. One can see some

temperature decrease at the end of the mixing. The effect may be explained by a competition of mixing with relatively cold gas and heating due to chemical reactions. At the parameters of interaction chosen in this particular case a local temperature maximum is observed at the beginning of the mixing. Figure 5 shows the temperature evolution at variation of V/V_0 . For the time scale $t < 500 \mu\text{s}$ the mixing degree $V/V_0 = 10$ is a critical value. At reduced time of mixing the time of ignition is increased dramatically. In this case the cooling is prevailed over heat release.

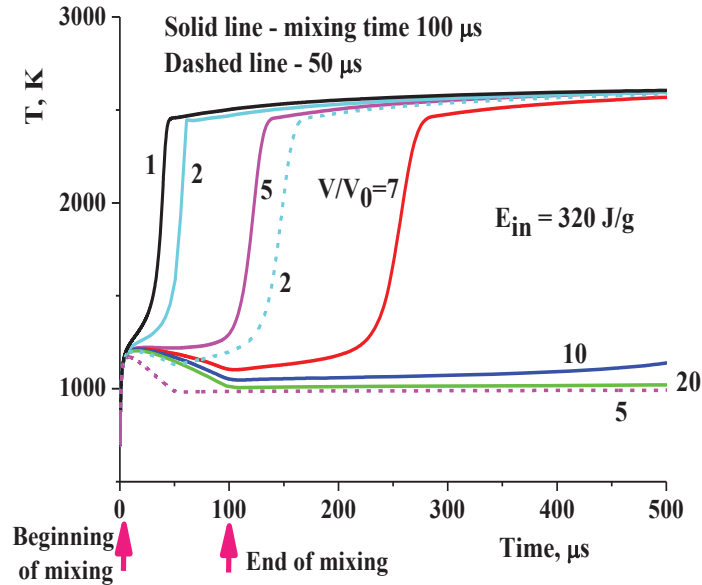


Fig.4.8.5. Dynamics of gas temperature depending on mixing degree V/V_0 and the mixing duration t_{mix} . Solid lines are for $t=100 \mu\text{s}$, dashed lines are for $t=50 \mu\text{s}$.

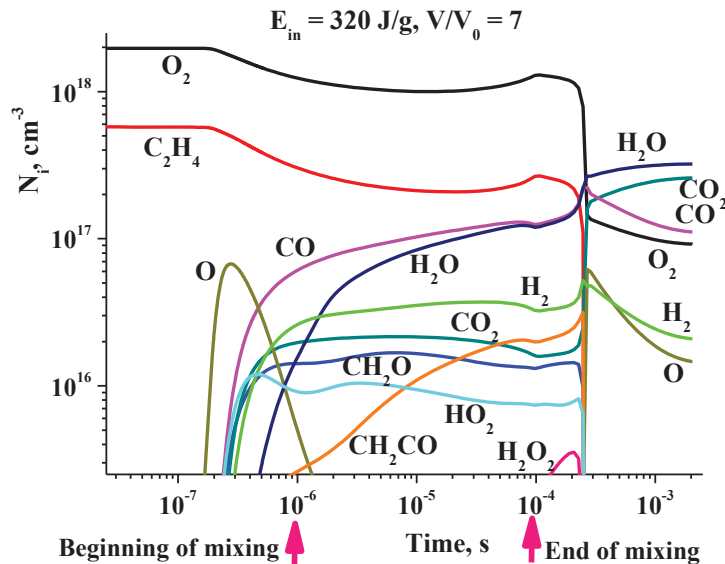


Fig.4.8.6. Dynamics of molecules and radicals concentration at discharge initiation and distributive mixing. The conditions are the same as in Fig.4.8.4.

The dynamics of molecules and radicals concentration is presented in Fig.4.8.6. At the beginning one can see a significant increase of the atomic oxygen concentration. Then so-called «cool flame» takes place, when the molecules CO, CH₂O, H₂, HO₂, CH₂CO, and others are generated. At $t > 10 \mu\text{s}$ but before the end of mixing, some rise of the O₂ and C₂H₄ concentration is observed due to coming of fresh gas. Depending on conditions the full combustion may or may not follow these preliminary stages.

The ignition time is one of the most important characteristic of the combustion processes. At the analysis of results this time was defined as the point of maximal derivative of the temperature dynamics curve. Usually this time is equal to the maximal concentration of the CH radicals, and can be useful for optical diagnostics of the ignition process. Figure 4.8.7 illustrates the ignition time depending on mixing degree and the mixing time. At mixing time $100 \mu\text{s}$ and mixing degree $V/V_0 = 12$ the ignition time is more than $600 \mu\text{s}$. The faster mixing leads to faster cooling and bigger ignition time.

In practical problem of plasma-based ignition and flameholding in ducts there is more convenient to present data in terms of length of ignition than of ignition time. The curves in Fig.4.8.8 presents the results of simulation of the ignition length of ethylene-air mixture depending on mixing time at initial flow velocity $M = 2.0$. Well seen that the ignition can be realized on the length $X = 0.6 \text{ m}$ at plasma energy release $W/G = 45 \text{ J/g}$ for mixing time $t = 100 \mu\text{s}$, and $W/G = 175 \text{ J/g}$ for mixing duration $50 \mu\text{s}$. Figure 4.8.8 also shows how the predicted induction time for combustion of ethylene-air mixture depends on the energy input per mass of gas flow in the case of filamentary discharge for two values of mixing time. At $\Delta t_{\text{mix}} = 100$ and $\Delta t_{\text{ind}} = 50 \mu\text{s}$ the required reduced energy input is about 40 J/g , that is remarkably lower than for uniform discharge.

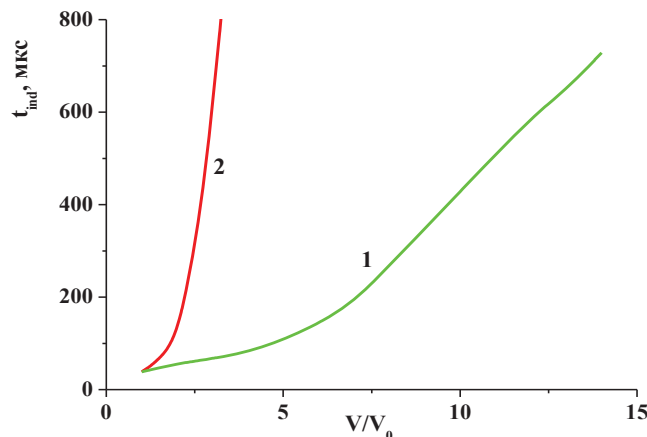


Fig.4.8.7. Ignition time vs mixing degree. 1 – mixing time $t = 100 \mu\text{s}$; 2 – $t = 50 \mu\text{s}$. The conditions are the same as for Fig.4.8.2.

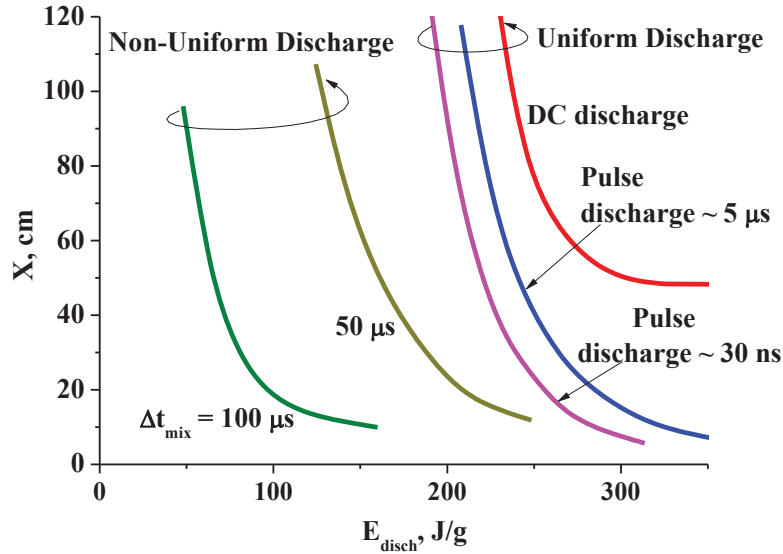


Fig.4.8.8. Length of ignition depending on energy release and the discharge mode. $M = 2$. Other conditions are the same as in Fig.4.8.2.

Herewith one can find the data for homogeneous DC discharge and pulse discharges of different pulse duration [3]. Non-homogeneous discharge possesses an obvious benefit in this regard. Comparison of the specific energies needed to ignite the mixture by non-homogeneous discharge, variety of homogeneous discharges, and by the heating is presented in Table.4.8.1. The use of non-homogeneous short-pulse discharge allows one to reduce the required power in 5times comparing with a homogeneous discharge, and in order of magnitude in comparison with the heating of the gas.

Table 4.8.1. Comparison of the energy levels required for the ethylene-air mixture ignition in $M=2$ flow. Combustor length 0.6m.

	Non-homogeneous	Homogeneous discharge			Heat
Mode	Pulse, mixing 100μs	Pulse ns discharge	Pulse μs discharge	DC discharge	
W/G, J/g	45	210	230	265	520

Figure 4.8.9 shows the ignition time vs specific energy deposition at different initial fuel concentrations: lean mixture, stoichiometric mixture, and rich mixture. It should be considered the less benefit of this method for a lean mixture due to less temperature elevation at the fuel oxidation.

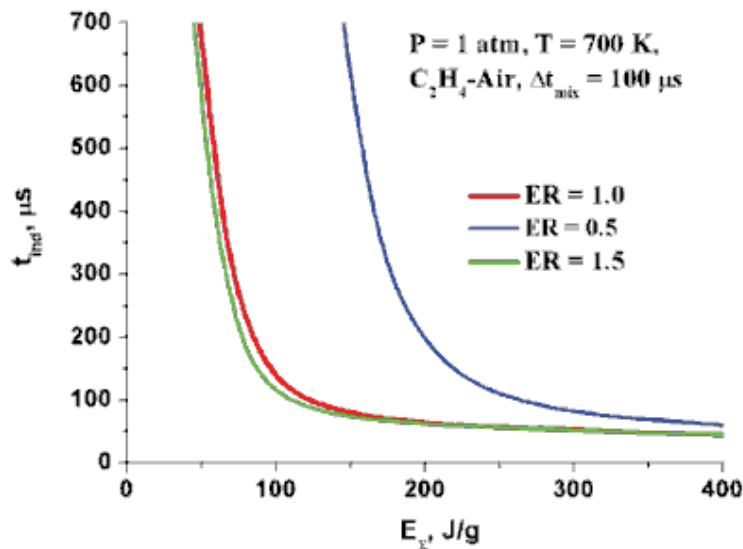


Fig.4.8.9. The ignition time vs specific energy deposition at variation of initial fuel concentrations. Mixing time $t=100\mu\text{s}$, $T=700\text{K}$, $P=1\text{Bar}$.

Reference to section 4.8.

1. I. Kochetov, A. Napartovich, and S. Leonov, "Plasma ignition of combustion in a supersonic flow of fuel-air mixtures: Simulation problems," *J. High Energy Chem.*, vol. 40, no. 2, pp. 98–104, 2006.
2. Pushkarev A., Zhu Ai-Min, Li Xio-Song, Sazonov R., V International Symposium on Theoretical and applied Plasma Chemistry, I.1, 23, 2008
3. Sergey B. Leonov, Yury I. Isaenkov, Dmitry A. Yarantsev, Igor V. Kochetov, Anatoly P. Napartovich, Michail N. Shneider "Unstable Pulse Discharge in Mixing Layer of Gaseous Reactants", 47th AIAA Aerospace Sciences Meeting and Exhibit (Orlando, FL, USA, 5-8 January 2009), AIAA-2009-0820.
4. Sergey B. Leonov, Yury I. Isaenkov, Alexander A. Firsov, Dmitry A. Yarantsev, Michail N. Shneider, "High-Power Filamentary Pulse Discharge in Supersonic Flow", 48th AIAA Aerospace Sciences Meeting and Exhibit (Orlando, FL, USA, 4-7 January 2010), AIAA-2010-0259.
5. I. Kochetov, A. Napartovich, and S. Leonov, "Numerical simulation of plasma ignition in supersonic flow", 5-th International Symposium "Thermochemical and Plasma Processes in Aerodynamics". St-Petersburg. "Radioavionica". 2006. p.25.
6. Sergey B. Leonov, Dmitry A. Yarantsev, Campbell Carter "Transversal Electrical Discharge as a New Type of Flameholder", 15th AIAA International Spaceplanes and Hypersonic Systems and Technology Conference, Dayton, OH, Apr-May 2008, AIAA-2008-2675.

5. Task 2. Experimental Efforts

5.1. Experimental facility description

In frames of the Task 2 the experiments were fulfilled to study of the pulse discharge dynamic in ambient gas, in high-speed flow, and in two-component flow (subsonic and supersonic).

Experiments in quiescent gas: The experimental scheme of test in quiescent gas is shown in Fig.5.1.1. The facility consists of test section, system of the pulse-repetitive feeding (pulse-repetitive discharger PD-100/2.5), and diagnostic arrangement. The test facility is equipped with high-quality optical windows. The diagnostic set consists of the following instrumentation:

- < schlieren device with spatial resolution not worse than 0.2mm and temporal resolution 0.1 μ s;
- < set of transducers and probes for
 - o pressure,
 - o voltage,
 - o current,
 - o radiation measurements;
- < spectroscopic system;
- < high speed CCD and CMOS cameras;
- < line-scan camera, etc.

The pulse transversal discharge is excited by means of the specially designed power supply made on the base of Tesla coil with impact excitation. The typical parameters of the tests are the following:

- gas pressure $P=0.1-2Bar,$
- discharge's main pulse duration $\tau=50-150ns,$
- maximal voltage $U_{max}=120kV,$
- maximal current $I_{max}=2.4kA,$
- maximal power release $W_{max}=110MW,$
- typical energy deposition in short-pulse mode $E=1-2.5J.$

The photo of test section is shown in the Fig.5.1.2. In the most experimental events two configurations of electrodes were applied in tests considered below, as it is presented in the Fig.5.1.3a,b: in the first scheme the top electrode looks like a single needle on axis of gas-feeding pipe; in the second scheme two anodes were applied near the wedge of the pipe. It was

done to locate the top electrode close to a boundary of gas jet flowed from the top pipe to bottom one. In two last cases the basic layout were modified to meet the specific test's task

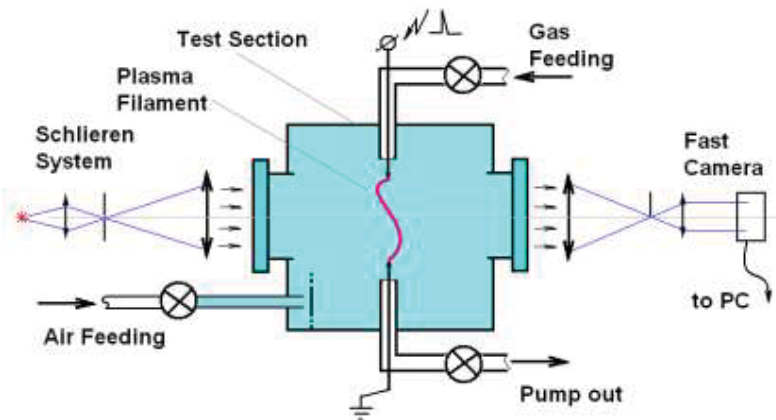


Fig.5.1.1. Experimental scheme of test in quiescent air.

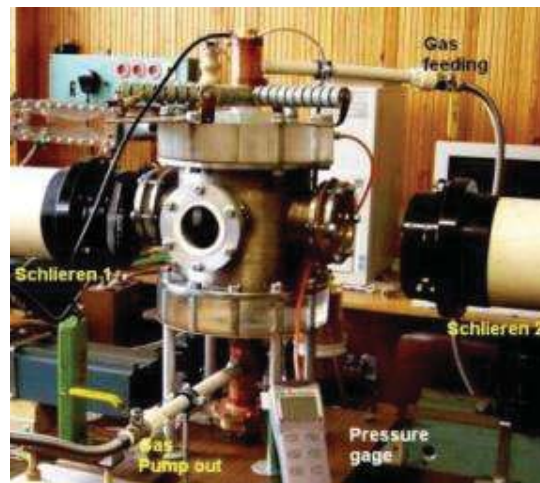


Fig.5.1.2. Photo of the test section.

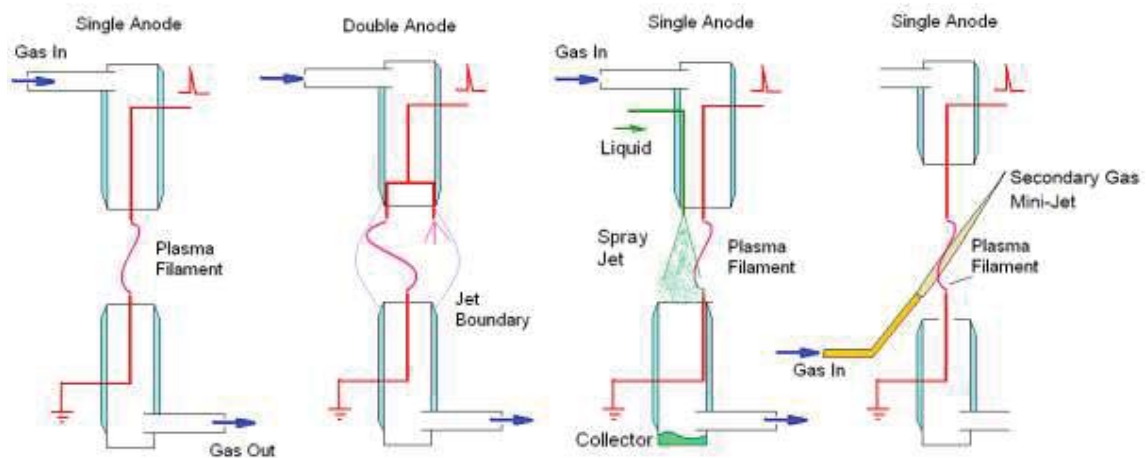


Fig.5.1.3. Variants of electrodes configuration for the test in quiescent air. (a) – single gas; (b) – two gases; (c) – spray-gas; (d) – gaseous mini-jet.

The experiments with sprays were performed at using of pulse system to avoid a dangerous situation with flammable fluids. The parameters of the spraying injection system are the following:

- ◆ Type of the injector spraying through 4 pinholes;
- ◆ Pressure of the injection 2÷6Bar;
- ◆ Pulse duration 1÷1000ms;
- ◆ Fluid mass flow-rate $G_f=10\div400\text{mg/pulse}=1\div4\text{g/sec}$.

The photo of spraying injector is presented in Fig.5.1.4a. The control of the fuel mass flow-rate occurs by the pressure in fuel tank and the pulse duration of EM control. Calibration curves obtained experimentally are presented in Fig.5.1.5 for two values of the pressure $P_{inj}=2$ and 4Bar . In this case the injection was carried out to ambient atmosphere. The value of fuel mass flow-rate is saturated on the level $G_f=4\text{g/sec}$ at the injection pressure increase over 5Bar . The photo of spray jet being illuminated by light spot $d\approx 3\text{cm}$ is shown in Fig.5.1.4b.

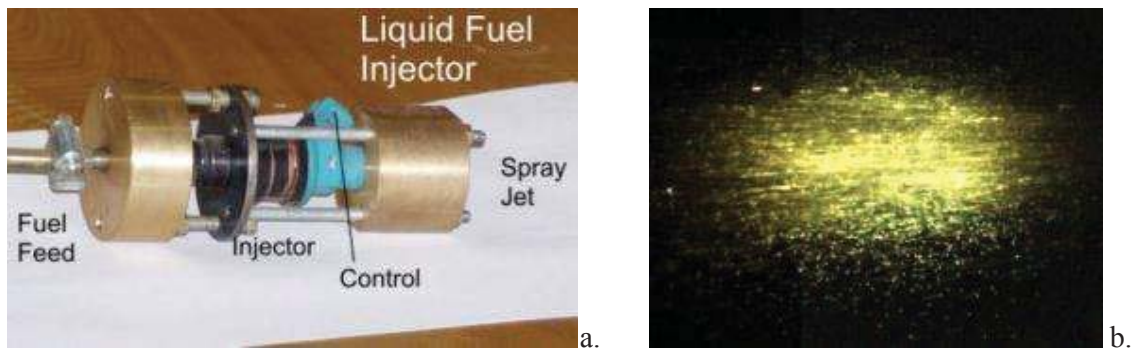


Fig.5.1.4. Photo of test sample of the spraying injector (a) and photo of spray jet (b).

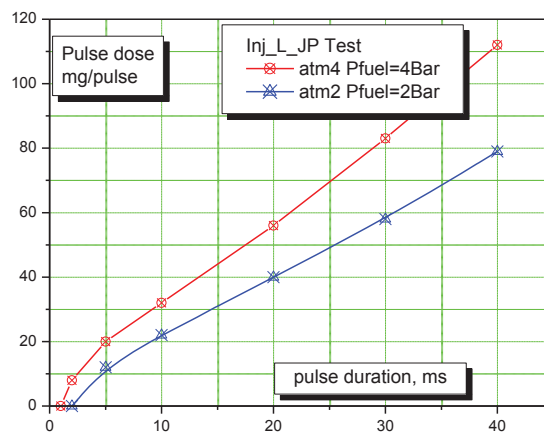


Fig.5.1.5. Spraying injector's characteristic measured.

Experiments in flow. These experiments were aimed at study the pulse discharge dynamic and localization in subsonic and supersonic airflow also at presence of second gas jet and spray jet of liquid hydrocarbons. The experiments were conducted in a short-duration blowdown wind tunnel PWT-50H with a closed test section $Y \times Z = 72 \times 72 \text{ mm}$ at Mach number of nozzle $M = 2$ and 2.5 and stagnation pressure $P_0 < 2.5 \text{ Bar}$, see Fig.5.1.6. The technical parameters of experimental test bed PWT-50HL are presented in Table 5.1.1 below.

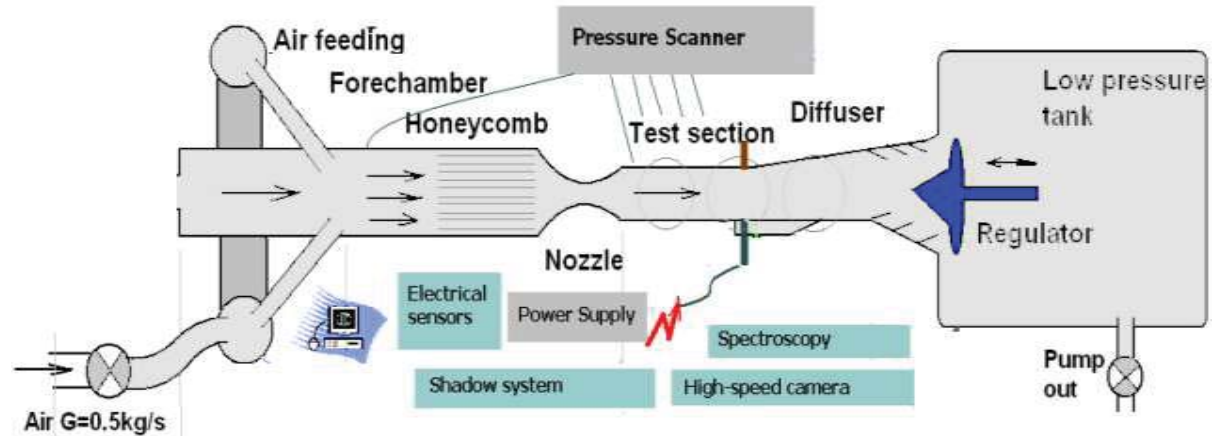


Fig.5.1.6. Scheme of the wind tunnel PWT-50H.

Table 5.1.1. Technical parameters of the facility PWT-50HL.

Parameter	PWT-50HL
Test section cross-dimensions, mm	72 (60)*72
Mach Number	2, 2.5
Maximal stagnation pressure, Bar	2.5
Stagnation temperature, K	300-750
Typical air mass flow rate, kg/s	0.5-1.0
Maximal fuel mass flow rate, g/s	0.1-8
Operation time, s	1.5
Steady stage duration, s	0.8
Runs per 8 hours, range	10-30
Lifetime, runs between services	200

Two experimental series were performed in single-phase flow: (1) study of pulse discharge dynamic in subsonic and supersonic flow in the test section 60*72mm; and (2) study of pulse discharge dynamic in supersonic flow in the test section 25*65mm, Fig.5.1.7. In the last case the static pressure of the air in M=2 flow was $P_{st}=350-450Torr$ comparing with $P_{st}=140-220Torr$ in the first case. A special geometric configuration was applied in the second series to avoid the near-wall breakdown of the discharge (narrow test section). Three main methods were applied for the visualization of plasma-flow interaction: instant schlieren images; schlieren-streak records; and schlieren based sensors records.

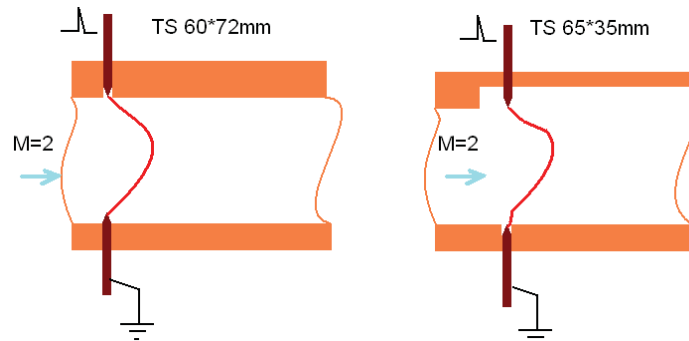


Fig.5.1.7. Experimental schemes for tests in flow.

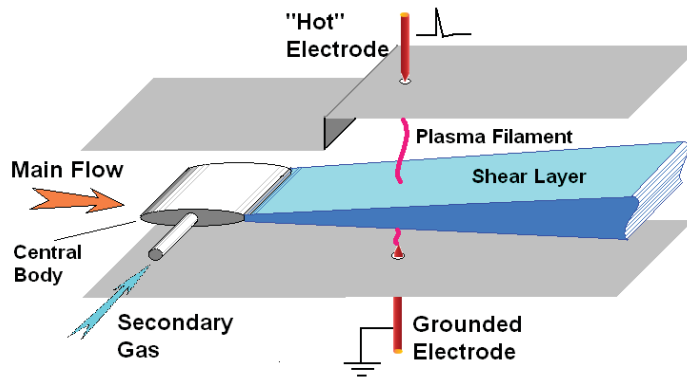
In the next experimental series a main attention was paid for study of the pulse discharge interaction with two-component flow. Three basic configurations were applied as they described in the Table 5.1.2 below and shown in Fig.5.1.8. It should be noted that air-fuel runs are not necessary supposed for configurations #1 and #2 because of their high-level hazard.

Table 5.1.2.

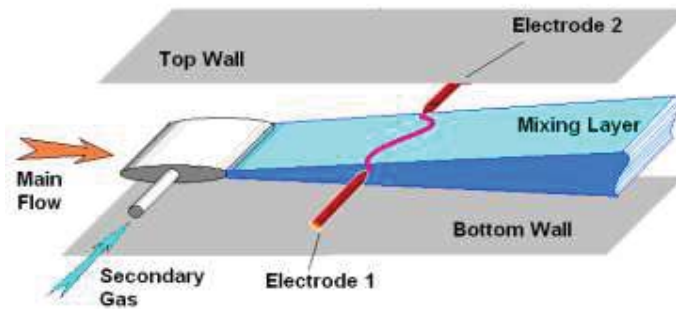
mode ##	Objectives	Gases	Discharge direction
1	Study of the discharge localization, mixing intensification	Air – CO ₂ ; Air – He	Transversally to flow, Cross boundary
2	Study of the discharge localization, mixing	Air – CO ₂ ; Air – He	Transversally to flow, Along the boundary
3	Study of the discharge localization, mixing, ignition	Air – CO ₂ ; Air – He; Air – H ₂ ; Air – C ₂ H ₄	Along the second gas transversal jet

In the first and the second configurations a plane jet of secondary gas is used to create the two-phase flow. For the gas feeding a central contoured body is installed to the duct. To avoid the electrical field aberration the central nozzle is made of dielectric material. The photo of insertion is shown in Fig.5.1.9. The first configuration was tested successfully. In the second

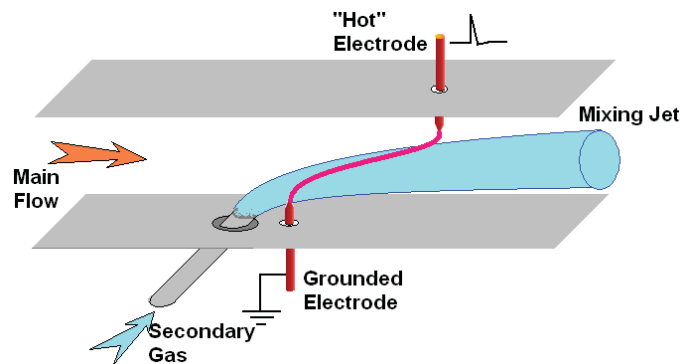
one there were some difficulties in diagnostics and visualization. The third scheme was explored in the most details.



Scheme 1



Scheme 2



Scheme 3

Fig.5.1.8. Three experimental configurations for two-component flow runs.

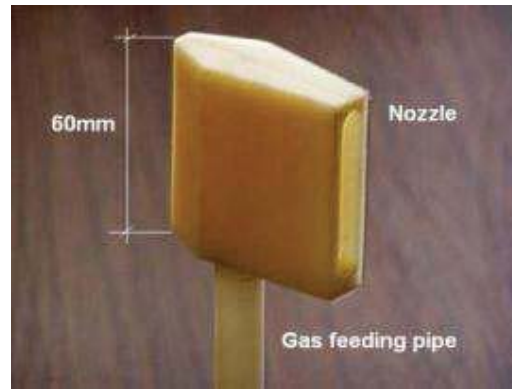


Fig.5.1.9. The photo of the central nozzle for the secondary gas injection.

Power supply for combined short-long pulses: New power supply (PS) was designed, assembled, and tested for experiments on afterspark channel dynamics in stagnant conditions. This PS was prepared to provide an extra supply of the discharge gap by the electrical pulse of millisecond duration. Principal scheme is shown in Fig.5.1.10.

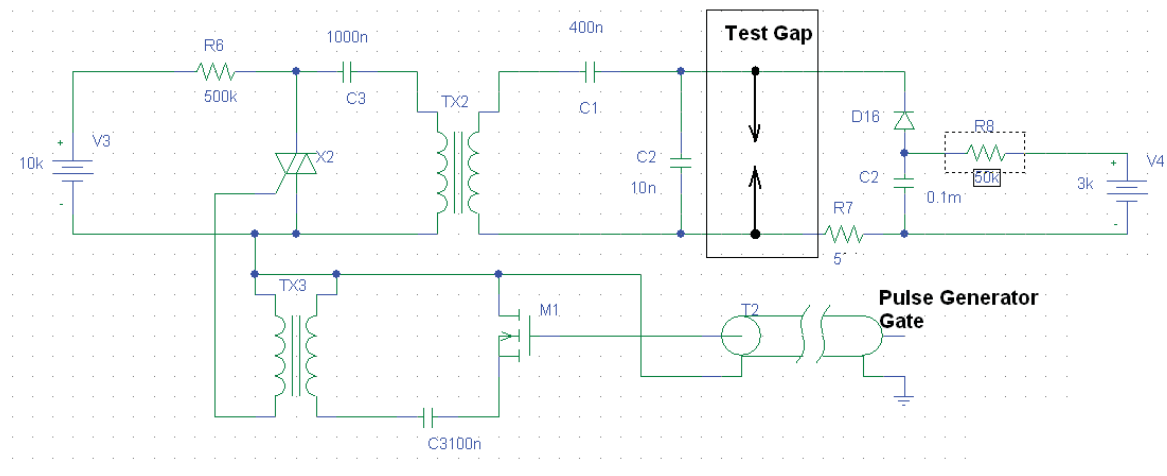


Fig.5.1.10. Principal scheme of the power supply for combined short-long pulses generation.

Main spark gap (in test section) is connected to pulse transformer through the dividing capacitance $C=0.4\mu\text{F}$. Magnetic coupling factor was established as large as

$$K = \frac{M}{\sqrt{L_1 \times L_2}} \approx 0,8.$$

Such a value leads to maximum amplitude of the voltage in the first half-period of the oscillation. At the same time it avoids a negative polarity of the voltage on diode D1. After the gap initial breakdown the diode D1 opens and the electrical current flows from the secondary capacitance $C2=100\mu\text{F}$ of value to the discharge filament. The pulse transformer is excited by discharge of $1\mu\text{F}$ capacitance initially charged with voltage $U \approx 10\text{kV}$. The capacitor is steering

by controlled gap, which is managed by pulse transformer TP2. The start of the controlled gap is being made by means of industrial pulse generator, which is synchronized with the system of optical registration.

Power supply for pulse-repetitive operation mode: The next generation of PS was prepared for the test with pulse-repetitive operation mode. The repetition frequency of the discharge power source must be not less than $f=10kHz$ in order to simulate pulse periodic mode of the interaction between spark discharge channel and supersonic flow $V=480m/s$. At such parameters the shift of the discharge region downstream the electrodes during the time between pulses is about the discharge gap. At smaller repetition frequency of the HV pulses the mode is the same as for a single pulse. At higher frequency there is a possibility of the secondary breakdown through a previous zone of disturbance because a recovery speed of the electric strength is not high enough.

Generation of powerful HV pulses at high repetition frequency is a complex technical problem. Several schemes of the power source have been analyzed to realize the mode mentioned above. All of them are based on the application of the controlled spark discharges as commutator of the primary circuit. Application of the solid commutator is limited due to its high cost and relatively low repetition frequency at needed power of commutation. Scheme on the base of resonant transformer with application of one primary capacity storage and one discharger in the primary circuit has been tested experimentally in order to achieve the maximal possible repetition frequency of the pulses. Simplified scheme is shown in the Fig.5.1.11.

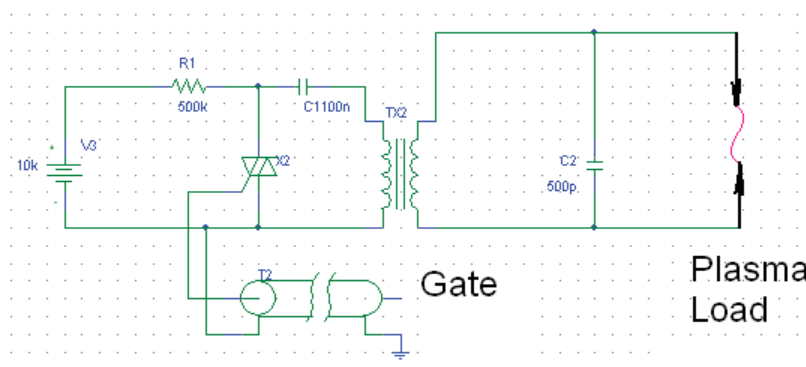


Fig.5.1.11. Principal scheme tested.

This scheme allows to operate at repetition frequency as high as of $f=2kHz$, that corresponds to the averaged power of the power source $W_{av}=5kW$.

Modification of pulse-repetitive power supply. Several principal schemes have been considered for the spark discharge excitation at high repetition rate within the supersonic airflow. It is clear that HV switchers are needed to be applied in order to form high voltage pulses. In last version the spark gap switchers were used for this purpose. This decision allows realizing scheme of the frequency HV generator in most simple way. Maximum achievable pulse repetition rate is determined by the recovery rate of switchers. Recovery rate depends on many factors, such as value of the switched energy, discharge gap, kind of the gas in the switcher, gas pressure, etc. Switchers filled with hydrogen possess the highest recovery rate of the breakdown strength. This statement is applied to the pressurized switchers without blowdown of the gap.

The previous scheme in Fig.5.1.11 allowed to get repetition rates at tandem modes up to 2-2,5 kHz, that relates to the average switched power of 6-7 kW. These values occurred limit ones for the single switcher filled with hydrogen. The process of storage capacitor C charging differs by the following in the tested scheme: charge current arises immediately after the switcher run. Current at this moment is influencing the de-ionization process of the switcher in spite of the small value of the current. It is known that much better switch properties may be obtained if to apply a sleep-sided pulse of the voltage on the switcher. A scheme shown in the Fig.5.1.12 has been adjusted and tested in order to achieve repetition rates of 10 kHz. Mode with zero voltage on the switcher after the run until the operation of the next switcher is provided by this scheme due to the application of the high-resistance (1 MOhm) buffer resistors. This fact facilitates the process of the switcher electrical strength recovery and allows to get delays of the switcher operation of 100 μ s that relates to the pulse repetition rate of 10 kHz.

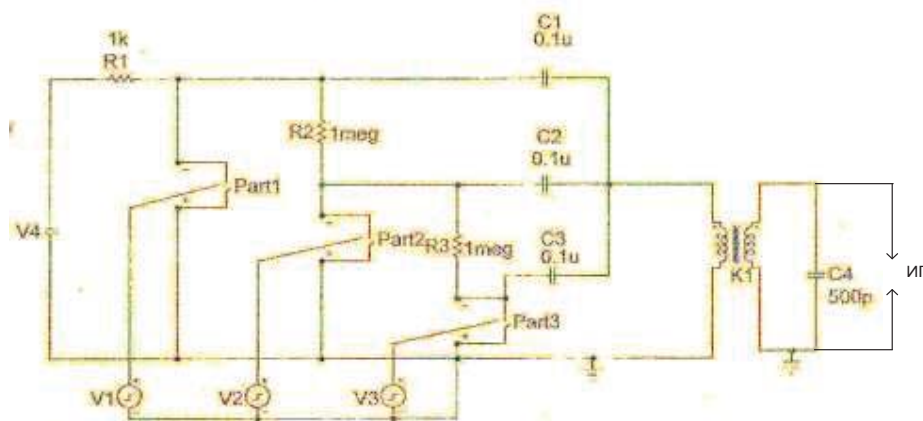


Fig.5.1.12. Triple pulse adjusted scheme.

Nevertheless the switch process is complicated by the over-voltage pulse that is generating on the other switchers (for example II and III) after the operation of the one of them (for example I). It occurs due to the existence of the capacitance driver C_2 ; C_p or C_3 ; C_p (C_p – parasitic capacity of the switcher). Therefore sum of the voltages that is equal to the voltage of the capacitors charge plus voltage on the primary circuit of the Tesla transformer is generating at this moment at the idle switchers. If the exit spark gap is possessing the electrical strength at this moment than there is an over-voltage factor of 1.5 on the idle switchers and switchers on the primary side of the Tesla transformer hold this over-voltage. Such an over-voltage factor is conditioned by the shape of the changing voltage on the primary circuit of the Tesla transformer at the magnetic coupling ratio of 0,6. If the exit spark gap doesn't have electrical strength at the moment of switching, than fading harmonic vibrations on the transformer dissipation inductance arises in the scheme and over-voltage factor achieves value of 2 that may cause to their undesirable operation.

If the load of the generator is a long spark gap that is connected in the secondary circuit of the Tesla transformer and positioned within the high speed airflow, than electrical strength recovery time of the long spark gap is determined by the flow velocity. Consequently, flow velocity determines the pulse repetition rate.

References to section 5.1:

1. “Study of Mechanisms of Filamentary Pulse Electric Discharge Interaction with Gaseous Flow of Nonuniform Composition”, Project ISTC #3793p, The First Year Report, October 2008.
2. “Study of Mechanisms of Filamentary Pulse Electric Discharge Interaction with Gaseous Flow of Nonuniform Composition”, Project ISTC #3793p, The Third Year Report, October 2010.
3. *Sergey B. Leonov, Yury I. Isaenkov, Alexander Firsov*, “Mixing Intensification in High-Speed Flow by Unstable Pulse Discharge, 40th AIAA PDL Conference, San-Antonio, June 22-25, 2009, Paper AIAA-2009-4074

5.2. Experimental study of plasma channel and low-density zone dynamics in ambient conditions.

In this experimental series the facility consisted of test section considered above, system of the single pulse discharge feeding (pulse discharger PD-100/2.5), and diagnostic equipment. The dynamics of afterspark channel was explored in 4 gases: Ar (noble gas), Air (oxidizer), CO₂ (product of combustion), and C₂H₄ (fuel). The gas breakdown and afterspark channel cooling and expansion in 5 cm gap in different gases at normal conditions was studied for the basic consideration.

The typical voltage-current and power characteristics of the discharge in air at atmospheric pressure are presented in Fig.5.2.1. It is seen that current in air has several vibrations after the main pulse. This rule is not universal (see below for CO₂) but shows that the inductive processes are not negligible. The data were refined for correct evaluation of the power release as it shown in the right picture.

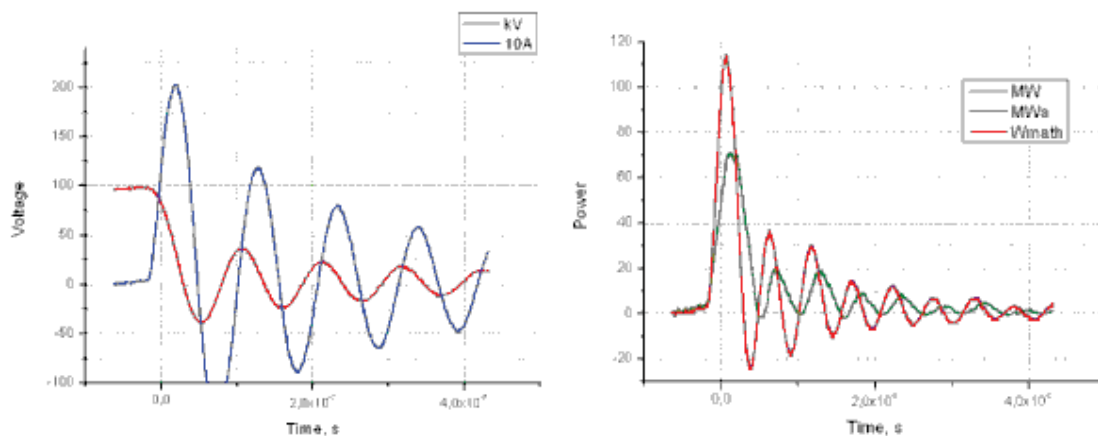


Fig.5.2.1. Voltage-current and power characteristics of electrical pulse in air. Power (in MW): green line taking into account inductive processes. Energy deposition is about 2.5J.

At high level of pressure and fixed 2-electrodes configuration the discharge appears in form of filamentary long spark. The filamentary discharge penetrates cross flow between “hot” electrodes with the speed about $V \approx 10^7 \text{ m/s} = 1 \text{ cm/ns}$. This value was estimated based on the schlieren pictures of the shock waves propagation away from initial streamers.

One of the most difficult parameters to be measured is the discharge channel diameter and its dynamics. It is clear that the plasma filament dimensions can be considered by different ways depending on which parameter and when is determined. The discharge channel diameter

and dynamics were recorded by streak technique. As the result we evaluate that the diameter of high-temperature zone at the maximum of discharge current is about $d=0.5mm$. At the same time a visible diameter of the plasma channel is $d=5-8mm$, which corresponds with expanded stage of heated zone. The visualization of the plasma filament in ambient conditions was done by means of fast camera, and line-scan (streak) camera. The photographs of the discharge filament in long current mode are shown in Fig.5.2.2.

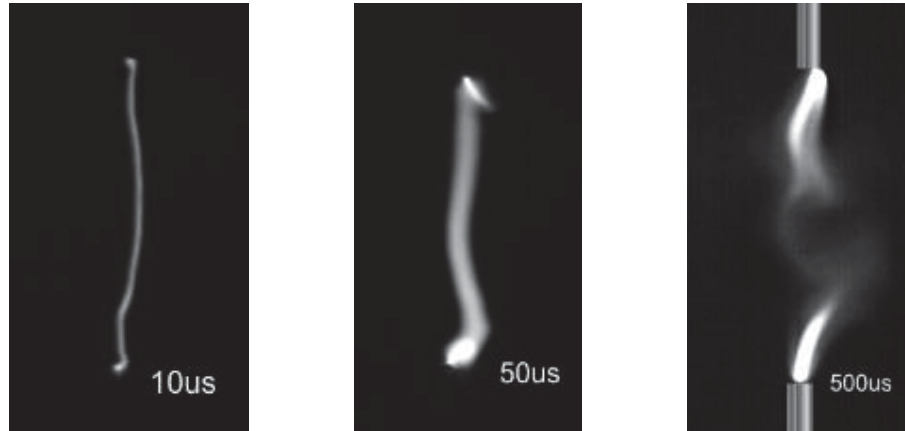


Fig.5.2.2. Discharge channel images at different moments of time.

The plasma temperature was estimated in $T_{pl}=15-17kK$ on the base of spectroscopic measurements of continuum luminescence. The analysis of radiation profile concludes the plasma as optically thick at the phase of high current [1-3].

Estimation on the base of deposited energy gives the same result. The initial volume of the discharge channel is about $Vol=10^{-8}m^3$. Specific energy release (specific enthalpy) is about $H=10^8 J/kg$ (up to 25% of the energy deposited to air is lost due to radiation). Such enthalpy is corresponded to air with the following parameters: temperature $T_0=16kK$, ionization degree $\alpha \approx 0.9$, mean conductivity is about $\sigma \approx 10^2 (Ohm \cdot cm)^{-1}$, channel resistance is $R=25 Ohm$ roughly (that is very close to directly measured value). The maximal radius of the heated zone expansion can be also estimated on the base of Sedov's hypothesis, that the expansion is defined only by integral energy release. By that way the maximal radius is equal to:

$$r_{\max} = \sqrt{\frac{2E}{5\pi \times l \times p_0}};$$

where l – is the length of the channel, p_0 – is the external pressure. The estimation gives value $r_{\max} \approx 5mm$, which is close to experimental one.

The thermal distortion, which is generated by the spark, was observed by schlieren and schlieren-streak methods based on thin laser beam deviation. On the first stage of expansion ($t < 50 \mu\text{s}$) the post-discharge channel looks quite classical: cylindrical thermal cavity. At $t \approx 150 \mu\text{s}$ (depending on conditions) the shape of the after-spark channel occurs unstable. In [1, 4] there were announced the physical mechanism of this instability: cooling of the axial zone leads to the pressure decrease with sequential gas reverse movement. Such a movement occurs unstable due to the Raleigh-Taylor mechanism. The followed behavior can be characterized by generation of intensive lateral jets with sequential fast turbulization of significant volume of the gas (the diameter is inter-gap distance, approximately). The sample of schlieren image of the jets generation is shown in Fig.5.2.3. In such a way the analysis of experimental data gives some not obvious results concerning the size of disturbed zone: its value occurs in several times bigger than it could be in accordance with laminar or turbulent diffusion law. The result of measurements and appropriate simulation is presented in Fig.5.2.4. Well seen that the second phase of expansion is not supported by the model. An observation of the experimental graph allows us to conclude two important things: the diameter of the plasma zone after the fast expansion is about $d = 8 \text{ mm}$, and the mean “velocity” of the plasma disturbances expansion on the phase of jets generation is more than $V = 100 \text{ m/s}$ under the conditions of this experiment. The data on the base of fast-response pressure transducers have verified the data of schlieren observations as a whole. A strong turbulent motion can be seen for hundreds of microseconds.



Fig.5.2.3. Typical schlieren image of post-discharge thermal distortion, $t = 200 \mu\text{s}$.

Comparison of measured channel radius and a channel radius calculated using the “standard” model [3] (not accounting for jets formation) is shown in Fig.5.2.4a. Theoretical predictions are very close to a so-called “minimum” radius, but “maximum” radius values, resulting from the jets expansion (Fig.5.2.4b), are much larger. Therefore, we need to develop a theory which can describe a “fast” expansion regime with gas jets formation (see section 4).

The after-spark channel development with time is shown in Fig.5.2.5, where a strong turbulent motion can be seen after several tens of microseconds. The image was recorded by means of schlieren streak technique. The plane of cutting was perpendicular to the current

direction and crossed the after-spark channel on centerline. Each line was exposed during $20\mu\text{s}$. The schlieren-streak method gives a more information on the dynamics of the after-spark channel expanding. The photo was processed using OriginPro© software.

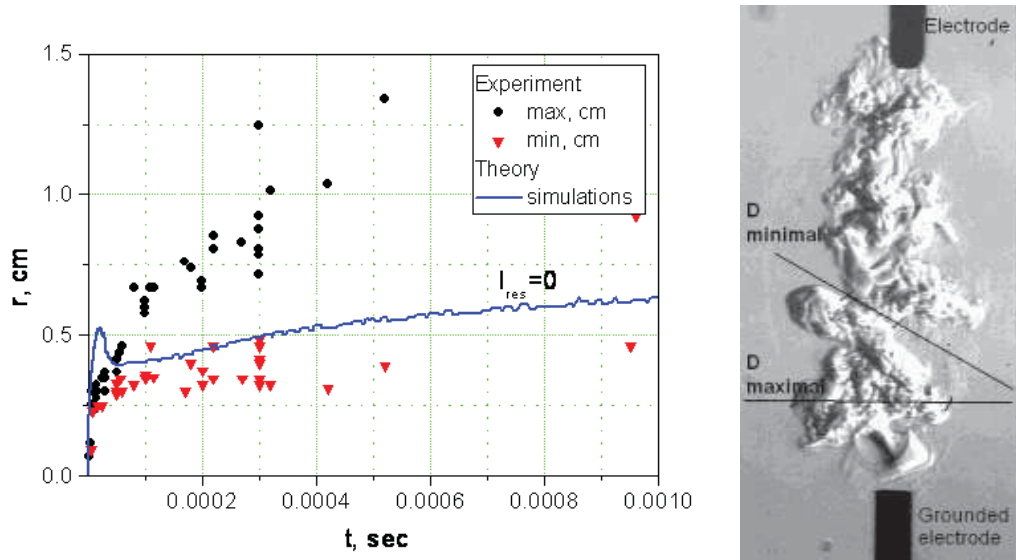


Fig.5.2.4. Experimental measurements and theoretical estimates of channel radius (left). Definition of maximum and minimum channel radius (right)

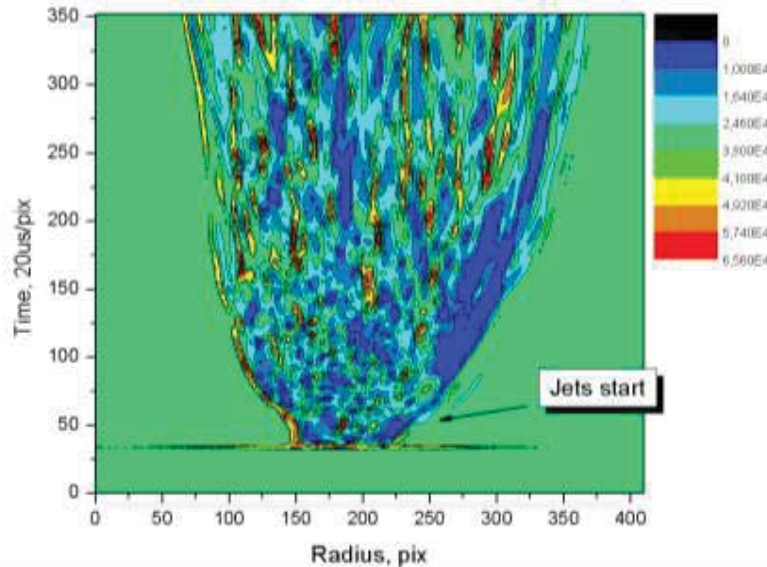


Fig.5.2.5. After-spark expanding channel with delay time from 0 to $500\mu\text{s}$ by schlieren-streak technique.

To recognize the beginning of lateral jets development the initial stage of the channel expansion was stabilized by small residual current during $200\mu\text{s}$. As it can be considered the turbulence leads to fast increase of the disturbed zone effective radius. Note that the turbulence leads to a rapid expansion of the after-spark channel and thus it has got the potential for fast mixing of the gaseous composition.

It is known that a primary ionization is considered necessary for obtaining a stable breakdown voltage in the discharge gap with sharply non-homogeneous field. Here the initial pre-ionization in the discharge gap was occurred due to appearance of the intensive corona discharge on the electrodes when voltage is tending to the breakdown level. Value of the corona discharge current was measured in a range 5 – 10A at the moment 5ns before breakdown. Light emission reaches the maximum at $t = 40\text{ns}$, then intensity reduces during the $0.6\mu\text{s}$.

The electrical characteristics of the discharge in different gases and the dynamics of disturbed zone were explored recently in special series of tests. As it is clearly shown below, the important information can be obtained by detail analysis of electrical parameters of the discharge. The main pulse duration was $t \approx 100\text{ ns}$, rate of the voltage rise before breakdown $dU/dt \approx 3 \times 10^{10}\text{ V/s}$, gas pressure $p = 1\text{ Bar}$, inter-electrodes gap $d = 50\text{ mm}$. Table 5.2.1 presents some factual data. Among the molecular gases the gaseous hydrocarbon fuel provides the best conditions for discharge development on the first phase (breakdown itself). With further growth of the electric current the situation can be changed. This statement is confirmed by measuring history of E/N and current in high-current phase of the discharge in different gases.

Table 5.2.1: Experimental data, pulse discharge in different gases. Short current $\tau = 100\text{ ns}$.

Gas	Air	C ₂ H ₄	CO ₂
Typical breakdown voltage, kV	100	98	93
Energy deposition in main pulse, J	2.1	2.4	2.9
Typical plasma channel resistance at $t/2$, Ohm	18	30	65

The Fig.5.2.6 presents the result of measurements of the volt-ampere characteristic of the discharge in air, CO₂, and ethylene. All other conditions were the same. It is seen that the shape of current-voltage curves is different. The strongest distinction may be considered between the air and CO₂: the channel resistance in CO₂ is larger and the process is aperiodic consequently. The Fig.5.2.7 compares the input power in case of the Air and CO₂. Though a so different behavior, the power occurred almost the same! A small difference in energy deposition (see table 5.2.1) can be explained by some variation in pulse duration.

The Fig.5.2.8 presents the result of resistance and reduced electrical field recalculation based on experimental data. It is seen that in first stage of the discharge the highest field is observed in CO₂, but in the second stage the higher value is realized in air. This result can be

posed as an experimental demonstration of the discharge location controllability with electrical parameters. This mechanism can enhance mixing additionally.

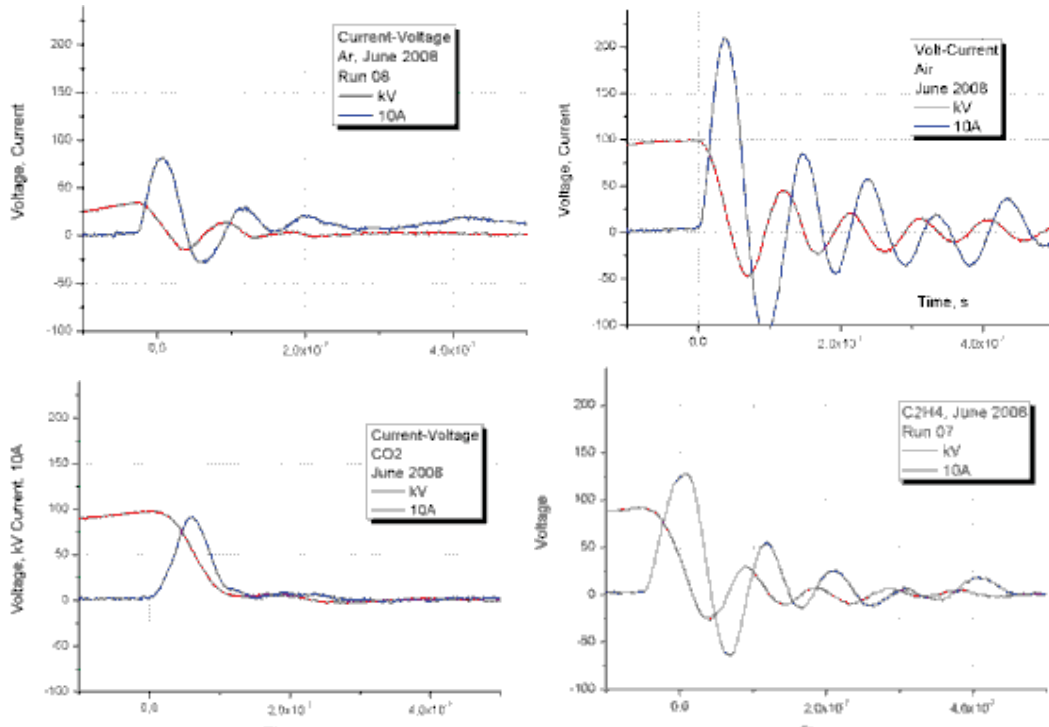


Fig.5.2.6. Experimental data for 100ns discharge in Ar, Air, CO₂, and C₂H₄. Volt-ampere characteristics.

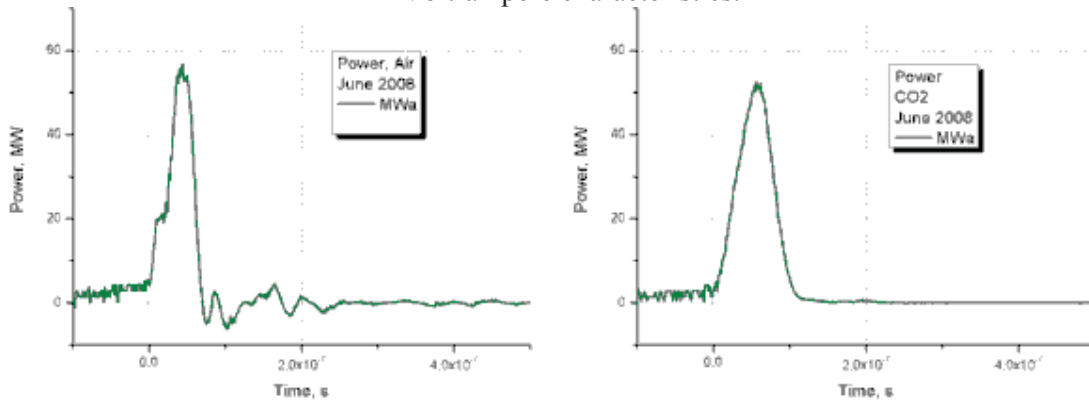


Fig.5.2.7. Experimental data for 100ns discharge in Air, and CO₂. Dynamics of power release.

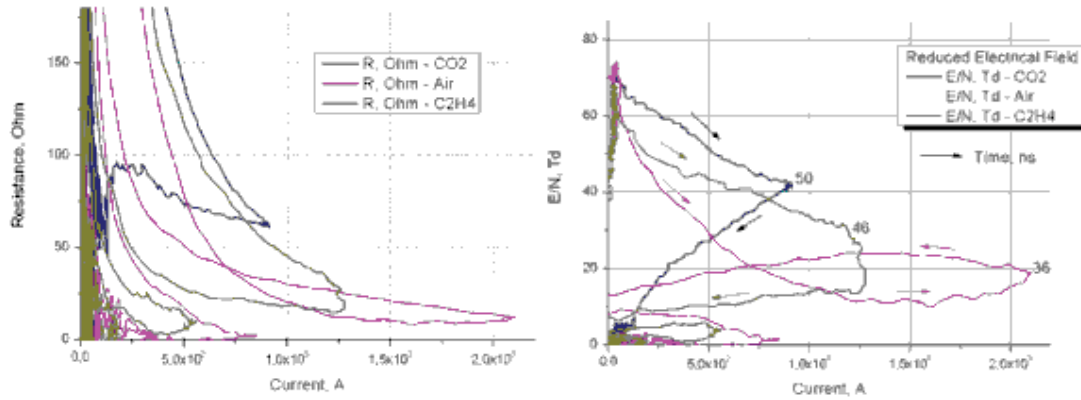


Fig.5.2.8. Experimental data for 100ns discharge in Air, CO₂, and C₂H₄. Dynamics of discharge channel resistance and reduced electrical field. Counts on graph are the time in ns.

The figures above may not give a full view on the processes. All discharge parameters depend on time and each on others. The V-I diagrams in Fig.5.2.9 present more visual information.

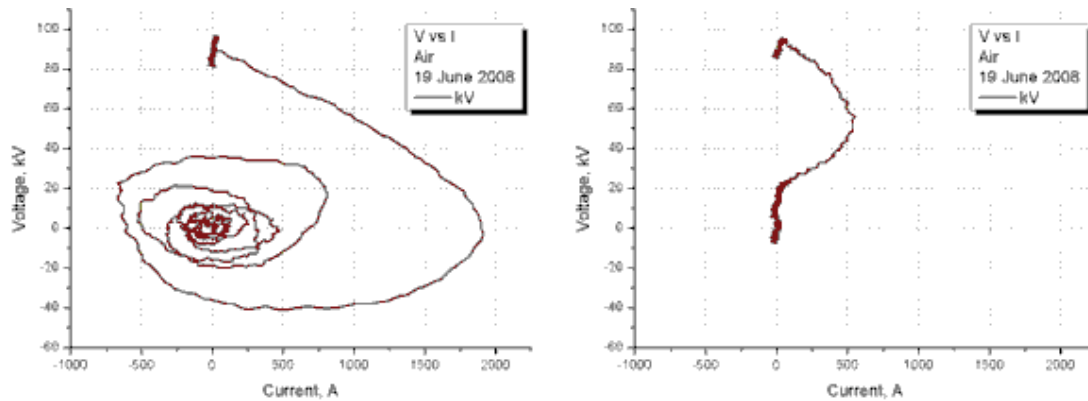


Fig.5.2.9. Experimental data for 100ns discharge in Air, and CO₂. V-I diagrams.

It has to be noted that in a case of “long” pulse the typical parameters of the filamentary discharge are not much differed each other but very distinct in respect of the short pulse case. The comparative data are shown in Table 5.2.2.

Table 5.2.2: Experimental data, pulse discharge in different gases. Long current $\tau=300\mu s$.

Gas	U, V	I, A	W, kW	R, Ohm
Air	350	86	30	4
C ₂ H ₄	550	70	38.5	8
CO ₂	480	112	54	4.3

In the case of “long” pulse the V-I diagrams show a principal difference in behavior of the discharge in gases mentioned above as it is presented in Fig.5.2.10. Such kind of diagrams was used for the analysis further.

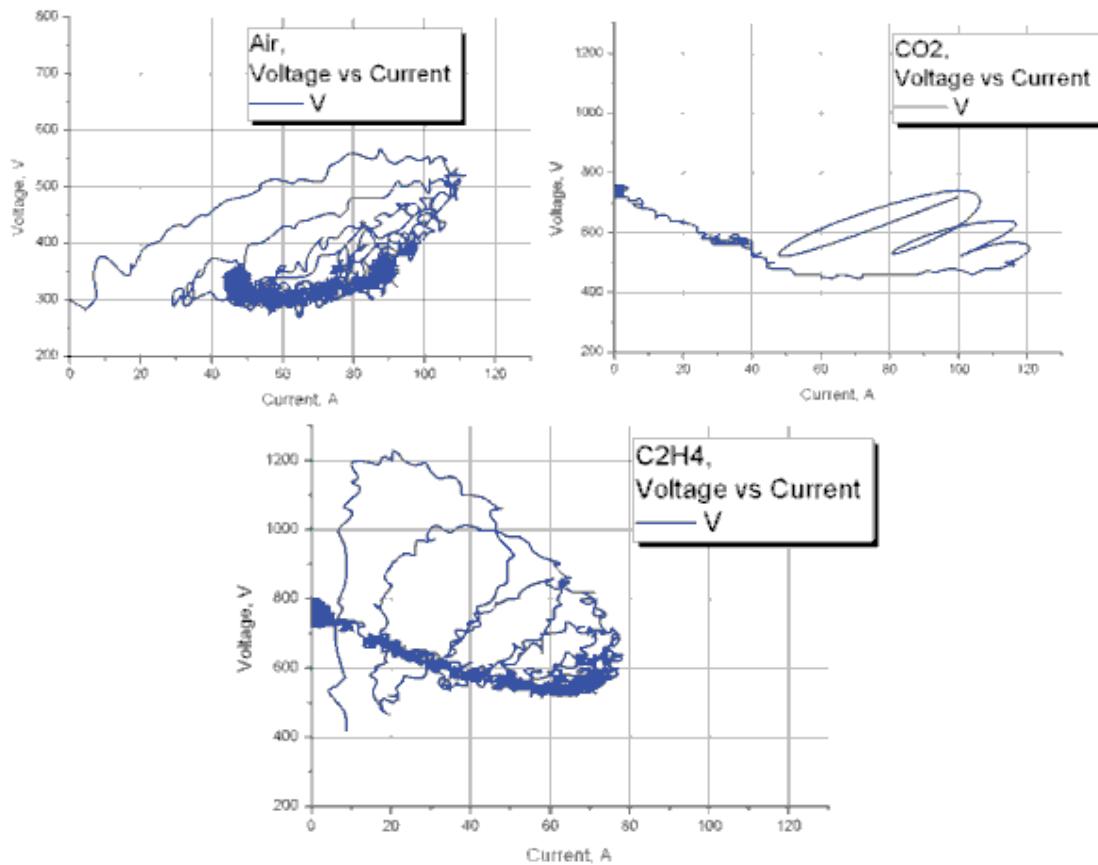


Fig.5.2.10. Experimental data for 300 μ s discharge in Air, CO₂, and C₂H₄. V-I diagrams.

The visualization of the discharge induced flow dynamics was made using schlieren technique for the short-pulse mode. The set of data is presented in the next pages. Preliminary observation of those images allows considering some peculiarities in post-discharge channel behavior in different gases.

- Ar: size of disturbance is minimal, very often the discharge has several channels.
- Air: maximal speed of expansion in time range 20-200 μ s.
- CO₂: the turbulence has smaller scale than in the Air, a “bubble” generation of unknown nature.
- C₂H₄: very similar with CO₂.

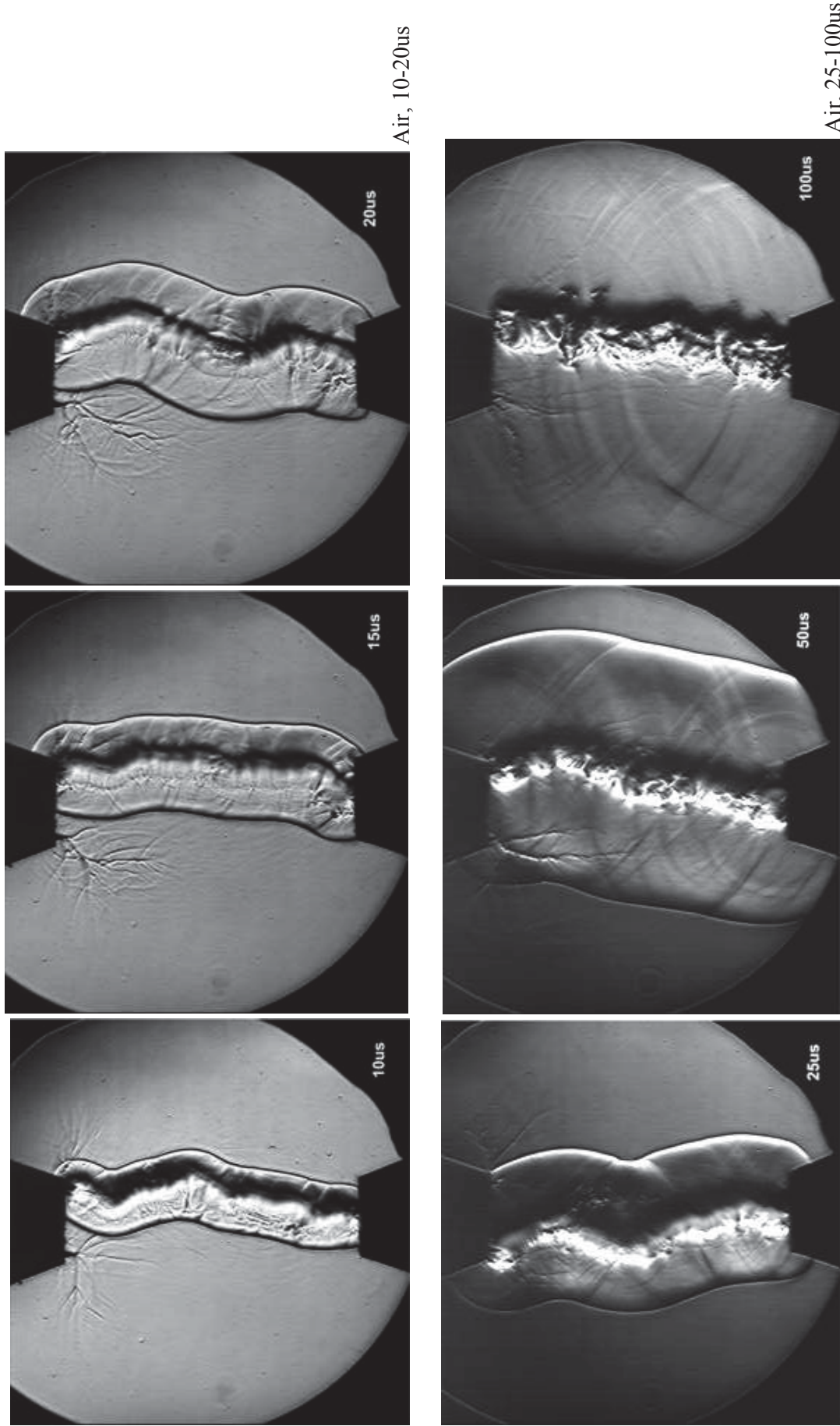


Fig.5.2.11. Typical short range dynamics of post-discharge disturbance in Air. Double anode.

May 2013

This work was supported financially by EOARD and performed under the agreement to the International Science and Technology Center (ISTC), Moscow.

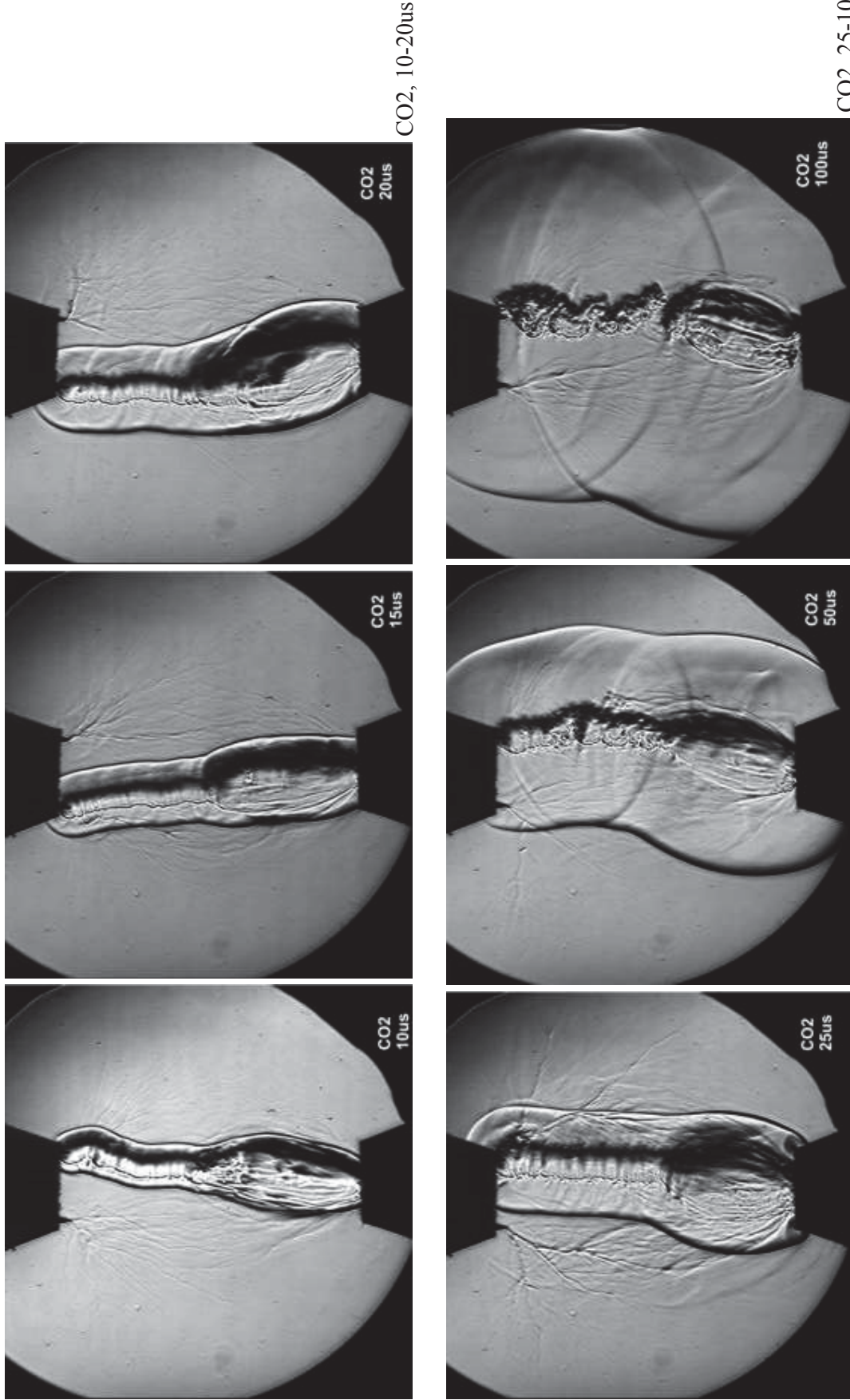


Fig.5.2.12. Typical short range dynamics of post-discharge disturbance in CO2. Double anode.

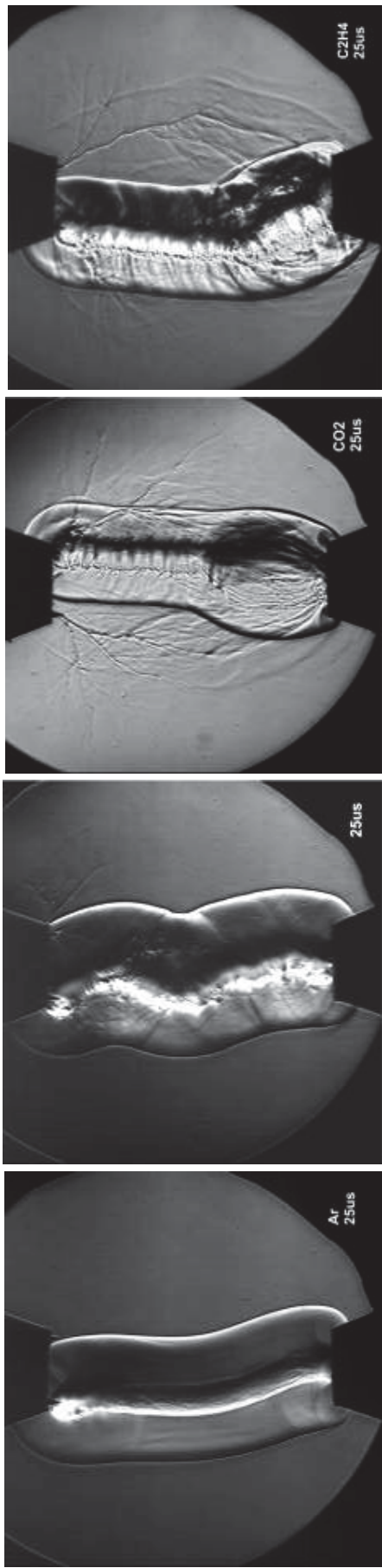


Fig.5.2.13. Difference of post-discharge disturbance at delay of 25 μ s in Ar, Air, CO₂, and C₂H₄. Double anode.

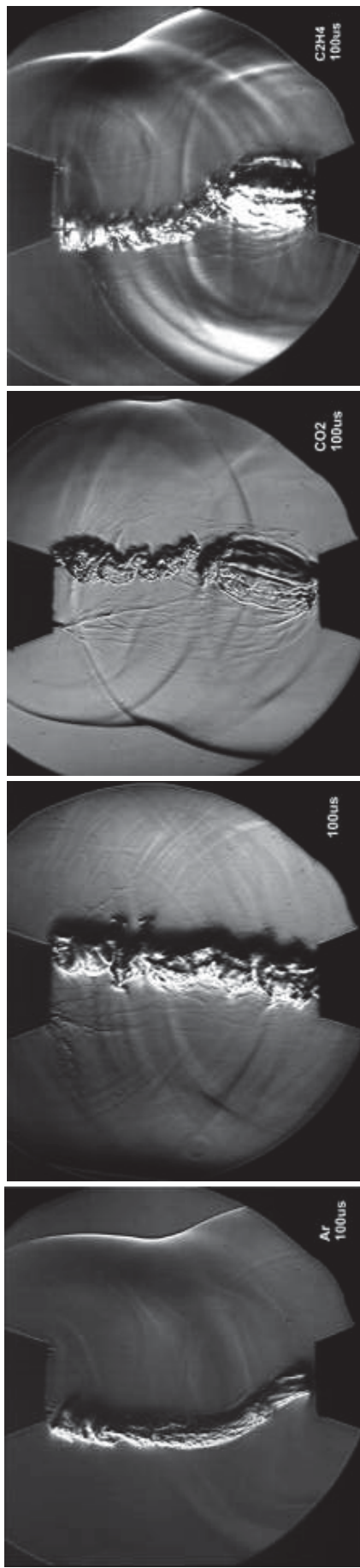


Fig.5.2.14. Difference of post-discharge disturbance at delay of 100 μ s in Ar, CO₂, and C₂H₄. Double anode.

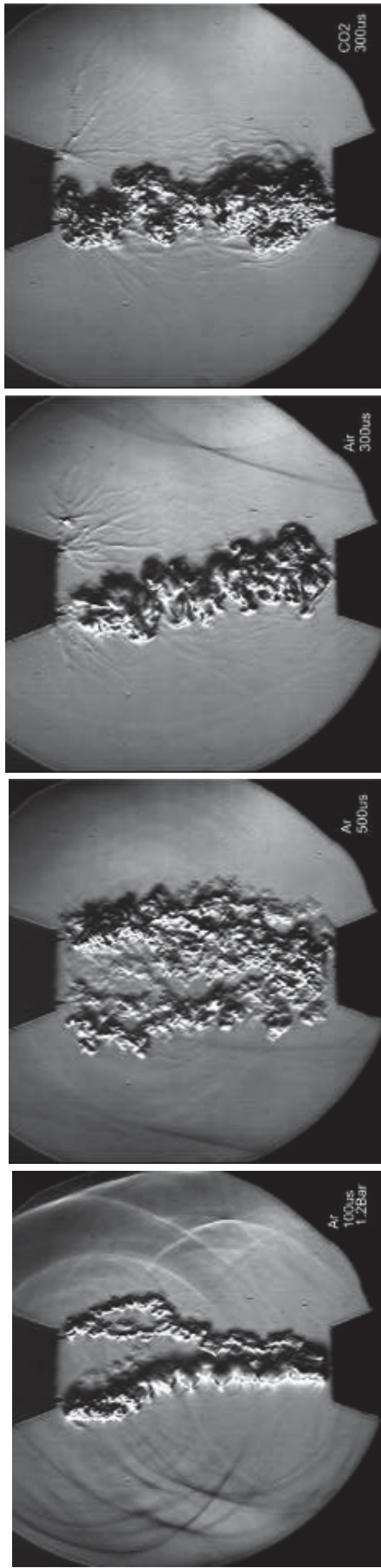


Fig.5.2.15. Difference of post-discharge disturbance at delay of 300us in Air and CO2, Ar 100us and 500us at 1.2Bar. Double anode.

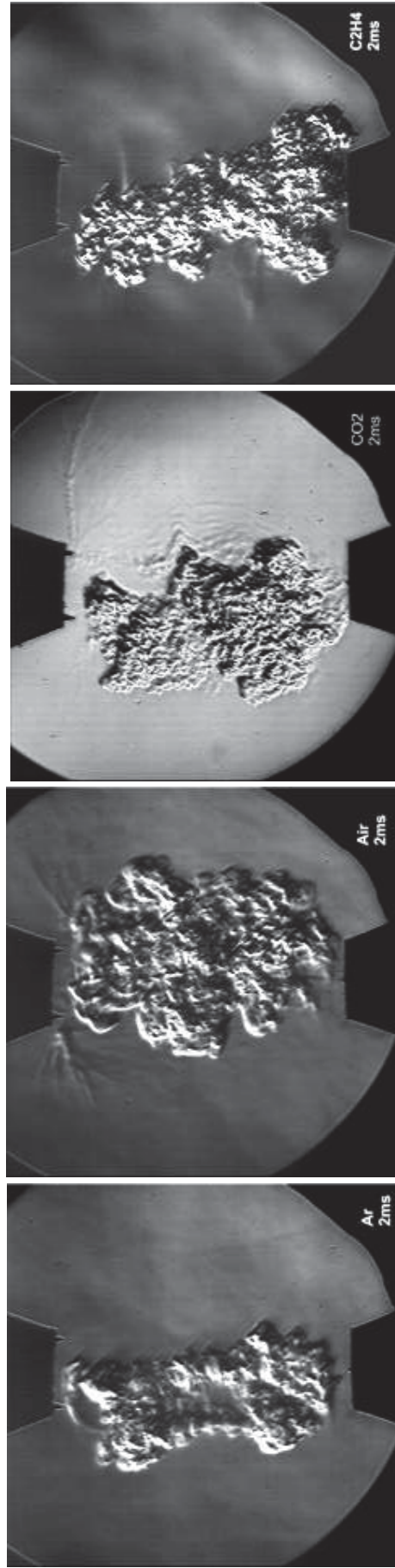


Fig.5.2.16. Difference of post-discharge disturbance at delay of 2ms in Ar, Air, CO2, and C2H4. Double anode.

References to section 5.2.

1. *S. Leonov, M. N. Schneider, D. Yarantsev* “Fast Mixing by Pulse Discharge in High-Speed Flow” // Paper AIAA-2006-8129, 14th AIAA/AHI Space Planes and Hypersonic Systems and Technologies Conference, Canberra, Australia, Nov. 6-9, 2006
2. *Sergey B. Leonov, Dmitry A. Yarantsev, Yury I. Isaenkov* “Properties of Filamentary Electrical Discharge in High-Enthalpy Flow”, 43rd AIAA Aerospace Sciences Meeting & Exhibit, 10-13 January 2005/ Reno, NV, AIAA-2005-0159.M.N.
3. *M. Shneider*, “Gasdynamic and turbulent cooling of after-spark and arc channels”, 26th AIAA Plasmadynamic and Lasers Conf., AIAA-95-1994, June 19-22, San Diego, 1995.
4. *S. Leonov, Yu. Isaenkov, M. Shneider, D. Yarantsev* “Fast Mixing by Pulse Discharge in High-Speed Flow”, Presented to 37th AIAA Plasmadynamics and Lasers Conference, San Francisco, USA, June 2006,
5. *Yu. I. Isaenkov, S. B. Leonov, M. N. Shneider* “Mixing Intensification by Electrical Discharge in High-Speed Flow” Proceeding of the Fifth International Conference on Fluid Mechanics, Aug.15-19, 2007, PaperF28; Shanghai, China; Tsinghua University Press & Springer
6. *Sergey B. Leonov, Yuri I. Isaenkov, Mikhail N. Shneider* "Suppression of the turbulent decay of an afterspark channel with residual current", PHYSICS OF PLASMAS 14, 123504 _2007.

April 2013

This work was supported financially by EOARD and performed under the agreement to the International Science and Technology Center (ISTC), Moscow.

Distribution A: Approved for public release; distribution is unlimited.

5.3. Experimental runs under stable and unstable operational modes.

It is a well-known fact that turbulent gas motion develops in a cooling post discharge channel, replacing molecular heat conduction as the dominant mechanism of the heat transfer. The rates of cooling and expansion of the channel increase dramatically in turbulent mode. This turbulent motion can significantly increase the rate of the fuel-gas mixing, which may control the mixing rate in ramjet or scramjet engines. The result of interaction of a pulsed filamentary discharge with gas flow strongly depends on its decay time. A simplified theoretical model of the cooling of a post-discharge channel in gas has been proposed (see section 4), which takes into account the development of turbulence and its effect on the channel cooling and expansion process. The model is based on a standard set of one-dimensional gas dynamics equations and the equation of state with Joule heating by the current pulse and heat losses due to the radiation transfer and molecular and turbulent heat conductivities [1-2]. It was predicted [2] and shown recently [3-5] that the afterspark plasma decay and intensity of mixing process can be controlled by the current pulse with residual current for the turbulence suppression. In the “standard” model the rate of gas cooling and expansion is determined by the average speed of the turbulent pulsations. Turbulence starts as a result of the Raleigh-Taylor instability in the region of large density gradient at the channel boundary. Typical turbulence scale is much smaller than the channel radius.

As it was shown experimentally [3, 6], there is another, much faster, mechanism of the afterspark channel expansion. Expansion occurs because high velocity radial jets are formed during afterspark channel cooling. It cannot be described by the “standard” model.

The experimental approach considers the generation of pulse electrical discharge in the form of long spark in atmospheric air under ambient conditions, measurement of its main parameters, and observation of the dynamic of the after-discharge channel expansion in two modes: unstable and stabilized by the residual current. Experimental facility consists of two-electrode discharge cell, pulse power supply, and a measuring technique. The copper electrodes were blunted; gap distance was varied in a range $d=30-60mm$. The power supply was built on the base of three-cascade scheme, as it is shown in Fig.5.3.1:

- short high-voltage pulse generator for an initial breakdown based on Tesla coil with impact excitation;
- main pulse circuit;
- generator of variable residual current.

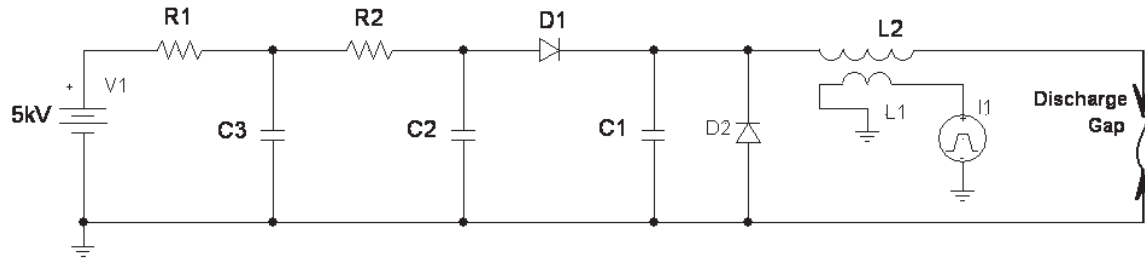


Fig.5.3.1. Principal electrical scheme of the power supply.
C1L2 – first contour, C2D1 – second contour, C3R2 – third contour.

The experiments were performed in air at pressure $p_0=1$ Atm and $T_0\approx 300$ K. In such two-electrode configuration and atmospheric pressure the discharge appeared in form of filamentary long spark. The discharge current, voltage, spectra, and radiation intensity were recorded each run. The thermal distortion, which was generated by the spark, was measured by schlieren and schlieren-streak methods. The discharge channel diameter and dynamics were recorded by frame-streak technique. The plasma temperature was estimated on the base of analysis of spectroscopic measurements. The temporal resolutions were as follows: $10\ \mu\text{s}$ for photo-images; $0.1\ \mu\text{s}$ for schlieren images, and $6\ \mu\text{s}$ for streak images. The best spatial resolution was about $0.2\ \text{mm}$.

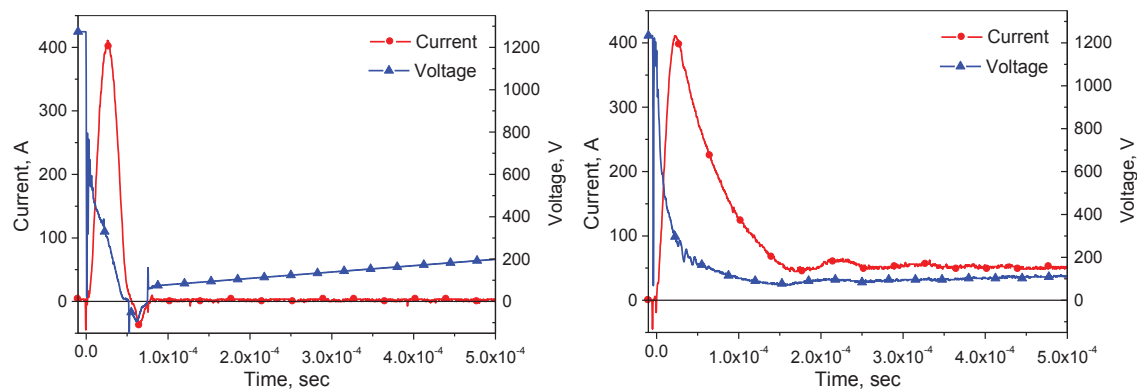


Fig.5.3.2. Typical current and voltage oscillograms of two main modes:
no residual current and $I_{\text{res}}\approx 50\ \text{A}$.

Two main modes of the discharge generation were explored in accordance with an idea of the turbulence stabilization by a small residual current:

- the “short pulse” at $I_{\text{max}} \approx 400\ \text{A}$, $\tau_{\text{pulse}} \approx 50\ \mu\text{s}$, $I_{\text{res}}=0\ \text{A}$, $\tau_{\text{res}}=0\ \text{s}$; and
- the “long pulse”: “short pulse” plus a long residual current $I_{\text{max}} \approx 400\ \text{A}$, $\tau_{\text{pulse}}\approx 50\ \mu\text{s}$, $I_{\text{res}}=10\text{-}50\ \text{A}$, $\tau_{\text{res}}>2\ \text{ms}$.

Typical oscillograms of these two modes are shown in Fig.5.3.2. An initial breakdown pulse is invisible here due to incomparably short duration. Below the data will also be presented for special regime with decaying residual current.

The intensity of discharge radiation varies in ~ 1000 times during the discharge current. It leads to some uncertainty in determination of the discharge channel diameters. At the breakdown moment the diameter occurs less than the resolution of the apparatus employed in our experiment. In moment $t=20\mu s$ it increases to $d=2\text{ mm}$ and stabilizes further on the $d=3\text{ mm}$ of magnitude up to the time $t=150-200\mu s$. A visible expansion is proceeded after the $t=200\mu s$ exceeding $d=8-15\text{ mm}$ before $t\sim 1\text{ ms}$. The analysis of radiation profile concludes the plasma as optically thick at the phase of high current. The gas temperature measured that time by optical method was $T=16000 \pm 1000\text{ K}$ that is in a good agreement with theoretical data. The streak image of discharge luminosity is presented in Fig.5.3.3 for “long current” operation modes. For “short pulse” mode the temporal resolution of apparatus is not enough to recognize the details.

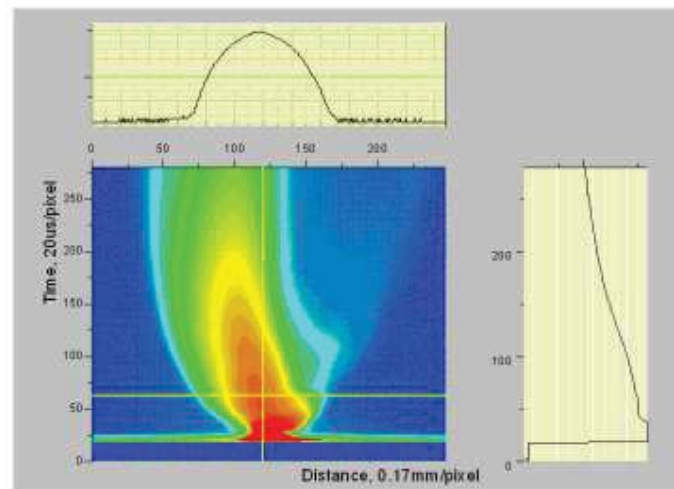


Fig.5.3.3. Streak image of the discharge luminosity in mode of “long pulse” after processing.
Initial stage is overexposed.

As was shown in references [1,5], theory predicted the effect of turbulent decay stabilization at small residual current presence for post-pulse heating of the central part of the low-density channel. In the present work this effect was observed experimentally as is shown in Fig.5.3.4 where the channel dynamics is registered by schlieren streak technique. A development of gasdynamic instability resulting in arising of intensive turbulent motion was observed at the “short pulse” ($I_{res}=0$) mode. The instability development occurs during the first $t=200\mu s$ after the discharge (Fig.5.3.4, left). The residual current with amplitude about 10% of the current amplitude of “short pulse” totally stabilizes the afterspark channel in a condition of

a quasi-stationary arc, as it shown in Fig.5.3.4, right. The result of images processing is shown in Fig.5.3.5. It allows recognizing the transversal modes of instability, mentioned in section 4. In Fig.5.3.6 the instantaneous schlieren images at $t=500\mu s$ are shown.

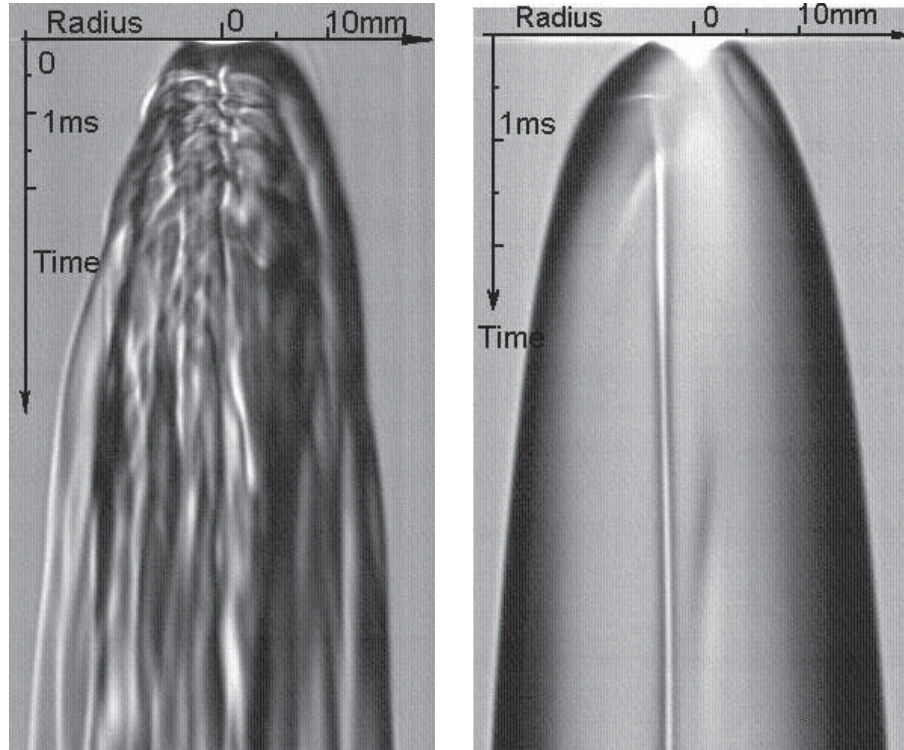


Fig.5.3.4. Schlieren-streak images: (left) – $I_{res}=0$; (right) – $I_{res}=50$ A.

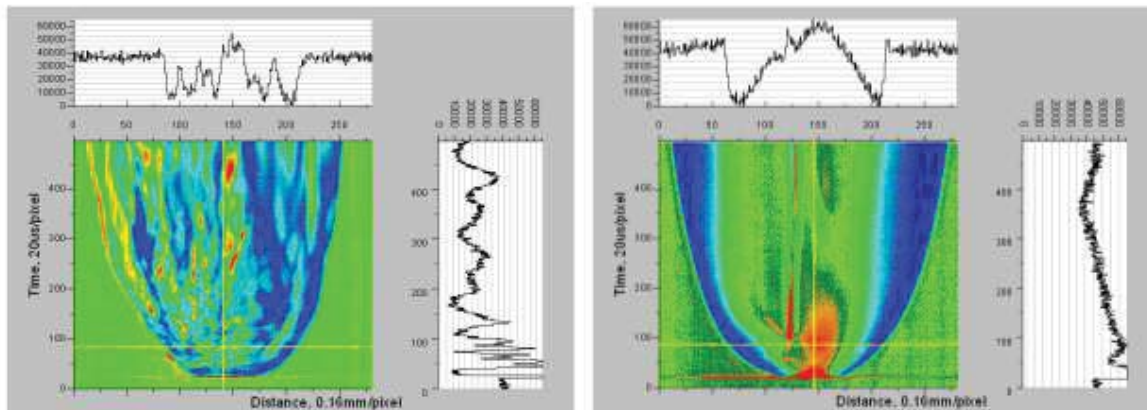


Fig.5.3.5. Processed schlieren-streak images: (left) – $I_{res}=0$; (right) – $I_{res}=50$ A.

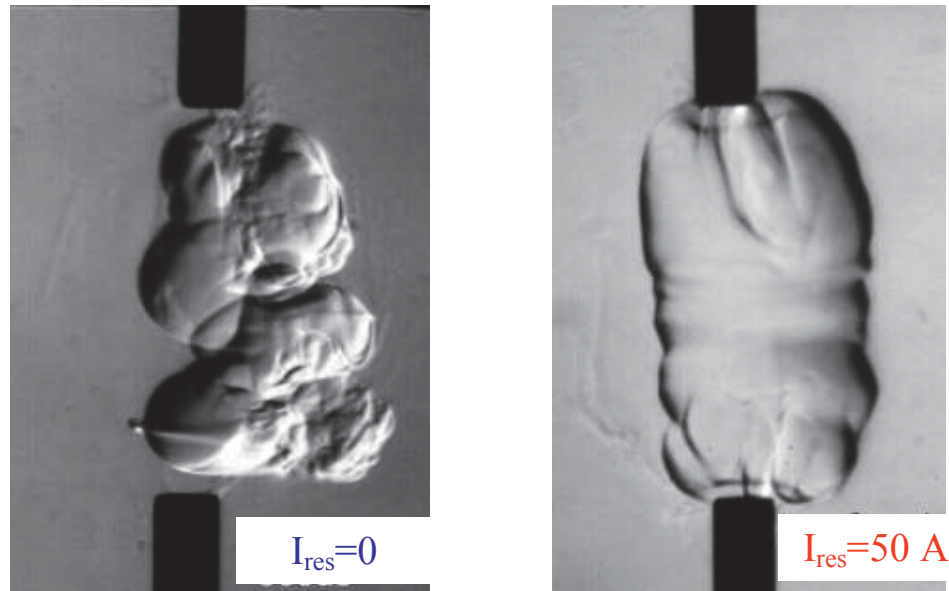


Fig.5.3.6. Instantaneous schlieren images at $t=500 \mu s$ for the cases $I_{res}=0$ and $50 A$.

A decrease of residual current value below $I_{res} \approx 50 A$ in described conditions weakens the effect of stabilization. A threshold of the effect has not been found: the current decrease leads to increase of instability gradually. The effect of stabilization was observed consistently in each run if the residual current was $I_{res} > 20 A$. Nevertheless, the regime with decaying residual current demonstrates that the instability can be suppressed temporarily, when the residual current has enough magnitude. The instability doesn't restore the development if it was being stabilized during 1ms or longer.

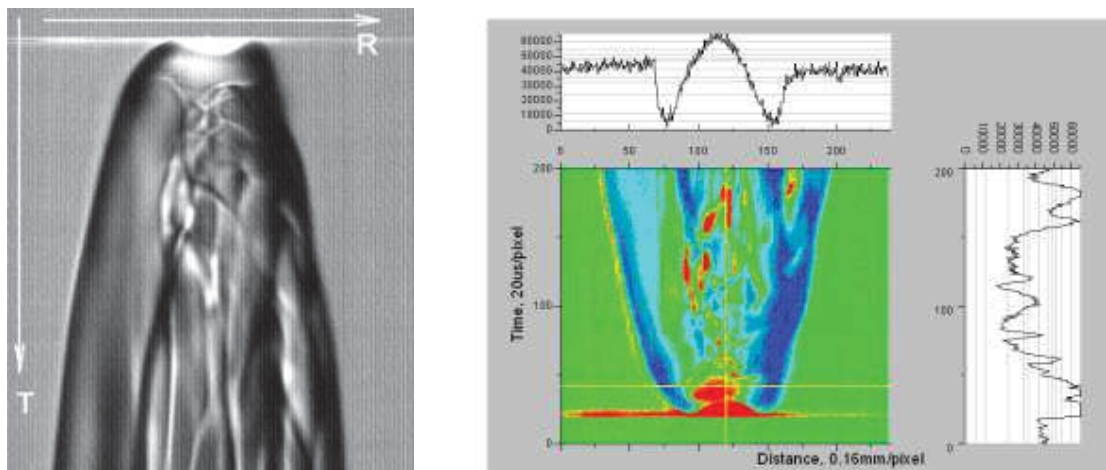


Fig.5.3.7. Schlieren-streak image and processed image in case of decaying residual current.

Special experiment was arranged to study the details of the filamentary discharge dynamics on the first stage of expansion. The current amplitude was $I \approx 1 kA$; no residual current was applied. The graph in the Fig.5.3.8 shows comparison the experimental and computational data that proves the fact of the reverse flow.

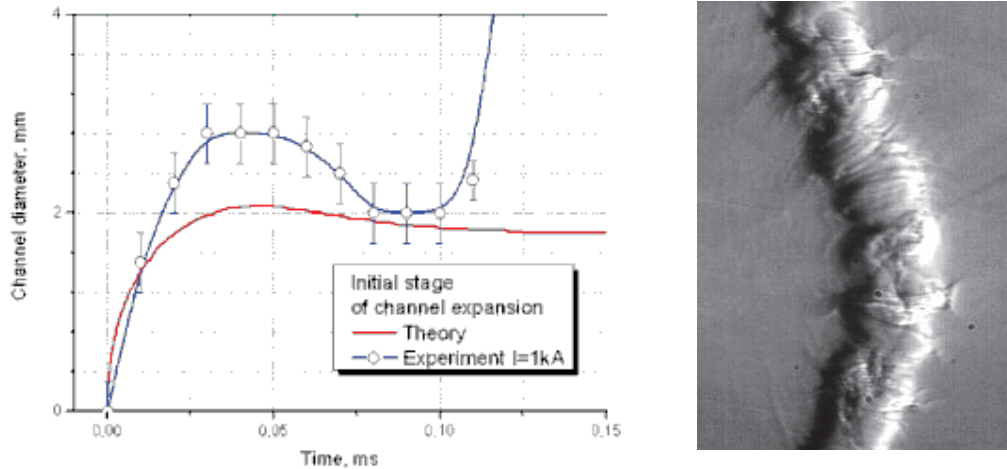


Fig.5.3.8. Dynamics of the after-spark channel expansion and schlieren photo of the disturbed zone in early stage of instability development.

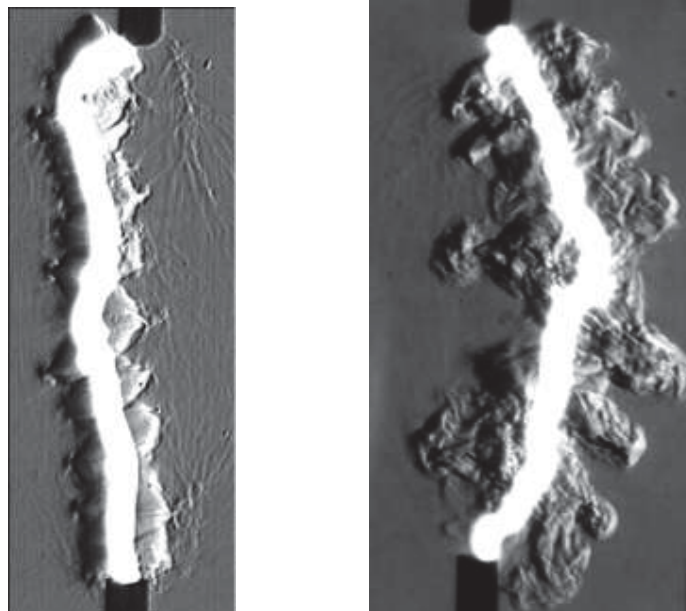


Fig.5.3.9. After-spark expanding channel with delay time 150 and 300 μs by schlieren technique. Plasma luminosity is not rejected.

Prove the physics of jets formation. Jets are developing in quasi-isobaric stage, when $p(r,t) \approx p_0$. Depending on whether the surface of the channel boundary is concave or convex, flow from the periphery to the center, arising in a process of cooling, can be contracting or expanding. If the flow is contracting (concave surface), the static gas pressure increases, however, expanding flow from the convex surface decreases the pressure. As a result, we can expect the formation of jets in the direction opposite to pressure gradients. Figure 5.3.9 presents two instant schlieren photos of jets' initial stage development. Here the plasma luminosity is not rejected. It allows recognizing favorite places of jets origination: the strongest

cumulative flows are associated with the plasma channel curvatures. Small initial jets flown in the same direction are combined together to form a bigger one later. The Fig.5.3.10 shows the frame sequence of the same pulse with consecutive delays to illustrate the idea above. Time between frames is equal with $270\mu\text{s}$. The delay of the first frame is $60\mu\text{s}$.

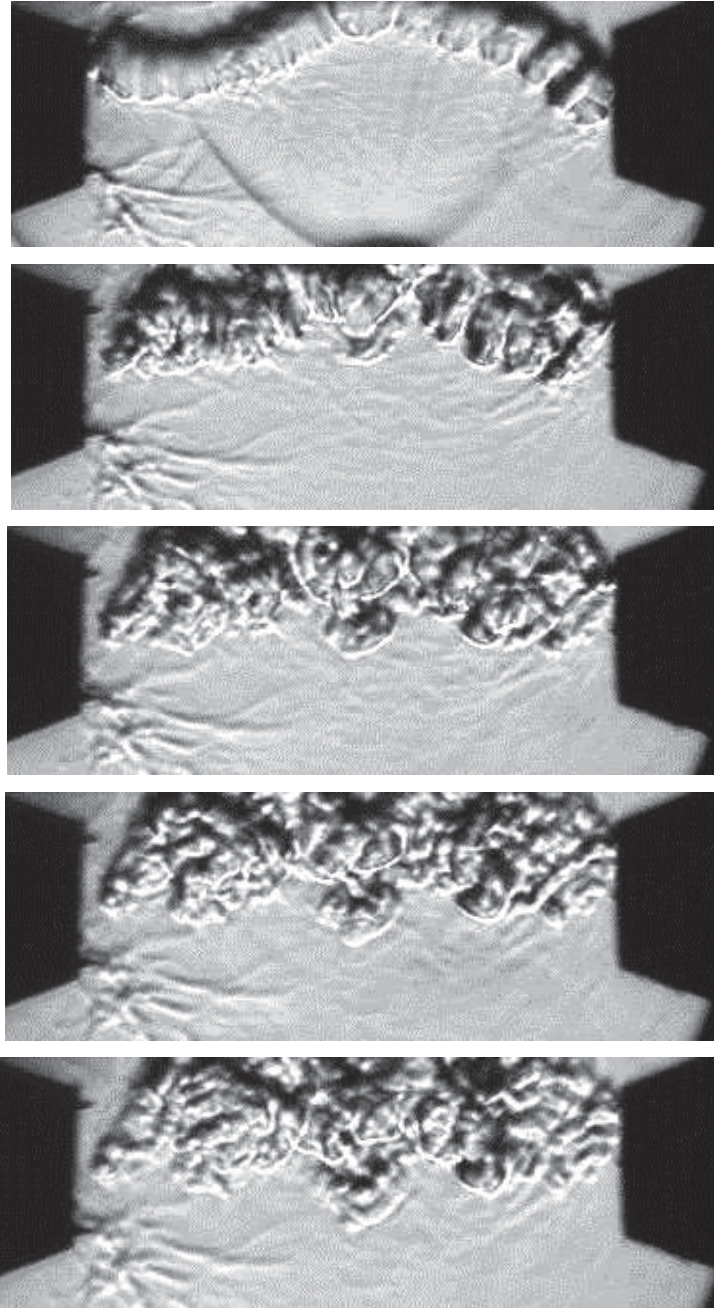


Fig.5.3.10. After-spark expanding channel. Consecutive frames at delay $60\mu\text{s}$ - $1140\mu\text{s}$.

References to section 5.3.

1. Sergey B. Leonov, Yuri I. Isaenkov, Mikhail N. Shneider "Suppression of the turbulent decay of an afterspark channel with residual current", PHYSICS OF PLASMAS 14, 123504_2007.

2. Shneider M.N., The effect of residual current on turbulent cooling of after-spark channels, 38th Aerospace Sciences Meeting and Exhibit, AIAA-2000-0721, Reno, 10-13, Jan., 2000.
3. Leonov S., Yarantsev D., Isaenkov Y. "Properties of Filamentary Electrical Discharge in High-Enthalpy Flow", 43rd AIAA Aerospace Sciences Meeting & Exhibit, 10-13 January 2005/ Reno, NV, AIAA-2005-0159.
4. Leonov S., Isaenkov Yu., Yarantsev D., Shneider M., "Fast Mixing by Pulse Discharge in High-Speed Flow", AIAA-2006-8129, 14th AIAA/AHI Space Planes and Hypersonic Systems and Technologies Conference, Canberra, Australia, Nov. 6-9, 2006
5. Shneider M.N., "Turbulent decay of after-spark channels", Phys. Plasmas, Vol. 13, 073501 (2006)
6. Sergey B. Leonov, Dmitry A. Yarantsev, Instability in Post-Discharge Thermal Cavity, IEEE Transactions, Plasma Science. June 2008, DOI 10.1109/TPS.2008.922479

5.4. Experimental study of plasma channel and low-density zone dynamics in high-speed flow.

Two experimental series were performed in respect of titled objective: (1) measurements of the short-pulse discharge parameters in air at variable pressure; (2) and study of pulse discharge dynamic in supersonic flow. The first series appears to be needed because the static pressure in high-speed flow is lower than atmospheric value: $P_{st}=100\text{-}250\text{Torr}$ at $M=2$. The tests were made in test-section of facility PWT-50. The electrical parameters were measured in coupling with schlieren images acquisition to detect the instability presence. Power supply worked in three modes as they are listed in table 5.4.1 below. In some range of parameters a shorter pulse may be more efficient in order to energy release to low-density gas.

Table 5.4.1.

	Capacitance of secondary circuit, pF	Maximal voltage of secondary circuit, kV	Maximal energy saved, J	Nominal energy saved, J	Half-cycle duration at $R=0$, ns
Mode 1	940	110	5.7	4.7	94
Mode 2	470	110	2.85	2.4	65
Mode 3	254	105	1.4	1.25	45

Figures 5.4.1-3 summarizes the electrical parameters of the discharge depending on the gas pressure. The first graph gives the detail data for the Mode 1. The next figures present similar data for modes 2 and 3.

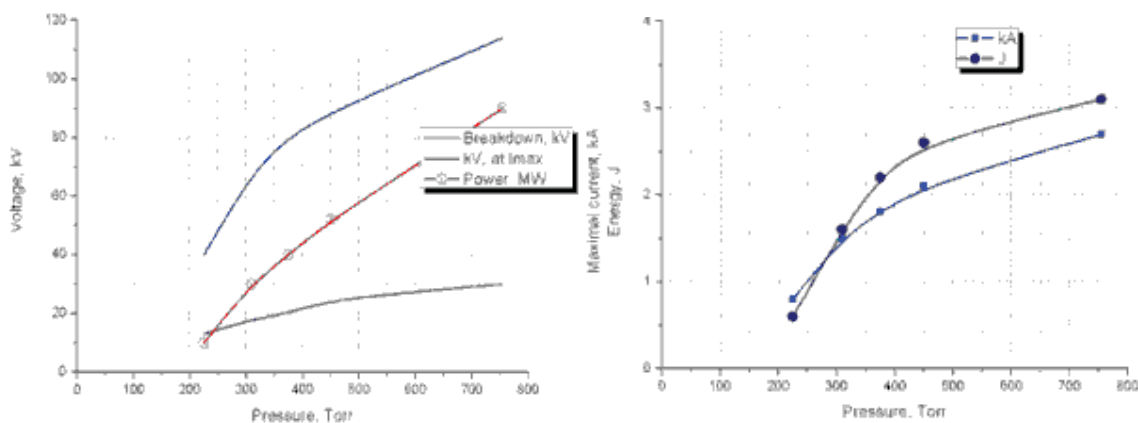


Fig.5.4.1.1. Data for the Mode 1. Breakdown voltage, gap voltage at maximal current, power deposited, maximal current, and energy deposited.

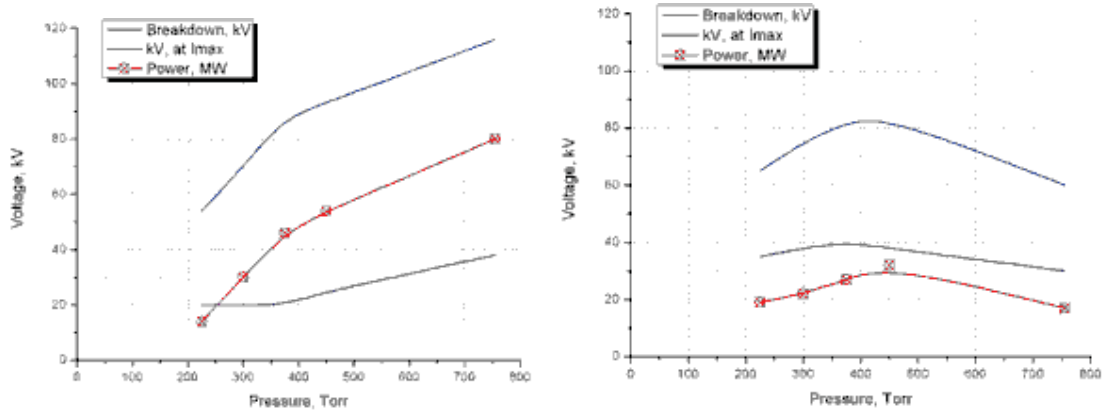


Fig.5.4.2. Data for the Modes 2 and 3. Breakdown voltage, gap voltage at maximal current, and power deposited.

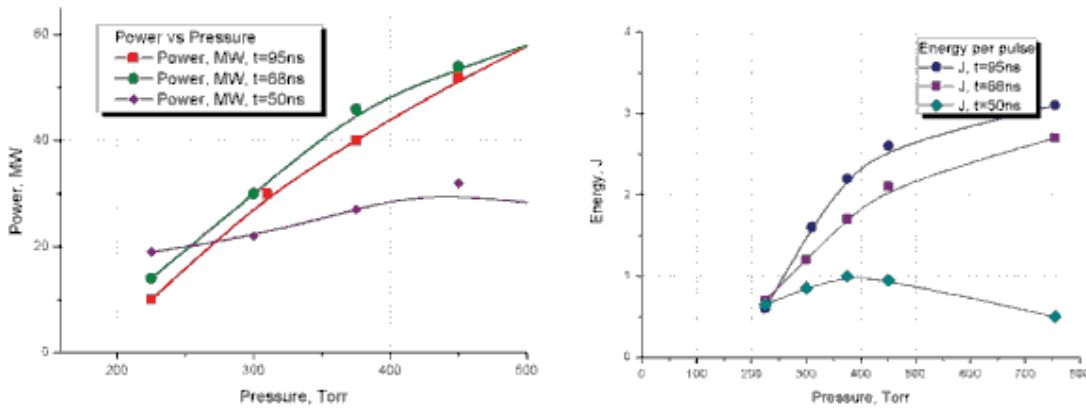
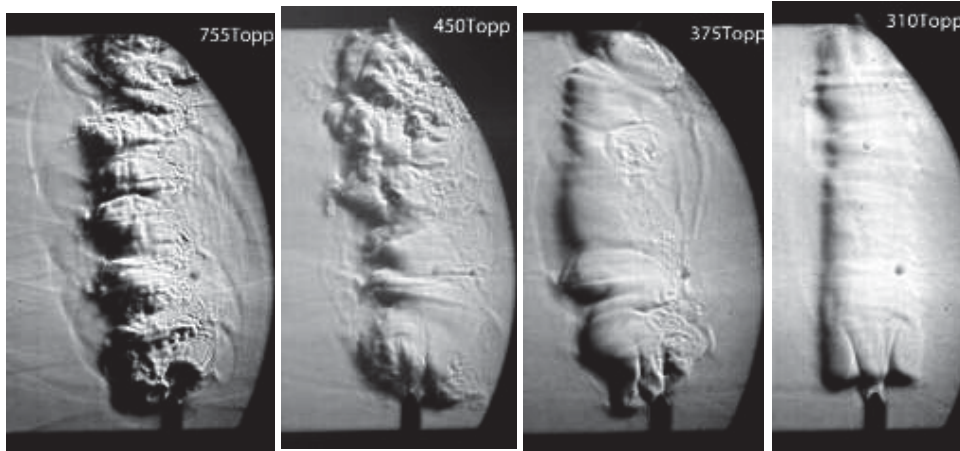


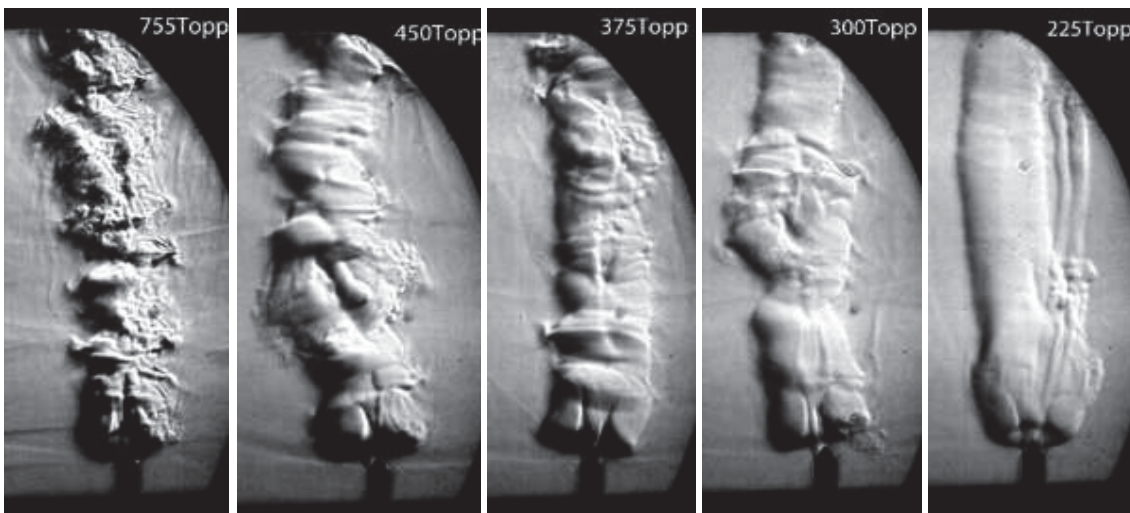
Fig.5.4.3. Comparison of the discharge modes in terms of power and energy deposition.

It is seen that the mode 3 has too short pulse for the discharge channel development at $P=1\text{Atm}$ but has demonstrated some benefit at lower gas density. The comparison of energy deposition is shown in Fig.5.4.3. Despite of large difference in initial energy saved in capacitance, the energy deposition is almost the same at lower gas density. This fact is posed as critically important for a further work.

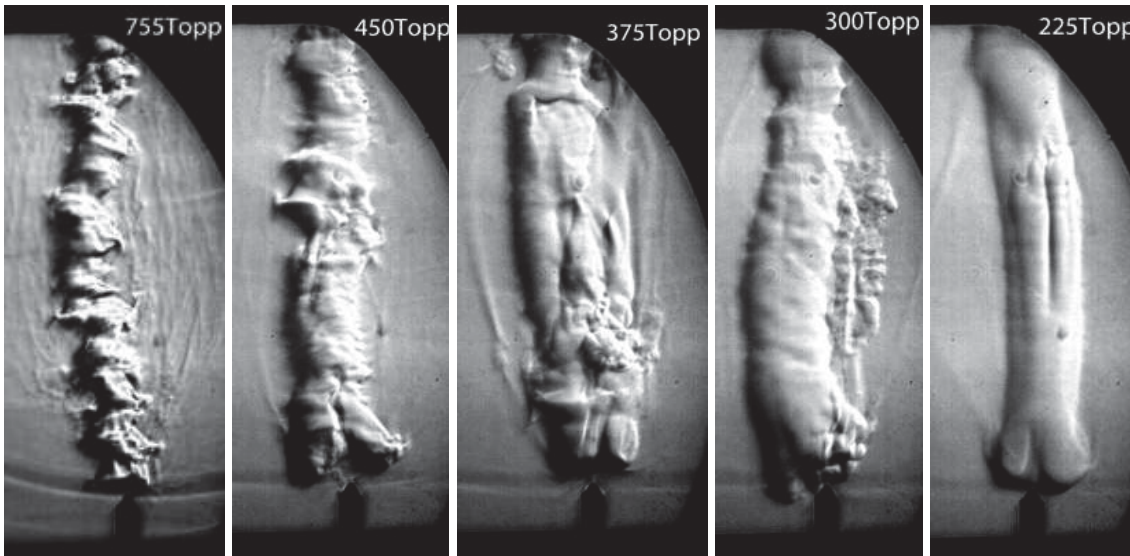
Typical schlieren images for the modes, described above, are presented in Fig.5.4.4 at different pressure. Time delay was $150\mu\text{s}$ in all these cases.



Mode 1



Mode 2



Mode 3

Fig. 5.4.4. Typical schlieren images vs air pressure in different modes.

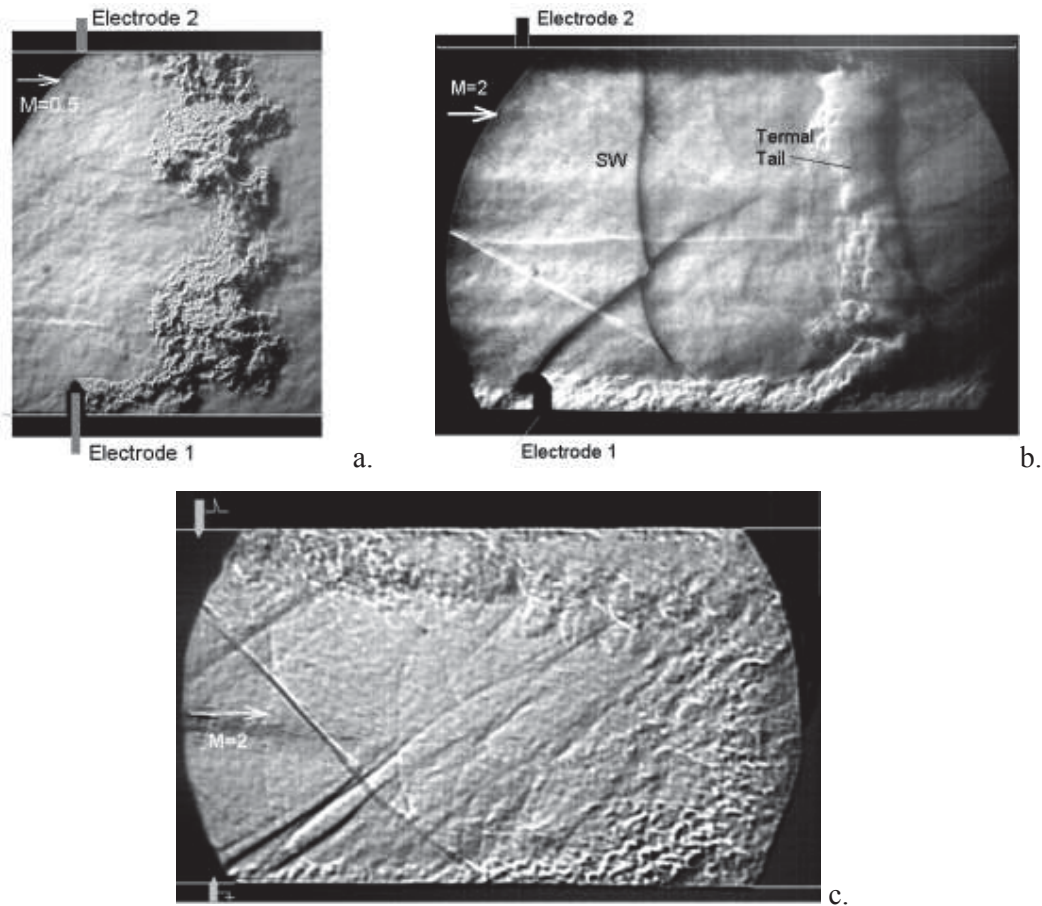


Fig.5.4.5. Schlieren image of pulse discharge in $M=0.5$ and $M=2$ flow.
 a.- $P_{st}=670$ Torr, b. - $P_{st}=220$ Torr, c. - $P_{st}=450$ Torr, respectively.

Typical schlieren images of pulse discharge in $M=0.5$ and $M=2$ flows are shown in Fig.5.4.5 at static pressure $P_{st}=670$ Torr, $P_{st}=220$ Torr, and $P_{st}=450$ Torr, respectively. Time delay was $150\mu s$, $100\mu s$ and $150\mu s$ in these cases. The graphs in Fig.5.4.6 demonstrate the data on the thermal cavern movement and expansion at flow and ambient conditions. A specific feature of the after-discharge channel dynamics is an amplification of instability in subsonic flow. This effect was observed previously [2]; it has no proper explanation yet. The difference in new data for the supersonic flow, which prove a previous expectation: in supersonic flow the rate of the after-discharge expansion very similar to behavior in subsonic flow.

For the better temporal resolution the schlieren-streak records were made under the conditions mentioned above. The line-scan camera has the frequency of operation up to 2×10^5 lines/s. The results of observation are presented below in Fig.5.4.7 for ambient conditions (a); for subsonic flow (b); and for supersonic flow (c). In all those cases the power supply gave two sequential pulses with time delay $\Delta t=150-220\mu s$. The features of interaction are well seen: outgoing shock waves (SW); and zone of the flow perturbation.

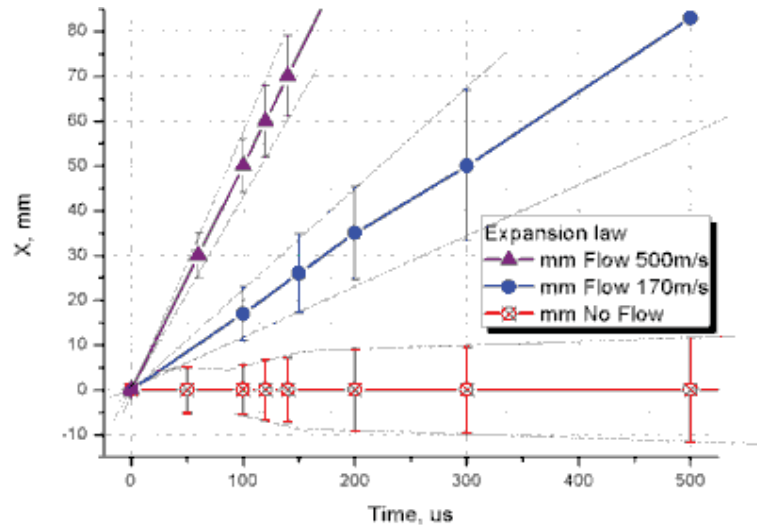
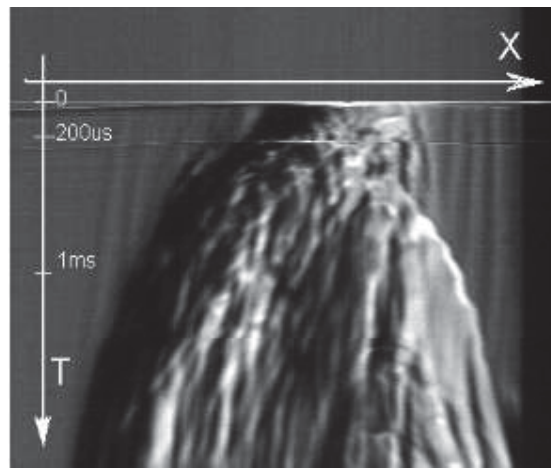
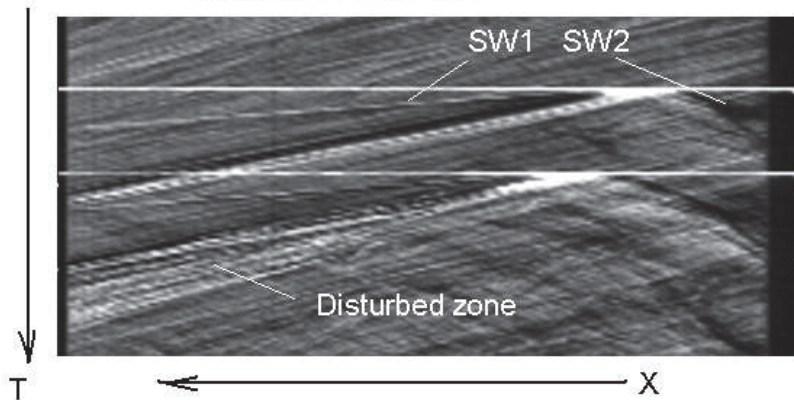


Fig.5.4.6. The rate of expansion in ambient air, in subsonic and supersonic flow.



(a)

Subsonic Flow $M=0.5$



(b)

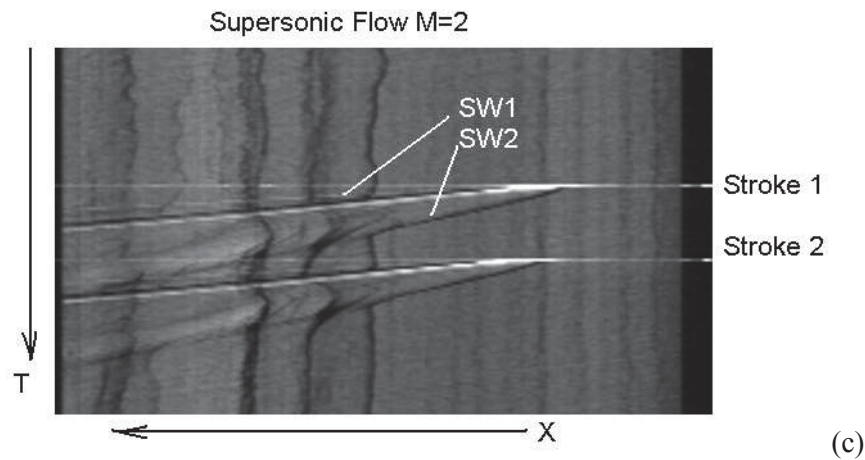


Fig.5.4.7. Schlieren-streak images of the discharge in ambient air (a) and in flow (b-M=0.5; c-M=2).

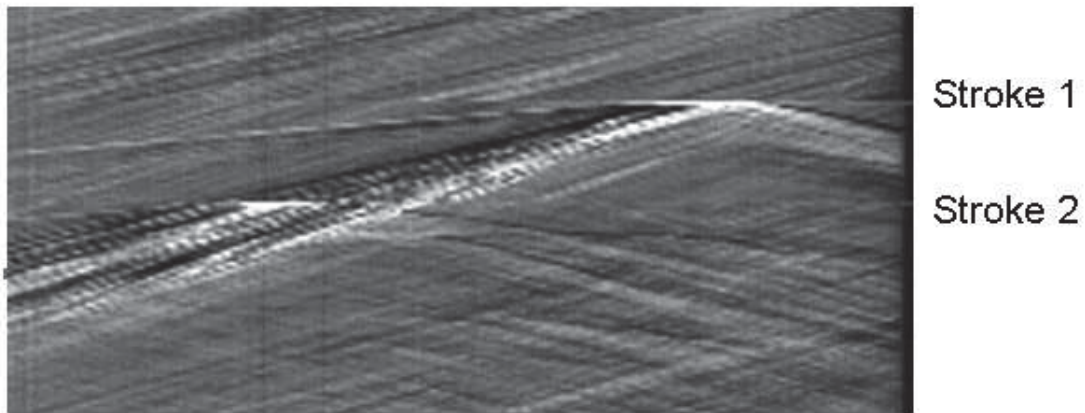


Fig.5.4.8a. Schlieren-streak image of the effect of strokes conjunction.

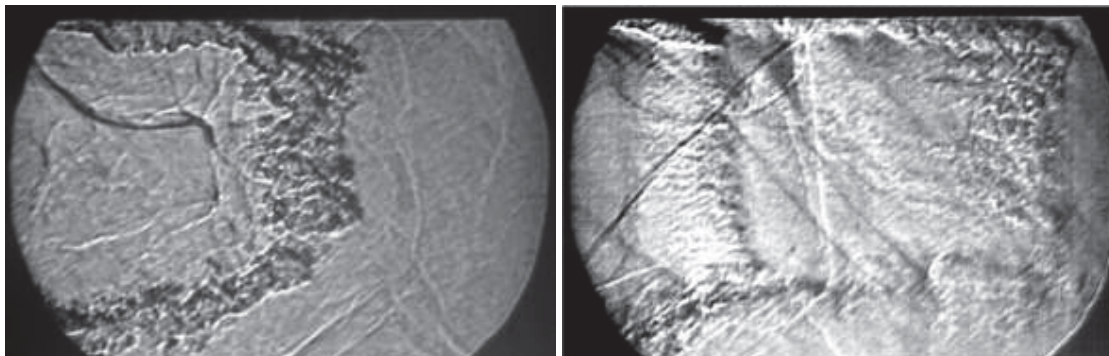


Fig.5.4.8b. Schlieren images of the effect of strokes conjunction/separation.

The decrease of the delay time below $\Delta t=90\mu\text{s}$ for the supersonic flow and below $\Delta t=150\mu\text{s}$ for subsonic flow leads to the effect of conjugation of sequential strokes (the second pulse follow the way of the previous one). The realization of this effect is shown in the Fig.5.4.8a in schlieren-streak image and in Fig.5.4.8b in two schlieren images. The breakdown of the second

discharge occurs in already disturbed zone by previous pulse. The criterion of the effect appearance is the distance to the previously disturbed zone must be higher than the inter-electrodes gap. It is reflected also in reducing of the breakdown voltage as it is shown in Fig.5.4.8c.

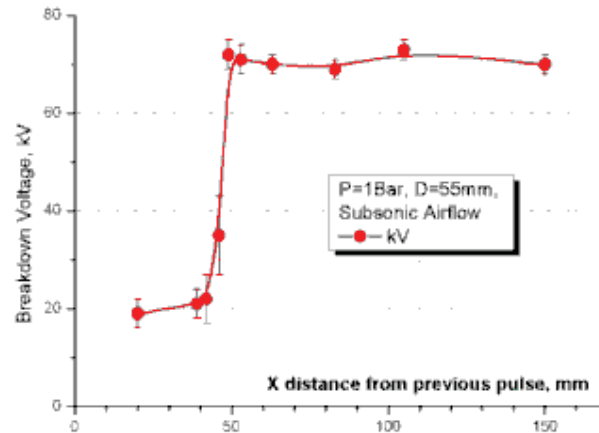


Fig.5.4.8c. Breakdown voltage reduction due to the effect of strokes conjunction.

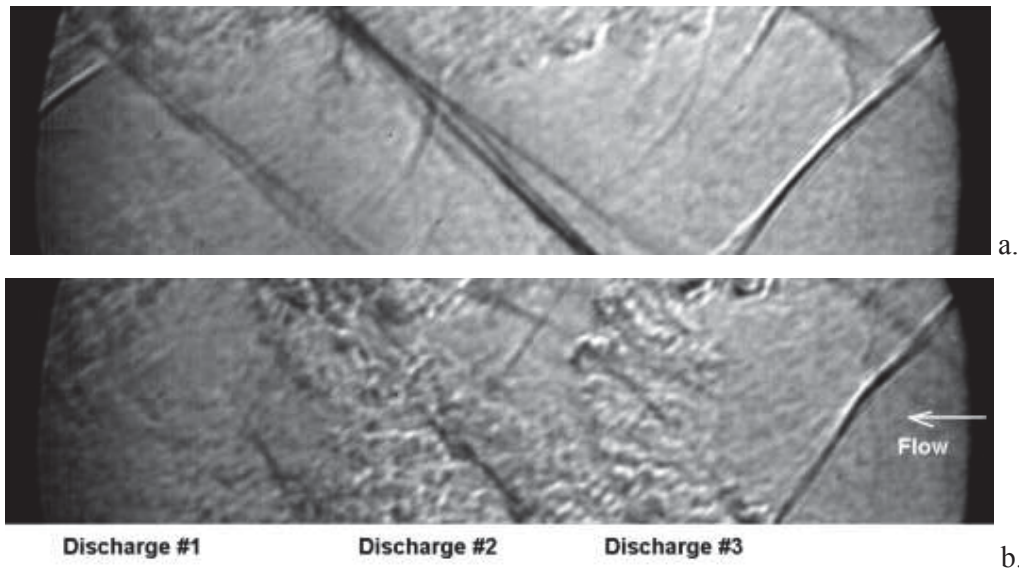


Fig.5.4.9. Schlieren image of triple pulse effect on the flow.
a. – no discharge, b. – triple pulse.

The second series of tests appears to be needed because the static pressure in the first case was critically lower than atmospheric value: $P_{st}=100-250Torr$ at $M=2$. The tests were made in test-section of facility PWT-10. The electrical parameters were measured in coupling with schlieren images acquisition to detect the instability presence in operation modes with 2 or 3 sequential pulses. The typical schlieren pictures are shown in the Fig.5.4.9 for undisturbed and disturbed flow (triple pulse). One can see that the disturbed zone occupies almost whole flow. At the same time there is no any significant modification of the averaged flow parameters.

The quantitative analysis of images allows estimating a main characteristic size of the plasma-induced disturbances. The Fig.5.4.10 presents a comparison of Fourier spectra of the processed images. The statistically averaged value is calculated as of $\Delta y=1-3\text{mm}$.

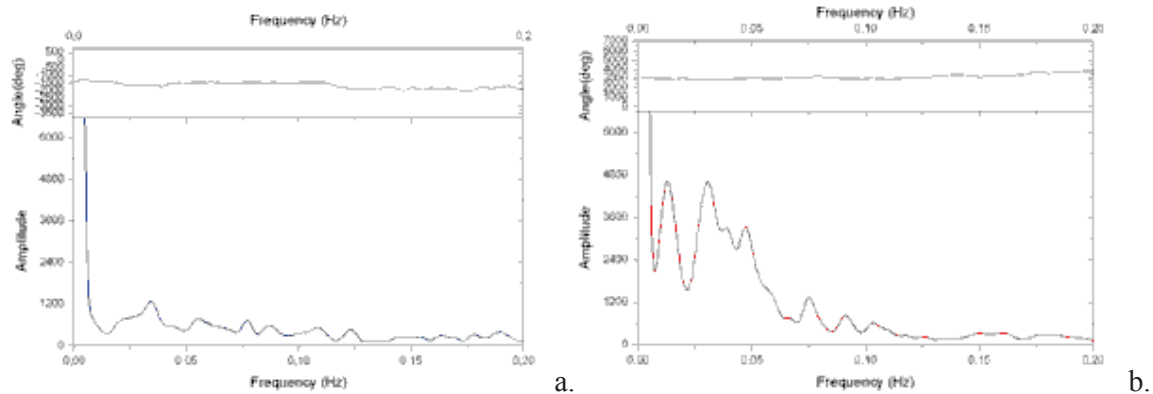


Fig.5.4.10. Fourier spectra of density disturbances in two cases: no discharge (a); and triple pulse (b).

Laser diode-based optical system has been used to determine spectra of perturbations in supersonic flow. Beam of light $\varnothing 2$ mm from the diode module passes through the supersonic flow ($M = 2$) and was received by photodiode with $1\mu\text{s}$ rise and fall response time. The photodiode is connected to the oscilloscope Agilent™ 54621A with maximum rate of data recording 2×10^8 points per second and ability to transmit array of 2×10^6 points to computer. The wavelength of the laser diode module is $\lambda=655$ nm and the power $W=6$ mW. In the last experimental series the dimensions of the test section were 25×65 mm, the beam passes through the center of the bigger wall at distance about 60 mm downstream the electrodes. The distance between the channel and photodiode was about 4 m. The power supply used was capable to stroke 1-3 discharges in the stream with $140 \mu\text{s}$ delay between the 1th and the 2nd pulses and $110 \mu\text{s}$ delay between the 2nd and the 3rd pulses. The scheme of measurements is shown in Figure 5.4.11.

The signal recorded is processed by PC by the following method: the data are divided into fragments with the length of $80 \mu\text{s}$ (partial intersection is possible), then amplitude Fourier-spectrum is calculated for each fragment in the range of $0 - 500$ kHz. Under the circumstances the frequency step is $\Delta f = 12,5$ kHz. After data processing the following graphs are constructed: amplitude spectrum $A(f)$ and dependence of $\lg(\langle A \rangle)$ on time, where $\langle A \rangle$ is the frequency-averaged amplitude calculated for $(f, f \pm \Delta f)$, i.e. for three points.

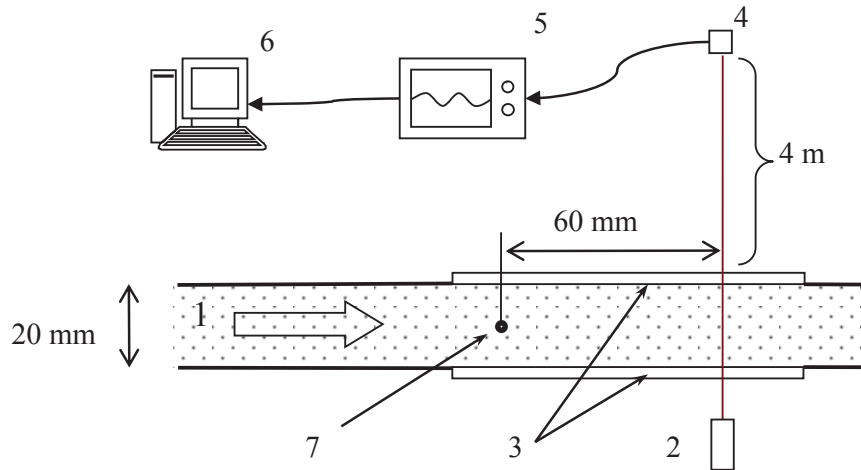


Fig.5.4.11. Scheme of the experiment. 1 – supersonic flow ($M = 2$); 2 – laser diode module; 3 – optical windows; 4 – photodiode; 5 – oscilloscope; 6 – computer; 7 – electrodes location.

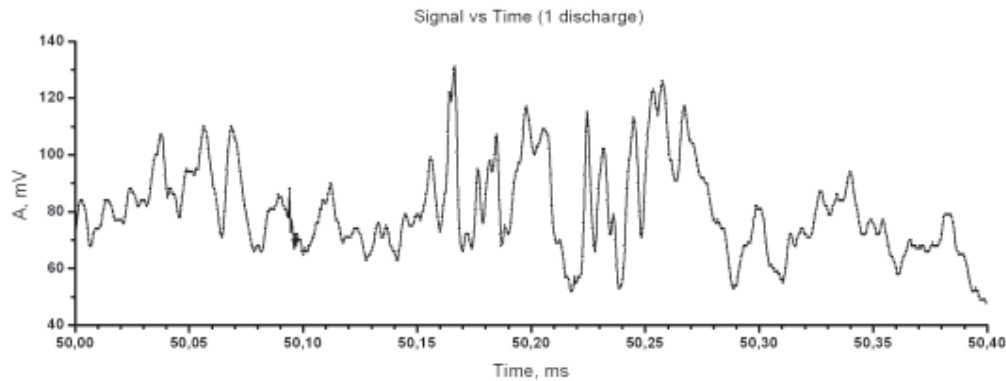


Fig.5.4.12. A sample of the signal record.

The time-dependence of photodiode signal for the case of one discharge is presented in Figure 5.4.12. In the range of $t=50,15\div 50,30$ ms the increase of the oscillation amplitude associated with passing of the disturbances, which were excited by the discharge, through the beam. The spectra for different time intervals are presented in Figure 5.4.13: at 49,88 ms - before the passage of disturbances, at 50,20 ms and 50,26 ms - during the passage of disturbances, at 50,58 ms - after the passage of disturbances. These spectra show that discharge generation leads to an amplitude increase in a wide frequency range of 100 - 400 kHz. Figures 5.4.14 and 5.4.15 present dependences of $\lg(\langle A \rangle)$ of time for the cases of one and three discharges, respectively. One can see that in the case of three discharges the increase of the amplitude at the frequencies mentioned above occurs in a wider time range and the disturbances almost merge into one.

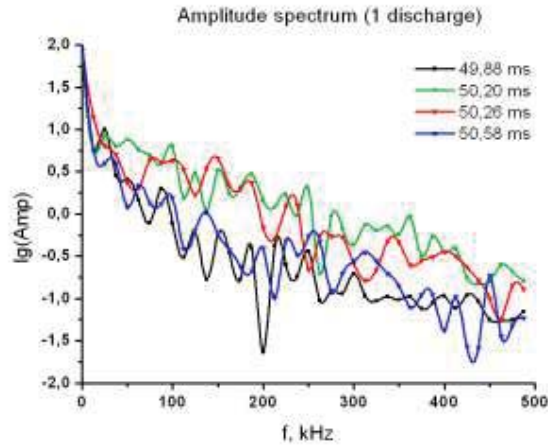


Fig.5.4.13. Spectra recalculated for the single discharge stroke.

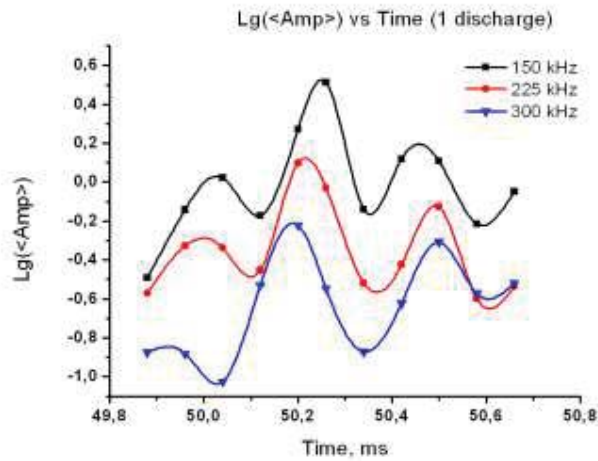


Fig.5.4.14. Spectral data dynamics at single stroke.

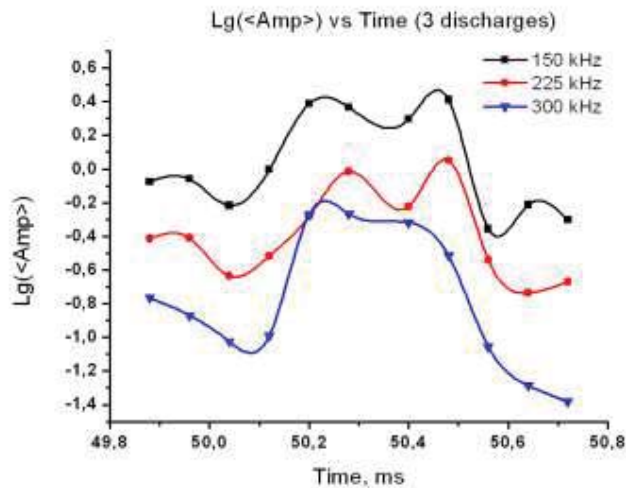


Fig.5.4.15. Spectra dynamics at triple stroke.

Additional analysis of physical effect of multi-pulse operation mode on gas' characteristics shows that zone of disturbances occupies not less than 70% of gas volume at distance more than 100mm downstream the discharge generation zone (electrodes position). From one side the repetition rate is limited by the effect of strokes conjugation, but, from the other side, must be enough high to disturb as much gas as possible on reasonable distance.

Following conclusions may be currently made based on experimental data obtained in this experimental series:

- The intensity of discharge instability drops with gas density;
- Shorter pulse – higher efficiency of energy deposition in explored range of gas parameters;
- Discharge structure modification prevents the instability development at lower gas density;
- Velocity of post-discharge thermal cavity in supersonic flow is equal with the flow;
- The time scale of the flow turbulence ($3\mu\text{s}$) corresponds to spatial scale of discharge excited disturbances, which is measured as $\Delta x=1-2\text{mm}$;
- Optimal repetition rate allows to provide the turmoil ☺ of gas in whole volume.

References to section 5.4.

7. *S. Leonov, M. N. Schneider, D. Yarantsev* “Fast Mixing by Pulse Discharge in High-Speed Flow” // Paper AIAA-2006-8129, 14th AIAA/AHI Space Planes and Hypersonic Systems and Technologies Conference, Canberra, Australia, Nov. 6-9, 2006
8. *Sergey B. Leonov, Dmitry A. Yarantsev, Yury I. Isaenkov* “Properties of Filamentary Electrical Discharge in High-Enthalpy Flow”, 43rd AIAA Aerospace Sciences Meeting & Exhibit, 10-13 January 2005/ Reno, NV, AIAA-2005-0159.M.N.
9. *M. Shneider*, “Gasdynamic and turbulent cooling of after-spark and arc channels”, 26th AIAA Plasmadynamic and Lasers Conf., AIAA-95-1994, June 19-22, San Diego, 1995.
10. *S. Leonov, Yu. Isaenkov, M. Shneider, D. Yarantsev* “Fast Mixing by Pulse Discharge in High-Speed Flow”, Presented to 37th AIAA Plasmadynamics and Lasers Conference, San Francisco, USA, June 2006,
11. *Yu. I. Isaenkov, S. B. Leonov, M. N. Shneider* “Mixing Intensification by Electrical Discharge in High-Speed Flow” Proceeding of the Fifth International Conference on Fluid Mechanics, Aug.15-19, 2007, PaperF28; Shanghai, China; Tsinghua University Press & Springer
12. *Sergey B. Leonov, Yuri I. Isaenkov, Mikhail N. Shneider* "Suppression of the turbulent decay of an afterspark channel with residual current", PHYSICS OF PLASMAS 14, 123504 _2007.
13. *Sergey B. Leonov, Dmitry A. Yarantsev, Campbell Carter* Transversal Electrical Discharge as a New Type of Flameholder, 15th AIAA International Spaceplanes and Hypersonic Systems and Technology Conference, Dayton, OH, Apr-May 2008, AIAA-2008-2675.

5.5. Experimental study of plasma localization in mixing layer of gas-gas and spray-gas systems at ambient conditions.

The experimental part of the project in frames of Task 2 was aimed at the tests to study of the filamentary discharge interaction with a spray medium in vicinity of its boundary. The actual electrodes configuration is drawn in Fig.5.5.1 below.

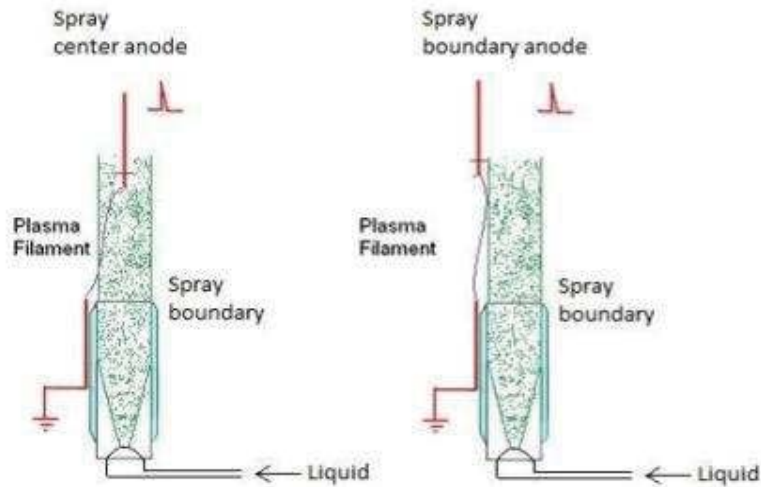


Fig.5.5.1. Variants of electrodes configuration for the first scheme: left – gas-spray, center anode; right – gas-spray, boundary anode.

In previous reports an idea of discharge filament localization under nonhomogeneous medium was discussed. Cases with gas jet in stationary gas and high speed flow were studied theoretically and experimentally. As a proceeding of these investigations we consider studying the discharge filament localization in case of spray jet under variety of conditions. Two schemes shown in Fig.5.5.1 were used in the last modification of the experimental setup.

The power supply for discharge studied is shown in Fig.5.5.2. It is based on the high voltage Tesla transformer using in regime of impact load. High voltage capacitance C_0 (1 μF , up to 12 kV) switched to the first coil of Tesla transformer by means of controllable high-pressure spark gap. Capacitance C of approximately 367 pF served a load of transformer. These schemes allow obtaining voltages on load up to ~ 120 kV, with the rise time of about 500 nanoseconds.

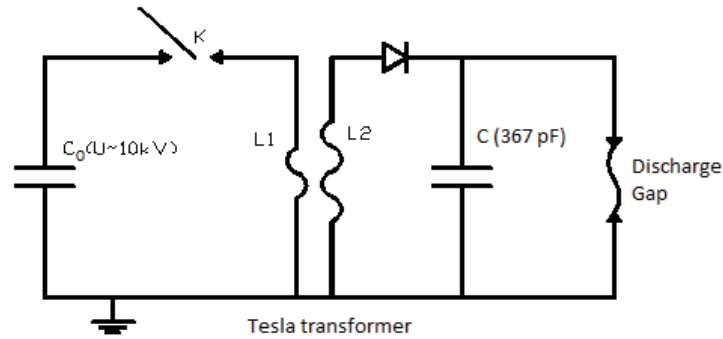


Fig.5.5.2. Principal scheme of the high voltage power supply.

Optical output pulse generator was used for synchronization. Scheme of optical coupler generating high voltage (~ 7 kV) pulse on the input of spark gap K is shown in Fig.5.5.3. The discharge voltage was measured by means of high speed divisor and current was measured by means of Rogovsky coil.

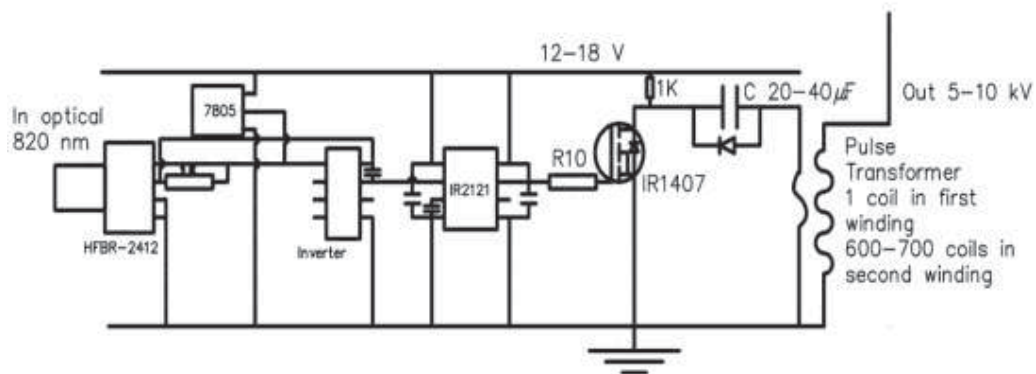


Fig.5.5.3. Scheme of discharge synchronization (optical coupler).



Fig.5.5.4. Schlieren photo of spray jet.

Series of experiments with the spray jet in ambient air were performed. In this experiments jet was formed by means of long tube connected to externally gated injector. Such configuration allows obtaining uniform cylindrical spray jet. The schlieren photo of jet without discharge is shown at Fig.5.5.4. The grounded electrode was placed along the surface of the tube. The high voltage electrode (anode) was placed in flexible goffer tube, which allows one to change its position. The

breakdown voltage is one of the main characteristics of the discharge. The values of averaged breakdown voltage under different configurations with spray and without spray are presented in Table.5.5.1. As it follows from comparison of these table data, there is a considerable decrease of breakdown voltage, when discharge propagated at the presence of spray jet.

Table 5.5.1. Average breakdown voltage under different conditions.

With spray jet		Without spray jet	
Position of anode relatively to the jet. Distance and orientation.	Average breakdown voltage, kV	Configuration of anode	Average breakdown voltage, kV
		30 mm border	86
40 mm border	94	40 mm border	109,86
50 mm border	99,74	50 mm border	120,67
40 mm center	103,11	40 mm center	108,33
50 mm center	107,45	50 mm center	122,5

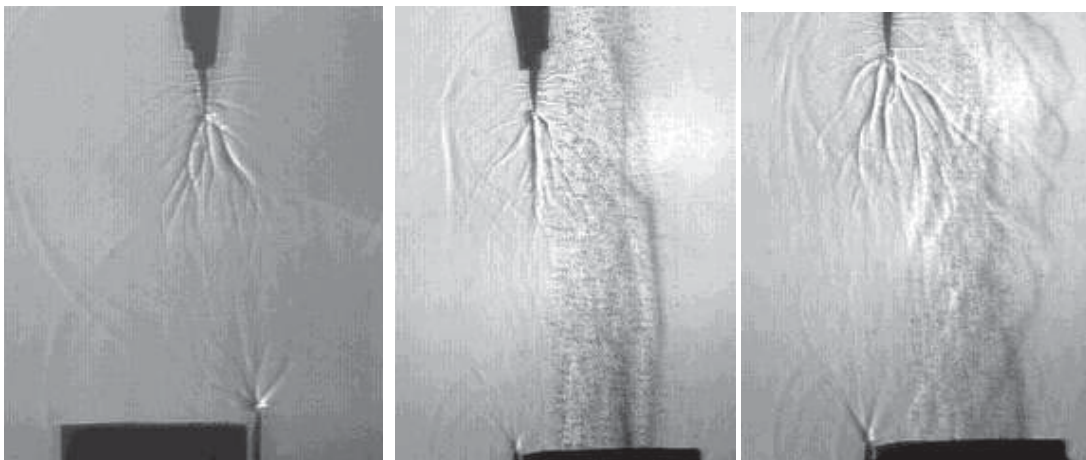


Fig.5.5.5. Schlieren photos of streamers without and with spray jet.

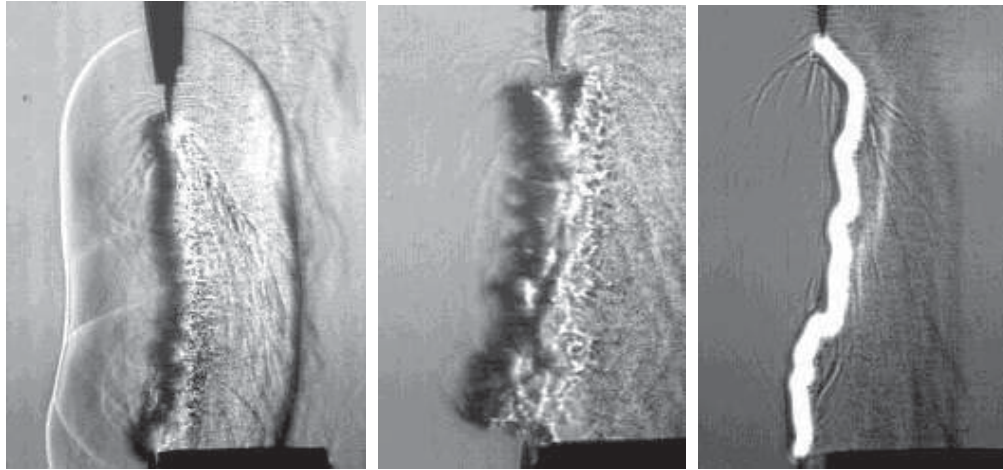


Fig.5.5.6. Schlieren photos of discharge propagation and plasma channel decay with the spray jet.

One can see the schlieren photos of streamers with and without spray jet in Fig.5.5.5. It is clear, that there is an influence of spray jet on the process of streamers propagation. They tend to propagate along the border between the spray jet and ambient air, at least at the first stage of propagation (before the first bend). Such a situation was observed at not every run. The preliminary idea is that there wasn't precise control of intensity of spray jet. The difference of average concentration of droplets in spray jet may be observed in the schlieren photos. Influence of spray jet on the process of streamers propagation was observed in runs with intensive spray jet. The second stage of development of the discharge (that was discussed in previous report) is even more responded to the spray jet. As it can be seen in Fig.5.5.6 the discharge tends to propagate along the border of the spray. This effect is rather similar to one in configuration with gas jet in ambient air. But the plasma filament is not straight as it was in case of gas jet. Contrary it's strongly bended, even more then in air without spray jet. The irregularity of spray boundary may be an explanation of this effect.

The next experimental portion of the work includes among others the tests on the discharge localization affected by thin laminar jet of He and heated air. The principal scheme of experimental arrangement is shown in Fig.5.5.7. A thin laminar gas jet is blown out from quartz or ceramic pipe in the same plane as the inter-electrode gap with a small angle in respect of axis. Schlieren images and photos were taken in perpendicular directions.

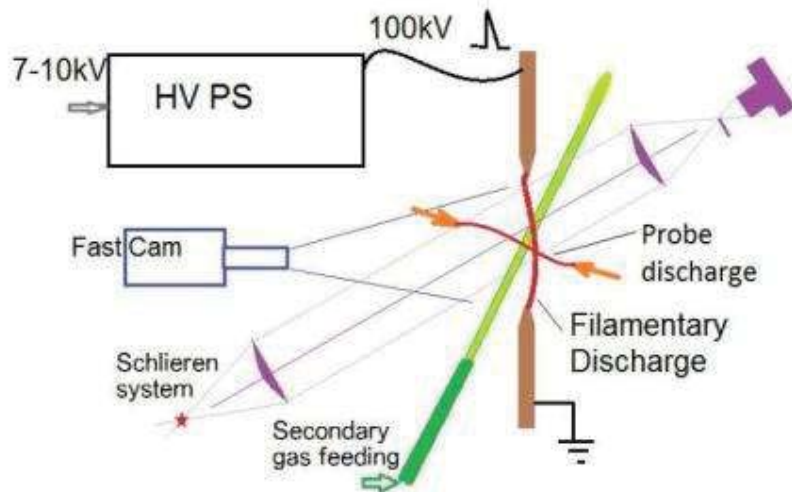


Fig.5.5.7. Experimental arrangement of the test on HV discharge interaction with secondary gas mini-jet.

Two experimental series were performed: (1) He jet; and (2) heated air jet. In the first case the effect of specific localization should be appears definitely due to much higher ionization rate in He vs air. In the second case a thermal effect (read: density effects) is revealed.

Figure 5.5.8 shows the schlieren image and photo of the high voltage discharge interaction with He laminar jet. Of course the discharge follows the jet. Of interest is that streamers may turbulize the laminar jet even without main HV discharge, see image in Fig.5.5.9a at delay time 2ms. The result of interaction of spark discharge and jet at the same delay time, presented in Fig.5.5.9.b, demonstrates an amplification of the instability development due to artificial bending of the discharge channel.



Fig.5.5.8. Schlieren image HV discharge + He jet (delay 20 μ s) and photo of the discharge.

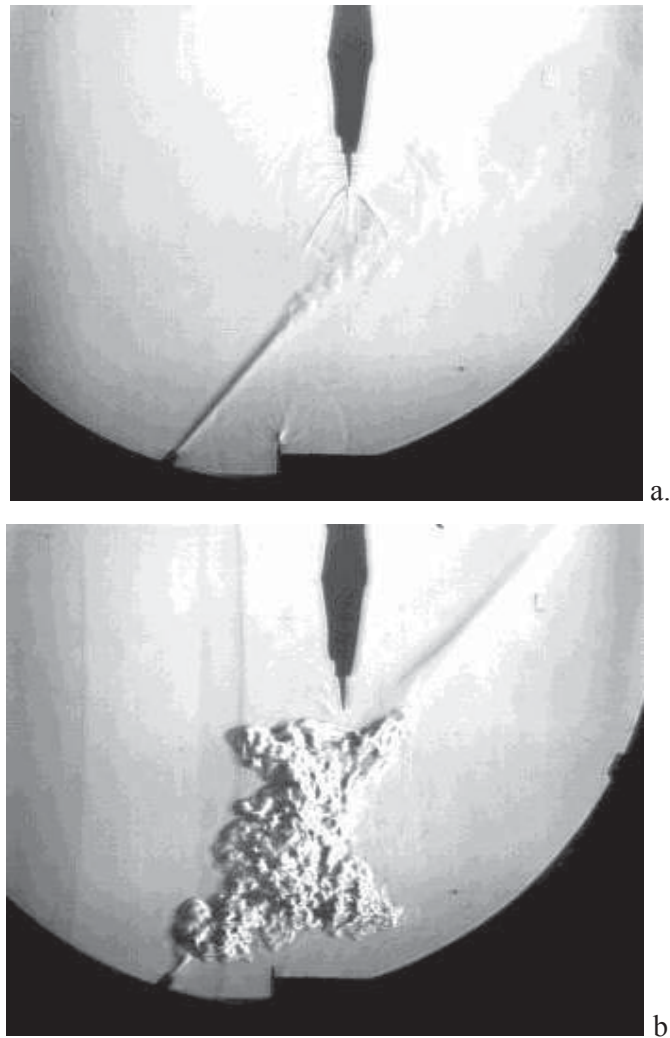


Fig.5.5.9. Schlieren images of HV discharge interaction with He jet (delay 2ms). a - streamer phase only; b - spark discharge.

In the second test the temperature elevation of heated air was in range $\Delta T=20-80K$. Based on (pd) scaling we could expect 10-15% of breakdown voltage reduction. In fact an insignificant effect of air temperature on the discharge location and negligible effect on breakdown voltage were observed under considered conditions. The schlieren image in Fig.5.5.8 is the best in terms of the discharge guiding.

5.6. Experimental runs with second gas and spray injection in high-speed flow.

5.6.1. Experimental runs with co-flowing jet of second gas.

Three experimental series were fulfilled in frames of the project to study the discharge interaction with two-component flow:

- Discharge through the jet of second gas, no external flow;
- Discharge in external flow with a central body without the second gas injection;
- Discharge through co-flowing jet of second gas in supersonic airflow.

The figures below show the typical schlieren photos for these three cases. It should be considered that the presence of schlieren images is insufficient for deep quantitative analysis of the discharge generation effect on the mixing processes.

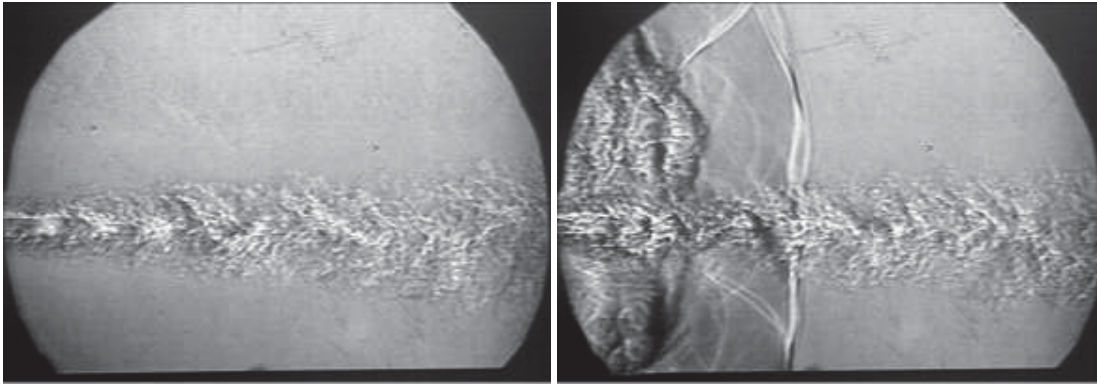


Fig.5.6.1. Discharge interaction with CO₂ jet. No flow.
Left – initial structure, right – 75 μ s after the discharge.

Without the secondary gas injection the central body produces the aerodynamic trail, where the gas velocity is negligibly small comparing the main flow. As the result the after-discharge channel possesses a sophisticated shape shown in Fig.5.6.2.

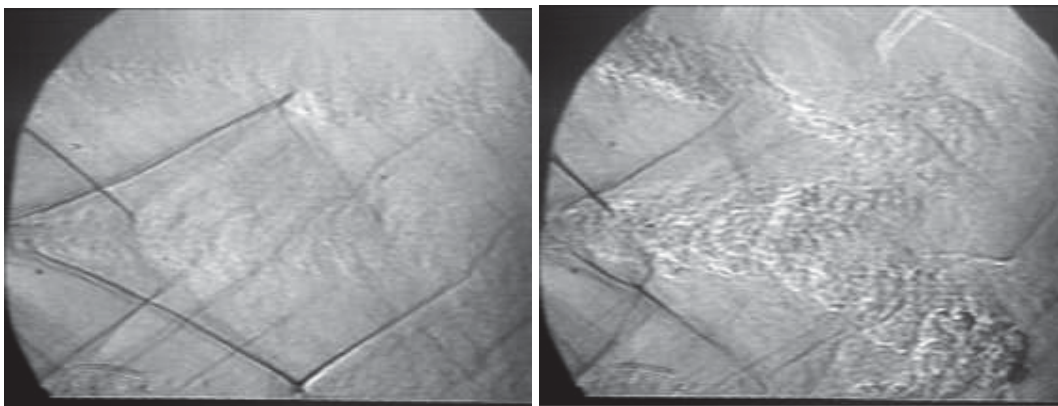


Fig.5.6.2. Discharge interaction in M=2 flow. No CO₂ injection.
Left – initial structure, right – 100 μ s after the discharge.

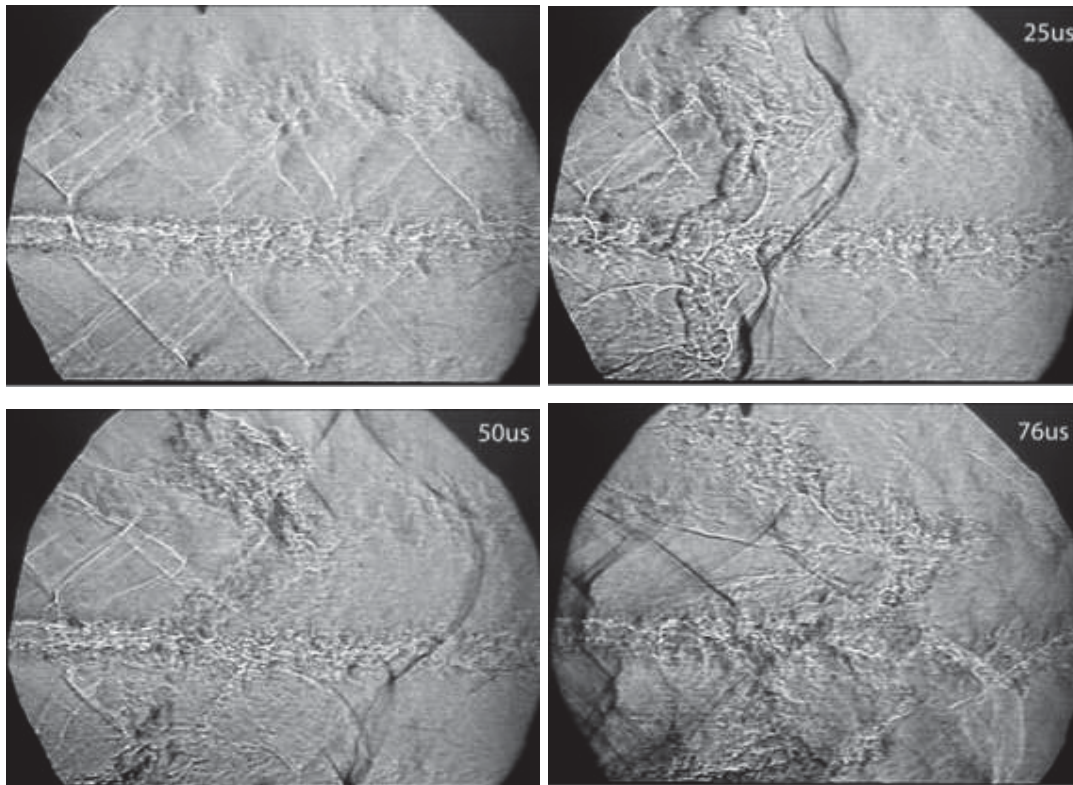


Fig.5.6.3. Discharge interaction with CO₂ jet in M=2 flow.
Left, top – initial structure, right and bottom – 25, 50 and 76 μ s after the discharge.

The Fig.5.6.3 demonstrates the dynamics of the flow structure after the discharge excitation through the supersonic flow and co-flown jet of CO₂. The influence of the discharge on visible appearance of the jet is recognized at time delay about 70 μ s and later. There were considered that at such an approach the volume of interaction is rather small to affect the mixing layer significantly.

5.6.2. Experimental runs with wall jet of model gas.

The experimental approach includes the following key points: subsonic and supersonic duct-driven airflow at $M=0.3-0.5$, $M=2$, and $M=2.5$; direct injection of gaseous fuel (wall jet of model gas, gaseous fuel, He or CO_2 , preliminary); transversal short-pulse repetitive electrical discharge, crossing flow along air-fuel boundary; plasma-induced artificial turbulence; zone of improved mixing. The experimental scheme is shown in Fig.5.6.4.

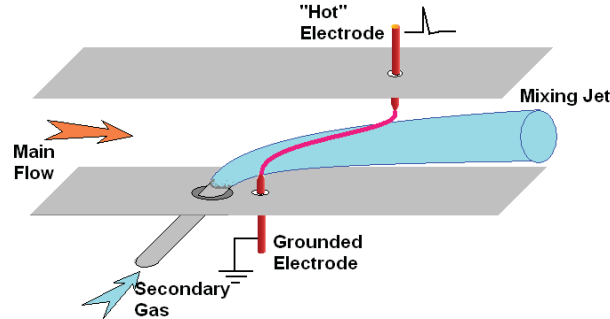


Fig.5.6.4. Experimental scheme.

The pulse transversal discharge was excited by means of the pulse-repetitive power supply of the discharge made on the base of Tesla transformer. The typical parameters of the tests are the following: total air pressure $P_t \approx 1 \div 2 \text{ Bar}$, discharge pulse duration in a range $t=40-100 \text{ ns}$, maximal voltage, current and power were $U_{max}=100 \text{ kV}$, $I_{max}=2.5 \text{ kA}$, $W_{max}=90 \text{ MW}$. Three main methods were applied for the visualization of plasma-flow interaction: instant schlieren images; schlieren-streak records; and high-speed photographs [1, 2].

The experimental scheme shown in Fig.5.6.4 was explored in subsonic and supersonic flow. Two secondary gases were used in preliminary tests: CO_2 as a model of hydrocarbon gaseous fuel, and He as a model of hydrogen. The jet was injected orthogonally to the wall through $D=4\text{mm}$ orifice with the sonic velocity. The grounded electrode was combined with the nozzle. The "hot" high-voltage electrode was installed on the opposite wall of the duct a bit downstream in respect of the grounded one.

Before presentation of the results obtained it is important to remind one feature of the discharge behavior near the boundary of two different gases. As there were announced in section 4 [4], "On one side, the breakdown voltage is lower in a fuel (experimentally and by the calculations, as well), on the other side the discharge channel loses the resistance much faster in the air. A priori it is difficult to predict the discharge filament location, when the electrodes position is close to boundary of two different gases. Special tests were performed to

clarify this point experimentally. It was found, that in the most cases the discharge was located inside a mixing layer between the gases”. Up to now there is no comprehensive explanation of this fact although it may be principally important for a practical implementation.

At flow velocity $M=0.3$ and 2.5 static pressure were $P_{st}=400$ and 125 Torr. Injected gases were CO_2 and He. Schlieren photos in Figs.5.5.2 demonstrate CO_2 jet in flow, discharge operation without CO_2 jet and discharge with jet under conditions of subsonic (top series) and supersonic (bottom series) flow.

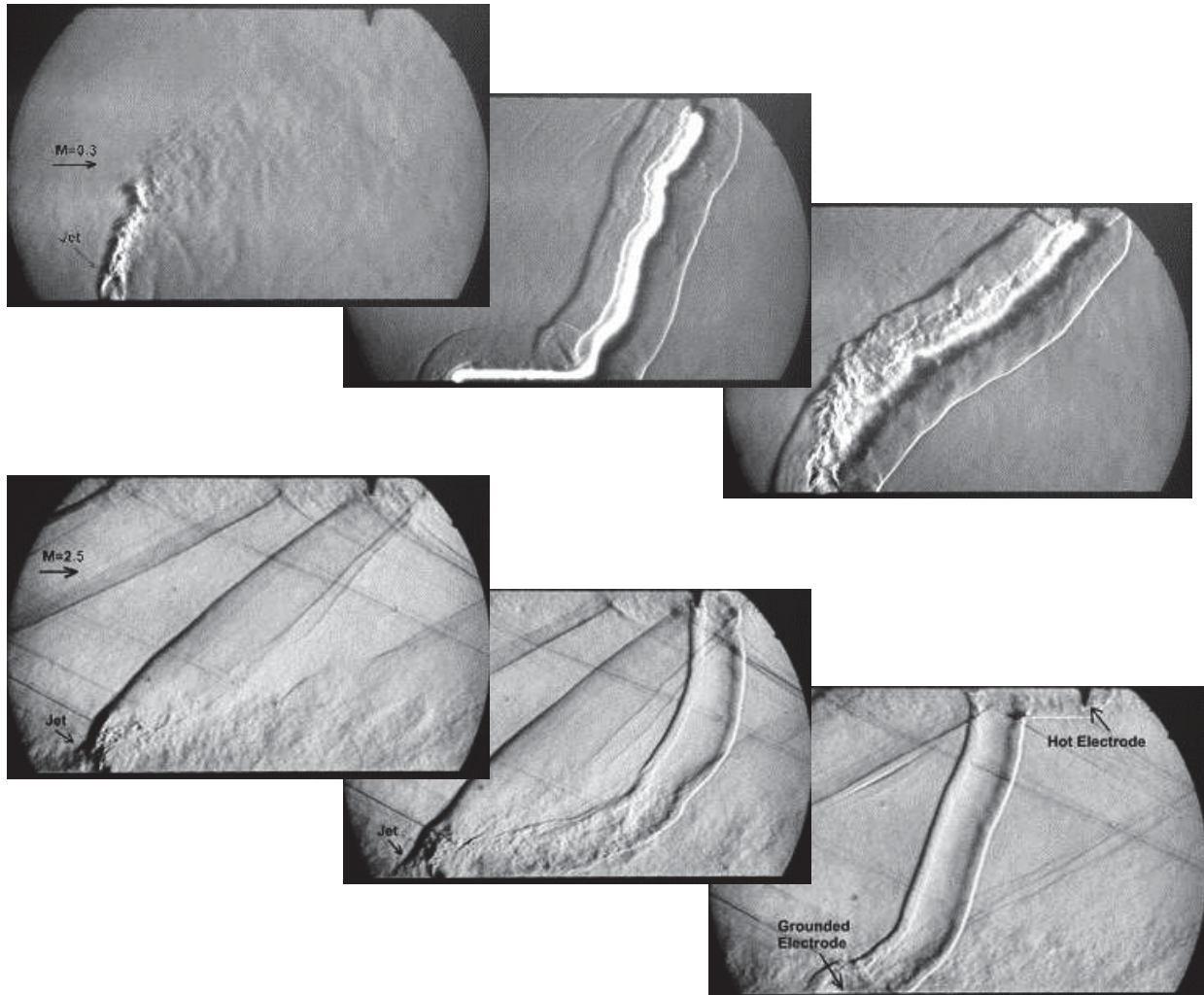


Fig.5.6.5. Typical schlieren images of the discharge operation in airflow with wall-injected secondary gas. Top line– subsonic flow, $M = 0.3$; bottom line – supersonic flow, $M = 2.5$.

Left column – CO_2 jet within the flow; middle column – discharge within the flow; right column – discharge and jet.

It is clearly seen, that discharge breakdown occurs along the jet. This fact was proved during number of experiments. Localization of the discharge’s filament may vary from run to run in the experimental mode without jet, but it doesn’t vary significantly in different runs with

jet injection. The shock wave arises on the jet in the supersonic flow as it is seen in Fig.5.6.5, but the discharge doesn't "feel" it. It means that the type of gas injected is more important for the breakdown than a strong density gradient.

CO₂ jet models the hydrocarbon fuel jet. Helium jet was used in order to model hydrogen fuel because breakdown voltages for both gases are definitely lower than in air. The schlieren photos of the discharge's interaction with CO₂ jet and He jet in the subsonic (M=0.3) airflow at different delays are shown in Fig.5.6.6.

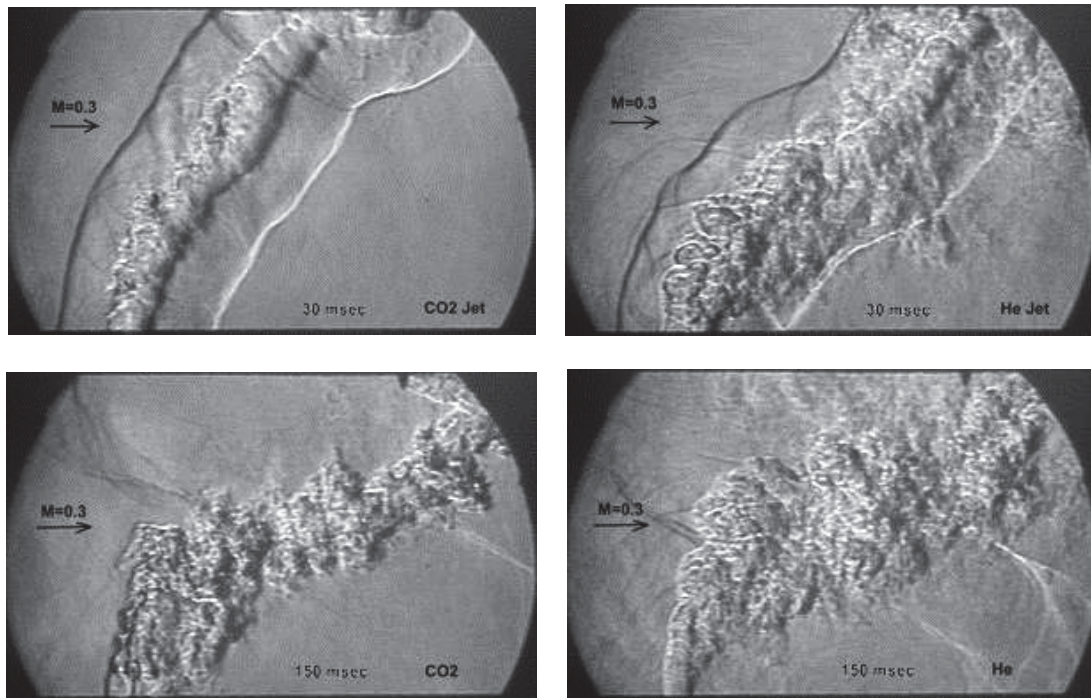


Fig.5.6.6. Schlieren photos of the discharge interaction with CO₂ jet (left) and He jet (right). M=0.3. Top row – time delay 30 μ s; bottom row – 150 μ s.

Helium jet itself occurs more turbulent in airflow than CO₂ jet, discharge interaction with helium jet is stronger than with CO₂ jet.

Comparison between schlieren photo of the CO₂ jet in Fig.5.6.5 and schlieren photo of the discharge interaction with CO₂ jet at delay 150 μ s in Fig.5.6.5 allows concluding that the discharge strongly influences on jet mixing with subsonic airflow. A several times longer distance is needed to analyze the discharge influence on jet appearance in supersonic flow. It was made using the second window of the test section to confirm the previous conclusion.

The discharge visualization was made by means of high-speed CCD camera IMPERX – VGA210GCCN. Camera was installed at 2 meters from the discharge plane, which is coincided with the middle plane of test section containing electrodes and place of gas injection.

The camera and power supply of discharge were synchronized by optical pulse generator. Camera was triggered on 1 ms before the discharge with exposure time being 2 ms. The image was filtered to avoid an matrix saturation. The discharge images at different operating conditions of flow and injection are shown in Figures 5.6.7a-f (flow from left to right).

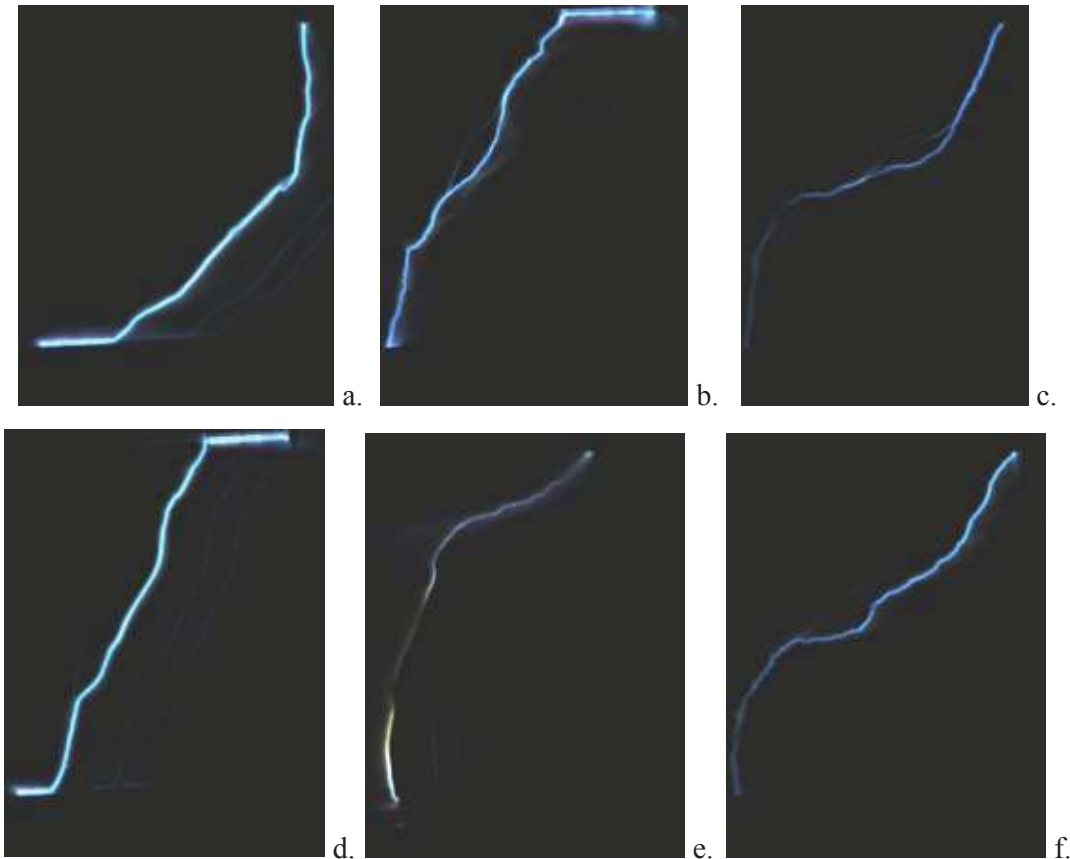


Fig.5.6.7. a- subsonic flow without injection; b - subsonic flow with injection of CO_2 ; c - subsonic flow with injection of helium; d - supersonic ($M=2,5$) flow without injection; e - supersonic ($M=2,5$) flow with injection of CO_2 ; f - supersonic ($M=2,5$) flow with injection of helium.

As follows from the comparison of discharge images with schlieren image of these experiments, the discharge breakdown occurs along the dielectric surface and discharge tends to propagate vertically at conditions of air flow without gas injection. The propagation of the discharge with the presence of gas jet occurs along flow-jet boundary. It is difficult to locate discharge filament position accurately. However at helium injection one can observe (by sight) that discharge luminosity becomes having more red color, this implies that helium is presented within the discharge channel. This fact was verified by spectroscopic methods. The discharge breakdown without jet is stochastic process: it may occur straight between electrodes, or it may arise along one dielectric surface and then turn vertically to the electrode, etc. Presence of the jet defines the way of discharge propagation within the jet area.

The analysis of current and voltage oscillograms allows determining the power input to the discharge, the total enclosed energy, breakdown voltage, resistance of the channel, etc. It is of interest the dependence of electric parameters on the mode of the flow and jet. The characteristic oscillogram of process is shown in Fig.5.6.8.

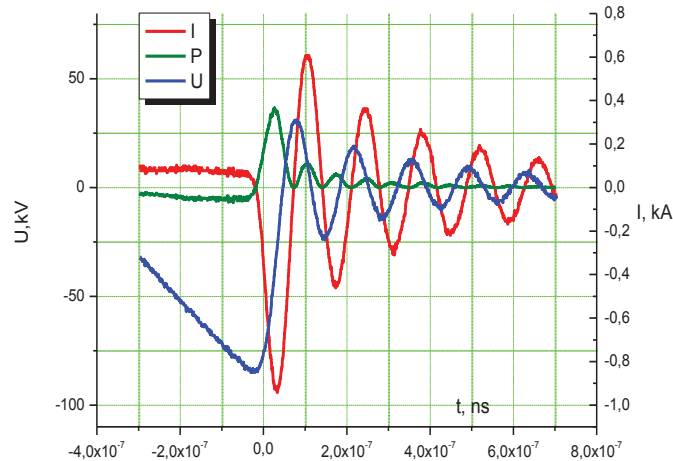


Fig.5.6.8. Current and voltage oscillograms. Power is recalculated.

It is possible to estimate qualitatively the change of gas composition in discharge channel by analysis of the electric parameters. Energy reserved in capacity depends on breakdown voltage, which in turn depends on the discharge channel length. The length of the discharge channel is a stochastic variable. Besides, it can be expected a change of gas composition within the discharge channel. These factors should affect the average electric parameters of the discharge. Table 5.6.1 below presents the averaged experimental results of discharge electrical characteristics in different operating conditions.

Table 5.6.1. Electric characteristics of discharge in various conditions of flow and jet.

N	U _{bd} , kV	E, J	R(I _{max})	Mode
1	100	2,06	42	no flow; P = 0,5 atm
2	75	1,35	44	supersonic flow; no jet
3	85	1,67	40	subsonic flow; no jet
4	73	1,24	42	subsonic flow; CO ₂ jet
5	69	1,14	37	subsonic flow; helium jet
6	61	0,98	44	supersonic flow; helium jet

Average breakdown voltage is 75 – 90 kV, and the power release is 1,5 – 1,7 J at conditions of the airflow without jet. At addition of CO₂ jet breakdown voltage on the average reduces to 65-75 kV, and power contribution reduces to 1-1,5 J. Resistance of the channel, defined at the first maximum of the current, does not vary significantly, although the reduction of the average resistance on by 1-2 ohms is observed (at full resistance of the channel 40 – 50 Ohm).

The electric parameters of the discharge vary much more essentially at the presence of the helium jet in airflow. Breakdown voltage on the average falls reduces down to 60 – 70 kV. Power release in the discharge decreases to 0,9 – 1,2 J. The effect of helium injection on electric parameters of the discharge is stronger, and its presence is easier to detect by the changes mentioned above. But the variation of breakdown parameters still remains notable. At transition to a supersonic flow, breakdown voltage appears the same, while resistance of the channel a bit increases. Breakdown occurs along the jet as it was in subsonic flow.

Estimation of gas composition in the discharge channel by electric parameters of breakdown is a qualitative because of strong variation of these parameters at all gas flow modes. It is possible to define discharge channel position only by average parameters. The spectroscopic method may give more essential information.

Following conclusions may be considered based on experimental data obtained in this test series:

- In two-component flow the filamentary discharge strives for the location between two molecular gases, if the experimental arrangement allows it;
- The discharge disposition into a mixing layer and the instability development are favorable for the kinematic mixing.

5.6.3. Experimental runs with gaseous hydrocarbons injection, double pulse pattern

The next experimental approach includes the following features: duct-driven airflow $M=0.5$ and $M=2.35$; direct injection of gaseous fuel (C_2H_4); transversal short-pulse electrical discharge along air-fuel boundary. Simplified scheme is shown in Fig.5.6.9. In respect of the previous layout the difference is in electrodes location.

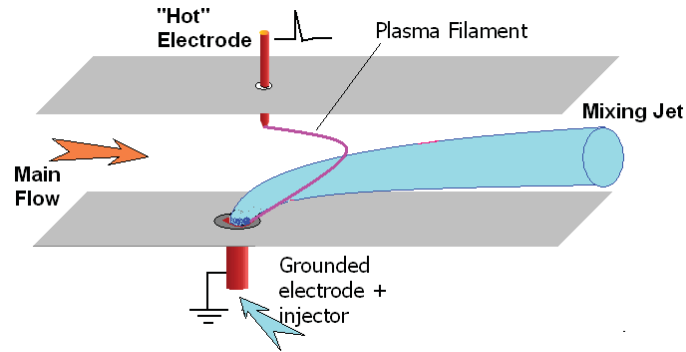


Fig.5.6.9. Experimental scheme applied at C_2H_4 injection.

Double pulse discharge excitation scheme was applied in the most runs. Typical fuel mass flow rate $G=1-5g/s$ was provided through sonic nozzle of diameter $d=4mm$. The grounded electrode was combined with the nozzle. The “hot” high-voltage electrode was installed on the opposite wall of the duct in the same cross-section $X=0$ as the grounded one. The following methods of measurements and visualization were used:

- Instant schlieren imaging;
- High-speed photograph;
- Optical spectroscopy;
- Electrical measurements of the discharge parameters;
- System sensors of pressure.

Typical schlieren image of the discharge interaction with C_2H_4 jet in high-speed flow is shown in Fig.5.6.10.

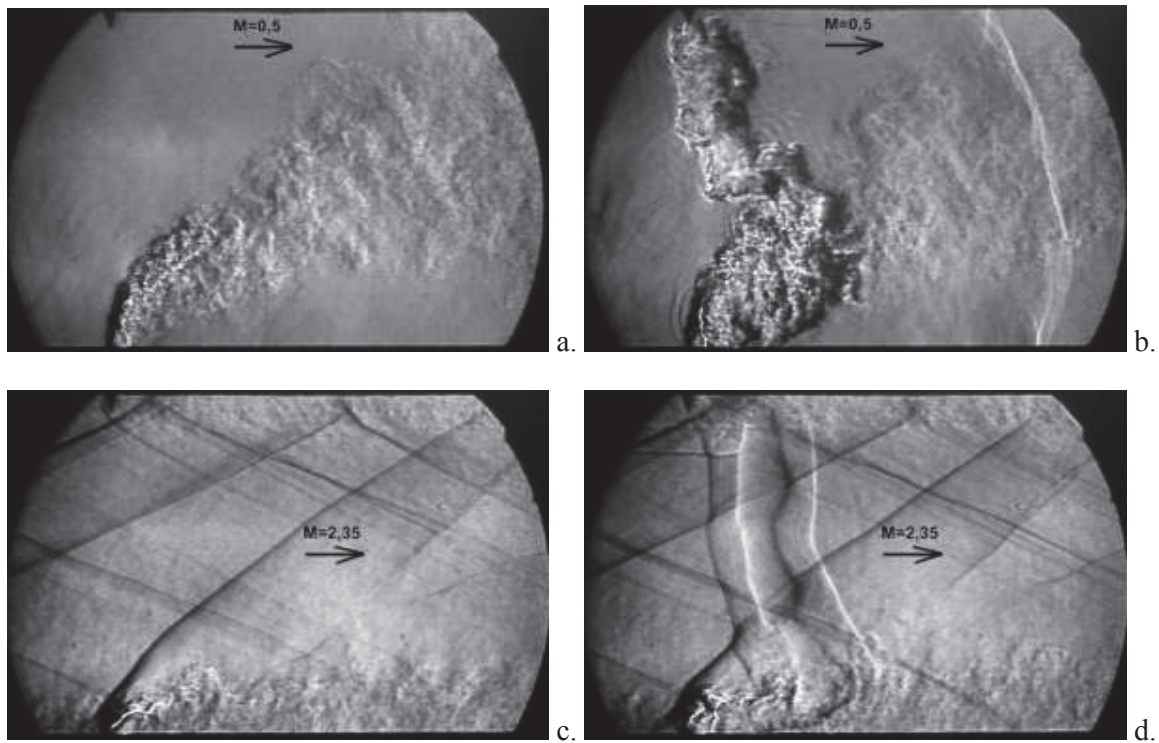


Fig.5.6.10. Schlieren images of the discharge in flow at C_2H_4 jet injection. a, b, – subsonic flow $M=0,5$ without discharge and with discharge, correspondingly; c, d – supersonic flow $M=2,35$ without discharge and with discharge, correspondingly.

Spectroscopic diagnostics. Scheme of spectroscopic observations is shown in Fig.5.6.11. Optical head collects radiation from narrow zone ($X*Y=5*5mm$), which locates downstream of the electrodes cross-section $X=X1$. Signal is transmitted to optical spectrograph (monochromator). Selected waveband is received by photo-amplifier (PMA) and recorded by oscilloscope. Result is the discharge's or the discharge tail's luminosity from predefined zone in specific wavelength (which can be corresponded with specific molecule). The following molecular bands were observed:

- Continuum - $\lambda=400nm$, discharge radiation in initial phase;
- CN - $\lambda=389nm$, fact of discharge-air-fuel interaction;
- CH - $\lambda=431nm$, roughly can be related to combustion;
- C2 - $\lambda=516nm$, typical for discharge luminosity in hydrocarbons.

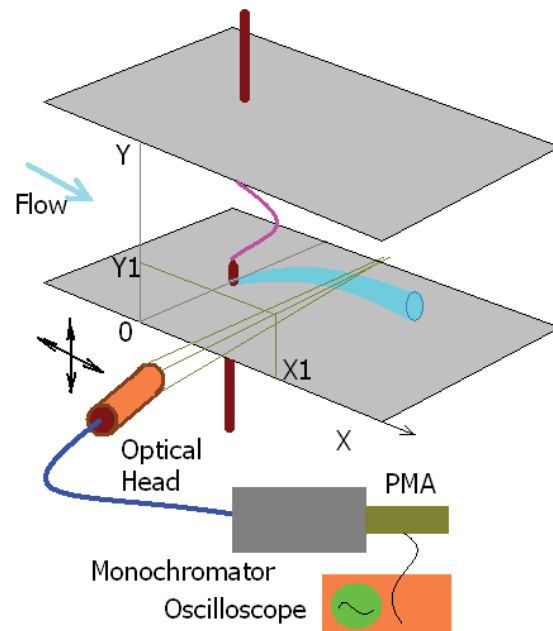


Fig.5.6.11. Scheme of spectroscopic observations.

Figures 5.6.12 and 5.6.13 present typical oscillograms of the post-discharge tail luminosity in $M=0.5$ flow without fuel injection and at injection, accordingly. In the first case an intensive CN radiation is absent and the wavelength $\lambda=389\text{nm}$ is related to continuous part of the spectra. Well seen that an excited zone moves with airflow downstream. Intensity of luminescence drops quickly with X distance; at $X=30$ no signal was recorded.

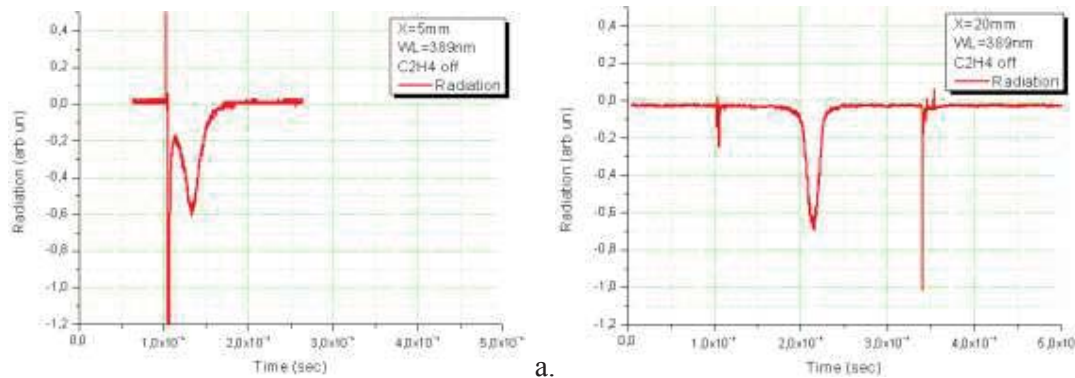


Fig.5.6.12. Behavior of continuum radiation of the discharge tail: a – $X=5\text{mm}$, b – $X=20\text{mm}$. No ethylene injection.

Under the C_2H_4 injection magnitude of signal on this wavelength increases in about 100 times, reflecting the CN band radiation. High-amplitude CN luminosity appears for the secondary pulse as well, i.e. the secondary discharge locates in C and N - containing media. At the same time the radiation in CH and C2 bands was not detected at $X=30\text{mm}$.

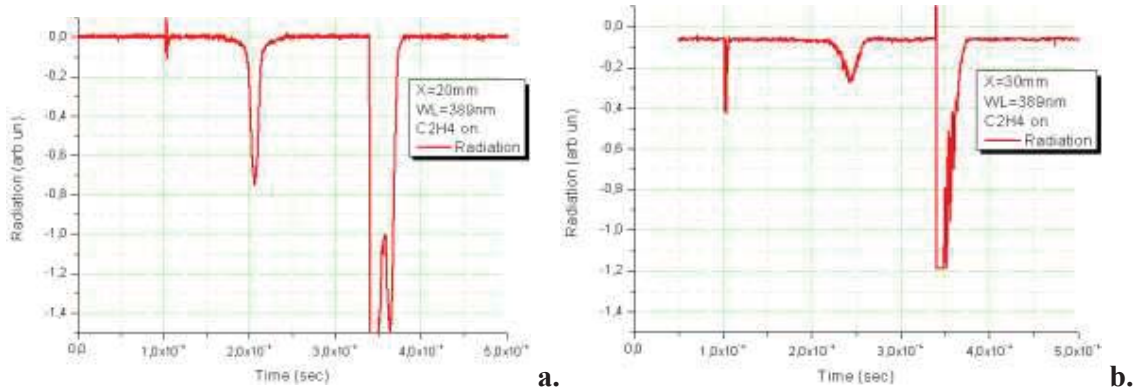


Fig.5.6.13. Behavior of CN band in discharge tail: a – X=20mm, b – X=30mm. Ethylene injection on. Sensitivity of PMA in Fig.13a is 100 times less than in Fig.5.6.12, approximately. Sensitivity of PMA in Fig.13b is approximately the same as in Fig.5.6.12.

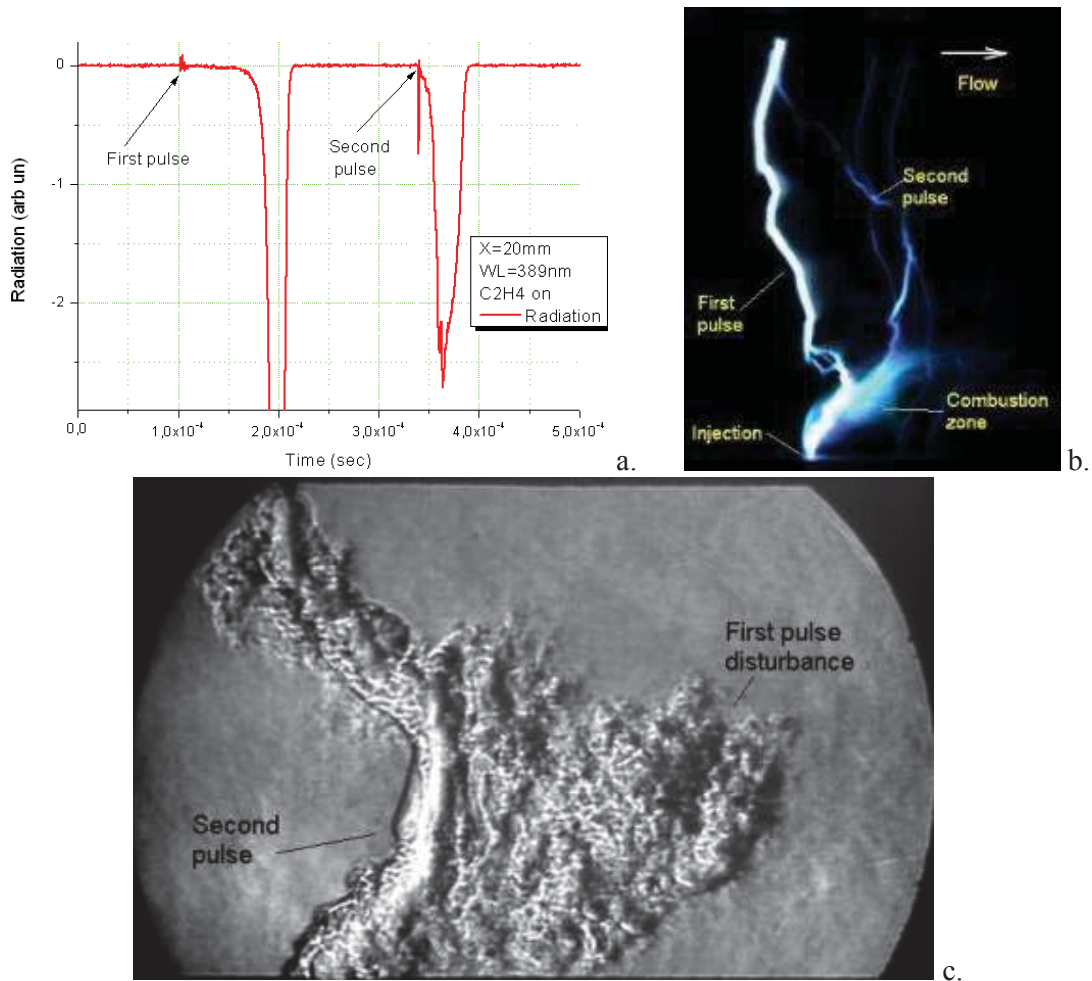


Fig.5.6.14. Two-pulse mode of the discharge excitation. (a) Discharge tail radiation in CN band. (b) Photo of the C₂H₄ ignition. (c) Typical schlieren image at delay time t=245μs.

Following conclusions/comments can be made based on experimental data obtained in this test series:

- Presence of intensive luminosity of CN band at direct fuel injection prove the previously made conclusion that the filamentary discharge strives for the location between two molecular gases, if the experimental arrangement allows it;
- The second pulse breakdown occurs not at the position of the first pulse and not right between electrodes but in some intermediate position – this fact was not emphasized before; Fig.5.6.14a shows typical oscillogram, which allows to make this comment; Fig.5.6.14c presents schlieren image at delay time $t=245\mu\text{s}$ after the first pulse, right after the second pulse;
- C_2H_4 ignition by filamentary discharge was detected in this test only in vicinity of the discharge root, probably, due to rather fast cooling of the post-discharge channel. This zone is well visible in photos, see example in Fig.5.6.14b. Zone of combustion moves downstream following the main flow, as it is shown in Fig.5.6.14c.

5.6.4. Experimental study of efficiency of plasma-based mixing by means of PBF in high-speed flow.

Efforts during this experimental series were aimed on estimation of the plasma-based mixing enhancement in high-speed flow by means of probe breakdown fluorescence method (PBF), see section 4.5 for details about PBF.

The first experimental series was made for the spark discharge at subsonic flow and $P_{st} = 450$ Torr, and the second series of experiments was made for the supersonic flow $M=2$, $P_{st} = 150$ Torr. The arrangement of the experiment is shown in Fig.5.6.15. It has been slightly changed comparing to the scheme considered in previous sections. Grounded electrode was posed a bit upstream the injection orifice in order to increase interaction of the afterspark channel and jet.

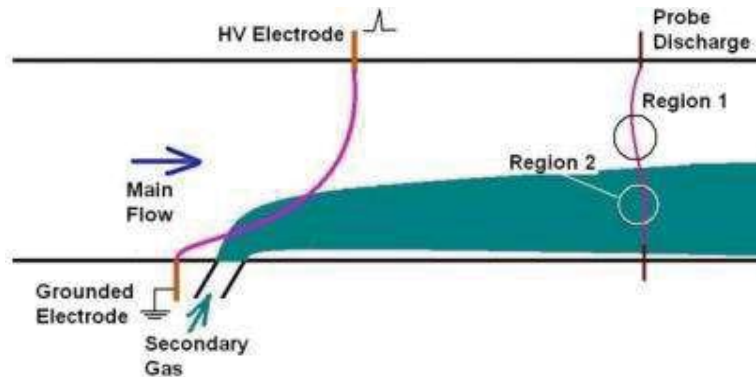


Fig.5.6.15. Experimental arrangement of the PBF measurements in high-speed flow.

The probe discharge was initiated downstream of the main one. Distance between top electrodes was 100 mm, and between bottom electrodes was 130 mm. The emission of the discharge was collected from different regions along the Y axis of the probe discharge between Region 1 and Region 2.

The first preliminary series of experiments was fulfilled to find the proper delay between the main discharge and the probe one for subsonic and supersonic flow. It has been found out that optimal delay for the subsonic flow is about $\Delta T = 800 \mu s$ and for the supersonic flow it is about $\Delta T = 200 \mu s$. Nevertheless, it should be noted that delay varies at variation of the measurement region due to the curvature of the main discharge.

The next series of experiments was dedicated to variation of the measurement region. It was found that boundary between CO_2 jet and air is unsteady. Fortunately, the width of boundary fluctuation zone was smaller than dimension of the region perturbed by the main discharge. As a result there have been found measurement regions somewhere in between

Region 1 and Region 2 on the Fig.5.6.15 for subsonic and supersonic flow. Experimental data for supersonic flow is presented on the Fig.5.6.16.

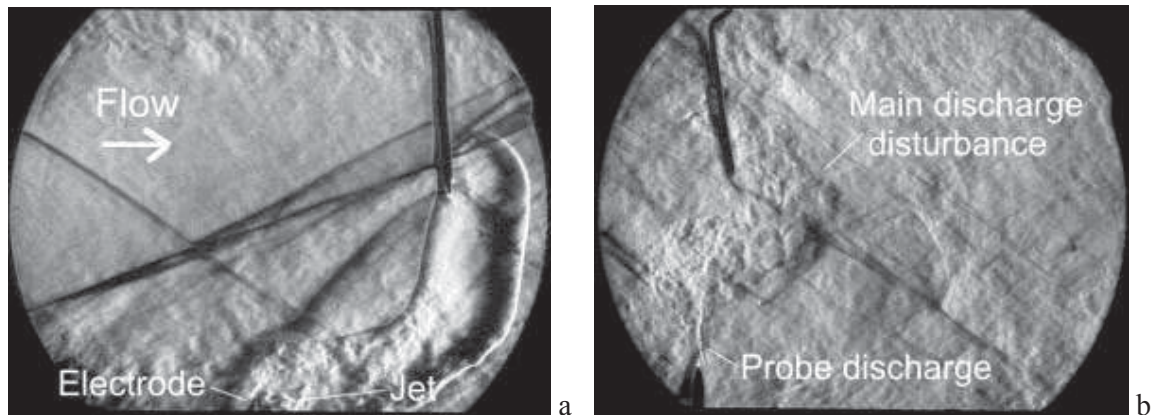
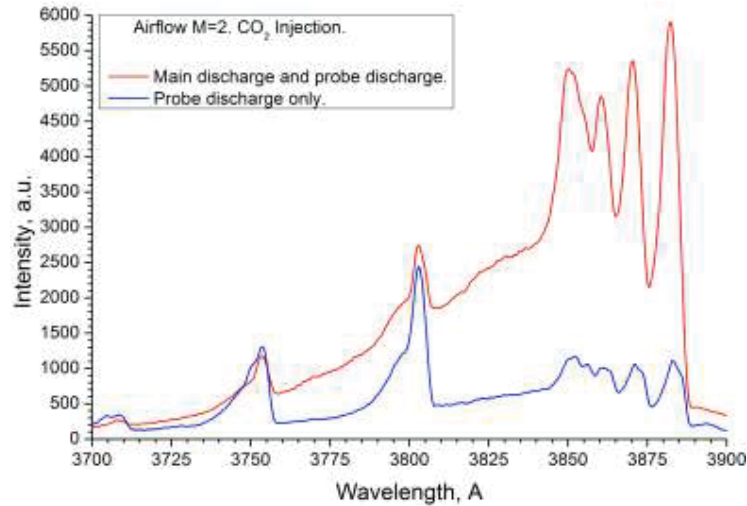


Fig.5.6.16. Spectra and schlieren photos for supersonic flow. Main discharge in the 2nd window (a) and probe discharge in the 3rd window of the test section (b). $R=0.45$.

It is seen the dramatic difference between spectrum of probe discharge for CO_2 jet (blue on the Fig.5.6.16) and spectrum of probe discharge for CO_2 jet perturbed by the main discharge. Arising of the strong CN bands and reducing of the N_2 bands mean that there is essential amount of CO_2 within the measurement region in the second case. At the same time CN bands are almost absent with strong N_2 bands are presenting in the spectrum when CO_2 jet does not perturbed by the main discharge in the first case. Mixing ratio may be estimated as $R=0.45$ according to calibration curve obtained due to the previous work, see section 4.6.

The same result has been obtained for the subsonic flow, see Fig.5.6.17. Energy release of the probe discharge was higher for the subsonic flow due to the higher static pressure. This cause to the spectra shape changes due to the higher temperature. Mixing ratio is about $R=0.4$ for spectra on the Fig.5.6.17.

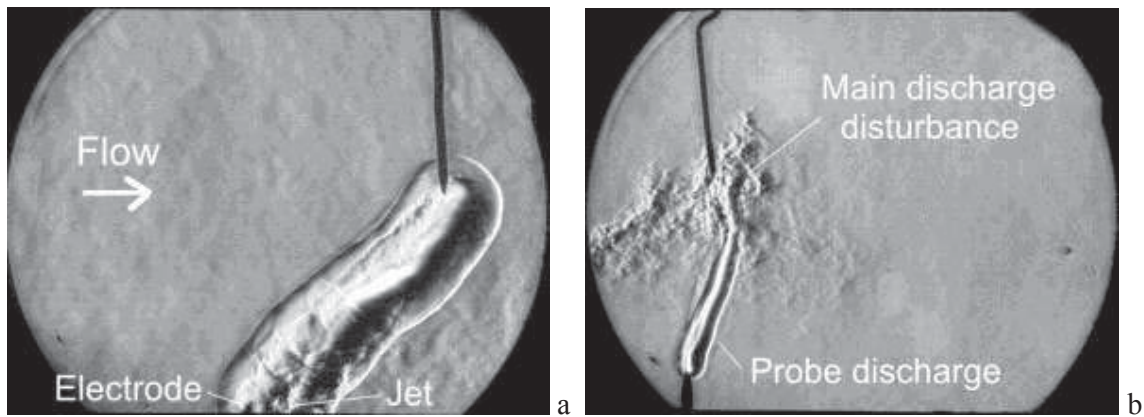
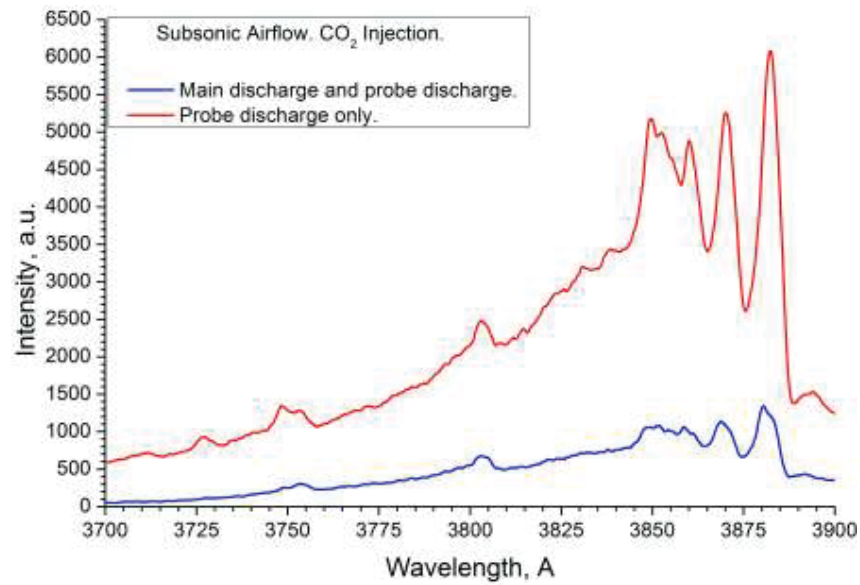


Fig.5.6.17. Spectra and schlieren photos for subsonic flow. Main discharge in the 2nd window (a) and probe discharge in the 3rd window of the test section (b). $R=0.4$.

There was some variation of the spectrum from run to run due to the unsteady jet boundary but in average the positive influence of the main discharge on the CO₂ jet mixing in airflow has been found to be evident.

5.6.5. Experimental runs with liquid hydrocarbons injection.

This experimental series was aimed at study the pulse discharge dynamic and localization in airflow at presence of spray jet of liquid hydrocarbons. The experiments were conducted in a short-duration blowdown wind tunnel PWT-50H with a closed test section $Y \times Z = 72 \times 72 \text{ mm}$ at Mach number of nozzle $M = 2.5$ and stagnation pressure $P_0 < 2.5 \text{ Bar}$. The scheme and technical parameters of experimental test bed PWT-50HL as well as power supply for discharge studied were described in section 5.1.

The experimental arrangement of the discharge generation inflow at presence of liquid spray jet is shown in Fig.5.6.18. Two schemes of discharge generation were tested. The main difference between them is the relative position of the spray jet and discharge. Duration of the injection was about 10ms. The moment of the discharge breakdown was adjusted during the preliminary test series. Synchronization of the discharge, spray injection and flow mode is visualized in Fig.5.6.19.

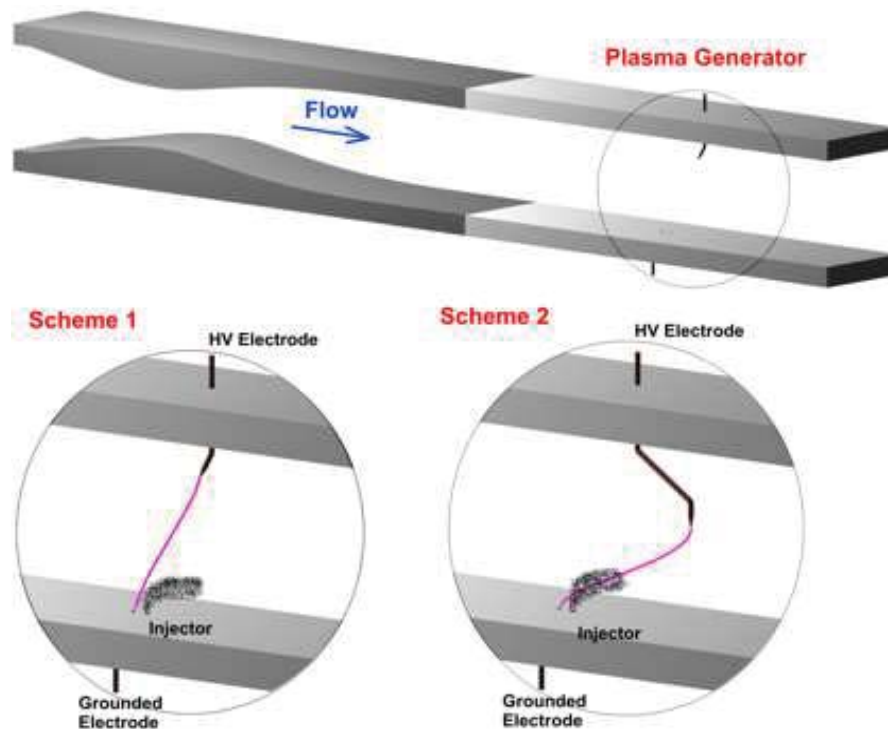


Fig.5.6.18. Experimental arrangement.

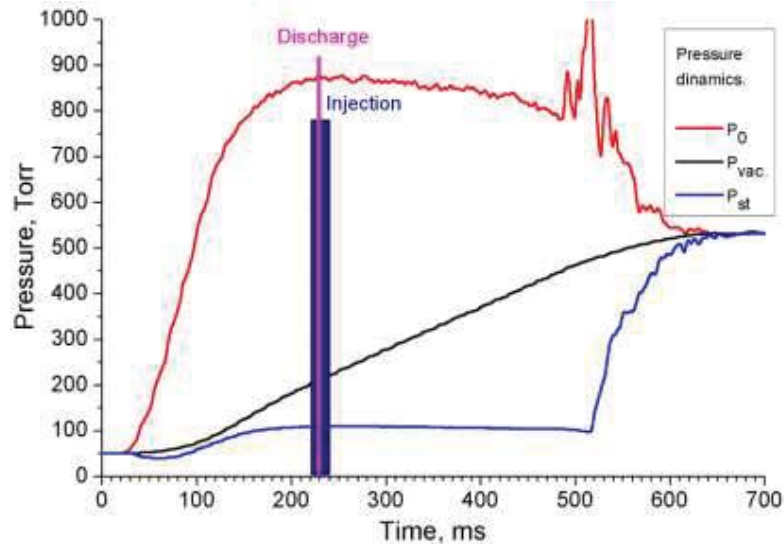


Fig.5.6.19. Pressure dynamics within the test section and experiment synchronization.

The schlieren photos of the discharge breakdown (scheme 1) in subsonic and supersonic flow at presence of spray jet are presented in Fig.5.6.20. It has been found out that discharge almost does not “feel” spray jet at such configuration both for subsonic and supersonic flow.

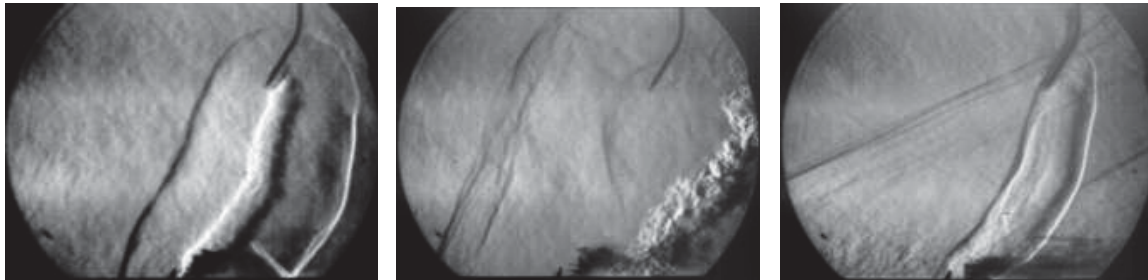


Fig.5.6.20. Schlieren photos of the discharge in flow at presence of spray jet; 1 – subsonic, schlieren delay 50 μ s; 2- subsonic, 150 μ s; 3 – supersonic, 20 μ s.

When the axis of the discharge gap is closer to the spray jet as for the scheme 2, than breakdown becomes to be sensitive to the spray injection. Schlieren photos of the pulse discharge breakdown in subsonic flow at presence of the spray jet and without jet are presented in Fig.5.6.21. It is seen that breakdown occurs in the same way for both cases.

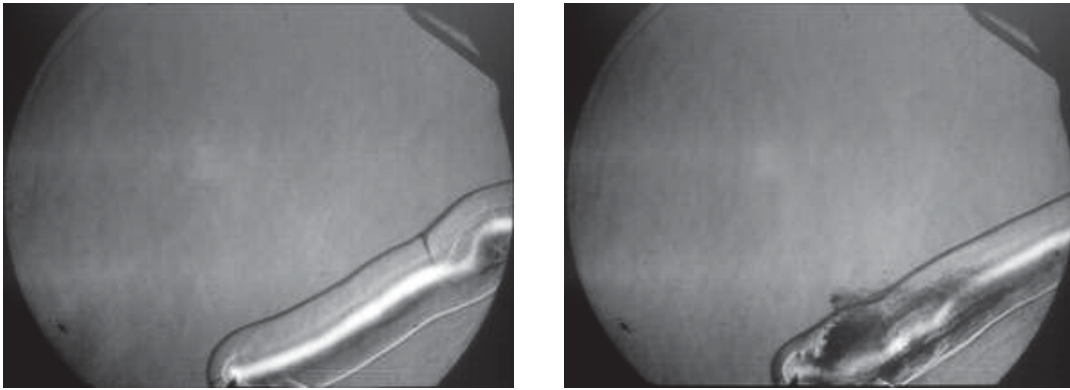


Fig.5.6.21. Schlieren photos of the discharge in subsonic flow for scheme 2. Left – without spray jet; right – with spray jet. Schlieren delay 50 μ s.

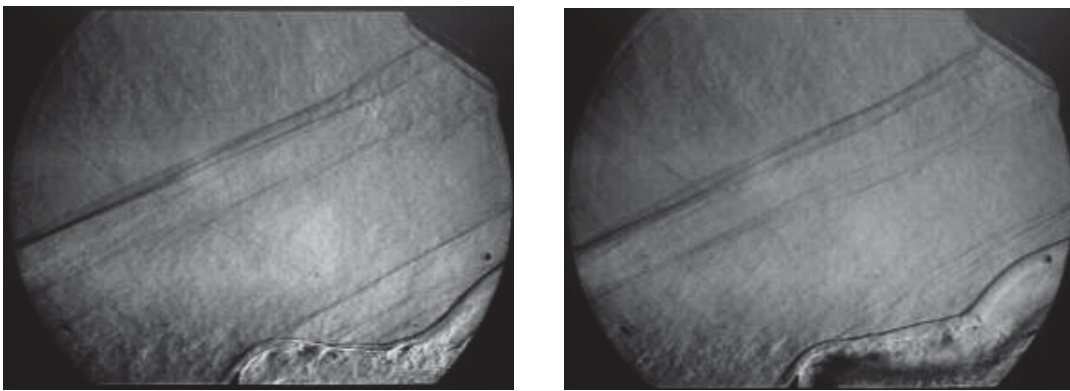


Fig.5.6.22. Schlieren photos of the discharge in supersonic flow for scheme 2. Left – without spray jet; right – with spray jet. Schlieren delay 50 μ s.

The same configuration in supersonic flow has demonstrated different behavior. Schlieren photos of the pulse discharge breakdown in supersonic flow at presence of the spray jet and without jet are presented in Fig.5.6.22. Breakdown path is different if there is a spray jet.

Spectroscopic study of the pulse discharge breakdown has been fulfilled for variety of conditions, see also section 4.6. Emission was collected from the whole discharge region. Spectra of the discharge for scheme 2 in supersonic flow are shown in Fig.5.6.23 for the C_3H_7OH spirit spray jet and without it. Presence of the intensive CN emission for the case of the spray jet proves that discharge region contains carbons, that means breakdown occurs inside the spray jet.

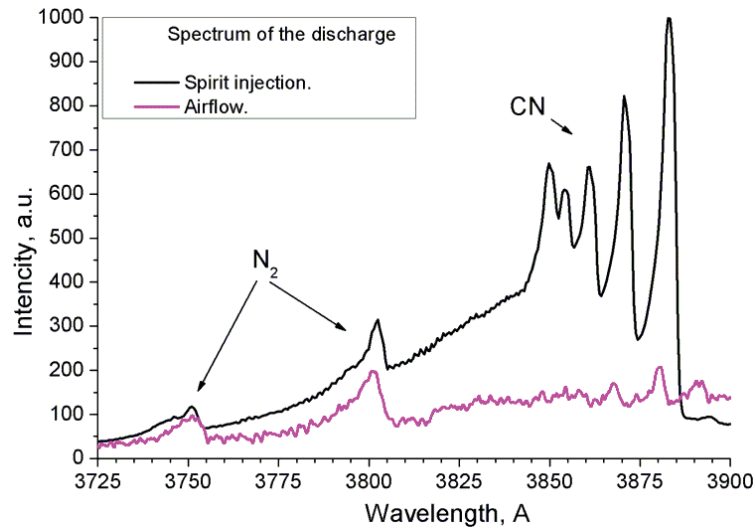


Fig.5.6.23. Pulse discharge spectrum. Magenta – discharge generation in airflow; black – discharge in airflow at presence of the fuel spray jet (propanol C_3H_7OH in this particular case).

References to the section 5.6:

1. “Study of Mechanisms of Filamentary Pulse Electric Discharge Interaction with Gaseous Flow of Nonuniform Composition”, Project ISTC #3793p, The First Year Report, October 2008.
2. “Study of Mechanisms of Filamentary Pulse Electric Discharge Interaction with Gaseous Flow of Nonuniform Composition”, Project ISTC #3793p, The 2nd Year Technical Report, October 2009.
3. *Sergey B. Leonov, Yury I. Isaenkov, Alexander Firsov*, “Mixing Intensification in High-Speed Flow by Unstable Pulse Discharge, 40th AIAA PDL Conference, San-Antonio, June 22-25, 2009, Paper AIAA-2009-4074
4. *Sergey B. Leonov, Yury I. Isaenkov, Dmitry A. Yarantsev, Igor V. Kochetov, Anatoly P. Napartovich, Michail N. Shneider* “Unstable Pulse Discharge in Mixing Layer of Gaseous Reactants”, 47th AIAA Aerospace Sciences Meeting and Exhibit (Orlando, FL, USA, 5-8 January 2009), AIAA-2009-0820.

6. Conclusions.

An effective mixing, flameholding and complete combustion of fuel and oxidizer mixture in the combustor at compressible conditions are important problems of high-speed propulsion. The problems are essential due to short residence time of gas mixture in the combustor of limited length. To solve those problems the extra method is required to keep mixing efficiency high enough with a minimum total pressure loss. The project ISTC#3793p is aimed at study the pulse filamentary discharge effect on mixing processes at ambient conditions and in high-speed flow.

The pulse-periodic filamentary electrical discharge of submicrosecond duration may be effective low-power method of the mixing intensification and, probably, of the combustion enhancement. From the other hand, properties of such a discharge at compressible flow were needed to be studied additionally for better understanding of basic features and dynamics of turbulent gas motion appeared during after-discharge phase.

In this way, the project objective was *to study the properties of filamentary transversal pulse-repetitive discharge and mechanisms of plasma-gas interaction under non-premixed conditions in high-speed flow.*

Effect of the fast turbulent expansion of the post discharge channel within the high speed flow was observed experimentally and it was described in details. The results obtained in this work show that the effect of strong instability can be efficient for improvement of the mixing in multicomponent flows. Plasma influence on the flow parameters is occurred to be local and it doesn't result in sufficient total pressure loss. It was demonstrated also that the filamentary discharge trail is localized along the boundary of two different gases at favorable conditions. If the discharge gap is longer than distance to the previously disturbed zone than the next breakdown occurs along the nearest boundary of thermal cavity generated by the previous discharge, when pulse repetitive discharge operates within the high speed flow. At such mode the generation of sequential pulses at some optimal repetition rate causes the flow disturbance that is spatially looks to be uniform over the flow.

Reasons and consequence of gasdynamic instability arisen after the electrical discharge in surrounding airflow were analyzed based on experimental, analytical and computational data. The turbulent gas motion develops in a cooling post discharge channel, replacing molecular heat conduction as the dominant mechanism of the heat transfer. The rates of cooling and expansion of the channel increase dramatically. Turbulence starts as a result of the Raleigh-

Taylor instability in the region of large density gradient at the channel boundary. Initially a typical turbulence scale is much smaller than the channel radius. Based on measurements and observations a few types of instabilities, regularly appeared in the system, were described, including the jet type of gas motion that considered for such a configuration at the first time. The physical model of lateral jets generation after the discharge breakdown was formulated and verified.

The experimental data were obtained and proved by means of wide set of diagnostic methods. All main parameters of plasma and of the thermal cavity were measured with high spatial and temporal resolution. The dynamics of gasdynamic processes was visualized by image acquisition and schlieren systems. The method of Probe Breakdown Fluorescence (PBF) were developed and applied for the mixing efficiency quantitative and qualitative estimation. Authors can't find any evidence of PBF use for mixing diagnostic in scientific publications worldwide.

It might be concluded that the formal objective of the project were reached; expected results were obtained and considered in this Technical Report, namely:

1. Data on the pulse discharge dynamics in ambient gas and in flow.
2. Result of theoretical analysis of physical mechanisms of the discharge channel the fast expansion. Description of physical models of turbulent motion of the gas affected by the discharge in non-homogeneous media.
3. Experimental data on the mixing intensification in two-component medium by the pulse-repetitive discharge.
4. Experimental data on the submicrosecond filamentary discharge dynamic in mixing layer of gas1-gas2 and spray-gas systems at static conditions and in high-speed flow.
5. Description of kinetic and dynamic physical models of the discharge specific localization in vicinity of two gases and spray-gas boundary.
6. Physical demonstration of effectiveness of the two-pulse scheme for ignition of non-premixed air-fuel composition.
7. Quantitative experimental data on the mixing efficiency due to unstable submicrosecond discharge excitation in vicinity of the boundary between two gases, obtained by non-intrusive diagnostics.

It should be considered that as a whole the tasks of the project were fulfilled. The most of physical results were reported, and published [1-8] due to the project's efforts. Among of them:

- experimental data on the unstable filamentary plasma dynamics in static gas and in high-speed flow;
- analytical and computational models of the gasdynamic instability due to pulse discharge generation were described in details;
- development of the spectroscopic diagnostic of mixing based on probe discharge excitation (Probe Breakdown Fluorescence = PBF);
- dynamics of the discharge in two-components and two-phase flow were studied in single-pulse and multi-pulse modes at variety of conditions;
- the concept of plasma-based mixing actuation was developed for the pulse-periodic filamentary discharge with a high energy density release; etc.

Additionally to the formal tasks of the project several new physical effects were observed and described in publications. Among of them are following: the effect of filamentary discharge localization in the mixing layer between two different gases was considered for the first time; the jet type of gas instability were observed experimentally and highlighted with the detail explanation of physical model of the phenomena; the two-pulse mode was proposed as more effective than a single pulse in terms of mixing and ignition; new physical ideas were formulated to explain the effects observed. Extra the experimental data were obtained on the discharge interaction with a heated air mini-jet to verify the mechanism of a HV discharge guiding by a femtosecond laser, studied in collaboration with Princeton University [7]. The analytical model of jet-type instability development was successfully proved experimentally and by 3D Navier Stokes CFD.

In terms of optimization of the plasma-based mixing technique, authors may recommend the following scheme of further improvement, making them more feasible for practical purposes. Several issues are of the key importance: high level of the energy density to excite the gas-dynamic disturbances; the effect of specific localization of the discharge for some pairs of gases or active guiding of the discharge breakdown pass; multi-pulse or pulse-repetitive mode of the discharge operation; proper geometrical organization of the electrode system. Current understanding is that the system of mixing actuation could be arranged in conjunction with the plasma-based ignition method and active flameholder, or to be the part of them. One more attractive result is the geometrical optimization of the plasma-based mixing actuator. A sample of “square” mixing actuator is shown in Fig.6.1.

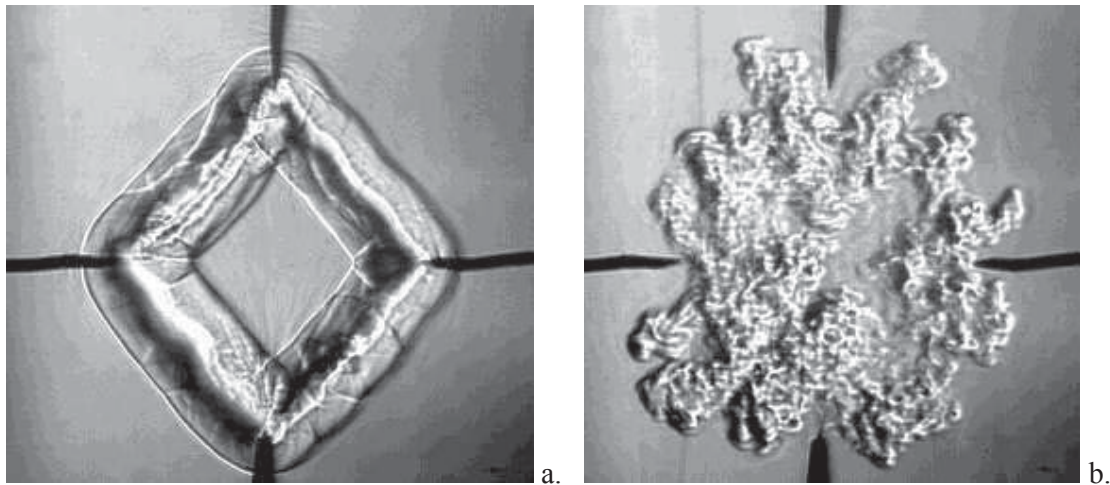


Fig.6.1. Schlieren images of HV mixing actuator. a – delay time $30\mu\text{s}$; b – delay time 2ms.

Authors are deeply grateful the organizations that have supported this work, including AFRL, EOARD, ISTC, JIHT RAS and Princeton University, and individuals personally interfere with this Project, especially Dr. Julian Tishkoff, Dr. Chiping Li, Dr. Campbell Carter, Prof. Richard Miles.

References for Conclusions:

1. “Control of Flow Structure and Ignition of Hydrocarbon Fuel in Cavity and behind Wallstep of Supersonic Duct by Filamentary DC Discharge”, Ed. S. Leonov, Project ISTC-EOARD-IVTAN #3793p, The Annual and Quarterly Technical Reports, 2007-2012.
2. S. B. Leonov, Y. I. Isaenkov, A. A. Firsov, S. L. Nothnagel, S. F. Gimelshein, and M. N. Shneider, “Jet Regime of the Afterspark Channel Decay”, *PHYSICS OF PLASMAS* **17**, 1, 2010
3. Sergey B. Leonov “Visualization of Unsteady electrical discharges in high-speed flow”, *Journal “International Review of Aerospace Engineering”*, International Review on Aerospace Science and Engineering by PRAISE, v.3, #4, August 2010, pp214-222.
4. A. Firsov, Yu. Isaenkov, S. Leonov, M. Shurupov, D. Yarantsev, “Pulse Filamentary Discharge in Mixing Layer of Reacting Gases”, *Proceedings of 18th International Conference on Gas Discharges and Their Applications*, Germany, Greifswald, 05 – 11 September 2010
5. A. A. Firsov, Yu. I. Isaenkov, I.V. Kochetov, S. B. Leonov, A.P. Napartovich, M.N. Shneider, M.A. Shurupov, D. A. Yarantsev, “Mixing Intensification by Electrical Discharge”, AFOSR Program Review “Fundamental Mechanisms, Predictive Modeling, and Novel Aerospace Applications of Plasma-Assisted Combustion”, November 9-10, 2011, OSU, Columbus, OH
6. Sergey B. Leonov, Plasma – Based Control of High-Speed Flow, Invited Lecture, *Proceedings of von Karman Institute, Fluid Dynamics Lecture Series*, Brussels, 21-24 February 2011
7. S. B. Leonov, A. A. Firsov, M. A. Shurupov, J. B. Michael, M. N. Shneider, R. B. Miles, and N. A. Popov “Femtosecond laser guiding of a high-voltage discharge and the restoration of dielectric strength in air and nitrogen”, *Physics of Plasmas*, vol.19, 123502, 2012
8. A. A. Firsov, M. A. Shurupov, D. A. Yarantsev, and S. B. Leonov “Mixing Actuation by Unstable Filamentary Discharge”, Paper AIAA-2013-1188

Attachment 1: List of published papers with abstracts

1.	<i>Yu. I. Isaenkov, S. B. Leonov, M. N. Shneider</i> “Mixing Intensification by Electrical Discharge in High-Speed Flow” Proceeding of the Fifth International Conference on Fluid Mechanics, Aug.15-19, 2007, PaperF28; Shanghai, China; Tsinghua University Press & Springer
The paper considers the results of experimental and analytic efforts on the filamentary transversal pulse discharge application for mixing intensification in high-speed gas flow. Two methods are demonstrated experimentally: active mixing by filamentary discharge in transversal magnetic field, and mixing due to development of huge instability with consequent fast turbulent expansion in after-discharge channel. The mechanism of the phenomena was described theoretically for quiescent ambient conditions. It is supposed that effect of fast turbulent expansion is effective for an acceleration of mixing in the non-premixed reactant multi-component flow.	
2.	<i>Sergey B. Leonov, Yuri I. Isaenkov, Mikhail N. Shneider</i> "Suppression of the turbulent decay of an afterspark channel with residual current", PHYSICS OF PLASMAS 14, 123504_2007.
The paper presents the results of an experimental study of the pulse discharge in air at atmospheric pressure and the post discharge channel decay. It is shown that a relatively small residual current suppresses the development of gasdynamic instability and stabilizes the channel. The results of experiments are compared with predictions of our theoretical model that was developed earlier.	
3.	<i>Sergey B. Leonov</i> “High-Speed Flow Control by Electro-Discharge Plasma Technique”, Invited paper, Proceedings of 2 nd International Conference “Recent Advances in Experimental Fluid Mechanics”, 3-6 March 2008, K.L.College of Engineering, Vijayawada, India
The paper presents a short review of world-wide efforts in a field of plasma-assisted aerodynamics and plasma-induced combustion, as well as the results of experimental work in this field obtained in the Laboratory of Experimental Plasma Aerodynamics JIHT RAS last years. The inflow mixing intensification is one of the key problems of high-speed combustion. Possible mechanisms of plasma/MHD-induced mixing are discussed. The experimental results on filamentary pulse discharge effect on flow in magnetic field and without it are demonstrated in different aerodynamic situations. The peculiarities of the filamentary discharge appearance in high temperature and high-speed flow explored experimentally are discussed in details.	
4.	<i>Sergey B. Leonov, Dmitry A. Yarantsev</i> , Instability in Post-Discharge Thermal Cavity, IEEE Transactions, Plasma Science. June 2008, DOI 10.1109/TPS.2008.922479
The pulse filamentary electrical discharge in atmospheric air heats the gas that leads to generation of post-discharge expanding thermal cavity. The dynamics of its unstable swelling is a subject of this paper.	
5.	<i>Sergey B. Leonov, Dmitry A. Yarantsev, Campbell Carter</i> Transversal Electrical Discharge as a New Type of Flameholder, 15 th AIAA International Spaceplanes and Hypersonic Systems and Technology Conference, Dayton, OH, Apr-May 2008, AIAA-2008-2675.
The paper describes experimental results on gaseous fuel ignition and flameholding controlled by an electrical discharge in high-speed airflow. The geometrical configuration does not include any mechanical or physical flameholder. The fuel is non-premixed and injected directly into the air crossflow from the combustor wall. A multi-electrode, nonuniform transversal electrical discharge is excited on the same wall, between flush-mounted electrodes, upward the fuel injector. Initial gas temperature is much lower than the value for autoignition of hydrogen and ethylene. Results are presented for wide range of fuel mass flow-rate and discharge power deposited into the flow. This coupling between the discharge and the flow presents a new type of flameholder over a plane wall for high-speed combustor.	
6.	<i>Яранцев Д. А., Леонов С. Б., Фирсов А. А.</i> Особенности применения диагностик в экспериментах по взаимодействию электрического разряда со сверхзвуковым

	потоком. Proceedings of 3 rd School-Workshop on MagnetoPlasma Aerodynamics, JIHT RAS, Moscow, April, 2008
	Поведение электрического разряда в скоростном (до $M=2$) потоке воздуха сильно зависит от конкретной аэродинамической конфигурации тестовой секции (плоская стенка, обратная ступенька, каверна). Как правило, разряд является неоднородным по структуре и нестационарным как по положению в пространстве, так и по основным параметрам плазмы. Диагностика разряда и его воздействия на поток в таких условиях предъявляет ряд специфических требований к средствам измерения. Длительность измерений не должна превышать характерного газодинамического времени (≈ 10 мкс). Пространственное разрешение измерений должно быть не хуже 1 мм. В качестве примера реализации приведены результаты измерения скорости газа в зоне горения топлива за разрядной областью.
7.	<i>Sergey B. Leonov, Yury I. Isaenkov, Dmitry A. Yarantsev, Igor V. Kochetov, Anatoly P. Napartovich, Michail N. Shneider</i> “Unstable Pulse Discharge in Mixing Layer of Gaseous Reactants”, 47th AIAA Aerospace Sciences Meeting and Exhibit (Orlando, FL, USA, 5-8 January 2009), AIAA-2009-0820.
	The paper describes results of experimental and computational efforts on the filamentary transversal pulse discharge dynamics in ambient conditions, different gases (mixtures), and high-speed airflow. The effect of fast turbulent expansion of the post-discharge channel is studied experimentally in order to enhance mixing processes of fuel and oxidizer and reduce the time of ignition. The idea of extra benefit possessed with nonequilibrium, unsteady, and non-homogeneous discharge is verified numerically.
8.	<i>M.N. Shneider, S.B. Leonov, Y.I. Isaenkov, S.F. Gimelshein, N.E. Gimelshein</i> , JET REGIME OF THE AFTERSPARK CHANNEL DECAY, 47th AIAA Aerospace Sciences Meeting and Exhibit, Orlando, FL, USA, 5-8 January 2009, AIAA-2009-691.
	The paper presents the results of an experimental study of the pulse discharge in air at atmospheric pressure and the post discharge channel decay. It is shown that a relatively small residual current suppresses the development of gasdynamic instability and stabilizes the channel. The results of experiments are compared with predictions of our theoretical model that was developed earlier.
9.	<i>A. P. Napartovich, I. V. Kochetov, S. B. Leonov</i> Modeling of premixed ethylene-air flow ignition by non-uniform non-thermal plasma, The 8th International Workshop on Magneto-Plasma Aerodynamics, Moscow, Russia, March 31 — April 2, 2009
	The paper presents a short review of world-wide efforts in a field of plasma-assisted aerodynamics and plasma-induced combustion, as well as the results of experimental work in this field obtained in the Laboratory of Experimental Plasma Aerodynamics JIHT RAS last years. The inflow mixing intensification is one of the key problems of high-speed combustion. Possible mechanisms of plasma/MHD-induced mixing are discussed. The experimental results on filamentary pulse discharge effect on flow in magnetic field and without it are demonstrated in different aerodynamic situations. The peculiarities of the filamentary discharge appearance in high temperature and high-speed flow explored experimentally are discussed in details.
10.	<i>S. B. Leonov, Yu. I. Isaenkov, D. A. Yarantsev, A. P. Napartovich, I. V. Kochetov</i> “Mixing and Ignition in High-Speed Flow by Long-Spark Electrical Discharge”, The 8th International Workshop on Magneto-Plasma Aerodynamics, Moscow, Russia, March 31 — April 2, 2009
	A subject of consideration is the dynamic of filamentary pulse discharge generated along contact zone of two co-flow gases. Experimental facility consists of blow-down wind tunnel PWT-50, system of the high-voltage pulse-repetitive feeding, and diagnostic equipment (schlieren device; pressure, voltage, current, radiation sensors; spectroscopic system; etc.) Typical parameters: $p=0.2-1$ Bar, velocity $M=0-2$, pulse duration $t=0.1-1$ us, power release $W=20-100$ MW. Предметом рассмотрения является динамика расширения тепловой каверны, образующейся после филаментарного искрового разряда. Экспериментально показано, что развитие газодинамической неустойчивости границы каверны может приводить к возникновению струйных течений в плоскости, перпендикулярной разрядному каналу. В статье обсуждается результат параметрического исследования развития неустойчивости в неподвижном газе и во внешнем высокоскоростном потоке. Предполагается, что разряд подобного типа может применяться для эффективного смешения компонент в камерах сгорания, в т.ч., ГПВРД.

11.	<i>Sergey B. Leonov, Yury I. Isaenkov, Alexander Firsov</i> , “Mixing Intensification in High-Speed Flow by Unstable Pulse Discharge, 40th AIAA PDL Conference, San-Antonio, June 22-25, 2009, Paper AIAA-2009-4074
The effect of fast development of the post-discharge channel instability at stagnant conditions and in high-speed flow was observed experimentally. This instability possesses form of lateral jets escaping. The mechanism of acceleration of post-discharge channel turbulent expansion was described earlier for ambient conditions. But the experiment has shown a wider zone of disturbance and a higher speed of spreading out. The second discussed idea is the filamentary discharge movement in medium at gradient concentration of different components. The discharge position and dynamics of mixing layer depend on the discharge parameters and physical properties of gases involved. It is considered that the result of interaction can be controlled by means of small additives in the gas. The effects found are supposed to be applied for high-speed combustion enhancement due to non-equilibrium excitation of air/fuel composition and mixing acceleration of non-premixed multi-components flow. The problem of plasma-assisted mixing was discussed earlier, particularly in frames of MHD approach.	
12.	<i>Sergey B. Leonov, Alexander A. Firsov, Yury I. Isaenkov, Michail N. Shneider, Dmitry A. Yarantsev</i> , "High-Power Filamentary Pulse Discharge in Supersonic Flow", 48th AIAA Aerospace Sciences Meeting and Exhibit (Orlando, FL, USA, 4-7 January 2010), AIAA-2010-0259
The paper considers the results of experimental and computational efforts on study of the filamentary transversal pulse discharge dynamics in high-speed airflow. The effect of fast turbulent expansion of the post-discharge channel is studied experimentally in order to enhance mixing processes of fuel and oxidizer and reduce the time of ignition. It is shown experimentally that the pulse-repetitive discharge disturbs the flown gas significantly if the time period between individual pulses is about d/V , where d = inter-electrode gap, V = flow velocity. The phenomenon of the discharge localization near boundary of two gases is demonstrated experimentally; the physical mechanism is discussed. Experimental results presented in this work demonstrate that turbulent and directed motion arising in the after-spark channel can essentially enhance the rate of fuel-gas mixing, which may control the mixing rate in engines with high-speed gas flow.	
13.	<i>D. Yarantsev, Yu. Isaenkov, S. Leonov, M. Shurupov</i> , “Localization of the Pulse Discharge in Two-Gases Flow” The 9th International Workshop on Magneto-Plasma Aerodynamics, Moscow, Russia, April 13-15, 2010
The idea discussed is the mechanism of the discharge localization in a mixing layer of two gases. The effects found are supposed to be used for high-speed combustion enhancement owing to nonequilibrium excitation of air/fuel composition and mixing acceleration of nonpremixed multicomponents flow.	
14.	<i>A. P. Napartovich, I. V. Kochetov, S. B. Leonov</i> “Modeling of premixed ethylene-air flow ignition by non-uniform non-thermal plasma”, Journal of Thermophysics, №1, 2010
The detailed modeling of a system of agitated streams is a very complicated task, taking into account necessity to describe correctly combustion chemistry. To evaluate ignition efficiency in conditions of non-uniform excitation, a model of distributed mixing for finite time was formulated, the numerical code was modified, and numerical simulations were performed for ignition of supersonic ethylene-dry air mixture by the system of transverse discharges. Calculations were made for the stoichiometric composition of the premixed mixture at the static pressure 1 bar and gas temperature 700 K Развита теоретическая модель воспламенения предварительно перемешанной смеси воздуха с этиленом, инициированного стримерным разрядом в сверхзвуковом потоке. Анализируется система, включающая в себя микро-стримерный разряд с последующим смешением возбужденных и невозбужденных областей. Численно продемонстрировано, что использование неоднородного разряда с последующим смешением возбужденной и невозбужденной областей потока смеси этилена с воздухом может резко уменьшить вкладываемую в разряде энергию в расчёте на полный поток, минимально необходимую для инициирования горения.	
15.	<i>M. A. Deminsky, I. V. Kochetov, A. P. Napartovich, S. B. Leonov</i> “Numerical Study of Stages of Ignition of Ethylene-Air Mixture by Plasma Initiation”, The 9th International Workshop on Magneto-Plasma Aerodynamics, Moscow, Russia, April

	13-15, 2010
	It was numerically demonstrated that usage of the non-uniform discharge with following mixing of excited and unexcited gas portions can reduce essentially the threshold energy input required for combustion initiation of premixed fuel – oxidizer flow. The predicted induction time for combustion of ethylene-air mixture depends on the energy input per mass of gas flow in the case of filamentary discharge for two values of mixing time. At $\Delta t_{mix}=100$ and $\Delta t_{ind}=500 \mu s$ the required reduced energy input is about 40 J/g, that is remarkably lower than for uniform discharge.
16.	<i>S. B. Leonov, Y. I. Isaenkov, A. A. Firsov, S. L. Nothnagel, S. F. Gimelshein, and M. N. Shneider</i> , “Jet Regime of the Afterspark Channel Decay”, PHYSICS OF PLASMAS 17 , 1, 2010
	Experimental and computational analyses of jet formation at the boundary of a decaying pulse discharge in an ambient quiescent air at 1 atm are presented. High velocity jets are observed attributed to the channel curvature set during the initial breakdown phase. The general convex-to-concave jet direction is explained, and the mechanisms of jets formation are discussed.
17.	<i>С.Б. Леонов, А.А. Фирсов, М.А. Шурупов, Д.А. Яранцев</i> “Субмикросекундный высоковольтный разряд в неоднородной газовой среде “, The 9th International Workshop on Magneto-Plasma Aerodynamics, Moscow, Russia, April 13-15, 2010
	Была проведена серия экспериментов при различных конфигурациях электродов. При расположении электродов внутри струи CO ₂ , разряд распространяется внутри струи, т.е. не наблюдается выход разряда на границу струя-газ. В данной конфигурации наблюдаются характерные для CO ₂ напряжения пробоя и динамика расширения канала (более интенсивное расширение в нижней части), известные из экспериментов в неподвижном газе. При выводе одного электрода на границу струи, разряд распространяется по границе струя-газ примерно две трети расстояния, потом замыкается уже внутри струи на электрод. При выводе обоих электродов на границу струи, разряд проходит четко по границе струя-газ, при этом пробойный канал становится прямым, в отличие от той же конфигурации, но без струи.
18.	<i>Sergey B. Leonov, Alexander A. Firsov, Yuri I. Isaenkov, Michail A. Shurupov, Dmitry A. Yarantsev, Michail N. Shneider</i> “Long-Spark Discharge In Mixing Layer Of Two Molecular Co-Flown Gases”, ICOPS Proceedings, Norfolk, VA, June 2010
	There was found experimentally that in two-phase flow the filamentary discharge strives for the location between two molecular gases, if the experimental arrangement allows it. The physical mechanism can be considered as the following. The first stage of the spark breakdown is the multiple streamers propagation from the “hot” electrode toward the grounded one. In case of high-power electrical source those streamers occupy a huge volume of the gas, covering all possible paths for the further development. The next phase consists of the real selection of the discharge path among the multiple channels with non-zero conductivity. It is the key point – which channel appears to be the best in terms of the current increase, i.e. possessing higher conductivity and lower inductivity. In non-uniform media the favorite path may not be the shortest one. The second effect appears in fast turbulent expansion of the post-discharge. The mechanism of phenomena is in development of fast gas cumulative jets escaping from the disturbed zone after strong shock wave passage. For the effect realization the shock wave must be curved due to initial multiple bends of the discharge channel. In the paper the experimental data are supported by theoretical and computational analyses.
19.	<i>Sergey B. Leonov, Alexander A. Firsov, Yuri I. Isaenkov, Michail A. Shurupov, Dmitry A. Yarantsev</i> “Pulse Filamentary Discharge In Mixing Layer Of Reacting Gases”, Proceedings of 18 th International Conference on Gas Discharges and Their Applications, Germany, Greifswald, 05 – 11 September 2010
	A subject of this work is the dynamics of long filamentary pulse discharge generated along the contact zone of two co-flown gases. Two main ideas are discussed: the mechanism of lateral jets generation after the discharge run and the mechanism of the discharge localization in a mixing layer of two gases. The effects found are supposed to be used for high-speed combustion enhancement owing to nonequilibrium excitation of air/fuel composition and mixing acceleration of nonpremixed multicomponents flow. Experimental results presented in this work demonstrate that turbulent and directed motion arising in the after-spark channel can essentially enhance the rate of fuel-gas mixing, which may control the mixing rate in engines with high-speed combustor.

20.	<i>Leonov S.; Yu. Isaenkov; A. Firsov; M. Shurupov; D. Yarantsev</i> , “Plasma-Based Fast Mixing and Ignition in Supersonic Combustor”, 17th AIAA International Space Planes and Hypersonic Systems and Technologies Conference, <i>Paper AIAA-2011-2327</i>
The effective mixing of fuel and oxidizer in the combustor at high-speed flow is a well-known problem. It is difficult to be solved due to very short residence time of supersonic flow in the combustor of limited length. The plasma method potentially is able to enhance mixing efficiency with minimum total pressure losses. The effect of fast turbulent expansion of the post-discharge channel in high-speed flow was experimentally observed and described in details. Now such an effect is supposed to be applicable for the mixing acceleration of non-premixed multi-component flow. The plasma influence occurs in a gas portion and a negligible, in average, energy release does not lead to any remarkable change of the flow bulk parameters in duct and therefore to the thermal choking.	
21.	<i>Sergey B. Leonov</i> , Plasma – Based Control of High-Speed Flow, Invited Lecture, Proceedings of von Karman Institute, Fluid Dynamics Lecture Series, Brussels, 21-24 February 2011.
The paper considers several examples of lab-scale experiments demonstrating successful plasma application for an accurate steering of structure and parameters of supersonic airflow. The principal focus is on phenomena associated with problem of drag reduction, plasma-induced generation of shock waves, and artificial flow separation.	
22.	<i>Sergey B. Leonov</i> “Plasma-Based Supersonic Flameholding at low ER”, 3th International Scientific and Technical Conference “Aeroengines of XXI century”, 30Nov-3Dec 2010.
The paper and presentation are dedicated to theoretical and experimental investigation of the process of hydrocarbon fuel plasma-chemical reforming and combustion in the airflow for the purpose of reduction of the combustion induction time.	
23.	<i>A. Firsov, Yu. Isaenkov, S. Leonov, M. Shurupov, D. Yarantsev, M. Shneider</i> , Interaction of Pulse Filamentary Discharge with Heterogeneous Media, Invited Lecture, 11th Asian Symposium on Visualization, NIIGATA, JAPAN, June 2011
A subject of consideration is the dynamic of filamentary discharge generated along contact zone of two co-flown gases. The effects found are supposed to be applied for high-speed combustion enhancement due to non-equilibrium excitation of air/fuel composition and mixing acceleration of non-premixed multi-components flow. In the paper the experimental data are supported by theoretical and computational analyses.	
24.	<i>Sergey B. Leonov</i> Review of Plasma-Based Methods for High-Speed Flow Control, Sixth International Conference on Fluid Mechanics, Guangzhou, China, June 30-July 3, 2011
The paper considers a general approach on plasma aerodynamics and some examples of lab-scale experiments demonstrating successful plasma application for an accurate steering of structure and parameters of supersonic airflow. The principal focus is on specific properties of electrical discharges due to high-speed flow and, contrariwise, on phenomena associated with plasma impact on flow. The results of model experiments are discussed specifically in two domains: (1) supersonic flow structure control by near-surface discharge; (2) mixing intensification by unstable high-power filamentary discharge.	
25.	<i>M.A. Shurupov, A. A. Firsov, Yu. I. Isaenkov, S. B. Leonov, D. A. Yarantsev, M.N. Shneider, I.V. Kochetov, A.P. Napartovich</i> , “Gasdynamic Effects of High-Voltage Breakdown in Non-Homogeneous Atmosphere”, Proceedings of 11th International Conference on Fluid Control, Measurements and Visualization: FLUCOME 2011 – Paper No. 064; December 5-9, 2011, Taiwan
A subject of paper is the appearance and dynamic of sub-microsecond long filamentary high-voltage discharge generated in atmosphere, in airflow, and in non-homogeneous gaseous media. Two effects are particularly discussed: strong gasdynamic instability of post-discharge disturbed zone, and the discharge specific localization in immediate vicinity of two gases. The effects found are supposed to be applied for lightning prediction/protection, and for high-speed combustion enhancement due to non-equilibrium excitation of air/fuel composition and mixing acceleration of non-premixed multi-components flow. In the paper the experimental data are supported by theoretical and computational analyses.	

26.	<i>Sergey B. Leonov</i> , “Plasma-Based Method for Precisious Control of Airflow”, Invited Lecture, 11th International Conference on Fluid Control, Measurements and Visualization: FLUCOME 2011; December 5-9, 2011, Taiwan
The Paper and presentation considers several examples of lab-scale experiments demonstrating successful plasma application for an accurate steering of structure and parameters of supersonic airflow. The principal focus is on phenomena associated with problem of flow actuation; drag reduction; plasma-induced generation of shock waves; and artificial flow separation.	
27.	<i>S. B. Leonov, A. A. Firsov, Yu. I. Isaenkov, M.A. Shurupov, D. A. Yarantsev, M.N. Shneider, I.V. Kochetov, A.P. Napartovich</i> , “Specific Localization of High-Voltage Discharge in Vicinity of Two Gases”, 64th Annual Gaseous Electronics Conference, November 14-18, 2011, Salt Lake City, Utah
For the short-pulse discharge the physical mechanism appears as the following. The first stage of the spark breakdown is the multiple streamers propagation from the “hot” electrode toward the grounded one. In case of high-power electrical source those streamers occupy a huge volume of the gas, covering all possible paths for the further development. This statement is illustrated by the well-adjusted schlieren photos of the streamers’, where the spark phase was prevented due to the voltage reducing. The next phase consists of the real selection of the discharge path among the multiple channels with non-zero conductivity. It is the key point – which channel appears to be the best in terms of the current increase, i.e. possessing higher conductivity and lower inductivity. If the media is non-homogeneous the favorite path may not be the shortest one. Experiments and calculations are presented for Air-CO ₂ and Air-C ₂ H ₄ pairs. Some practical approaches are demonstrated experimentally due to the discharge excitation near directly injected gaseous fuel to high-speed flow.	
28.	<i>M. A. Deminsky, I. V. Kochetov, A. P. Napartovich, S. B. Leonov</i> , “Modeling of plasma assisted combustion in premixed supersonic gas”, International Journal of Hypersonics, Vol 1, #4, 2011, pp.209-223
A model for plasma assisted combustion of ethylene-air mixtures at conditions typical for scramjet combustion chamber is developed combining classical mechanisms of thermal combustion with non-thermal plasma chemistry. Numerical simulations showed that sufficiently strong reduction of ignition induction time at a reasonable energy cost can be realized with help of filamentary discharges. Starting from the discharge region, the gas mixture is heated due to exothermic reactions involving atomic oxygen and secondary chemical radicals. Temperature increment to the end of this stage for ethylene-air mixture is relatively small. An important effect of this stage is not heating but production of transient species. Then, a period with slow growth of temperature follows, which terminates by fast combustion. Processes causing the first fast growth of gas temperature are analyzed, and intermediate species controlling acceleration of ignition are determined numerically for plasma assisted combustion of stoichiometric mixture of ethylene with air. The value of the calculated induction time defined as a moment of the fast combustion is rather sensitive to the particular combustion mechanism adopted. This manifests a necessity to refine combustion mechanisms for conditions typical for scramjet combustion chamber with plasma initiation – one atmosphere pressure, static gas temperature around 700 K and appearance of atomic oxygen.	
29.	<i>Leonov, S. B., Kochetov, I. V., Napartovich, A. P., Sabel'nikov, V. A., Yarantsev, D. A.</i> “Plasma-Induced Ethylene Ignition and Flameholding in Confined Supersonic Air Flow at Low Temperatures” Plasma Science, IEEE Transactions on, V.39, Issue 99, No2, 2011, pp.781-787.
The results of laboratory-scale experiments on plasma-induced hydrogen and ethylene ignition and flameholding by means of near-surface electrical discharge are presented. The ignition and flameholding were demonstrated for direct fuel injection into the supersonic air. Two-zone model of plasma-induced ignition is proposed to explain the experimental data. Numerical simulations were performed to confirm the two-zone model of plasma-assisted ignition.	
30.	<i>Sergey B. Leonov</i> , “Faster and Smarter”, Aviation Week and Space Technology, Oct 24/31, 2011, pp.77-79
N/A	
31.	<i>Sergey Leonov, D. Yarantsev, V. Sabelnikov</i> , Electrically Driven Combustion near the plane wall in a supersonic duct, Progress in Propulsion Physics, Advances in

	Aerospace Science, EUCASS book series, Vol 2, 2011, pp. 519-530
	An ultimate objective of this work is to enhance the performance of air-breathing engines in transient modes. The paper presents the result of laboratory-scale experiments on ignition of non-premixed fuel-air composition in high-speed flow by near-surface electrical discharge. The experiments were fulfilled under conditions of model supersonic combustor on the plane wall without any mechanical flameholder. The ignition and flameholding of hydrogen-air and ethylene-air compositions were demonstrated for direct fuel injection into the flow at low ($T_0=300-750\text{K}$) gas temperature. The power deposited was $W_{pl}/H_{tot}<2-5\%$ of flow total enthalpy. The power threshold of fuels ignition over the plane wall was measured by variation of power deposition and the fuel mass flow rate. The combustion completeness was estimated to be reasonably high, $\eta>0.9$, with both hydrogen and ethylene fuels under optimal conditions.
32.	<i>S.B. Leonov, A.A. Firsov, M.A. Shurupov</i> , Flow structure analysis by cross-correlation image processing, The 10th International Workshop on Magneto-Plasma Aerodynamics, Moscow, Russia, March 22-24, 2011
	The paper describes method of velocity profile measurements by processing of images obtained by schlieren optical system with using of line-scan camera. The images acquired by line-scan camera present set of instantaneous states of flow disturbances: exposure time of one line is $6\ \mu\text{s}$ at the $f=100\ \text{kHz}$ scan rate. In regular case the velocity of each small disturbance in the flow is equal to speed of flow. The method is based on determination of the shift of disturbance dx for two nearest lines of line-scan camera image. Knowing the shift dx , we can find the velocity as $V=f\times dx$. The image is divided to several parts by time and length to find out the local velocity for each part at fixed time. Utilizing the cross-correlation image processing of line-scan camera image, the time-depended lengthwise flow velocity profile averaged by flow width can be calculated.
33.	<i>Фирсов А.А., Леонов С.Б.</i> , Моделирование распада перегретого канала, возникающего при электрическом пробое в воздухе, Proceedings, Engineering Systems 2012
	В работе представлено исследование возмущений, возникающих при распаде разрядного канала в воздухе; также обсуждается механизм возникновения быстрых вихреобразных структур. Данные исследования обусловлены задачами по ускорению перемешивания топлива с окислителем в камерах сгорания. Образующиеся вихреобразные структуры хорошо видны на теневых снимках. Однако получить информацию о трехмерной структуре этих возмущений, а также о параметрах газа в области распада разрядного канала крайне сложно в реальном эксперименте. Наиболее удобным шагом в данном случае является проведение численного моделирования.
34.	<i>A. M. Frolov, S. B. Leonov, V.R. Soloviev</i> , Spatial and dynamic characteristics of dielectric barrier discharge (DBD) at variation of dielectric's parameters, The 11th International Workshop on Magneto-Plasma Aerodynamics, Moscow, Russia, Apr 10-12, 2012
	In present work the influence of dielectric's parameters and characteristics of power supply on dielectric barrier discharge (DBD) luminosity is studied. The supply voltage has amplitude up to 16 kV and frequency up to 5 kHz. To explore the behavior of the discharge luminosity area optical measurements of its length have been carried out simultaneously with the recording of the electrical parameters. Linear dependence of DBD length upon voltage amplitude with rising or falling potential of the exposed electrode was observed. The discharge length and, consequently, appearance and propagation of DBD is supposed to be independent on the dielectric's parameters.
35.	<i>I. V. Kochetov, A. P. Napartovich, S. B. Leonov</i> , The discharge development along the border of the gases jets, The 11th International Workshop on Magneto-Plasma Aerodynamics, Moscow, Russia, Apr 10-12, 2012
	It was found experimentally that the pulse discharge in co-flowing gas jets has a trend to develop along the boundary layer between jets composed of two different gases (air, CO ₂ , He). This effect may be important in plasma assisted combustion technology as far as correlation between plasma and gas-dynamic movement may enlarge gas mixing rate and make ignition initiation more effective. In order to estimate reality of such effects, the first step is evaluation of plasma properties in fuel/air mixtures of various compositions. The most important quantity governing discharge breakdown is the rate of electron multiplication equal to difference between electron impact ionization and attachment rates. The electric current increase rate under voltage growing is analyzed numerically as a function of C ₂ H ₄ -air mixture composition.
36.	<i>M. Shurupov, S. Leonov, K. Savelkin, D. Yarantsev</i> , Spectral diagnostics of mixing,

	induced by high voltage discharge, by means of probe discharge, The 11th International Workshop on Magneto-Plasma Aerodynamics, Moscow, Russia, Apr 10-12, 2012
	One of the most serious problems of the mixing study in compressible flow is the experimental estimation of fuel and oxidizer components in predefined volume. In order to estimate mixing efficiency of the discharge the <i>laser breakdown fluorescence (LBF)</i> could be used. In spite of all its advantages (high temporal and spatial resolution, nonintrusivity) this method have very high cost of the laser system required. It has been proposed to modify this method and to use discharge breakdown instead of laser breakdown. The idea is to realize breakdown of so-called “probe” discharge that possess much less power than the main one at some delay after the main breakdown. The temporal resolution of this method is equal to the probe discharge fluorescence duration – 1 μ s and it is rather small. The spatial resolution is determined by the collecting optical system and can be no more than $l \times d = 3 \times 1$ mm, approximately. It is a little bit worse than spatial resolution of the LBF but it still seems enough for mixing efficiency estimation.
37.	<i>Dmitry A. Yarantsev, Sergey B. Leonov, Konstantin V. Savelkin, M.A. Bolshov, Yu. A. Kuritsyn, V.V. Liger, V.R. Mironenko</i> , Comparison of injection schemes for ignition of nonpremixed fuel by surface discharge in supersonic flow. The 11th International Workshop on Magneto-Plasma Aerodynamics, Moscow, Russia, Apr 10-12, 2012
	This paper is devoted to the comparison of the two schemes of plasma generator and fuel injectors' arrangement on the plane wall of supersonic duct in experiments on ethylene ignition and flameholding in supersonic airflow. The following measurements were carried out in experiments: static pressure distribution along the duct; water temperature and concentration within the combustion zone were measured by means of tunable diode laser absorption spectroscopy (TDLAS); flow structure visualization was made by means of schlieren method; besides, electrical parameters of the discharge were measured and fast visualization of discharge was carried out.
38.	<i>S. Leonov, A. Firsov, D. Yarantsev, M. Bolshov, Y. Kuritsyn, V. Liger</i> , “Temperature Measurement in Plasma-Assisted Combustor”, AIAA Paper #2012-3181
	The paper is focused on study of particular mechanisms of plasma impact on high-speed combustion. A tunable diode laser absorption spectroscopy (TDLAS) technique and appropriate instrumentation was developed for the measurement of temperature and water vapor concentrations in reacted gases. The technique is based on the detection of the spectra of H ₂ O absorption lines with different energies of low levels. Spectra were recorded using fast frequency scanning of a single distributed feedback (DFB) laser. Under conditions of high level of flow disturbances an optimal technique for fitting the experimental spectra was developed based on presentation of the transient absorption spectra as 2D images in the first step of data processing. In the most cases the high signal-to-noise ratio enabled the reconstruction of the temporal behavior of temperature with a resolution of ~ 1 ms. The validated TDLAS technique was applied for detection of temperature and H ₂ O concentration in the combustion zone of a supersonic ($M = 2$) air-fuel flow. Direct wall-injected hydrogen and ethylene were used as the fuels. The combustion process was initiated and sustained by near-surface electric discharge. The data of DLAS measurements have proved the idea of two-stage mechanism of plasma-assisted combustion.
39.	<i>S. Leonov, A. Firsov, M. Shurupov, J. Michael, R. Miles, M. Shneider</i> , “Femtosecond laser guiding of high-voltage discharge and the restoration of dielectric strength”, AIAA Paper #2012-3178
	We investigate the dynamics of a long filamentary submicrosecond high-voltage pulse discharge generated after a femtosecond laser pulse. A femtosecond laser focused in the inter-electrode gap results in a weakly-ionized plasma filament and results in guiding of the high voltage discharge through this laser channel. The energy of laser pulse is about 2 mJ, the energy of electrical discharge is more than 1 J. The laser-guiding effect is considered for variety of geometric configurations and delay times between the laser pulse and HV pulse up to $\square\square 100\mu$ s. An initial stage of breakdown – development a streamer tree – was observed in detail with and without a laser guiding pulse. Tests were performed in air and nitrogen to better illuminate the mechanism of our observed laser-based guiding at large (~ 100 μ s) delays. We present the results which may be of potential application for aircraft lightning protection.
40.	<i>Sergey B. Leonov</i> “Supersonic Flow Structure on Compression Surfaces under Plasma Impact”, Proceedings of International Congress on Theoretical and Applied Mechanics, Beijing, China, Aug 19-24, 2012, Paper FM04-009
	This paper reports the results of experimental and computational study of compressible flow control by weakly-ionized plasma of electrical discharge. Particular objective of this activity is to demonstrate the steering effect of

	near-surface electrical discharge on supersonic flow structure in a model two-dimensional aerodynamic configuration with two-shock compression ramp.
41.	<i>S. Leonov, Yu. Isaenkov, D. Yarantsev, M. Shurupov, J. Michael, A. Dogariu, M. Shneider, R. Miles</i> , “High-Voltage Breakdown, Guided by Femtosecond Laser and Gas Inhomogeneity”, Proceedings of 19th International Conference on Gas Discharges and Their Applications, Beijing, Sept 2012, paper 159
	The dynamics of a long filamentary submicrosecond high-voltage ($U_d > 100\text{kV}$, pulse duration 50-70ns) pulse discharge, generated after a femtosecond laser pulse, is investigated. A femtosecond laser focused in the inter-electrode gap results in a weakly-ionized plasma filament that results in guiding of the high voltage discharge through this laser channel. The result of interaction of a pulsed filamentary discharge with a surrounded gas strongly depends on current amplitude and pulse duration. The energy of laser pulse is about 2mJ (at the electron density within the filament of $\sim 10^{16}\text{ cm}^{-3}$), the energy of electrical discharge is more than 1 J. The laser-guiding effect is considered for variety of geometric configurations and delay times between the laser pulse and HV pulse up to 100 μs . An initial stage of breakdown – development a streamer tree – was observed in detail with and without a laser guiding pulse.
42.	<i>S. B. Leonov, A. A. Firsov, M. A. Shurupov, J. B. Michael, M. N. Shneider, R. B. Miles, and N. A. Popov</i> “Femtosecond laser guiding of a high-voltage discharge and the restoration of dielectric strength in air and nitrogen”, Physics of Plasmas, vol.19, 123502, 2012
	The use of a low energy, high peak intensity ($> 100\text{ TW/cm}^2$) femtosecond laser pulse is investigated for guiding and control of a sub-microsecond high voltage discharge. Study of the laser induced plasma channel and measurements of the field required for breakdown in air and nitrogen at atmospheric pressure are presented. Direct imaging of the dynamics of discharge breakdown shows effective laser guiding which is critically dependent on the laser focusing geometry, timing, and location relative to the electrodes.
43.	<i>S. Leonov, J. B. Michael, R. B. Miles, M.N. Shneider, M. Shurupov</i> “High-Voltage Discharge In Air And Nitrogen, Guided By Femtosecond Laser”, 65th Gaseous Electronic Conference, Book of Abstracts, UF2.00004, 2012
	The ability of a low energy ($E_l < 2\text{mJ}$) femtosecond laser pulse to modify a high energy ($E_d > 1\text{J}$), high voltage discharge is examined in detail. The geometry and breakdown voltage of a long filamentary submicrosecond high-voltage pulse discharge are studied by noting the effect on initial streamer formation, the breakdown location and overall geometry, and through voltage and current waveforms. A femtosecond duration laser pulse is focused in the inter-electrode gap, producing a weakly-ionized plasma filament and effectively decreasing the high voltage breakdown and the geometry of both the initial streamer formation and the high voltage filamentary breakdown. The power supply supplies a rapid voltage rise, $dU/dt > 2 \times 10^{11}\text{ V/s}$, and the high voltage breakdown results in a current pulse of 30-80ns in duration with a high voltage amplitude of up to 120kV. The guiding effect of the laser pulse is considered for several geometric configurations and for delay times between the laser pulse and HV pulse up to $\approx 100\mu\text{s}$. The initial stage of breakdown – development a streamer tree – was observed in detail with and without a laser guiding pulse. Tests were performed in air and nitrogen to better illuminate the physical mechanism of our observed laser-based guiding, particularly at small ($< 0.2\text{mcs}$) and large (up to 100mcs) delays. The largest decrease in the breakdown voltage occurs at early time, and the effect remains significant in pure nitrogen mixtures at delay times up to 2mcs. Both gas kinetic and gasdynamic analyses are used to determine the effects due to ionization and density drops in both air and nitrogen.
44.	<i>A. A. Firsov, M. A. Shurupov, D. A. Yarantsev, and S. B. Leonov</i> “Mixing Actuation by Unstable Filamentary Discharge”, Paper AIAA-2013-1188
	The problem discussed in this work is the dynamics of long filamentary pulse discharge generated along the contact zone of two co-flown gases. The effect of the mixing actuation in compressible flow is observed because of the gasdynamic instability arisen after the discharge generation. The mixing efficiency is examined qualitatively by means of Probe Discharge Breakdown Fluorescence (PBF)
45.	<i>A.A. Firsov, S.B. Leonov, K.V. Savelkin, M.A. Shurupov, D.A. Yarantsev</i> “Unsteady Decay of Pulse Discharge Thermal Cavity”, The 12th International Workshop on Magneto-Plasma Aerodynamics, Moscow, Russia, March, 2013
	The problem of decay of thermal disturbances after the impulse energy deposition covers a wide range of studies of the plasma-excited gas dynamic disturbances. Also, this problem has a direct influence on the recovery of

dielectric strength post-discharge channel, which, in turn, is important for the safety of high-voltage equipment.

46. *A.A. Firsov, S.B. Leonov, M.A. Shurupov* “Gasdynamic Phenomena at Thermal Impact (Scientific Art)”, The 12th International Workshop on Magneto-Plasma Aerodynamics, Moscow, Russia, March, 2013

The paper considers the results of computational analysis of gas dynamics of long filamentary pulse discharge in free air. Simulation of after spark channel was performed by using FlowVision 3 software. Numerical modeling was based on solution of 3D time-dependent Reynolds averaged Navier-Stokes equations with (or without) utilization of the wide used two-equation $k-\epsilon$ model of turbulence. Discharge breakdown was simulated by volumetric heat source.

Attachment 2: List of presentations at conferences and meetings with abstracts

1. I.V. Kochetov, S.B. Leonov, A.P. Napartovich, E.A. Filimonova, D.A. Yarantsev “Plasma-chemical reforming of the hydrocarbon fuel in the air flow”, International Workshop on “Thermochemical and plasma processes in aerodynamics” Saint-Petersburg, 19-21 June, 2006.

The paper and presentation are dedicated to theoretical and experimental investigation of the process of hydrocarbon fuel plasma-chemical reforming in the airflow for the purpose of reduction of the combustion induction time.

2. Sergey B. Leonov, Igor B. Matveev “First Test Results of the Transient Arc Plasma Igniter in a Supersonic Flow”, Paper, Proceedings of IWEPAC-3, September 17-20, 2007, Falls Church, VA, U.S.A

This paper and presentation considers the idea and the first test results of the combined cycle plasma torch (CCPT) application for flame holding in high-speed combustors. The CCPT was developed by Applied Plasma Technologies (APT) and is based on a low-power transient discharge plasma pilot with fuel or air-fuel mixture feeding into the arc chamber, so that the main thermal effect is provided by chemical reactions in a plasma-activated medium.

3. Sergey B. Leonov, Dmitry A. Yarantsev, “Flameholding due to electrical discharge generation on plane wall of supersonic duct.”, Proceedings of ICPCD 2008, Moscow, Russia, 10-12 November 2008

The presentation dedicates the last achievements in a field of active flameholding in high-speed flow under non-optimal conditions by means of near-surface electrical discharge. В докладе представлены последние достижения в области стабилизации фронта высокоскоростного горения в неоптимальных условиях при помощи приповерхностного электрического разряда.

4. S. Leonov, Yu. Isaenkov, D. Yarantsev “Pulse Discharge in Mixing Layer of Reacting Gases”, Book of Abstracts, 61th Annual Gaseous Electronics Conference 14- 17 October, 2008, Dallas-Addison Marriott Quorum, Dallas, TX, USA

A subject of consideration is the dynamic of filamentary pulse discharge generated along contact zone of two co-flown gases. Experimental facility consists of blow-down wind tunnel PWT-50, system of the high-voltage pulse-repetitive feeding, and diagnostic equipment (schlieren device; pressure, voltage, current, radiation sensors; spectroscopic system; etc.) Typical parameters: $p=0.2-1\text{Bar}$, velocity $M=0-2$, pulse duration $\tau=0.1-1\mu\text{s}$, power release $W=20-100\text{MW}$. Recently the effect of enormously fast turbulent expansion of the post-discharge channel was observed experimentally [S. Leonov, oth., AIAA Paper 2005-0159 and S. Leonov, oth. “Physics of Plasmas”, v.15, 2007]. In this paper a result of parametrical study of the mixing efficiency due to instability development are discussed. The next announced item is that the discharge position and dynamics depend on the test parameters and physical properties of gases involved. The result of interaction can be controlled by the discharge’s duration and current as well as by small additives to the gas. The effects found can be applied for high-speed combustion enhancement due to mixing acceleration in multi-components flow.

5. *М. А. Деминский, И. В. Кочетов, С. Б. Леонов, А. П. Напартович, Б. В. Потанин*, Удельные энергии плазменного инициирования для обеспечения горения в сверхзвуковом потоке топливно-воздушной смеси, Труды 6го Международного симпозиума “Термохимические и плазменные процессы в аэродинамике”, Санкт-Петербург, 12-14 мая, 2008, Холдинговая компания “Ленинец”

Определены удельные энергии, необходимые для плазменного инициирования горения предварительно перемешанной водородно-воздушных и этилен-воздушных смесей в сверхзвуковом потоке в условиях типичных для ГПВРД. Исследовано влияние вида разряда на эффективность плазменного инициирования. Показано, что основными механизмами плазменного инициирования в рассматриваемых условиях являются диссоциация молекул кислорода при столкновениях с электронно-возбужденными молекулами азота и диссоциация электронами плазмы. Исследовано влияние молекул кислорода в нижнем синглетном электронно-возбужденном состоянии (СК) на порог плазменного инициирования в водородно-воздушных смесях. Из-за больших сечений возбуждения различных внутренних степеней свободы молекул азота на возбуждения СК идет незначительная доля мощности разряда, и его влияние на плазменное инициирование незначительно.

6. *С.Б. Леонов*, Стабилизация фронта пламени электрическим разрядом за уступом и на плоской стенке сверхзвукового канала. Труды 3й Школы-семинара по Магнито-плазменной Аэродинамике, Москва, ОИВТ РАН, апрель 2008.

Подробно представлены экспериментальные результаты по зажиганию топлива в сверхзвуковом потоке и стабилизации фронта пламени при $T_0=300-760\text{K}$. В качестве топлива используются водород и этилен, непосредственно инжектируемые со стенки в поток $M=2$ при $ER<0.1$. В работе использовался приповерхностный разряд на плоской стенке между электродами, установленными «заподлицо». Величина вложенной в разряд электрической мощности составляла $W_{pl}/H_{tot}<2\%$ от полной энтальпии потока, тогда как тепловая мощность вследствие горения превышала $W_{com}/H_{tot}>100\%$ при низкой начальной температуре газа. Стабилизация фронта горения получена при полноте сгорания топлива $\eta>0.9$. Приведены данные по положению фронта и росту давления и зависимости от начальной температуры. Специально отмечается, что разряд несет как функцию инициатора пламени, так и регулятора структуры потока. Выключение разряда приводит к немедленному срыву горения. Приведены данные по порогу горения в зависимости от мощности разряда и расхода топлива.

7. *Sergey Leonov* “Ignition and Flameholding in $M>1$ Airflow by Electrical Discharge: 10years’ Experience”, Invited Lecture, 47th AIAA Aerospace Sciences Meeting and Exhibit (Orlando, FL, USA, 5-8 January 2009), AIAA-2009-0000.

A main objective of this work as a whole is to enhance the performance of air-breathing engines in transient modes. The concept of Plasma-Induced Ignition and Plasma-Assisted Combustion is considered on the basis of three main ideas: the medium heating/excitation by discharge, fuel-air mixing intensification, and flow structure control in the vicinity of reaction zone. A short review of recent works is done based on available publications. The paper presents also the result of lab-scale experiments on ignition of non-premixed fuel-air composition in high-speed flow by electrical discharge made during the last 10 years. The experiments were fulfilled under conditions of model supersonic combustor in standard aerodynamic configurations with backwise wallstep, in cavity, and on the plane wall. The electrical discharge was organized in specific electrodes arrangement where the plasma filaments crossed an area of gas circulation. The ignition and flameholding of hydrogen-air, ethylene-air, and kerosene-air compositions were demonstrated for direct fuel injection into the fixed separation zone at low gas temperature. An energetic threshold of fuel ignition under separation and in a shear layer of supersonic flow has been measured. Some ideas for the mixing intensification are discussed as well. They are proved by model experimental demonstrations.

8. *Leonov S. B.*, “Ignition and Flameholding of Gaseous Fuels by Electrical Discharge in $M>1$ Airflow”, Invited lecture, 2nd EUCASS ATW, Les Houches, France, October 11-16, 2009

Main idea pushed forward by this lecture is that the plasma assistance for combustion enhancement occurs on sophisticated multistage manner. Under some conditions the multistage combustion is observed without plasma of electrical discharge. But at the plasma assisted combustion the kinetic mechanism of ignition looks to be principally multistage (at least, two stages) process, as it is pointed in some last publications. To prove such a mechanism of combustion the diode laser absorption spectroscopy (DLAS)

was applied for the remote measurement of temperature, total pressure and concentration of water vapor. The comparison of these data with results of visualization and pressure records are made for the first time.

9. *С.Б. Леонов, А.А. Фирсов, М.А. Шурупов, Д.А. Яранцев* “Субмикросекундный высоковольтный разряд в неоднородной газовой среде”, The 9th International Workshop on Magneto-Plasma Aerodynamics, Moscow, Russia, April 13-15, 2010
The idea discussed is the mechanism of the discharge localization in a mixing layer of two gases. The effects found are supposed to be used for high-speed combustion enhancement owing to nonequilibrium excitation of air/fuel composition and mixing acceleration of nonpremixed multicomponents flow.
10. *Leonov S. B.*, Visualization of unsteady electrical discharges in high-speed flow, Keynote Lecture, 10th ASV International Conference, SRM University, Chennai, India, March 2010
Specific experimental technique, applied in Plasma-Assisted Aerodynamics, is considered in the paper. The results of several experiments are presented to demonstrate abilities of non-standard methods of visualization to make evident the gasdynamic effects appeared due to the plasma-flow interaction. These phenomena are mostly hidden for unaided eye. The examples shown include the unsteady near-surface discharge in supersonic flow; the DBD over a contoured airfoil; the high-power pulse discharge instability; and some others for the demonstration in appropriate presentation.
11. *Sergey B. Leonov* “Plasma-based method for precise control of high-speed airflow”, Invited lecture for the 8th European Fluid Mechanics Conference by the *European Mechanics Society*, Bad Reichenhall, Germany, September 13-16, 2010.
The lecture considers several examples of lab-scale experiments demonstrating successful plasma application for an accurate steering of structure and parameters of supersonic airflow. The principal focus is on phenomena associated with plasma-induced shocks generation and artificial flow separation.
12. *S. Leonov*, Supersonic Airflow Control by Electrical Discharges, Invited Lecture, AIAA International Space Planes and Hypersonic Systems and Technologies Conference, San Francisco, CA, 11-14 April 2011
The presentation is dedicated to theoretical and experimental investigation of the plasma-based flow control.
13. *S. B. Leonov, A. A. Firsov, Yu. I. Isaenkov, M.A. Shurupov, D. A. Yarantsev, M.N. Shneider, I.V. Kochetov, A.P. Napartovich*, “Mixing Intensification by Electrical Discharge”, AFOSR Program Review “Fundamental Mechanisms, Predictive Modeling, and Novel Aerospace Applications of Plasma-Assisted Combustion”, November 9-10, 2011, OSU, Columbus, OH
The presentation considers last ideas and experimental data on plasma-based mixing intensification in high-speed flow.
14. *S. Leonov*, Plasma-based method for precision control of airflow, Invited lecture (IS06), 11th International Conference on Fluid Control, Measurements and Visualization: FLUCOME 2011 – Paper No. IS06; December 5-9, 2011, Taiwan
The presentation considers several examples of lab-scale experiments demonstrating successful plasma application for an accurate steering of structure and parameters of supersonic airflow. The principal focus is on phenomena associated with problem of flow actuation; drag reduction; plasma-induced generation of shock waves; and artificial flow separation.
15. *S. Leonov* Inlet Regulation by Electrical Discharge, Invited Lecture: 11th International Workshop on Magneto-Plasma Aerodynamics, 10 - 12 April 2012, JIHT RAS, Moscow, Russia
The presentation presents results of experimental and computational study of near-surface electrical discharge effect on shocks configuration in a compression ramp and 2D inlet performance in M=2-3 supersonic flow. It is shown that the plasma deposition allows an accurate regulation of shock angle and reflection line position on opposite wall of the first model and in vicinity of cowl lip of the second model. The plasma effect is considered on mass flowrate (MFR) and pressure recovery coefficient (PRC). The

magnitude of regulation effect depends on the power release. While the PRC increases in few percent, the MFR modification strongly varies, being constituent with the operation mode. The CFD efforts in 3D NS approach clarify some extra features of plasma-flow-surface interaction.

16. *S.B. Leonov* “Plasma for High-Speed Propulsion” (invited presentation). The 12th International Workshop on Magneto-Plasma Aerodynamics, Moscow, Russia, March, 2013

Review of last trends in Plasma-assisted Combustion. The talk examines the possibility and technical feasibility of plasma technology application to expand the limits of operation of the ramjet/scramjet depending on the parameters of incoming stream, and the conditions in the combustion chamber. Three examples of successful laboratory scale experiments are considered: (1) control of air inlet parameters; (2) ignition of fuel and maintenance of the flame front; and (3) acceleration of mixing of components in high-speed flow. In the management of air inlet the regulation problem of shock-wave structure on compression surface and promotion of laminar-turbulent boundary layer transition are under analysis. As part of the combustion problem discuss, the concept of surface discharges as a flameholder in scramjet is presented. The gasdynamically unstable discharge of submicrosecond duration, localized in the mixing layer of fuel and oxidizer, is considered to be an agent of the mixing enhancement in combustor.

Attachment 3: Information on patents and copy rights

No